EMERGING INFECTIOUS DISEASES®

U.S. CENTERS FOR DISEASE CONTROL AND PREVENTION

Zoonotic Infections

May 2026

Cassius Marcellus Coolidge, *A Friend in Need*, 1903. Oil on canvas. 129.5 cm x 160.6 cm (51 in × 63.22 in). Smithsonian American Art Museum, Washington, DC, USA.

Pages 675–838

EMERGING INFECTIOUS DISEASES

A Peer-Reviewed Journal Tracking and Analyzing Disease Trends

Emerging Infectious Diseases is published monthly by the Centers for Disease Control and Prevention, 1600 Clifton Rd NE, Mailstop H16-2, Atlanta, GA 30329-4018, USA. Telephone 404-639-1960; email eideditor@cdc.gov

EMERGING INFECTIOUS DISEASES®

Zoonotic Infections **May 2026**

On the Cover

Cassius Marcellus Coolidge, *A Friend in Need,* 1903. Oil on canvas. 129.5 cm × 160.6 cm (51 in × 63.22 in). Smithsonian American Art Museum, Washington, DC, USA.

About the Cover p. 833

Synopses

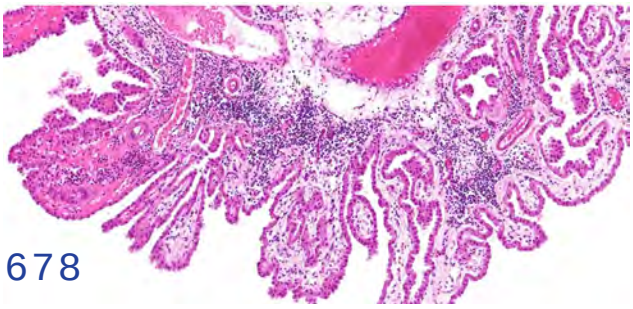

678

EMERGING INFECTIOUS DISEASES®

May 2025

Research

Medscape EDUCATION ACTIVITY

Dispatches

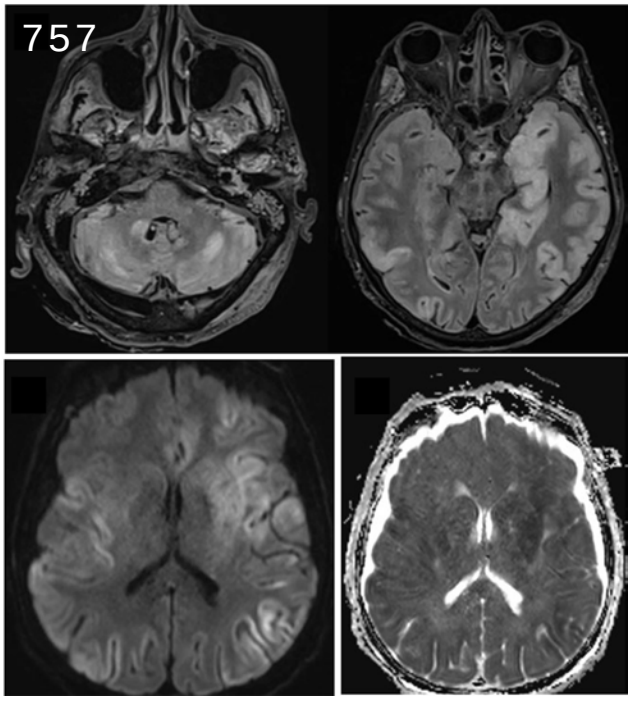

757

EMERGING INFECTIOUS DISEASES®
May 2025

Photo Quiz

Research Letters

Comment Letter

Books and Media

About the Cover

Etymologia

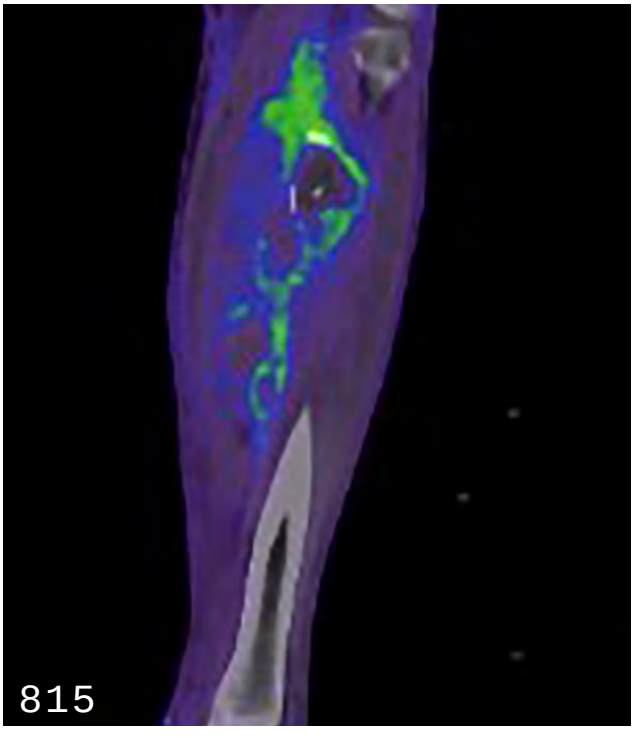

Emerging Infectious Diseases
Photo Quiz Articles

Volume 14, Number 9
September 2008

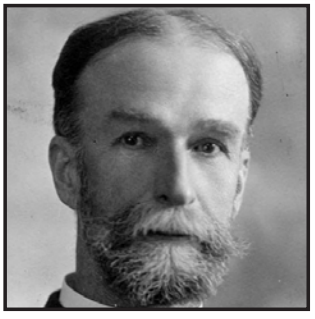

Volume 14, Number 12
December 2008

Volume 15, Number 9
September 2009

Volume 15, Number 10
October 2009

Volume 16, Number 6
June 2010

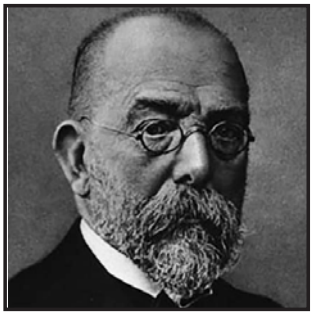

Volume 17, Number 3
March 2011

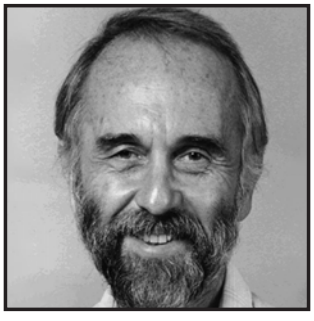

Volume 17, Number 12
December 2011

Volume 19, Number 4
April 2013

Volume 20, Number 5
May 2014

Volume 21, Number 9
September 2015

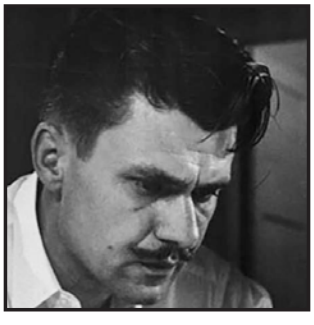

Volume 22, Number 8
August 2016

Volume 28, Number 3
March 2022

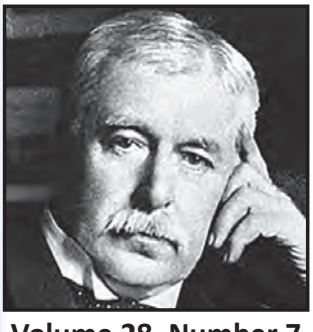

Volume 28, Number 7
July 2022

Click on the link below to read about the people behind the science.

https://bit.ly/3LN02tr

See requirements for submitting a photo quiz to EID.

https://bit.ly/3VUPqfj

EID Journal

Borna Disease Virus 1 as Cause of Fatal Meningoencephalomyelitis in Wild Hedgehogs, Germany, 2022–2025

Effrosyni Michelakaki, Benjamin Schade, Brigitte Boehm, Eva Kappe, Marcel Suchowski, Anne Kupca, Magdalena Schumacher, Anna Maria Gager, Friederike Liesche-Starnecker, Sonja Fiedler, Eva Schwarz, Zoltan Bago, Andreas Blutke, Martin Beer, Dennis Rubbenstroth,[1] Kaspar Matiasek[1]

Borna disease virus 1 (BoDV-1) causes encephalitis with a fatality rate of ≥90% in domestic mammals and humans. Currently, the bicolored white-toothed shrew is the only known reservoir host. We report BoDV-1 infections in 15 wild European hedgehogs from an endemic area in Germany. Because hedgehogs are distant relatives of shrews and often cared for by humans, the cases raise concern regarding a potential zoonotic risk. All the hedgehogs that tested positive for BoDV-1 died of neurological disease and exhibited severe polio-predominant lymphoplasmohistiocytic meningoencephalitis. However, because of the detection of viral antigens in nonneural cells in 1 animal, we cannot completely exclude that some infected hedgehogs shed the virus. Although direct BoDV-1 transmission is known to be inefficient, our results emphasize the necessity of hygiene measures when handling hedgehogs, especially those with neurological signs who are from BoDV-1–endemic regions.

Borna disease virus 1 (BoDV-1; species *Orthobornavirus bornaense*, family Bornaviridae) is known as the causative agent of Borna disease, a usually fatal, immune-mediated meningoencephalitis identified throughout endemic areas of Germany, Austria, Liechtenstein, and Switzerland (*1*). Borna disease can affect a broad range of domestic mammals, particularly horses, alpacas, and sheep (*1*–*4*). Since 2018, BoDV-1 has also been shown to cause encephalitis in humans. Up to 6 cases are reported each year, and the case-mortality rate is ≥90% (*1*,*5*–*7*). Domestic mammals and humans are known to serve as dead-end hosts, in which the virus possesses an almost exclusively neurotropic tissue distribution without detectable viral shedding (*3*,*8*). Those infections resulted from spillover transmission from a natural reservoir (*1*,*9*,*10*). Currently, the insectivorous bicolored white-toothed shrew (*Crocidura leucodon*) is the only known reservoir host species (*11*–*13*). Infected shrews develop lifelong viral persistence with a broad tissue distribution and continuous viral shedding but no apparent tissue lesions or clinical disease (*11*).

The European hedgehog (*Erinaceus europaeus*) is another insectivorous species indigenous to Europe that often comes into close contact with humans, particularly when being cared for during hibernation in private households and rescue centers. Although hedgehogs have been associated with various zoonotic diseases (*14*,*15*), we have been unable to find reports of hedgehog BoDV-1 infection.

We present a study of BoDV-1 infection and fatal encephalitis in 15 wild European hedgehogs from an endemic area in Germany. The first case was detected in 2022. BoDV-1 was identified by quantitative reverse transcription PCR (qRT-PCR) of brain tissue from infected hedgehogs. Previous testing for various encephalitic pathogens reported in this or other species, such as tickborne encephalitis virus (TBEV)

Author affiliations: Centre for Clinical Veterinary Medicine, Ludwig Maximilians-Universität München, Munich, Germany (E. Michelakaki, S. Fiedler, E. Schwarz, A. Blutke, K. Matiasek); Bavarian Animal Health Service, Poing, Germany (B. Schade, B. Boehm, E. Kappe); Bavarian Health and Food Safety Authority, Oberschleißheim, Germany (M. Suchowski, A. Kupca, M. Schumacher, A.M. Gager); University Medical Center Ulm, Ulm University, Ulm, Germany (F. Liesche-Starnecker); Institute for Veterinary Disease Control, Mödling, Austria (Z. Bago); Institute of Diagnostic Virology, Friedrich-Loeffler-Institut, Greifswald-Insel Riems, Germany (M. Beer, D. Rubbenstroth)

DOI: https://doi.org/10.3201/eid3205.250952

[1]These senior authors contributed equally to this article.

(*16*), rabies virus (*17*), canine distemper virus (CDV) (*18*) and rustrela virus (RusV) (*19*), yielded negative results. After the diagnosis of a second case in May 2024, the awareness of BoDV-1 among hedgehog rescue centers and diagnostic institutions in the region increased considerably, which led to the identification of a series of additional cases.

The taxonomic proximity of hedgehogs with shrews (*20*), the known BoDV-1 reservoir hosts, raised concerns about hedgehogs being able to shed the virus, leading to potential human exposure. Therefore, we performed a comprehensive analysis of the confirmed cases, including detailed histopathologic study and extensive characterization of the viral tissue distribution and cell tropism by using immunohistochemistry (IHC), RNAscope (Advanced Cell Diagnostics, Inc., https://acdbio.com) in situ hybridization (ISH), and phylogeographic analysis of hedgehog-derived BoDV-1 sequences. In addition, we initiated a screening of nonencephalitic hedgehogs from endemic areas that is ongoing.

Methods

Case Selection, Sample Collection, and Diagnostic Investigations

Our investigation focused on 16 wild hedgehogs that died or were euthanized because of nonsuppurative encephalitis with a histopathologic diagnosis at postmortem examination. In addition, we included 33 deceased nonencephalitic hedgehogs from endemic regions in Bavaria as controls (Appendix Table 1, http://wwwnc.cdc.gov/EID/article/32/5/25-0952-App1.pdf).

All animals underwent a complete postmortem examination, and we fixed a broad set of organs and tissues in 10% neutral buffered formalin for ≥24 hours for histopathologic analysis. From most cases, we snap-froze brain tissue and additional samples for further investigation. In addition, we collected fecal samples, urine samples, and oral swab samples beginning with case 7.

We tested fresh-frozen or formalin-fixed paraffin-embedded (FFPE) brain tissue of all animals by using a BoDV-1–specific qRT-PCR for BoDV-1 RNA (*1*,*3*). We also tested all available fresh-frozen samples and swab samples of BoDV-1–positive animals.

For all BoDV-1–positive animals, we performed staining for BoDV-1 antigen and RNA by IHC and RNAscope ISH. In addition, we tested brain samples from encephalitic animals for other known encephalitic viruses, including TBEV and RusV by qRT-PCR (Appendix Table 2) (*21*,*22*), rabies virus (*23*), and CDV (*24*) by IHC (Appendix section B, Table 3).

Screening for BoDV-1 Antigen Distribution by IHC

We conducted IHC for BoDV-1 nucleoprotein (N) by using mouse monoclonal antibody Bo18 (*25*) on all sections of all available tissues. We also used rabbit anti–BoDV-1 nucleoprotein polyclonal hyperimmune serum #201 (*3*) on select central nervous system (CNS) and peripheral nonneural tissue sections of case 5. All procedures are described in detail (Appendix section B, Table 3).

Screening for BoDV-1 RNA Tissue Distribution via RNAscope ISH

We conducted RNAscope ISH on tissue sections of the CNS of all BoDV-1–positive animals and a selection of peripheral organs for BoDV-1 RNA (probe V-BoDV1-G targeting viral RNA encoding for the matrix protein and glycoprotein genes; genome positions 2,236–3,747 of BoDV-1) (GenBank accession no. NC_001607.1). We conducted ISH as described previously (*26*).

Lesion Characterization

We macroscopically evaluated formalin-fixed tissues before and after fixation and trimming. We trimmed the brain at multiple planes and processed representative areas of telencephalon, diencephalon, brain stem, and cerebellum for microscopic examination. Spinal cord sections comprised transverse and longitudinal sections upon decalcification of the vertebral column by a 20% EDTA solution. We took representative sections from all available adequately preserved peripheral organs and tissues. All samples underwent an ascending alcohol series up to xylene by using an automatic histoprocessor. Thereafter, we embedded the samples in paraffin, cut into 2–4 μm–thick sections, and then stained all sections with hematoxylin and eosin stain for routine microscopic examination (*27*).

To phenotype the inflammatory cell infiltrations, we performed IHC by staining for T lymphocyte marker CD3, B lymphocyte marker Pax 5, and macrophage and microglial marker Iba1. We highlighted the degree and distribution of gliosis by using the astrocyte marker glial fibrillary acidic protein (GFAP). All procedures including detailed information on used antibodies are described (Appendix).

RNA Extraction and qRT-PCR Testing for BoDV-1

We extracted RNA from fresh-frozen tissue samples and swabs by using the NucleoMag VET kit (Macherey-Nagel, https://www.mn-net.com) with a KingFisher Flex Purification System (Thermo Fisher Scientific, https://www.thermofisher.com), whereas we used the RNeasy FFPE kit (QIAGEN, https://www.qiagen.com) for FFPE tissue, as described previously (*1*). We conducted semiquantitative detection of BoDV-1 RNA

Table. Overview of BoDV-1–infected European hedgehogs included in study of Borna disease virus 1 causing fatal meningoencephalomyelitis in wild hedgehogs, Germany, 2022–2025

Case no.	District	Rescue center	Date found	Date died	Survival time after admission or disease onset*
1	Rottal-Inn	A	2022 Jun 22	2022 Jul 16	24
2	Ebersberg	Private	2024 Apr 30	2024 May 5	5
3	Rottal-Inn	A	2024 Jul 1	2024 Jul 10	9
4	Ebersberg	B	2024 Jun 24	2024 Jul 12	20
5	Rottal-Inn	Private	2024 Jun 23	2024 Jul 24	24
6	Ebersberg	B	2024 Jun 18	2024 Aug 15	58
7	Rottal-Inn	A	2024 Sep 11	2024 Sep 12	1
8	Landsberg am Lech	C	2025 Apr 9	2025 Apr 29	5*
9	Eichstätt	D	2025 May 14	2025 May 23	9
10	Eichstätt	D	2025 May 17	2025 May 23	6
11	Ebersberg	E	2025 May 16	2025 Jun 3	18
12	Rosenheim	F	End of 2024	2025 Jun 7	4*
13	Traunstein	F	2025 May 28	2025 Jun 10	13
14	Roth	G	2025 Jul 17	2025 Jul 19	2
15	Landsberg am Lech	Private	2025 Jul 26	2025 Jul 31	5

*Case 8 was reported to demonstrate first clinical signs on 2025 Apr 24. Case 12 had been submitted to the rehabilitation center already several months earlier and had hibernated there. Case 12 began demonstrating neurologic signs on 2025 Jun 3.

by qRT-PCR BoDV-1 Mix-1 and Mix-6 (Appendix Table 2), as described previously (*1*,*7*). We compiled qRT-PCR results as cycle quantification (Cq) values. We used an RNA preparation of BoDV-2 isolate number 98 (GenBank accession no. AJ311524.1) as a positive control and for calibration of the Cq values.

For all BoDV-1-positive animals, we determined partial BoDV-1 genome sequences covering at least the N, accessory protein, and phosphoprotein genes (1,824 bases, positions 54 to 1,877) (GenBank accession no. U04608.1) by Sanger sequencing of overlapping conventional reverse transcription PCR products, as described previously (*1*,*3*). BoDV-1 sequences generated in this study were deposited in GenBank (accession nos. PV357162.1–8.1 and PZ000771.1–8.1). We performed phylogenetic analysis by using Geneious Prime version 2021.0.1 (Geneious, https://www.geneious.com). We calculated a neighbor-joining tree by using the Jukes-Cantor model of all 15 hedgehog-derived BoDV-1 sequences together with 258 N-X/P sequences from naturally infected animals and humans available from public databases (*1*,*9*). We used the sequence of isolate BoDV-2 No/98 (GenBank accession no. AJ311524.1) to root the tree.

Results

Diagnostic Testing, Time of Appearance, Geographic Origin, and Clinical Manifestation

Sixteen of the 49 evaluated hedgehogs from Bavaria demonstrated lymphoplasmohistiocytic meningoencephalitis. BoDV-1 RNA was detected in the brains

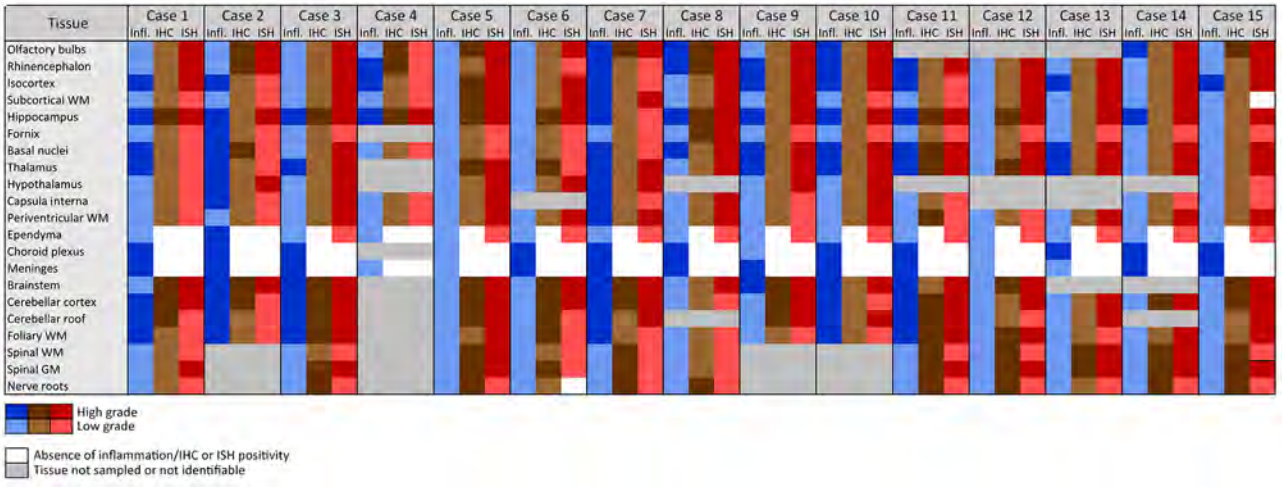

Figure 1. Inflammatory lesions and Borna disease virus 1 antigen and RNA detection in the central nervous system of infected European hedgehogs in study of the virus as cause of fatal meningoencephalomyelitis in wild hedgehogs, Germany, 2022–2025. GM, gray matter; IHC, immunohistochemistry; infl., inflammation; ISH, RNAscope in situ hybridization (Advanced Cell Diagnostics, Inc., https://acdbio.com); WM, white matter.

of 15 of those animals (Table) but not in any of the 33 nonencephalitic hedgehogs (Appendix Table 1). Differential diagnostic testing by IHC and qRT-PCR did not detect TBEV, RusV, CDV, or rabies virus in any of the encephalitis cases (data not shown).

The first BoDV-1–infected animal died in July 2022, followed by 6 BoDV-1–positive cases during May–September 2024 and 8 cases during April–July 2025 (Table). All BoDV-1–positive hedgehogs originated from the known BoDV-1–endemic area in Bavaria; they were submitted for necropsy by different hedgehog rescue centers or by private persons (Table). At necropsy, the hedgehogs weighed 400–960 g. Eight were female and 7 were male. All cases, except case 8 and case 12, had already exhibited neurologic signs by the time they were found. Clinical manifestations developed in case 8 after 15 days of care, whereas case 12 had already been in the rehabilitation center for >6 months and hibernated there before neurologic signs developing in June 2025 (Table). According to the information provided by the submitters, clinical manifestations included incoordination, gait abnormalities, seizures, apathy, spontaneous muscle twitching, impaired thermoregulation, and vestibular signs with unilateral head tilt (Appendix Table 4). As the clinical signs progressed and the animals were not responsive to the administered treatments, all hedgehogs were euthanized because of poor prognosis or died during days 1–58 of care (Table).

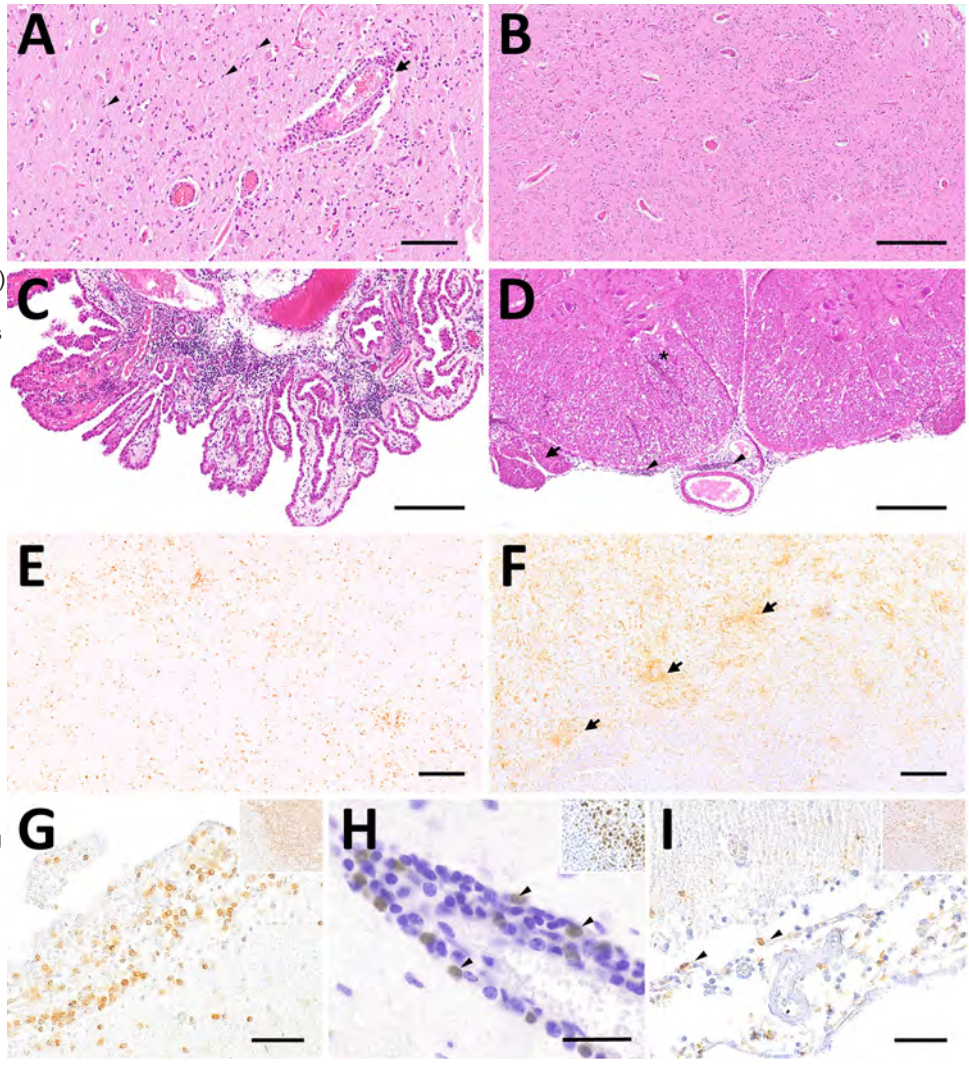

Figure 2. Representative changes and composition of immune cells in the central nervous system of Borna disease virus 1–infected hedgehogs in study of the virus as cause of fatal meningoencephalomyelitis in wild hedgehogs, Germany, 2022–2025. A) Multifocal lymphohistiocytic infiltrates with perivascular cuff formation (arrow) and microgliosis (arrowheads) from case 7. Scale bar represents 100 µm. B) Low-magnification section of brainstem from case 7 showing marked hypercellularity, with scattered lymphocytic infiltrates intermingled with astro- and microgliosis. Scale bar represents 250 µm. C, D) Infiltrates also extend into the choroid plexus in case 6 (C) and the subarachnoid space (arrowheads), nerve roots (arrow) and spinal white matter (asterisk) from case 5 (D). Scale bars represent 250 µm. E) CD3 immunohistochemistry of the corresponding brainstem region shown in Figure 1, panel B, confirms the widespread T lymphocyte infiltration, comprising the most invading immune cells. Scale bar represents 250 µm. F) The second most prominent cells involved in antiviral responses are Iba1-positive microglial cells and macrophages (arrows), as seen here in case 7. Scale bar represents 200 µm. G) Subarachnoid spaces contain numerous CD3-positive T lymphocytes in case 7. Scale bar represents 50 µm. H) Pax-5 positive B lymphocytes (arrowheads) resemble a minority of immune cells that are here seen concentrated around a blood vessel (arrowheads) from case 1. Scale bar represents 25 µm. I) Scattered Iba1-positive macrophages within subarachnoid spaces from case 7. Scale bar represents 50 µm. Insets in figures G, H, and I show the positive controls for each respective immunohistochemical staining (original magnification ×20). Stains: panels A–D, hematoxylin and eosin; E–I, 3,3′-diaminobenzidine, hematoxylin counterstain, immunohistochemistry using markers; E, CD3; F, Iba1; G, CD3; H, Pax5; I, Iba1.

Sample	Case no.														
	1*	2*	3	4	5	6	7	8	9	10	11	12	13	14	15
Brain	24.8	18.2	17.4	16.6	18.0	18.0	21.2	24.5	18.4	21.2	22.1	16.9	18.1	21.0	19.0
Spinal cord		29.3					18.1								19.8
Liver		Neg	29.0		31.2	Neg	Neg	Neg	32.6	Neg	Neg	Neg	Neg	Neg	Neg
Spleen		Neg	28.6		32.6		Neg	Neg			Neg	Neg	Neg	Neg	Neg
Kidney			26.4		35.1	Neg	Neg	Neg	33.1	Neg	Neg	Neg	Neg	Neg	Neg
Lung		Neg	30.0		25.0	Neg	Neg	Neg			Neg	Neg		32.3	Neg
Trachea		Neg													
Intestine								Neg						28.6	Neg
Adrenal gland								Neg						27.2	31.2
Salivary gland								Neg							Neg
Urinary bladder							Neg		34.7	Neg					Neg
Blood pellet									Neg	30.9		Neg	Neg	33.1	Neg
Oral swab							Neg	34.3	Neg	34.8	Neg	Neg	Neg	Neg	Neg
Rectal swab/feces							Neg	Neg	Neg	Neg	Neg	Neg	Neg	Neg	Neg
Urine								Neg	36.0	Neg	Neg	Neg	Neg	Neg	

Figure 3. Detection of Borna disease virus 1 RNA by quantitative reverse transcription PCR in hedgehogs in study of the virus as cause of fatal meningoencephalomyelitis in wild hedgehogs, Germany, 2022–2025. Samples tested were available fresh-frozen neural and extra-neural tissues and additional samples collected postmortem. Results are presented as cycle quantification values. *Only formalin-fixed paraffin-embedded brain tissue was available for cases 1 and 2. Neg, negative.

BoDV-1–Associated Lesion Patterns

No macroscopical alterations showed in the central or peripheral nervous system (PNS) of BoDV-1–infected hedgehogs. According to the histopathologic testing, the neurologic manifestations observed in all BoDV-1–positive animals included generalized angiocentric lymphoplasmohistiocytic meningoencephalitis (n = 4) or meningoencephalomyelitis (n = 11). The inflammatory infiltrates were widespread throughout all CNS regions of all 15 animals (Figure 1) and multifocally invaded the subarachnoid space, choroid plexus stromata, and neuroparenchyma (Figure 2, panels A–D). Neuronophagia and neuronal necrosis were observed in rare, scattered neurons. Moderate to marked, multifocal microglial activation and astrogliosis (highlighted by Iba-1 or GFAP staining) were most extensive in the gray matter of cerebral cortices, diencephalon, and brainstem, occasionally forming glial nodules (Figure 2, panels B, F). All cases featured mild to moderate intralesional edema.

IHC-based phenotyping of inflammatory cells revealed the affected hedgehog brains to be extensively infiltrated by CD3+ T lymphocytes, occasionally forming perivascular cuffs of up to 3–4-layer thickness (Figure 2, panels E, G), similar to other dead-end hosts, although more widespread (*28*–*30*). Inflamed zones also showed moderate numbers of Iba1-positive macrophages, activated Iba1-positive microglial cells (Figure 2, panels F, I) and GFAP-positive astrocytes, but only a few scattered and mostly perivascular Pax5-positive B cells (Figure 2, panel H). In addition, mild intraaxial vasculitic features were observed in cases 5 and 7.

The spinal cord was overall less severely affected, featuring multifocal lymphoplasmohistiocytic infiltration mostly within subarachnoid spaces (Figure 2, panel D). Of note, mild to moderate, multifocal infiltration and spongiosis of spinal white matter occurred in all animals, even in areas with spared gray matter (Figure 2, panel D). The inflammatory infiltrates also extended into adjacent nerve roots and dorsal root ganglia (Figure 1; Figure 2, panel D). Large fascicular nerves, distal, intramural ganglia and nerve branches showed minimal to no inflammation, except for mild to moderate, focally extensive, lymphocytic infiltration of the cranial mesenteric ganglia and nerves in case 3.

We did not observe intranuclear Joest-Degen inclusion bodies. We compiled information on concurrent pathologies in BoDV-1–positive hedgehogs (Appendix).

Cell Tropism and Tissue Distribution of BoDV-1 RNA and Antigen

We detected moderate to high levels of BoDV-1 RNA (Cq 16.6–24.8) in the brains of all BoDV-1–positive animals and in the spinal cord when available (Figure 3). Variable sets of fresh-frozen peripheral organs were available from 13 animals. Five animals had low to moderate BoDV-1 RNA levels (Cq 25.0–34.7) detectable in up to 4 peripheral tissue samples. Low levels of viral RNA (Cq 30.9–33.1) were also detectable in 2 of 6 blood samples collected (Figure 3). Postmortem oral swab, fecal, and urine samples were

collected from 9 animals. Very low viral RNA loads (Cq 34.3–36.0) were detectable in 2 oral swab samples and 1 urine sample (Figure 3).

IHC using the Bo18 antibody and RNAscope ISH revealed widespread cytoplasmic and nuclear positivity for the BoDV-1 N protein and genomic RNA across neurons and glial cells without consistent hot spots in the brains and spinal cords of all BoDV-1–infected animals (Figures 1, 4). We observed almost diffuse reactivity throughout the neuroparenchyma, including white matter areas. IHC and ISH results agreed with each other, except for the ependymal layer, in which only RNA was detected in 4 animals (Figure 4, panel G). Neither antigen nor RNA were detected in choroid plexus and meninges (Figure 1).

We analyzed peripheral nerves and organs by IHC. Fascicular nerve roots (dorsal and ventral), dorsal root ganglia, peripheral nerves, and distal and intramural ganglia showed positive signals (Figure 4, panel D; Figure 6, panels A–H). We observed antigen-positive peripheral nerve branches and ganglia extensively across various organs (Figure 5; Figure 6, panels A–H). We detected viral antigen in ganglion and satellite cells, axons, myelin sheath, and Schwann cells of the PNS. In addition, chromaffin cells of the adrenal medulla were multifocally to diffusely strongly positive in 5 of 8 tested cases (Figure 5; Figure 7, panel A). We observed the detection of viral antigen in nonneural cells in case 5, which exhibited a strong cytoplasmic immunopositivity in a single

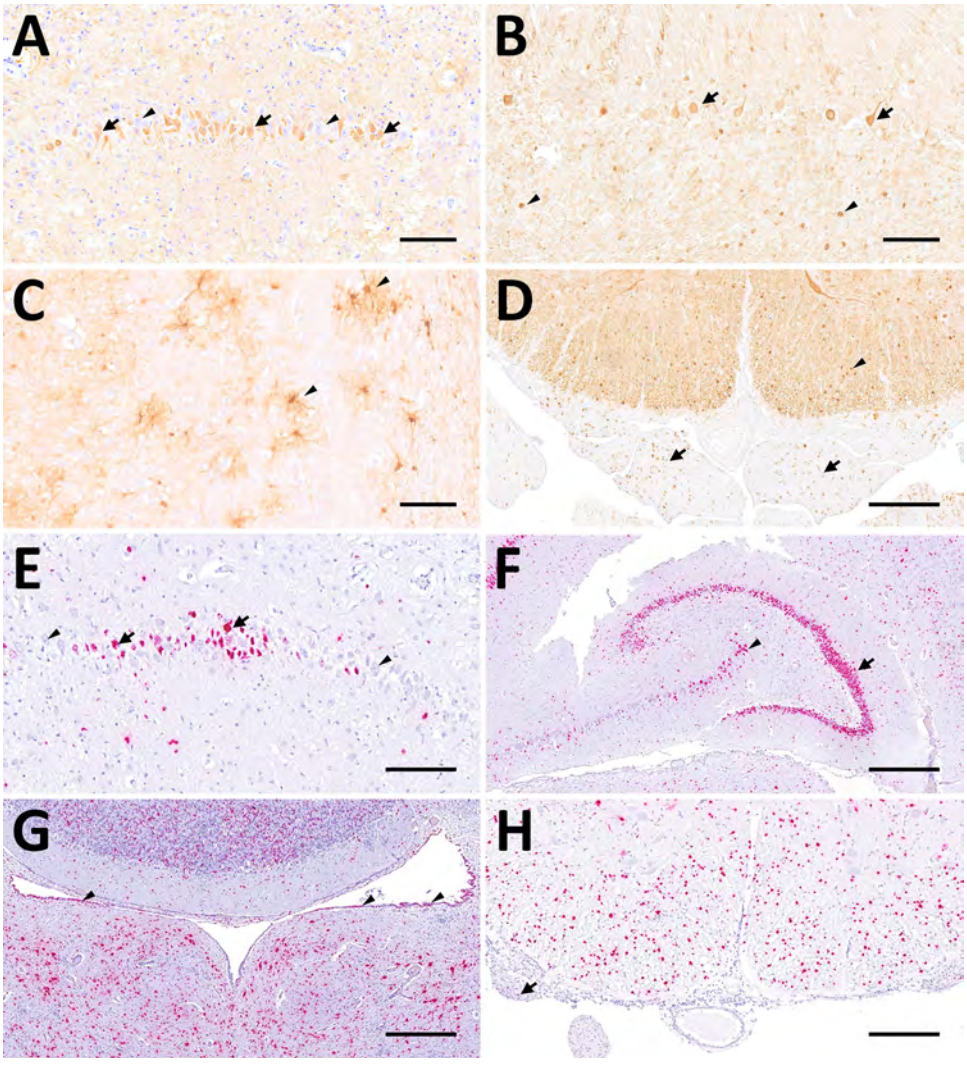

Figure 4. Distribution of Borna disease virus 1 detected within the CNS of infected hedgehogs in study of the virus as cause of fatal meningoencephalomyelitis in wild hedgehogs, Germany, 2022–2025. A–D) Antigen detected by immunohistochemistry by using Bo18 antibody. A) Multiple immunopositive neurons within the pyramidal layer of the hippocampus (arrows) mingling with negative neurons (arrowheads) from case 1. Scale bar represents 100 µm. B) Multiple immunopositive Purkinje (arrows) and few granule cells (arrowheads) within the cerebellar cortex from case 3. Scale bar represents 100 µm. C) Multiple positive astroglial cells within the spinal white matter (arrowheads) from case 6. Scale bar represents 100 µm. D) Multiple positive oligondendroglial cells within the spinal white matter (arrowhead), as well as multiple positive nerve fibers within the adjacent nerve roots (arrows) from case 5. Scale bar represents 250 µm. E–H) Virus RNA detected by RNAscope (Advanced Cell Diagnostics, Inc., https://acdbio.com) in situ hybridization (ISH). E) Numerous ISH-positive neurons (arrows) mingling with negative ones (arrowheads) within the corresponding area of the hippocampus shown in (A) from case 1. Scale bar represents 100 µm. F) Granule cells of dentate gyrus (arrow) are almost entirely ISH-positive as do multiple neurons of cornu ammonis (arrowhead) from case 5. Scale bar represents 500 µm. G) Numerous ISH-positive neurons, glial as well as ependymal cells (arrowheads) surrounding the fourth ventricle from case 7. Scale bar represents 500 µm. H) Numerous ISH- positive oligodendroglial cells within the spinal white matter and rare signals within nerve roots (arrow) from case 5. Scale bar represents 250 µm. Stains: A–I, 3,3′-diaminobenzidine with hematoxylin counterstain; E–H, 2.5 HD assay–RED with hematoxylin counterstain.

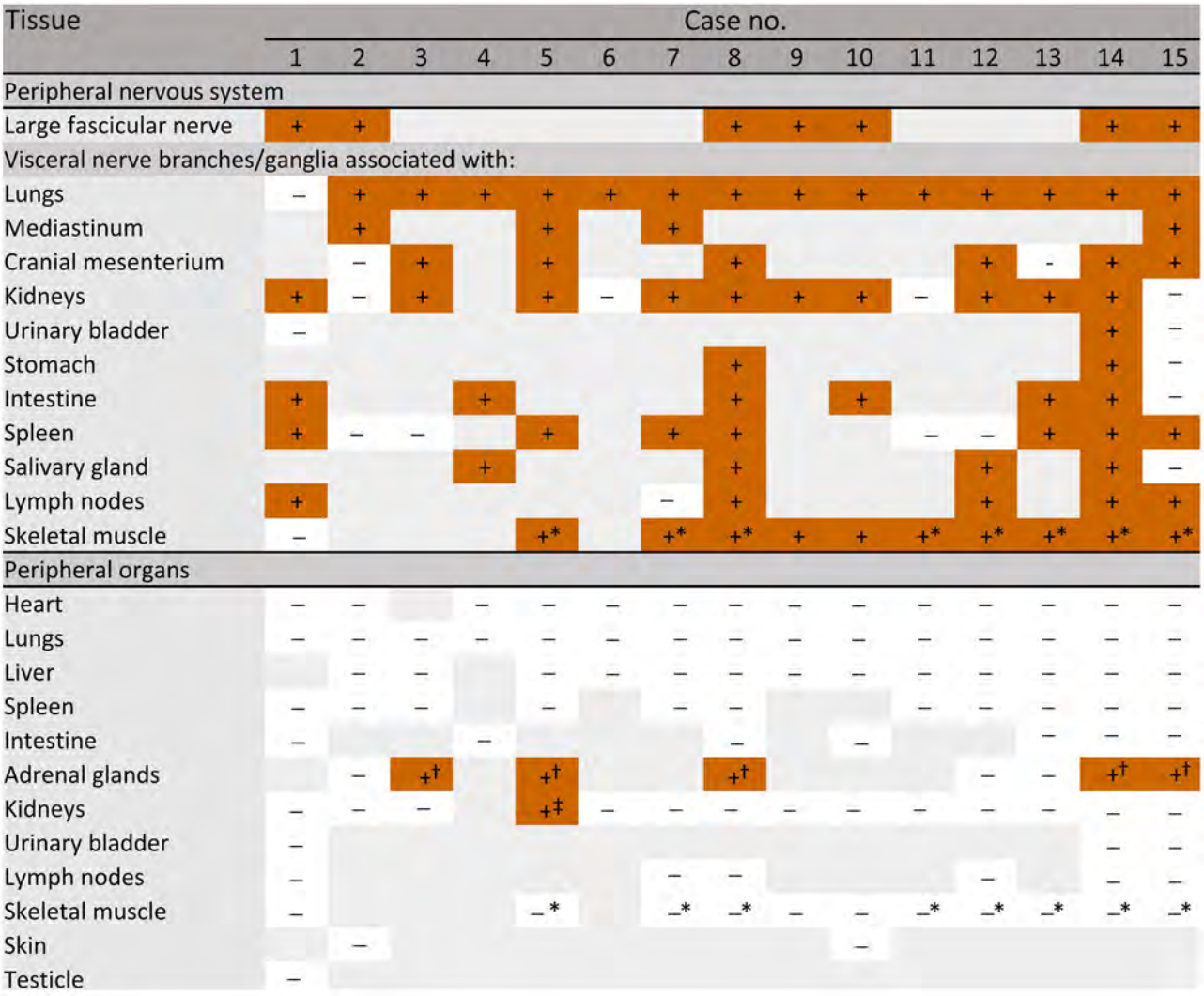

Figure 5. Borna disease virus 1 antigen detection by immunohistochemistry by using Bo18 antibody in peripheral nerves and peripheral organs of European hedgehogs in study of the virus as cause of fatal meningoencephalomyelitis in wild hedgehogs, Germany, 2022–2025. *Paravertebral musculature; †chromaffin cells; ‡1 focus of renal tubular epithelial cells. Nerve branches of organs that were not positive in any animal are not listed.

focus of renal tubular epithelial cells (Figure 5; Figure 6, panel I).

To confirm our findings, we conducted IHC by using rabbit polyclonal hyperimmune serum #201 and RNAscope ISH for various peripheral organs from case 5. Although the staining patterns were comparable for the tested peripheral nerves and the adrenal medulla (Figure 7), we could not reproduce the IHC Bo18 signal in the tubular epithelial cells of case 5 by either of the confirmatory methods (data not shown).

Phylogeographic Analysis of BoDV-1 Sequences from Hedgehogs

We determined the partial genomic sequences covering the BoDV-1 N, X, and P genes (1,824 nucleotides) for all 15 BoDV-1–positive hedgehogs. Phylogenetic analysis together with 258 BoDV-1 sequences derived from public databases (*1*,*9*) revealed the hedgehog-derived sequences belonged to the BoDV-1 sequence clusters 1A or 2, which is in agreement with their origin from Bavaria (Figure 8, panels A–C). A more detailed analysis identified the hedgehog-derived sequences as belonging to subclades 1A.SE-1 (cases 1, 3, 5; Rottal-Inn, Rosenheim, Traunstein), 1A.SE-2 (case 7, 12, 13; Rottal-Inn, Rosenheim, Traunstein), 1A.SE-3 (cases 2, 4, 6, 11; Ebersberg, Germany) (Figure 8, panels B, D), 2.MID (cases 9, 10, 14; Eichstätt, Roth, Germany), and 2.SW-1 (cases 8, 15; both Landsberg am Lech) (Figure 8, panels B, C). In all cases, sequences of the same subclade derived from infected shrews, domestic mammals, or humans were found in the same or neighboring districts as the hedgehog cases (Figure 8, panels E, F).

Discussion

Our study provides evidence of BoDV-1 infection causing meningoencephalomyelitis, radiculitis, and, in 1 case, focally extensive ganglioneuritis in wild European hedgehogs. Although BoDV-1 is known to cause fatal encephalitis in a broad range of mammalian species, well-documented cases in wild mammals are currently restricted to a single European beaver (*Castor fiber*) from 2013 (*31*). The first case of our series was detected in 2022, before 6 additional hedgehogs from the same relatively restricted area within a BoDV-1–endemic region in Bavaria, southern Germany, were submitted in 2024 within a 4-month period. In 2025, an additional 8 infected hedgehogs were submitted from a somewhat broader area in Bavaria. We cannot exclude that this temporal and regional accumulation might represent a local emergence or increase of BoDV-1 infections of hedgehogs. However, it appears possible that the initial cases raised the awareness of disease surveillance centers, leading to more frequent diagnosis of a previously underreported entity.

The relatively frequent detection of BoDV-1 in hedgehogs suggests hedgehogs might be particularly susceptible to BoDV-1 infection, possibly because of their biological relationship to shrews, the reservoir hosts of BoDV-1 that the virus is adapted to (*20*). This possibility raised the question whether infected hedgehogs might serve only as spillover dead-end hosts that develop disease without viral shedding or whether they also show broad viral tissue distribution, viral shedding, or even an asymptomatic infection, similar to BoDV-1 reservoir hosts (*11*). A similar intermediate role has been described for psittacines affected by parrot bornaviruses 1–8 (species *Orthobornavirus alphapsittaciforme* and *O. betapsittaciforme*). Affected birds suffer from neurologic disease and can transmit the virus to a broad range of other psittaciformes originating from different continents and are therefore unlikely to all represent original reservoir hosts of those viruses (*32*).

To date, neurological signs induced by a lymphoplasmohistiocytic meningoencephalitis developed in all BoDV-1–positive hedgehogs, similar to the case

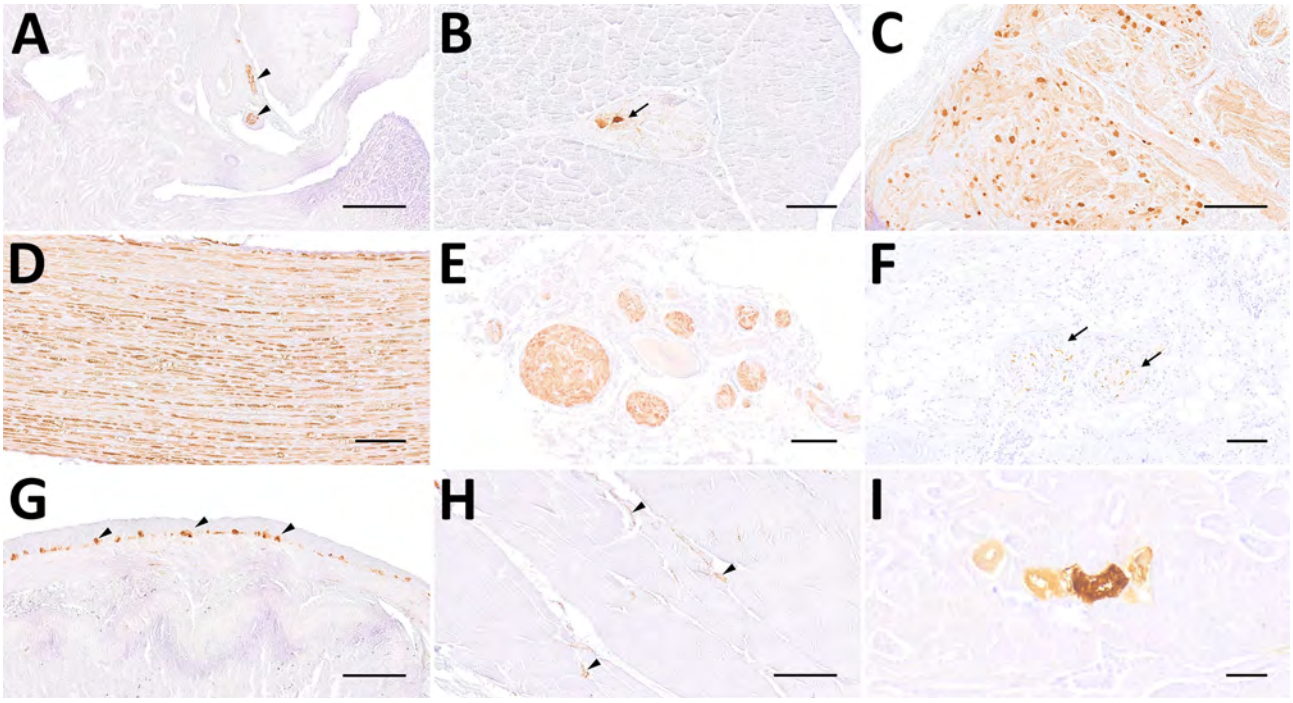

Figure 6. Distribution of virus antigen detected by immunohistochemistry using Bo18 antibody among peripheral organs and tissues of Borna disease virus 1–infected hedgehogs in study of the virus as cause of fatal meningoencephalomyelitis in wild hedgehogs, Germany, 2022–2025. A) Immunopositive nerve branches within the renal pelvis (arrowheads) from case 3. Scale bar represents 250 µm. B) Immunopositive ganglion neurons within salivary gland (arrow) from case 4. Scale bar represents 100 µm. C) Marked positivity within cranial mesenteric ganglion from case 3. Scale bar represents 250 µm. D) Diffusely immunopositive nerve fibers within a large fascicular nerve from case 1. Scale bar represents 100 µm. E) Large immunopositive visceral nerve branches within the mediastinum from case 2. Scale bar represents 200 µm. F) Pulmonary nerve branches with positive fibers (arrows) from case 7. Scale bar represents 100 µm. G) Widespread immunostaining of myenteric plexus (arrowheads) from case 4. Scale bar represents 250 µm. H) Immunopositive intramuscular nerve branches within the paravertebral musculature (arrowheads) from case 5. Scale bar represents 250 µm. I) A small group of immunopositive renal tubules from case 5. Scale bar represents 50 µm. All stains were 3,3′-diaminobenzidine with hematoxylin counterstain.

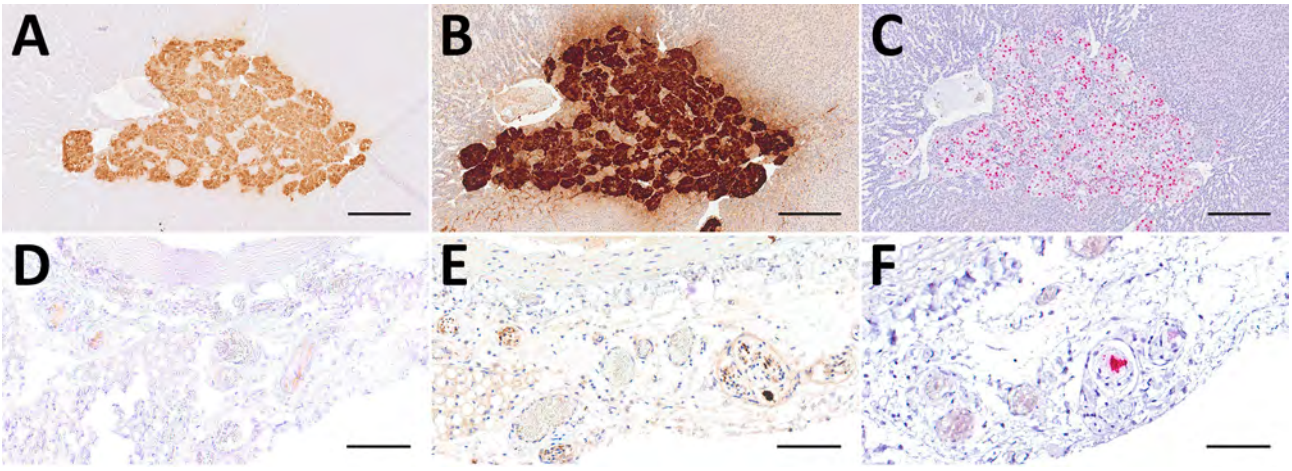

Figure 7. Comparison of 3 diagnostic methods, in the adrenal glands (A–C) and mediastinal nerve branches (D–F) of case 5, a hedgehog from Germany with Borna disease virus 1 (BoDV-1) infection, in study of the virus as cause of fatal meningoencephalomyelitis in wild hedgehogs, Germany, 2022–2025. Diffusely positive chromaffin cells and multifocal positive nerve branches are seen by immunohistochemistry by using BoDV-1 nucleoprotein mouse monoclonal antibody Bo18 (A, D), rabbit anti–BoDV-1 nucleoprotein polyclonal hyperimmune serum #201 (B, E) and RNAscope (Advanced Cell Diagnostics, Inc., https://acdbio.com) in situ hybridization (C, F). Scale bars: A–C, 250 μm; D–F, 100 μm. Stains: A, B, D, E, 3,3′-diaminobenzidine with hematoxylin counterstain; C, F, 2.5 HD assay–RED with hematoxylin counterstain.

for spillover hosts such as horses, alpacas, sheep, and humans (*28*–*30*). Because this finding might be biased by our initial case selection focusing on animals with neurologic abnormalities, we extended the study to nonencephalitic hedgehogs from endemic areas. We could not detect BoDV-1 in brains of 33 nonencephalitic hedgehogs. However, a larger survey of neurologically inconspicuous hedgehogs in BoDV-1–endemic areas is required to rule out the possibility of mild or asymptomatic BoDV-1 infections.

Of note, the BoDV-1–infected hedgehogs in our study exhibit differences from other affected species in terms of lesion and virus distribution spatial characteristics within the CNS. In horses, the most prominently affected CNS region is the hippocampal formation, followed by limbic system, basal ganglia, and brainstem (*29*,*30*). Humans seem to consistently show virus infestation hotspots in the brainstem and telencephalon or diencephalon (*28*). We did not observe the same distribution characteristics in the hedgehogs. Instead, we observed a uniform distribution of inflammatory infiltrates, virus antigen, and RNA throughout the entire CNS. Beyond neuronal infection, both IHC and ISH revealed a prominent infection of glial cells and Schwann cells, whereas viral RNA was also detected in ependymal cells of 12 animals (Figure 1). A similar cell tropism was previously described in the CNS of humans (*28*) and experimentally infected rats (*33*,*34*). In the studied hedgehogs, inflammation was mainly restricted to the CNS and spinal nerve roots, whereas only 1 animal showed ganglioneuritis of the cranial mesenteric ganglion. To our knowledge, distal ganglioneuritis is not a typical feature in naturally BoDV-1–infected horses or alpacas (*8*,*29*), but it is a hallmark of parrot bornavirus infection in parrots (*32*). Inflammation in peripheral nerves has been described for a few BoDV-1–infected human patients, whose illness manifested with Guillain-Barré–like neuropathy at early stages of infection (*5*,*28*,*35*).

Detection of BoDV-1 antigen or RNA in peripheral nerves and ganglia has been sporadically described also for alpacas and human patients as well as a BoDV-1–infected beaver (*28*,*29*,*31*). That finding has been discussed mainly as representing centrifugal virus dissemination from the brain, as experimentally shown for mice and rats (*36*,*37*). Compared with those species, BoDV-1–positive cells in the PNS were surprisingly common in the analyzed hedgehogs; we identified positive nerve fibers and ganglion cells in several organs for each of them.

In 5 animals, viral antigen was seen in chromaffin cells of the adrenal medulla, whereas in 1 animal we observed focal cytoplasmic immunopositivity in the focus of renal tubular epithelial cells. Although the cytoplasmic immunopositivity could not be confirmed by IHC by using another BoDV-1 N antibody or by RNAscope ISH, our concern is that individual BoDV-1–infected hedgehogs might shed the virus via mucosal surfaces. Unfortunately, urine, fecal, and mucosal swab samples were not available from this animal. However, we emphasize that the extent of viral presence on the epithelial surfaces of this single animal is much lower compared with infected bicolored white-

toothed shrews, in which viral antigen is usually found widespread on various epithelial surfaces (*11*). We detected BoDV-1 RNA in oral swab and urine samples of 2 hedgehogs at levels barely above the assay detection limit. We do not know if those low amounts of viral RNA represent shedding of infectious virus.

Most BoDV-1–infected hedgehogs displayed neurologic manifestations before or shortly after

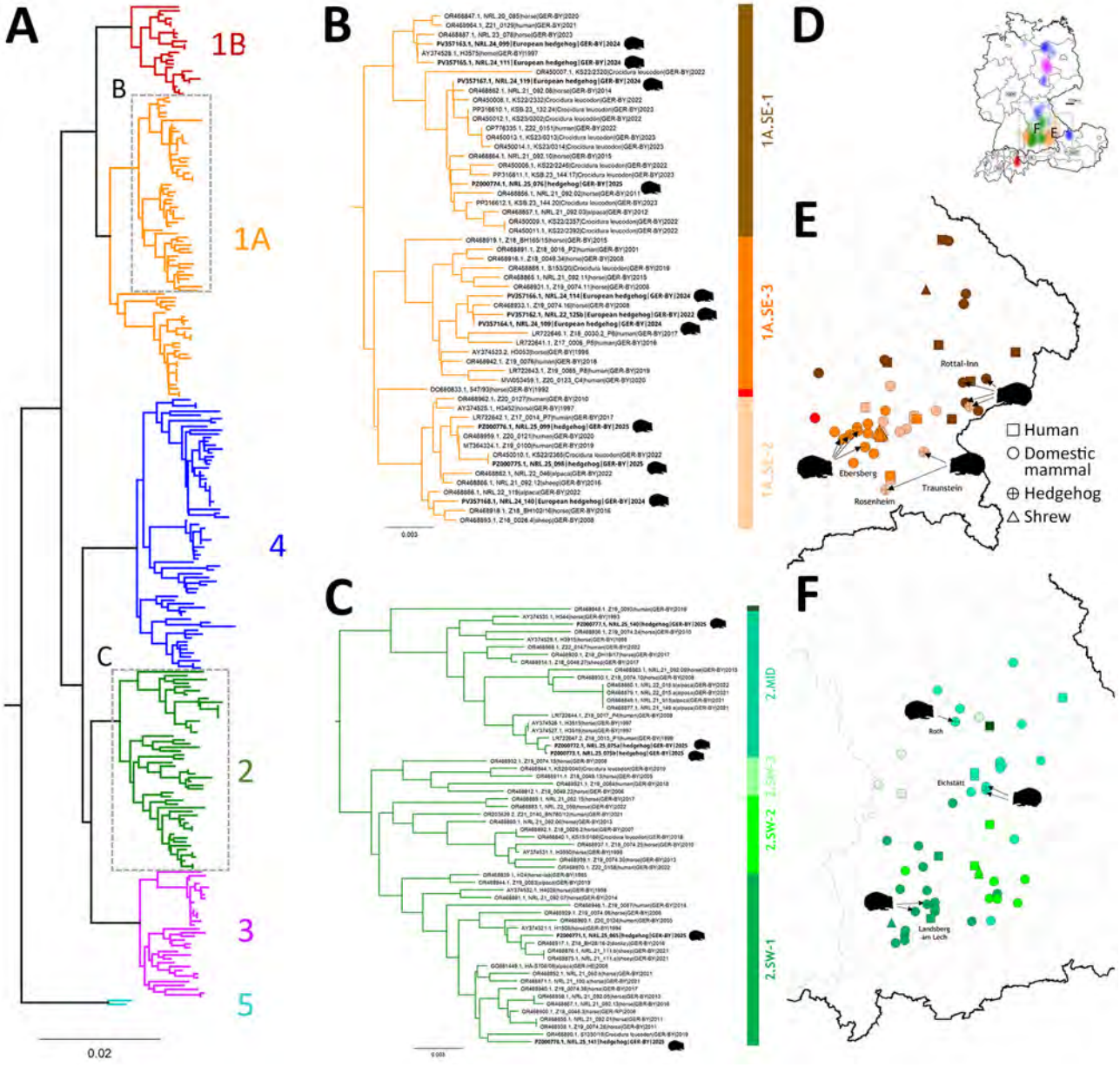

Figure 8. Phylogeographic analysis of Borna disease virus 1 (BoDV-1) infections in hedgehogs in Bavaria in study of the virus as cause of fatal meningoencephalomyelitis in wild hedgehogs, Germany, 2022–2025. A) Phylogenetic analysis of partial genomic BoDV-1 sequences (N, X, and P genes, encoding the nucleoprotein, accessory X protein, and phosphoprotein, respectively; 1,824 nucleotides, representing genome positions 54–1,877) of all 15 BoDV-1–infected hedgehogs in combination with 258 BoDV-1 sequences from naturally infected animals and humans available from public databases (*1*,*9*). Colors of tree branches represent BoDV-1 sequence clusters 1A, 1B, and 2–5. Grey boxes mark the subtrees shown in detail in panels B and C. B, C) Detailed presentation of a subtree of cluster 1A (B) and cluster 2 (C), which contain all 15 hedgehog-derived sequences (bold). Colors of vertical bars represent subclades of cluster 1A and 2 (1). D) BoDV-1-endemic area in Germany, Austria, Switzerland, and Liechtenstein, adapted from Ebinger et al. (*1*). Colors represent the phylogenetic clusters shown in panel A. Licensed under a Creative Commons Attribution 4.0 International License (https://creativecommons.org/licenses/by/4.0). E, F) Detailed phylogeographic mapping of BoDV-1 cases from the phylogenetic subtree of cluster 1A (E) as shown in panel B or cluster 2 (F) as shown in panel C, to their distribution areas in Bavaria. Colors represent the different subclades. For data protection, human cases are mapped no more precisely than to the center of the administrative district of their origin.

capture. Only case 12 had clinical signs >6 months after admission, indicating potential infection in the rescue center, given the assumed incubation period of several weeks to few months (*1*). However, it remains unknown if the hibernation-related metabolic suppression could delay the onset of this immune-mediated disease. The BoDV-1 sequences found in the 15 cases belonged to 5 different phylogenetic subclades, all reflecting the dominant virus types in the region in which each animal was found (*1*). That result argues for individual spillover events from the local shrew reservoir, rather than for a hedgehog-adapted BoDV-1 variant circulating in their populations.

In summary, we present a series of BoDV-1 cases in European hedgehogs. BoDV-1 infections might be greatly underreported in this species and wild mammals in general. It is therefore essential to consider BoDV-1 infection as a possible differential diagnosis in hedgehogs with CNS signs and encephalitic lesions in endemic regions, even if Joest-Degen inclusion bodies are not present. Despite being distant relatives of bicolored white-toothed shrews, the identified BoDV-1–infected hedgehogs showed the signature of typical spillover dead-end hosts, with fatal lymphoplasmohistiocytic encephalitis and an almost exclusively neurotropic infection. However, the broader viral presence across the PNS of hedgehogs and occasional detection of viral antigen in nonneural cells, possibly including renal epithelial cells in 1 animal, raise concerns if singular infected hedgehogs might shed virus. In such cases, the amount of excreted virus would likely be considerably lower than for regular reservoir hosts. Moreover, BoDV-1 spillover transmission to humans appears to be generally inefficient; only a few cases occur per year even in areas where the virus is endemic in the local shrew population (*1*,*9*). However, given the potentially close contact of humans and hedgehogs and the high case-fatality rate of zoonotic BoDV-1 infections, our results not only call for further investigations into the epidemiology of BoDV-1 infections in hedgehogs but also emphasize that standard hygiene measures should be implemented whenever handling hedgehogs, particularly for those with neurologic disorders.

This article was posted as a preprint at https://doi.org/10.1101/2025.07.08.663648.

Acknowledgments

We thank Sandra Aumiller, Sabine Brenner, Friedrich Faßler, Natalia Gerling, Gudrun Goldmann, Johann Gschlößl, Maximilian Hanslik, Weda Hoffmann, Lea Lenhard, Moritz Maier, Astrid Nagel, Marina Schneider, Marion Segl, Juliane Stephan, Kathrin Steffen, Philip Starcky, and Karin Stingl for their technical assistance.

This study was partially funded by the Bavarian State Ministry of Health, Care and Prevention project Zoonotic Bornavirus Focal Point Bavaria.

About the Author

Ms. Michelakaki completed her studies in veterinary medicine at the University of Thessaly in Greece and currently is a scientific assistant in the institute of veterinary pathology of Ludwig-Maximilians-Universität in Munich, Germany. Her research interests include wildlife pathology and veterinary neuropathology.

References

1. Ebinger A, Santos PD, Pfaff F, Dürrwald R, Kolodziejek J, Schlottau K, et al. Lethal Borna disease virus 1 infections of humans and animals—in-depth molecular epidemiology and phylogeography. Nat Commun. 2024;15:7908. https://doi.org/10.1038/s41467-024-52192-x
2. Malbon AJ, Dürrwald R, Kolodziejek J, Nowotny N, Kobera R, Pöhle D, et al. New World camelids are sentinels for the presence of Borna disease virus. Transbound Emerg Dis. 2022;69:451–64. https://doi.org/10.1111/tbed.14003
3. Schulze V, Große R, Fürstenau J, Forth LF, Ebinger A, Richter MT, et al. Borna disease outbreak with high mortality in an alpaca herd in a previously unreported endemic area in Germany. Transbound Emerg Dis. 2020;67:2093–107. https://doi.org/10.1111/tbed.13556
4. Vahlenkamp TW, Konrath A, Weber M, Müller H. Persistence of Borna disease virus in naturally infected sheep. J Virol. 2002;76:9735–43. https://doi.org/10.1128/JVI.76.19.9735-9743.2002
5. Schlottau K, Forth L, Angstwurm K, Höper D, Zecher D, Liesche F, et al. Fatal encephalitic Borna disease virus 1 in solid-organ transplant recipients. N Engl J Med. 2018;379:1377–9. https://doi.org/10.1056/NEJMc1803115
6. Korn K, Coras R, Bobinger T, Herzog SM, Lücking H, Stöhr R, et al. Fatal encephalitis associated with Borna disease virus 1. N Engl J Med. 2018;379:1375–7. https://doi.org/10.1056/NEJMc1800724
7. Niller HH, Angstwurm K, Rubbenstroth D, Schlottau K, Ebinger A, Giese S, et al. Zoonotic spillover infections with Borna disease virus 1 leading to fatal human encephalitis, 1999–2019: an epidemiological investigation. Lancet Infect Dis. 2020;20:467–77. https://doi.org/10.1016/S1473-3099(19)30546-8
8. Weissenböck H, Bagó Z, Kolodziejek J, Hager B, Palmetzhofer G, Dürrwald R, et al. Infections of horses and shrews with Bornaviruses in upper Austria: a novel endemic area of Borna disease. Emerg Microbes Infect. 2017;6:e52. https://doi.org/10.1038/emi.2017.36
9. Böhmer MM, Haring VC, Schmidt B, Saller FS, Coyer L, Chitimia-Dobler L, et al. One Health in action: investigation of the first detected local cluster of fatal borna disease virus 1 (BoDV-1) encephalitis, Germany 2022. J Clin Virol. 2024;171:105658. https://doi.org/10.1016/j.jcv.2024.105658
10. Rubbenstroth D, Schlottau K, Schwemmle M, Rissland J, Beer M. Human bornavirus research: back on track! PLoS Pathog.

2019;15:e1007873. https://doi.org/10.1371/journal.ppat.1007873
11. Nobach D, Bourg M, Herzog S, Lange-Herbst H, Encarnação JA, Eickmann M, et al. Shedding of infectious Borna disease virus-1 in living bicolored white-toothed shrews. PLoS One. 2015;10:e0137018. https://doi.org/10.1371/journal.pone.0137018
12. Hilbe M, Herrsche R, Kolodziejek J, Nowotny N, Zlinszky K, Ehrensperger F. Shrews as reservoir hosts of Borna disease virus. Emerg Infect Dis. 2006;12:675–7. https://doi.org/10.3201/eid1204.051418
13. Dürrwald R, Kolodziejek J, Weissenböck H, Nowotny N. The bicolored white-toothed shrew Crocidura leucodon (HERMANN 1780) is an indigenous host of mammalian Borna disease virus. PLoS One. 2014;9:e93659. https://doi.org/10.1371/journal.pone.0093659
14. Riley PY, Chomel BB. Hedgehog zoonoses. Emerg Infect Dis. 2005;11:1–5. https://doi.org/10.3201/eid1101.040752
15. Ruszkowski JJ, Hetman M, Turlewicz-Podbielska H, Pomorska-Mól M. Hedgehogs as a potential source of zoonotic pathogens—a review and an update of knowledge. Animals (Basel). 2021;11:1754. https://doi.org/10.3390/ani11061754
16. Schönbächler K, Hatt J, Silaghi C, Merz N, Fraefel C, Bachofen C. Confirmation of tick-borne encephalitis virus in a European hedgehog (*Erinaceus europaeus*) [in German]. Schweiz Arch Tierheilkd. 2019;161:23–31. https://doi.org/10.17236/sat00191
17. Faragó Z. Rabid hedgehog in inner-city area of Budapest [in Hungarian]. Orv Hetil. 1997;138:2231–2.
18. Duque-Valencia J, Sarute N, Olarte-Castillo XA, Ruíz-Sáenz J. Evolution and interspecies transmission of canine distemper virus—an outlook of the diverse evolutionary landscapes of a multi-host virus. Viruses. 2019;11:582. https://doi.org/10.3390/v11070582
19. Matiasek K, Pfaff F, Weissenböck H, Wylezich C, Kolodziejek J, Tengstrand S, et al. Mystery of fatal 'staggering disease' unravelled: novel rustrela virus causes severe meningoencephalomyelitis in domestic cats. Nat Commun. 2023;14:624. https://doi.org/10.1038/s41467-023-36204-w
20. Douady CJ, Chatelier PI, Madsen O, de Jong WW, Catzeflis F, Springer MS, et al. Molecular phylogenetic evidence confirming the Eulipotyphla concept and in support of hedgehogs as the sister group to shrews. Mol Phylogenet Evol. 2002;25:200–9. https://doi.org/10.1016/S1055-7903(02)00232-4
21. Steininger P, Ensser A, Knöll A, Korn K. Results of tick-borne encephalitis virus (TBEV) diagnostics in an endemic area in southern Germany, 2007 to 2022. Viruses. 2023;15:2357. https://doi.org/10.3390/v15122357
22. Thilén E, Rubbenstroth D, Tengstrand S, Pfaff F, Wensman JJ, Ley C. Evidence of rustrela virus-associated feline staggering disease in Sweden since the 1970s. Acta Vet Scand. 2024;66:59. https://doi.org/10.1186/s13028-024-00783-5
23. Li Z, Feng Z, Ye H. Rabies viral antigen in human tongues and salivary glands. J Trop Med Hyg. 1995;98:330–2.
24. Haines DM, Martin KM, Chelack BJ, Sargent RA, Outerbridge CA, Clark EG. Immunohistochemical detection of canine distemper virus in haired skin, nasal mucosa, and footpad epithelium: a method for antemortem diagnosis of infection. J Vet Diagn Invest. 1999;11:396–9. https://doi.org/10.1177/104063879901100502
25. Haas B, Becht H, Rott R. Purification and properties of an intranuclear virus-specific antigen from tissue infected with Borna disease virus. J Gen Virol. 1986;67:235–41. https://doi.org/10.1099/0022-1317-67-2-235
26. Wang F, Flanagan J, Su N, Wang L-C, Bui S, Nielson A, et al. RNAscope: a novel in situ RNA analysis platform for formalin-fixed, paraffin-embedded tissues. J Mol Diagn. 2012;14:22–9. https://doi.org/10.1016/j.jmoldx.2011.08.002
27. Garman RH. Histology of the central nervous system. Toxicol Pathol. 2011;39:22–35. https://doi.org/10.1177/0192623310389621
28. Liesche F, Ruf V, Zoubaa S, Kaletka G, Rosati M, Rubbenstroth D, et al. The neuropathology of fatal encephalomyelitis in human Borna virus infection. Acta Neuropathol. 2019;138:653–65. https://doi.org/10.1007/s00401-019-02047-3
29. Fürstenau J, Richter MT, Erickson NA, Große R, Müller KE, Nobach D, et al. Borna disease virus 1 infection in alpacas: comparison of pathological lesions and viral distribution to other dead-end hosts. Vet Pathol. 2024;61:62–73. https://doi.org/10.1177/03009858231185107
30. Bilzer T, Planz O, Lipkin WI, Stitz L. Presence of CD4+ and CD8+ T cells and expression of MHC class I and MHC class II antigen in horses with Borna disease virus-induced encephalitis. Brain Pathol. 1995;5:223–30. https://doi.org/10.1111/j.1750-3639.1995.tb00598.x
31. Ellenberger C, Heenemann K, Vahlenkamp TW, Grothmann P, Herden C, Heinrich A. Borna disease in an adult free-ranging Eurasian beaver (Castor fiber albicus). J Comp Pathol. 2024;209:31–5. https://doi.org/10.1016/j.jcpa.2024.01.003
32. Rubbenstroth D. Avian Bornavirus research—a comprehensive review. Viruses. 2022;14:1513. https://doi.org/10.3390/v14071513
33. Carbone KM, Moench TR, Lipkin WI. Borna disease virus replicates in astrocytes, Schwann cells and ependymal cells in persistently infected rats: location of viral genomic and messenger RNAs by in situ hybridization. J Neuropathol Exp Neurol. 1991;50:205–14. https://doi.org/10.1097/00005072-199105000-00003
34. Werner-Keišs N, Garten W, Richt JA, Porombka D, Algermissen D, Herzog S, et al. Restricted expression of Borna disease virus glycoprotein in brains of experimentally infected Lewis rats. Neuropathol Appl Neurobiol. 2008; 34:590–602. https://doi.org/10.1111/j.1365-2990.2008.00940.x
35. Coras R, Korn K, Kuerten S, Huttner HB, Ensser A. Severe bornavirus-encephalitis presenting as Guillain-Barré-syndrome. Acta Neuropathol. 2019;137:1017–9. https://doi.org/10.1007/s00401-019-02005-z
36. Shankar V, Kao M, Hamir AN, Sheng H, Koprowski H, Dietzschold B. Kinetics of virus spread and changes in levels of several cytokine mRNAs in the brain after intranasal infection of rats with Borna disease virus. J Virol. 1992; 66:992–8. https://doi.org/10.1128/jvi.66.2.992-998.1992
37. Enbergs HK, Vahlenkamp TW, Kipar A, Müller H; Haimo K Enbergs, Thomas W Vahlenkam. Experimental infection of mice with Borna disease virus (BDV): replication and distribution of the virus after intracerebral infection. J Neurovirol. 2001;7:272–7. https://doi.org/10.1080/13550280152403317

Address for correspondence: Dennis Rubbenstroth, Institute of Diagnostic Virology, Friedrich-Loeffler-Institut, Südufer 10, 17493 Greifswald–Insel Riems, Germany; email: dennis.Rubbenstroth@fli.de

Three Fatal Gestational Psittacosis Cases Caused by *Chlamydia psittaci* Strains Belonging to Closely Related Lineages, Japan

Atsuko Nishino, Yukiko Nakura, Yukiko Sassa-O'Brien, Momoko Soeda, Hirokazu Sugii, Kanako Shimizu, Shiro Miura, Yumiko Sato, Michinobu Yoshimura,[1] Michiko Kodama, Itaru Yanagihara

Gestational psittacosis is a rare infectious disease caused by *Chlamydia psittaci* that causes high maternal and fetal mortality rates. In Japan, gestational psittacosis has been reported in 7 patients, including 4 maternal deaths without antemortem diagnosis. We molecularly diagnosed *C. psittaci* infection postmortem in 3 patients treated during 2017–2024. We extracted DNA from formalin-fixed paraffin-embedded placenta, lung, and spleen tissues. Analysis of multilocus sequence typing indicated sequence type (ST) 269 in 1 patient and ST335 in 2; all 3 were closely related lineages that have not been previously reported in Japan or in animals. However, the *ompA* gene showed distinct clusters in the phylogenetic analysis. Quantitative PCR and immunostaining revealed higher amounts of *C. psittaci* detected in placenta than in lung or spleen, suggesting that proliferation of *C. psittaci* in the placenta might cause severe symptoms. ST335/ST269 lineage could be highly virulent strains for pregnant women.

Gestational psittacosis is a rare infectious disease caused by *Chlamydia psittaci* and is associated with high maternal and fetal mortality rates (*1*). *C. psittaci* is an obligate intracellular gram-negative bacterium that has been reported to cause 1%–2% of community-acquired pneumonia among hospitalized patients annually (*2*). The mortality rate for psittacosis when including nonpregnant periods is <1% with proper treatment. During pregnancy, the maternal immune system accepts the semiallograft fetus by controlling T helper (Th) 1/Th2 balance, T regulatory (Treg) cell activity, and Th9 to achieve immunologic tolerance (*3*). However, that immunotolerant status might reduce the protective nature against intracellular invasive bacteria, such as *Listeria monocytogenes*, *Coxiella burnetii*, and *Chlamydia* spp., resulting in adverse outcomes (*4*). Although fetal cases of gestational psittacosis have been reported less frequently than fetal pneumonia cases, gestational psittacosis poses a threat to life; rates of intrauterine fetal mortality (82.6%, 19/23) and maternal mortality (8.7%, 2/23) are high (*5*). Given that the maternal mortality rate is reported to be ≈9 times higher than the overall case fatality rate of psittacosis, rapid diagnosis and emergency medical care are necessary.

Psittacosis in humans is a notifiable disease in Japan; 5–11 cases were reported annually in recent years (*6*). Birds, particularly species in the families Cacatuidae and Columbidae, are considered the primary source of infection (*7*). Among the reported cases of human psittacosis in Japan during 2007–2016, the suspected source of infection was identified as birds in 79% of cases and unknown or unreported exposure histories in the remaining 21% of cases; the identified birds were from the order Psittaciformes (parakeets/parrots) in 53%, doves or pigeons in 35%, and other avian species in 12% of cases (*6*). In Japan, the recent prevalence of *C. psittaci* is <1% among pet birds but remains unclear among wild birds, although detection in pigeons and feral parrots has been reported (*6*,*8*–*10*). Reports on infections from wild birds,

Author affiliations: Research Institute, Osaka Women's and Children's Hospital, Osaka, Japan (A. Nishino, Y. Nakura, M. Yoshimura, I. Yanagihara); The University of Osaka, Osaka (A. Nishino, M. Kodama, I. Yanagihara); Tokyo University of Agriculture and Technology, Tokyo, Japan (Y. Sassa-O'Brien); NHO Nagasaki Medical Center, Nagasaki, Japan (M. Soeda, S. Miura); NHO Iwakuni Clinical Center, Yamaguchi, Japan (H. Sugii, Y. Sato); Tannan Health Welfare Center, Fukui, Japan (K. Shimizu); Maizuru Kyosai Hospital, Kyoto, Japan (K. Shimizu)

DOI: https://doi.org/10.3201/eid3205.252008

[1]Current affiliation: Fukuoka University, Fukuoka, Japan.

particularly outbreaks in Europe during 2023–2024, further illustrate that wild birds can serve as sources of infection (*11*–*13*). Although birds remain the primary source of human psittacosis, transmission between humans or through other mammals, such as horses and Siberian elk (*Alces alces cameloides*), have also been reported (*14*–*16*). This diversity of potential infection routes complicates epidemiologic investigations, and the wide range of hosts has made identifying the infection route more complicated.

In Japan, we have diagnosed 3 fatal gestational psittacosis cases among maternal deaths of unknown etiology during 2017–2024. In this study, we aimed to obtain epidemiologic information on those 3 cases by phylogenetic analysis of chlamydial marker *ompA* and by performing multilocus sequence typing (MLST), a valuable tool for estimating the source of infection with bacteria of the order Chlamydiales. In addition, we evaluated the distribution of *C. psittaci* in placentas, maternal spleens, and maternal lungs using quantitative real-time PCR (qPCR) analyses and immunofluorescent staining to investigate the pathogenesis of gestational psittacosis.

Materials and Methods

Samples and DNA Extraction

In cooperation with the Japan Maternal Death Exploratory Committee of the Japan Association of Obstetricians and Gynecologists, we evaluated 3 cases (FO-01 [*17*,*18*], YO-02 [*19*,*20*], and NO-03) of maternal and fetal death of unknown etiology for which autopsies were performed at different locations within Japan during 2017–2024. Formalin-fixed paraffin-embedded (FFPE) tissue samples were sent to our laboratory, and we extracted DNA from the placenta, maternal lungs, and maternal spleen using Maxwell RSC DNA FFPE Kit (Promega, https://www.promega.com) according to the manufacturer's instructions.

Molecular Diagnosis of Gestational Psittacosis

We performed PCR to detect chlamydial ribosomal DNA. For initial screening, we performed real-time PCR using the primer pair CPSI_F/CPSI_R, which amplifies the region spanning the 3′-region to the intergenic spacer region of 16S-23S rRNA gene, specific to *C. psittaci* and *C. abortus* (*21*). We prepared a 10-μL reaction mixture containing 5 μL of PowerUp SYBR Green Master Mix (Thermo Fisher Scientific, https://www.thermofisher.com), 0.5 μM of each primer, 3 μL of double-distilled water, and 1 μL of DNA template. The cycle conditions were 40 cycles at 95°C for 15 seconds, then annealing at 55°C for 15 seconds and 72°C for 1 minute. Next, we performed 16S rRNA gene PCR under the same conditions using the primers C.p.16S 45F/C.p.16S 320R and C.p.16S 1172F/C.p.16S 1370R to distinguish among *C. psittaci*, *C. abortus*, and *C. buteonis*. We used the primer pair C.p.16S 45F/C.p.16S 320R to amplify 276 bp 5′-region of 16S rRNA gene and used the primer pair C.p.16S 1172F/C.p.16S 1370R to amplify the 199-bp 3′ region of 16S rRNA gene. We retrieved 16S rRNA gene sequences of *C. psittaci*, *C. abortus*, and *C. buteonis* from the National Center for Biotechnology Information RefSeq database (https://www.ncbi.nlm.nih.gov/refseq). The alignments revealed 5 nucleotide polymorphisms among *C. psittaci*, *C. abortus*, and *C. buteonis*. Among the 5 nucleotide differences identified in the 16S rRNA gene, we selected the regions encompassing 4 of those polymorphic sites as the target for PCR amplification. We purified the PCR amplicons using NucleoSpin Gel and PCR Clean-up (MACHEREY-NAGEL, https://www.mn-net.com) after gel electrophoresis; subjected them to Sanger sequencing using Big Dye Terminator 3.1 kit on an SeqStudio Genetic Analyzer (Thermo Fisher Scientific); and compared them with reference sequences by using BLASTn (https://blast.ncbi.nlm.nih.gov).

Multilocus Sequence Typing

We performed PCR of 7 housekeeping genes (*enoA*, *fumC*, *gatA*, *gidA*, *hemN*, *hflX*, and *oppA_3*) using DNA extracted from the placenta, as previously described, and the reported primer sets (Table 1). The gene *hemN* could not be amplified with the previously reported primer sets YPhemN1 and YPhemN2; therefore, we prepared new primers designated as hemN-F2 and hemN-R2. For each sample, we prepared a 15-μL reaction mix by combining 1 μL of sample template, 0.075 μL of TaKaRa Ex Taq, 1.5 μL of 10x Ex Taq Buffer (Mg^{2+} plus), 1.2 μL of deoxyribonucleotide triphosphate mixture (TaKaRa Bio, https://www.takarabio.com), and 1.0 μL of each primer (10-μM stock). The cycle conditions were 35 cycles at 98°C for 10 seconds, 55°C for 30 seconds, and 72°C for 45 seconds. Subsequently, we purified and analyzed the PCR products as described previously. We concatenated the MLST alleles and determined the sequence type (ST) using the PubMLST Chlamydiales database (http://pubmlst.org/chlamydiales). We visualized MLST phylogenetic relationships among *C. psittaci* using GrapeTree, an interactive tool in EnteroBase (https://enterobase.warwick.ac.uk) for visualizing phylogenetic trees. The tool reconstructs and displays complex minimum spanning trees and integrates detailed metadata to enable epidemiologic interpretation (*24*).

Table 1. Primers and probes used for diagnosing *Chlamydia psittaci* and MLST in study of 3 fatal gestational psittacosis cases caused by *C. psittaci* strains belonging to closely related MLST lineages, Japan, 2017–2024*

Method	Target gene	Primer or probe	Sequence, 5′→3′	Amplicon size, bp	Reference
Real-time PCR	16S–23S rRNA operon	CPSI_F	AAGGAGAGAGGCGCCCAA	133	(*21*)
		CPSI_R	CAACCTAGTCAAACCGTCCTAA		
C. psittaci PCR	16S rRNA	C.p.16S 45F	TGGATGAGGCATGCAAGTCG	276	This study
		C.p.16S 320R	TGGCGGTCAATCTCTCAATC		
		C.p.16S 1172F	GGGTTAACCAGGAGGAAGGC	199	This study
		C.p.16S 1370R	AGCTGACACGCCATTACTAGC		
MLST PCR	*enoA*	YPenoA3	CCTATGATGAATCTCATTAATGG	428	(*22*); this study†
		YPenoA4	CCCAACCATCAAAATCTTCTTCCG		
	fumC	YPfumC1	GGGCTCCTGAGGTTATGCC	649	
		YPfumC2	CGCAAATAATGAATCACCTTATC		
	gatA	YPgatA3	GCCTTAGAGTTAAGAAATGCCG	509	
		YPgatA4	CCCCCTGTATCGGAACCTAACGC		
	gidA	YPgidA1	GCTTATTAGAGAGCTGTCCTGGC	693	
		YPgidA2	CGCGTTTTCTAACCCACGG		
	hemN	YPhemN1	GGATCCATTTCGGAGGAGGC	398	
		hemN-R2†	TAAGCGGTCAGGCCGCATGTG		
		hemN-F2†	GTCAAAGTCATGAAGAGTCAC	505	
		YPhemN2	CCTGAAAGGATTTTCTCATGG		
	hflX	YPhflX3	GAGATTTTTGCTAATCGAGCG	530	
		YPhflX4	GTAAAACATCTTCATGTAACGC		
	oppA	YPoppA3	ATGCGCAAGATATCAATGGG	500–610	
		YPoppA4	GGCAAGGTTTGGTGTAACTCGC		
PCR	*ompA*	CPsittGenoFor	GCTACGGGTTCCGCTCT	FO-01: 625; YO-02: 631; NO-03: 622	(*23*); this study†
		Cp ompA R3 †	CAATYTTAGGATTAGATTGAGC		
		Cp ompA F3 †	TGGGATCGCTYCGAYATTTTC	FO-01: 495; YO-02: 508; NO-03: 498	
		Cp ompA R4 †	TGCTCTTGACCAGTTTACGCC		
		Cp ompA F4 †	TATGGGAATGTGGTTGTGCAA	FO-01: 452; YO-02: 452; NO-03: 451	
		CPsittGenoRev	TTTGTTGATYTGAATCGAAGC		

*MLST, multilocus sequence typing.

We concatenated nucleotide sequences of 7 housekeeping genes for each strain among these 3 cases (FO-01, YO-02, and NO-03) and other strains (6BC, Mat116, and NJ1; GenBank accession nos. CP002586, CP002744, and CP003798), aligned them using MAFFT version 7 (*25*), and extracted single-nucleotide polymorphisms (SNPs) from the alignments using SNP-sites (*26*), then calculated the pairwise SNP distances using SNP-dists version 1.2.0 (https://github.com/tseemann/snp-dists). We visualized the resulting SNP distance matrix as a heatmap using the tidyverse version 2.0.0 and pheatmap version 1.0.13 packages in R version 4.5.1 (The R Project for Statistical Computing, https://www.r-project.org).

Phylogenetic Analysis of the *ompA* Gene and OmpA Protein

We performed PCR of the *ompA* gene using placental DNA with the primers (Table 1). The *ompA* gene could not be amplified with the previously reported primer sets CPsittGenoFor and CPsittGenoRev; therefore, we designed new primers and obtained overlapping sequences. We performed both nucleotide and amino acid sequence analyses using sequences obtained from BLAST searches. We aligned nucleotide sequences with the representative *ompA* genotype sequence (*27*), converted nucleotide sequences to amino acid sequences, aligned them using MAFFT version 7 (*25*), trimmed for alignment optimization using trimAl and ClipKIT (*28*,*29*), and phylogenetically analyzed them with IQ-TREE version 3 (T.K.F. Wong et al., unpub. data, https://ecoevorxiv.org/repository/view/8916), including visualization using iTOL versin 7 (*30*).

Quantitative Analyses

We performed qPCR targeting the 16S rRNA gene sequence of Chlamydiales using the primers CPSI_F and CPSI_R under previously described conditions. We performed relative quantification (RQ) using the $2^{-\Delta\Delta Ct}$ method, normalizing chlamydial DNA levels to β actin as internal control and calculating the relative fold change in the placenta and spleen compared with the lungs.

Hematoxylin and Eosin and Immunofluorescence Staining

We examined hematoxylin and eosin–stained tissue sections under an Eclipse Ti microscope equipped with a DS-Fi3 camera (both Nikon, https://www.nikon.com). Using serial sections, we performed antigen retrieval with Dako Target Retrieval Solution, Citrate pH 6 (Agilent Technologies, https://www.agilent.com), and blocked the sections with 5% bovine

serum albumin for 1 hour at room temperature. We stained the slides with a rabbit polyclonal (1:1,000) antibody raised against *C. psittaci* BC6 strain diluted with 1% bovine serum albumin (*10*). We used the anti-rabbit Alexa Fluor 488 (Thermo Fisher Scientific) as a secondary antibody and stained the nucleus with 4′,6-diamidino-2-phenylindole (Roche, https://www.roche.com). For immunofluorescence microscopy, we used a GFP/DAPI (green fluorescent protein/4′,6-diamidino-2-phenylindole) filter set (Chroma Technology Corp., https://www.chroma.com).

Statistical Analyses

We analyzed data using JMP 18 statistical analysis software (JMP Statistical Discovery LLC, https://www.jmp.com) or Igor Pro 9.05 software (WaveMetrics, https://www.wavemetrics.com). We evaluated significant differences in the RQ of qPCR among tissues using 1-way analysis of variance, followed by pairwise comparison using Tukey–Kramer's honest significant difference test. We considered a p value of <0.05 to be statistically significant.

Nucleotide Sequence Accession Numbers and pubMLST Identification Numbers

The nucleotide sequences obtained in this study have been deposited in DDBJ/EMBL/GenBank under accession numbers LC900811 and LC900812 (FO-01), LC900813 and LC900814 (YO-02), and LC900815 and LC900816 (NO-03) for the partial 16S rRNA gene; LC921559–65 (FO-01), LC888489–95 (YO-02), and LC888482–8 (NO-03) for housekeeping genes using for MLST analysis; and LC486816 (FO-01, protein identification [ID] BBL33230), LC923014 (YO-02), and LC923015 (NO-03) for the partial *ompA* gene. The pubMLST isolate ID numbers are 4431, 5398, and 5399.

Ethics Approval

Autopsy procedures were conducted with the informed consent of the families. This study was approved by the institutional review board and ethics committee of the Osaka Women's and Children's Hospital (no. 999, 999-2).

Results

Clinical Characteristics and Diagnosis of *C. psittaci*

The 3 cases FO-01, YO-02, and NO-03 occurred in different coastal cities in Japan in 2017, 2022, and 2024. In the case of FO-01, a 26-year-old pregnant woman demonstrated fever at 23 weeks and 4 days of gestation; vomiting began at 23 weeks and 6 days. In the case of YO-02, a 28-year-old pregnant woman demonstrated fever at 25 weeks and 5 days of gestation, and muscle pain also began at 26 weeks and 0 days. In the case of NO-03, a 32-year-old pregnant woman showed fever at 37 weeks and 2 days of gestation. The intervals from onset to death were 4 days in the case of FO-01, 4 days in the case of YO-02, and only 2 days in the case of NO-03. All 3 patients had fever and nonspecific symptoms, without respiratory complaints such as cough or sore throat (Table 2). At the initial visit, only mild elevations in leukocyte count and C-reactive protein were noted. Subsequently, septic shock developed in all 3 women. Laboratory tests revealed coagulation abnormalities, hepatic dysfunction, and renal impairment. Intrauterine fetal death was confirmed, and early termination was considered. However, because of the maternal poor systemic condition and coagulopathy, cesarean section could not be performed. Maternal death occurred before delivery of the fetus and placenta. On autopsy, although no infectious changes were observed in the lung, hemophagocytosis was noted in the spleen, consistent with hemophagocytic syndrome in all 3 cases.

In cases FO-01, YO-02, and NO-03, real-time PCR with primers CPSI_F and CPSI_R yielded positive results across all tissues. Pairwise comparison of the partial 16S rRNA gene sequences showed high similarity among the 3 isolates; percentage identities were 100.0% (FO-01-YO-02) and 99.8% (FO-01-NO-03 and YO-02-NO-03) as determined by BLAST analysis. Isolates LC900811 and LC900812 (FO-01) showed a 99.64% and 100% similarity to the 16S rRNA gene sequence of multiple *C. psittaci* strains, LC900813 and LC900814 (YO-02) showed a 99.64% and 100% similarity, and LC900815 and LC900816 (NO-03) showed a 100% and 100% similarity. On the basis of those results, *C. psittaci* infection was diagnosed in the patients.

MLST Analyses

MLST analyses revealed that FO-01 belonged to ST269 and YO-02 and NO-03 belonged to ST335 (Table 3). According to the MLST phylogenetic analysis, ST335 and ST269 were closely related; ST335 was considered a derived ST from ST269, STs of which had not been previously reported in Japan or in animals. ST335 and ST269 showed c. 414C>T (p. Gly138 = , synonymous) and c. 515C>T (p. Pro172Leu, nonsynonymous) in *gidA* and c. 558G>A (p. Gly186 = , synonymous) in *hflX*. Phylogenetically, ST269/ST335 are distinct from the lineages, including ST208, which was previously reported in Japan and caused outbreaks in animals and humans at animal

Table 2. Clinical findings in 7 cases of gestational psittacosis reported in Japan during 2000–2024*

Case identification	Year	Maternal age	Gestational age at onset	Parity	Symptoms	Antibiotics administered	Maternal death	Fetal death	Reference
1	2000	Not reported	35 wks 3 d	Not reported	Fever, cough	CLR, MNO	N	N	(*31*)
2 (FO-01)	2017	26	23 wks 4 d	0	Fever, vomiting	None	Y	Y	(*17*,*18*); this study
3	2017	31	17 wks 1 d	0	Fever, malaise, headache, muscle pain	MEM	Y	Y	(*5*)
4	2021	31	15 wks 3 d	3	Fever, cough, headache	MEM, CSL, MTR, AZM	N	Y	(*32*)
5	2022	24	25 wks 2 d	0	Fever, malaise	TCY	N	N	(*33*)
6 (YO-02)	2022	28	25 wks 5 d	1	Fever, muscle pain	MEM	Y	Y	(*19*,*20*); this study
7 (NO-03)	2024	32	37 wks 2 d	2	Fever	Not reported	Y	Y	This study

*AZM, azithromycin; CLR, clarithromycin; CSL, cefoperazone/sulbactam; MEM, meropenem; MNO, minocycline; MTR, metronidazole; TCY, tetracycline.

exhibition facilities, and ST35, which has been detected in asymptomatic feral parrots introduced to regions outside their native range (Figure 1). To date, ST269/ST335 occurrence has been limited to human patients; ST335 was isolated from bronchoalveolar lavage fluid of a male patient with pneumonia in China, then in the patients with gestational psittacosis in this study (*34*).

The heatmap based on the SNP distances of 7 housekeeping genes also revealed that FO-01, YO-02, and NO-03 were closely related: there were 0 SNPs between YO-02 and NO-03, and FO-01 differed by 4 SNPs from both YO-02 and NO-03. Not only 6BC and NJ1 but also Mat 116, which was isolated in Japan, differed by 16–27 SNPs from FO-01, YO-02, and NO-03 (Figure 2).

Phylogenetic Analysis Using the *ompA* Gene and OmpA Protein

Phylogenetic analyses of the OmpA protein revealed that FO-01, YO-02, and NO-03 belonged to a different cluster, and sequence variations existed in the hypervariable region (Figure 3, panel A). FO-01 corresponded to protein ID BBL33230 and was the closest to genotype D. YO-02 was clustered in genotype 1V, and NO-03 was clustered in genotype YP84, which was isolated from a king parakeet in Japan (Figure 3, panel B).

Chlamydial DNA Levels in the Placenta

In all 3 patients, qPCR indicated higher amounts of chlamydial DNA in the placenta than in the lungs and spleen (Figure 4). One-way analysis of variance revealed a significant difference in the RQ values of chlamydial DNA among tissues from the 3 female patients (case 1g $F(2,6) = 23.8$, $p<0.01$; case 2, $F(2,6) = 41.7$, $p<0.001$; case 3, $F(2,6) = 32.0$, $p<0.001$). Posthoc analysis using Tukey-Kramer's honest significant difference test indicated significant differences of the placenta with the spleen and lungs ($p<0.01$), with ≈20- to 100-fold changes.

C. psittaci Infection in Placenta

Hematoxylin and eosin staining showed marked intervillositis in the placenta, with pronounced inflammatory changes compared with the changes seen in the lung and spleen. Immunofluorescence staining revealed higher signals in placenta compared with lungs and spleen in all 3 cases. *C. psittaci* was markedly observed, especially in the syncytiotrophoblast cells (Figure 5).

Discussion

In Japan, there have been 7 cases of gestational psittacosis, resulting in a total of 4 maternal deaths (mortality rate 57.1%) and 5 fetal deaths (mortality rate 71.4%) (Table 2) (*5*,*17*–*20*,*31*,*32*,*33*). Of note, the route of infection remained unknown in all reported cases, except in 1 patient (case ID 1 in Table 2) who kept a parrot. Reports on patients with gestational psittacosis in various regions of Japan have been sporadic, making epidemiologic analysis difficult and control of this infectious disease challenging. After the announcement of the new classification of

Table 3. Sequence type and allelic profiles of three cases of gestational psittacosis complicated by maternal and fetal death in study of 3 fatal gestational psittacosis cases caused by *C. psittaci* strains belonging to closely related MLST lineages, Japan, 2017–2024*

Case ID	Year	GenBank accession no.	PubMLST ID	Sequence type	*enoA*	*hemN*	*fumC*	*gatA*	*gidA*	*hflX*	*oppA*
1 (FO-01)	2017	LC921559–65	4431	269	13	9	78	85	92	90	78
2 (YO-02)	2022	LC888489–95	5398	335	13	9	78	85	112	108	78
3 (NO-03)	2024	LC888482–8	5399	335	13	9	78	85	112	108	78

*ID, identification.

C. psittaci and *C. abortus* in 1999 (*35*), 5 cases of gestational psittacosis were reported in China during 2020–2025, 1 case in the United States in 2018, and 3 cases in Europe during 2006–2022. All cases in China had a history of contact with birds (parrots, pigeons, and poultry), whereas all cases in Europe had a history of contact with sheep (1 case also had contact with goats). The case in the United States had contact only with a pet cat as the animal source, and the clear source of infection was unknown (*36*–*43*; X. Wu et al., unpub. data, https://www.researchsquare.com/article/rs-53548/v1).

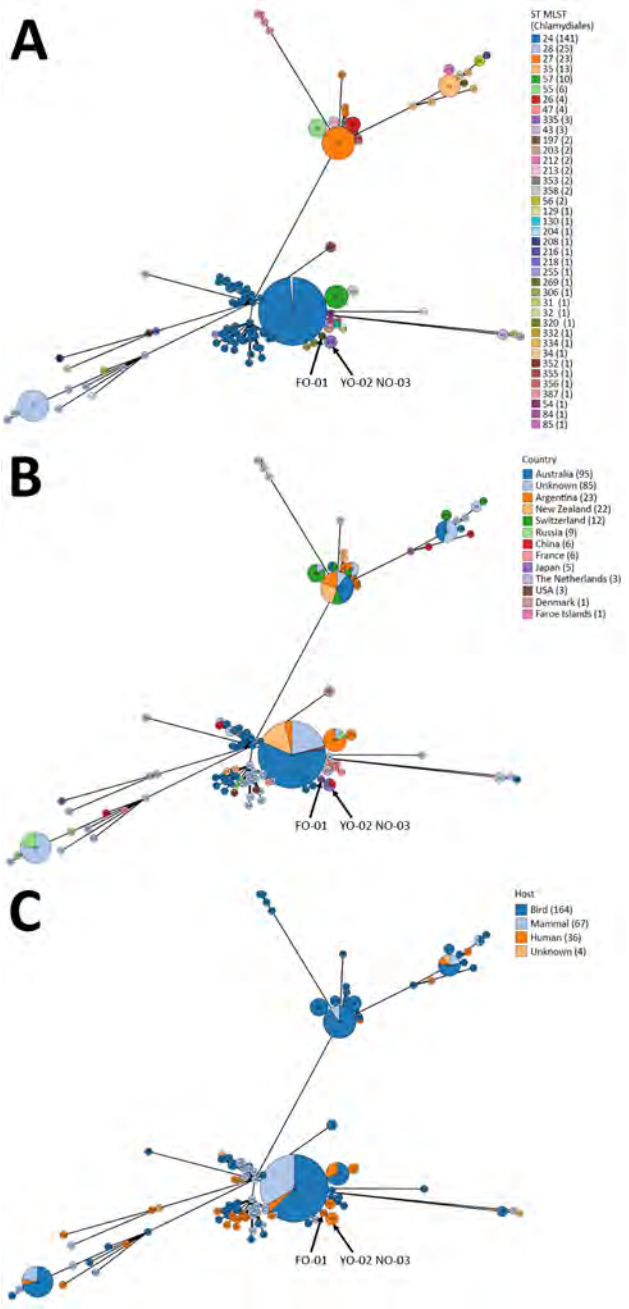

Figure 1. GrapeTree view showing MLST phylogenetic relationship among *Chlamydia psittaci* strains in study of 3 fatal gestational psittacosis cases (FO-01, YO-02, and NO-03) caused by *C. psittaci* strains belonging to closely related MLST lineages, Japan, 2017–2024. A) ST; B) country; C) source host. Strains include ST269/ST335. Numbers in parentheses indicate number of isolates. The MLST alleles are concatenated, and the ST is determined using the Chlamydiales database hosted at http://pubmlst.org/chlamydiales. MLST, multilocus sequence typing; ST, sequence type.

In Japan, all 3 surviving mothers had been administered antimicrobial agents, such as macrolides and tetracycline. However, for the 4 mothers who died, their conditions rapidly became severe after hospitalization, and no treatment was effective. Pneumonia was diagnosed in only 1 patient, and the other patients had no signs of respiratory infectious disease.

The fatal gestational psittacosis cases we describe belonged to closely related ST269/ST335 lineages, as indicated by MLST analysis. The phylogenetic analysis of the *ompA* gene revealed differences in the hypervariable region, grouping them into distinct clusters. Because the cases (FO-01, YO-02, and NO-03) occurred in geographically separate locations in Japan, they are considered to be independent cases of infection rather than an outbreak originating from a single source. MLST is a phylogenetic analysis using highly conserved housekeeping genes; the fact that the strains were identified as closely related in this analysis suggests that they might share a common phylogenetic background.

In this study, the higher bacterial loads in placentas than in maternal lungs and spleens indicated a pronounced proliferative potential of *C. psittaci* in the human placenta. The association of ST269/ST335 lineages with *C. psittaci* proliferation in human placenta remains unclear. Epidemiologically, in Japan, ST269/ST335 lineages have not been previously reported in humans and animals. Elucidating the sources of infection of those lineages remains crucial for effective prevention. Mat116 lineage was reported to circulate between human patients and wild birds (*44*). However, no obvious psittacosis patients were among the family members and medical personnel who had contact with these gestational psittacosis patients. Considering that human-to-human transmission has not been ruled out and the possibility that this *C. psittaci* strain is highly pathogenic to pregnant women, more detailed epidemiologic information on humans and animals is needed.

Diagnosis of *C. psittaci* infection is often challenging because of its nonspecific symptoms, such as fever, as seen in the patients we describe. The rarity of the disease makes it challenging to consider in the

differential diagnosis, and the diagnostic tests, such as isolation of *C. psittaci*, serology, and detection of *C. psittaci* DNA, are not routinely performed in most hospitals (*1*). Undiagnosed *C. psittaci* infection could account for some cases of sudden, unexplained maternal death, suggesting that the actual burden of gestational psittacosis is likely underestimated worldwide.

The cases we report, and other reports on gestational psittacosis, have noted extensive intervillous inflammation of the placenta on pathological examination (*17*–*20*,*32*). Acute intervillositis represents hematogenous spread of organisms from the mother to the fetus through the placenta, and *C. psittaci* is thought to reach the placenta through hematogenous spread. The presence of severe symptoms in pregnant women could be explained several ways. First, as pregnancy progresses through the second and third trimesters, the immune system shifts toward a tolerogenic state to support the developing semiallogenic fetus, uterine dendric cells and natural killer cells produce the regulatory interleukin 10, systemic Treg cell activity increases, and cytotoxic leukocyte activity decreases. Simultaneously, overall Th immunity shifts toward a Th2 profile, mediated in part by differentiation of naive T cells to Th2 cells and accumulation of Th2 cells in the uterus (*45*). That immunologic environment, characterized by a shift from Th1 to Th2 dominance, potentially favors the proliferation of intracellular bacteria, such as *C. psittaci*, which rely on evading Th1-type immune response. Second, during pregnancy, plasma volume at term can increase by nearly 1 L, 90% of which is used in the placenta (*46*). Those

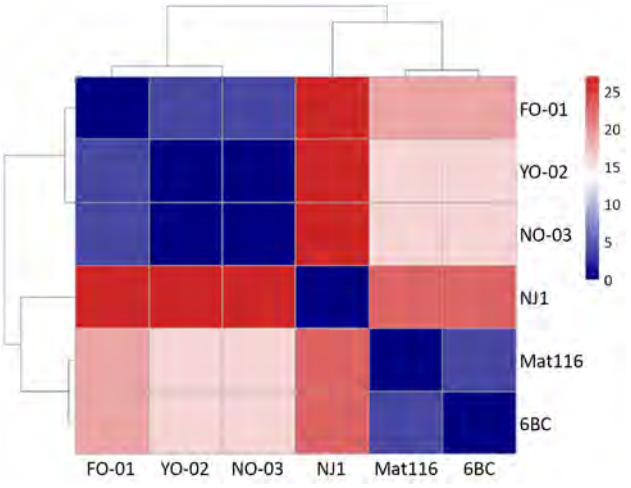

Figure 2. Heatmap of single-nucleotide polymorphism distances of housekeeping genes among 3 cases of gestational psittacosis (FO-01, YO-02, and NO-03) and other *Chlamydia psittaci* strains in study of fatal gestational psittacosis cases caused by *C. psittaci* strains belonging to closely related multilocus sequence typing lineages, Japan, 2017–2024.

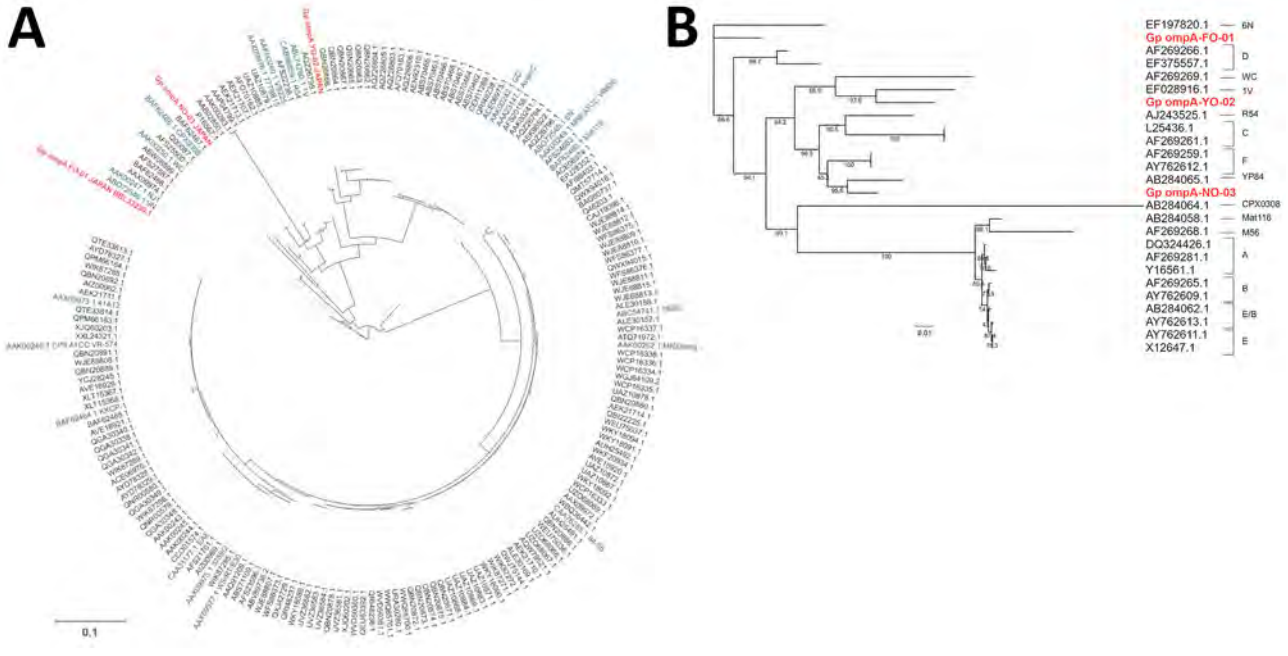

Figure 3. Phylogenetic analysis of the OmpA protein and *ompA* gene of *Chlamydia psittaci* in study of 3 fatal gestational psittacosis cases caused by *C. psittaci* strains belonging to closely related multilocus sequence typing lineages, Japan, 2017–2024. Red text indicates gestational psittacosis cases from in this study (FO-01, YO-02, and NO-03). A) Circular phylogenetic tree of the OmpA protein of 200 strains. Blue indicates representative *C. psittaci* strains. B) Phylogenetic tree of the *ompA* gene of the 3 strains from this study and representative *C. psittaci* genotypes. Scale bar indicates nucleotide or amino acid substitutions per site.

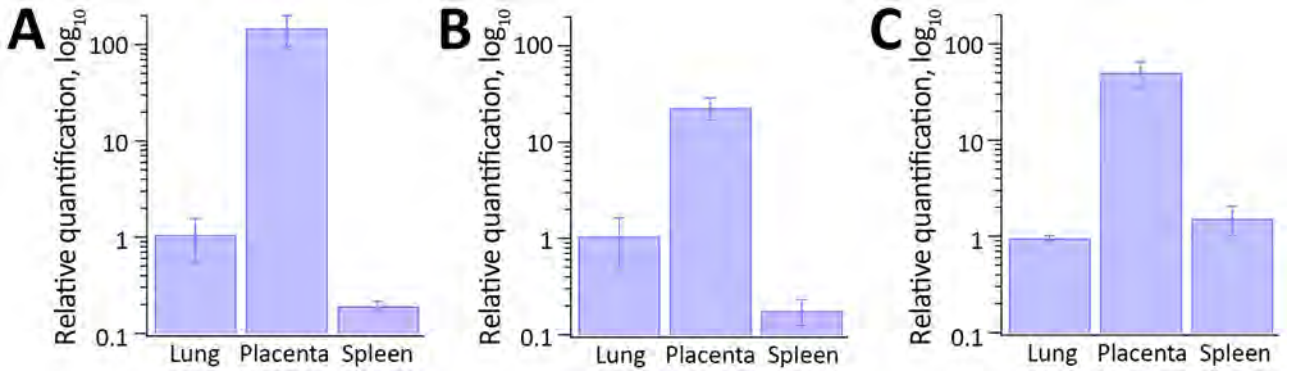

Figure 4. Relative quantification of chlamydial DNA from the maternal lungs, placenta, and spleen in study of 3 fatal gestational psittacosis cases caused by *C. psittaci* strains belonging to closely related multilocus sequence typing lineages, Japan, 2017–2024. Quantitative real-time PCR was performed targeting the 16S rRNA gene of the order Chlamydiales (n = 3). Relative quantification was performed using the $2^{-\Delta\Delta Ct}$ method, normalizing chlamydial DNA levels to β actin as internal control and calculating the relative fold change in the placenta and spleen compared with the lungs. A) Case FO-01; B) case YO-02; C) case NO-03.

hemodynamic changes during pregnancy might enable the spread of *C. psittaci* to the placenta. Compared with FO-01 and YO-02 in this study, NO-03 showed more rapid progression of the initial symptoms to maternal and fetal death at 37 weeks of gestation. That difference might reflect the high proliferative capacity of *C. psittaci* within the placenta, where bacterial load appears to correlate with placental weight (*47*). Fetal death in those 3 cases was considered to be associated with maternal systemic deterioration and placental dysfunction.

The first limitation of our study is that only fixed tissue samples were available, which precluded pathogen isolation and evaluation of virulence in animal models. Because DNA was extracted from FFPE tissue, only short DNA fragments could be amplified;

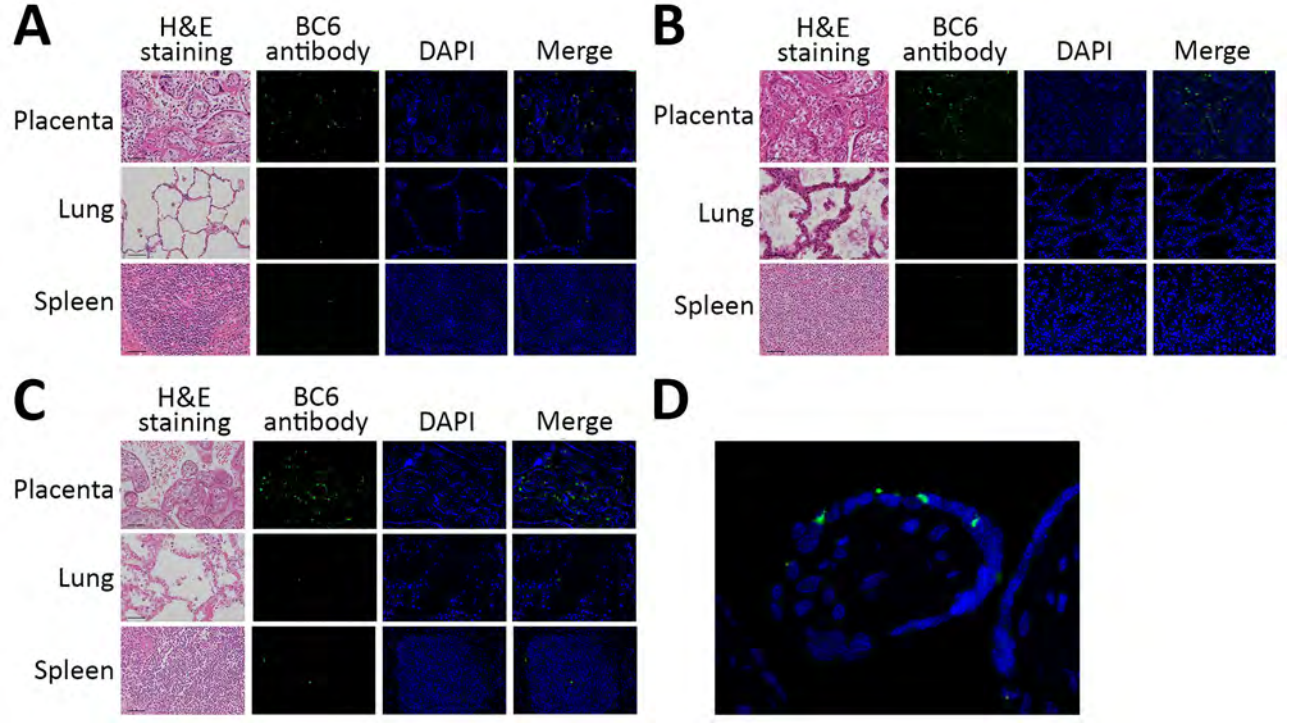

Figure 5. Histologic findings from 3 fatal gestational psittacosis cases caused by *C. psittaci* strains belonging to closely related multilocus sequence typing lineages, Japan, 2017–2024. A–C) Hematoxylin and eosin staining (scale bar = 50 μm; original magnification ×20) and immunofluorescence microscopy of the placenta, lung, and spleen are shown for case FO-01 (A), case YO-02 (B), and case NO-03 (C). Specific fluorescence observed via immunofluorescence using *C. psittaci* BC6 rabbit antibody staining. Nuclei were stained with DAPI. Merge column indicates BC6 antibody staining and DAPI. Original magnification ×20. D) High-magnification view (original magnification ×60) of the villi. DAPI, 4′,6-diamidino-2-phenylindole; H&E, hematoxylin and eosin.

we could not yet obtain the entire genome sequence. However, we successfully amplified and obtained the sequences required for MLST and *ompA* analyses, enabling reliable strain characterization. In addition, genetic data on *C. psittaci* in Japan remain scarce, limiting the generalizability of our findings.

In conclusion, our study identified ST335/ST269 as potential highly virulent lineages in gestational psittacosis. Continued surveillance, improved diagnostic approaches, and further research on transmission pathways and pathogenicity are needed. Our findings provide a basis for risk stratification and targeted surveillance, supporting earlier clinical recognition and prevention of severe outcomes in pregnant women.

This research was partially supported by AMED under grant numbers JP25fk0108677 (I.Y.) and MEXT KAKENHI JP25088336 (I.Y.). We thank Tomoaki Ikeda and Tomoko Wakasa for the nationwide maternal mortality survey in Japan.

I.Y. and Y.S-O. conceptualized the study; methodology was constructed by A.N., Y.N., Y.S-O., M.Y., and I.Y.; M.S., H.S., K.S., S.M., and Y.S. investigated; A.N., Y.N., Y.S-O., and M.Y. performed data curation; A.N., Y.N., Y.S-O., and I.Y. conducted formal analysis; A.N. wrote the original draft; Y.S-O. and I.Y. performed further review and editing; M.K. supervised the study; I.Y. acquired funding. All authors reviewed and edited the manuscript. All authors read and approved the final manuscript.

About the Author

Dr. Nishino is an obstetrician and a PhD student in the graduate school of medicine in The University of Osaka, Osaka, Japan. Her research interests include perinatal infectious diseases.

References

1. Tantengco OAG. Gestational psittacosis: an emerging infection. Lancet Microbe. 2022;3:e728. https://doi.org/10.1016/S2666-5247(22)00191-4
2. Hogerwerf L, DE Gier B, Baan B, VAN DER Hoek W. *Chlamydia psittaci* (psittacosis) as a cause of community-acquired pneumonia: a systematic review and meta-analysis. Epidemiol Infect. 2017;145:3096–105. https://doi.org/10.1017/S0950268817002060
3. Wang W, Sung N, Gilman-Sachs A, Kwak-Kim J. T helper (Th) cell profiles in pregnancy and recurrent pregnancy losses: Th1/Th2/Th9/Th17/Th22/Tfh cells. Front Immunol. 2020;11:2025. https://doi.org/10.3389/fimmu.2020.02025
4. Baud D, Greub G. Intracellular bacteria and adverse pregnancy outcomes. Clin Microbiol Infect. 2011;17:1312–22. https://doi.org/10.1111/j.1469-0691.2011.03604.x
5. Katsura D, Tsuji S, Kimura F, Tanaka T, Eguchi Y, Murakami T. Gestational psittacosis: a case report and literature review. J Obstet Gynaecol Res. 2020;46:673–7. https://doi.org/10.1111/jog.14217
6. Kozuki E, Arima Y, Matsui T, Sanada Y, Ando S, Sunagawa T, et al. Human psittacosis in Japan: notification trends and differences in infection source and age distribution by gender, 2007 to 2016. Ann Epidemiol. 2020;44:60–3. https://doi.org/10.1016/j.annepidem.2020.03.001
7. Stokes HS, Berg ML, Bennett ATD. A review of chlamydial infections in wild birds. Pathogens. 2021;10:948. https://doi.org/10.3390/pathogens10080948
8. Fukushi H, Itoh K, Ogawa Y, Hayashi Y, Kuzuya M, Hirai K, et al. Isolation and serological survey of *Chlamydia psittaci* in feral pigeons from Japan. Nippon Juigaku Zasshi. 1983;45:847–8. https://doi.org/10.1292/jvms1939.45.847
9. Tanaka C, Miyazawa T, Watarai M, Ishiguro N. Bacteriological survey of feces from feral pigeons in Japan. J Vet Med Sci. 2005;67:951–3. https://doi.org/10.1292/jvms.67.951
10. Sassa-O'Brien Y, Wu CF, Matsunaga S, Ohya K, Fukushi H. Isolation of "pigeon-type" *Chlamydia psittaci* and detection of *Chlamydia*-related bacteria in Indian ring-necked parakeets (*Psittacula krameri manillensis*) in introduced flocks in urban area of Japan. Vet Microbiol. 2025;309:110689. https://doi.org/10.1016/j.vetmic.2025.110689
11. Rehn M, Ringberg H, Runehagen A, Herrmann B, Olsen B, Petersson AC, et al. Unusual increase of psittacosis in southern Sweden linked to wild bird exposure, January to April 2013. Euro Surveill. 2013;18:20478. https://doi.org/10.2807/ese.18.19.20478-en
12. Chereau F, Rehn M, Pini A, Kühlmann-Berenzon S, Ydring E, Ringberg H, et al. Wild and domestic bird faeces likely source of psittacosis transmission—a case-control study in Sweden, 2014–2016. Zoonoses Public Health. 2018;65:790–7. https://doi.org/10.1111/zph.12492
13. World Health Organization. Psittacosis—European Region [cited 2026 Mar 25]. https://www.who.int/emergencies/disease-outbreak-news/item/2024-DON509
14. Zhang Z, Zhou H, Cao H, Ji J, Zhang R, Li W, et al. Human-to-human transmission of *Chlamydia psittaci* in China, 2020: an epidemiological and aetiological investigation. Lancet Microbe. 2022;3:e512–20. https://doi.org/10.1016/S2666-5247(22)00064-7
15. Jelocnik M, Jenkins C, O'Rourke B, Barnwell J, Polkinghorne A. Molecular evidence to suggest pigeon-type *Chlamydia psittaci* in association with an equine foal loss. Transbound Emerg Dis. 2018;65:911–5. https://doi.org/10.1111/tbed.12817
16. Fukushi H. Chlamydiosis in zoo [in Japanese]. Japanese Journal of Zoo and Wildlife Medicine. 2003;8:11–17.
17. Shimizu K, Nishijima K, Kawahara K, Banno Y, Yoshimura M, Yanagihara I, et al. The first case of maternal death due to psittacosis [in Japanese]. Obstetrical and Gynecological Practice. 2018;67:445–450.
18. Yoshimura M, Shimizu K, Nakura Y, Kawahara K, Katano H, Motooka D, et al. A fatal case of hemophagocytic lymphohistiocytosis associated with gestational psittacosis without symptoms of pneumonia. J Obstet Gynaecol Res. 2022;48:3325–30. https://doi.org/10.1111/jog.15429
19. Tanioka M, Sugii H, Kanemori M, Ito H. Gestational psittacosis: a case report and literature review [in Japanese]. Modern Trends in Obstetrics & Gynecology. 2023;72:215–220.
20. Miyauchi T, Hirata Y, Fukuda S. Postmortem diagnosis of gestational psittacosis: A case report. Acute Med Surg. 2024;11:e932. https://doi.org/10.1002/ams2.932
21. Opota O, Jaton K, Branley J, Vanrompay D, Erard V, Borel N, et al. Improving the molecular diagnosis of *Chlamydia psittaci*

and *Chlamydia abortus* infection with a species-specific duplex real-time PCR. J Med Microbiol. 2015;64:1174–85. https://doi.org/10.1099/jmm.0.000139
22. Pannekoek Y, Dickx V, Beeckman DS, Jolley KA, Keijzers WC, Vretou E, et al. Multi locus sequence typing of *Chlamydia* reveals an association between *Chlamydia psittaci* genotypes and host species. PLoS One. 2010;5:e14179. https://doi.org/10.1371/journal.pone.0014179
23. Heddema ER, Ter Sluis S, Buys JA, Vandenbroucke-Grauls CM, van Wijnen JH, Visser CE. Prevalence of *Chlamydophila psittaci* in fecal droppings from feral pigeons in Amsterdam, The Netherlands. Appl Environ Microbiol. 2006;72:4423–5. https://doi.org/10.1128/AEM.02662-05
24. Zhou Z, Alikhan NF, Sergeant MJ, Luhmann N, Vaz C, Francisco AP, et al. GrapeTree: visualization of core genomic relationships among 100,000 bacterial pathogens. Genome Res. 2018;28:1395–404. https://doi.org/10.1101/gr.232397.117
25. Katoh K, Rozewicki J, Yamada KD. MAFFT online service: multiple sequence alignment, interactive sequence choice and visualization. Brief Bioinform. 2019;20:1160–6. https://doi.org/10.1093/bib/bbx108
26. Page AJ, Taylor B, Delaney AJ, Soares J, Seemann T, Keane JA, et al. *SNP-sites*: rapid efficient extraction of SNPs from multi-FASTA alignments. Microb Genom. 2016;2:e000056. https://doi.org/10.1099/mgen.0.000056
27. Wang J, Wang B, Xiao J, Chen Y, Wang C. *Chlamydia psittaci*: a zoonotic pathogen causing avian chlamydiosis and psittacosis. Virulence. 2024;15:2428411. https://doi.org/10.1080/21505594.2024.2428411
28. Capella-Gutiérrez S, Silla-Martínez JM, Gabaldón T. trimAl: a tool for automated alignment trimming in large-scale phylogenetic analyses. Bioinformatics. 2009;25:1972–3. https://doi.org/10.1093/bioinformatics/btp348
29. Steenwyk JL, Buida TJ III, Li Y, Shen XX, Rokas A. ClipKIT: a multiple sequence alignment trimming software for accurate phylogenomic inference. PLoS Biol. 2020;18:e3001007. https://doi.org/10.1371/journal.pbio.3001007
30. Letunic I, Bork P. Interactive Tree of Life (iTOL) v6: recent updates to the phylogenetic tree display and annotation tool. Nucleic Acids Res. 2024;52(W1):W78–82. https://doi.org/10.1093/nar/gkae268
31. Nakajyo A, Sotome Y, Matsuyama T, Yoshioka M, Karube M, Matsubara H. A case of a female infant born from a pregnant woman who contracted psittacosis in late pregnancy [in Japanese]. J Pediatr. 2002;55:895–8.
32. Hattori A, Yoshida A, Oku K, Kamiya A, Kuroda Y, Kasamatsu A, et al. Gestational psittacosis of the placenta with massive perivillous fibrin deposition leading to intrauterine fetal demise: a case report [in Japanese]. Journal Japan Society of Perinatal and Neonatal Medicine. 2021;57:140–5.
33. Mitsuzuka K, Manabe T, Sakamoto N, Nakajima R, Kashiwagi H, Hayashi M, et al. A case of gestational psittacosis presenting with pneumonia similar to COVID-19 and disseminated intravascular coagulation [in Japanese]. In: Abstracts of the 58th Annual Congress of Japan Society of Perinatal and Neonatal Medicine; Kanagawa, Japan; 2022 Jul 10–12. Abstract O-015. Tokyo: Journal of Japan Society of Perinatal and Neonatal Medicine; 2022.
34. Huang W, Hu S, Zhu Y, Liu S, Zhou X, Fang Y, et al. Metagenomic surveillance and comparative genomic analysis of *Chlamydia psittaci* in patients with pneumonia. Front Microbiol. 2023;14:1157888. https://doi.org/10.3389/fmicb.2023.1157888
35. Everett KD, Bush RM, Andersen AA. Emended description of the order *Chlamydiales*, proposal of *Parachlamydiaceae* fam. nov. and *Simkaniaceae* fam. nov., each containing one monotypic genus, revised taxonomy of the family *Chlamydiaceae*, including a new genus and five new species, and standards for the identification of organisms. Int J Syst Bacteriol. 1999;49:415–40. https://doi.org/10.1099/00207713-49-2-415
36. Yang Z, Wang S, Xing D, Zhang H. Pregnancy combined with severe pneumonia caused by *Chlamydia psittaci* infection—a case report. Ginekol Pol. 2021;92:743–4. https://doi.org/10.5603/GP.a2021.0184
37. Sun L, Li P, Pang B, Wu P, Wang R. Gestational psittacosis with secondary hemophagocytic syndrome: a case report and literature review. Front Med (Lausanne). 2021;8:755669. https://doi.org/10.3389/fmed.2021.755669
38. Wang L, Lin C, Qi Y. Gestational psittacosis causes severe pneumonia and miscarriage: a case report and literature review. Radiol Case Rep. 2023;18:1959–62. https://doi.org/10.1016/j.radcr.2023.02.034
39. Liu Z, Luo L, Zhang Z, Li X, Zuo B, Wu D. Epidemiological investigation and clinical presentation of severe gestational psittacosis diagnosed using targeted next-generation sequencing: a case report. Medicine (Baltimore). 2025;104:e46860. https://doi.org/10.1097/MD.0000000000046860
40. Janssen MJ, van de Wetering K, Arabin B. Sepsis due to gestational psittacosis: a multidisciplinary approach within a perinatological center—review of reported cases. Int J Fertil Womens Med. 2006;51:17–20.
41. Imkamp F, Albini S, Karbach M, Kimmich N, Spinelli C, Herren S, et al. Zoonotic Chlamydiae as rare causes of severe pneumonia. Swiss Med Wkly. 2022;152:w30102. https://doi.org/10.4414/SMW.2022.w30102
42. Guscoth LB, Taylor DM, Coad F. Persistent renal replacement requirement following fulminant psittacosis infection in pregnancy. BMJ Case Rep. 2022;15:e250221. https://doi.org/10.1136/bcr-2022-250221
43. Paul L, Comstock J, Edes K, Schlaberg R. Gestational psittacosis resulting in neonatal death identified by next-generation RNA sequencing of postmortem, formalin-fixed lung tissue. Open Forum Infect Dis. 2018;5:ofy172. https://doi.org/10.1093/ofid/ofy172
44. Herrmann B, Aaziz R, Kaden R, Riedel HM, Spörndly-Nees E, Sandelin LL, et al. SNP-based high-resolution typing of *Chlamydia psittaci* from humans and wild birds in Sweden: circulation of the Mat116 genotype reveals the transmission mode to humans. Microbes Infect. 2024;26:105251. https://doi.org/10.1016/j.micinf.2023.105251
45. Creisher PS, Klein SL. Pathogenesis of viral infections during pregnancy. Clin Microbiol Rev. 2024;37:e0007323. https://doi.org/10.1128/cmr.00073-23
46. Fournier SB, D'Errico JN, Stapleton PA. Uterine vascular control preconception and during pregnancy. Compr Physiol. 2021;11:1871–93. https://doi.org/10.1002/j.2040-4603.2021.tb00168.x
47. Wallace JM, Bhattacharya S, Horgan GW. Gestational age, gender and parity specific centile charts for placental weight for singleton deliveries in Aberdeen, UK. Placenta. 2013;34:269–74. https://doi.org/10.1016/j.placenta.2012.12.007

Address for correspondence: Itaru Yanagihara, Department of Developmental Medicine, Research Institute, Osaka Women's and Children's Hospital, 840 Murodo-cho, Izumi, Osaka 594-1101, Japan; email: itaruy@wch.opho.jp

Frequency and Duration of Diagnostic Delays Associated with Coccidioidomycosis and Risk Factors for Missed Diagnoses, United States

Desmond D. Barber, Alan T. Arakkal, George R. Thompson, John W. Baddley, Joe E. Cavanaugh, Aaron C. Miller, Philip M. Polgreen

Medscape CME Activity

In support of improving patient care, this activity has been planned and implemented by Medscape, LLC and Emerging Infectious Diseases. Medscape, LLC is jointly accredited with commendation by the Accreditation Council for Continuing Medical Education (ACCME), the Accreditation Council for Pharmacy Education (ACPE), and the American Nurses Credentialing Center (ANCC), to provide continuing education for the healthcare team.

Medscape, LLC designates this Journal-based CME activity for a maximum of 1.00 ***AMA PRA Category 1 Credit(s)™***. Physicians should claim only the credit commensurate with the extent of their participation in the activity.

Successful completion of this CME activity, which includes participation in the evaluation component, enables the participant to earn up to 1.0 MOC points in the American Board of Internal Medicine's (ABIM) Maintenance of Certification (MOC) program. Participants will earn MOC points equivalent to the amount of CME credits claimed for the activity. It is the CME activity provider's responsibility to submit participant completion information to ACCME for the purpose of granting ABIM MOC credit.

All other clinicians completing this activity will be issued a certificate of participation. To participate in this journal CME activity: (1) review the learning objectives and author disclosures; (2) study the education content; (3) take the post-test with a 75% minimum passing score and complete the evaluation at https://www.medscape.org/qna/processor/77356?showStandAlone=true&isAspenArticle=true&src=prt_jcme_eid_mscpedu; and (4) view/print certificate. For CME questions, see page 837.

NOTE: It is the policy of Medscape Education to avoid the mention of brand names or specific manufacturers in accredited educational activities. However, trade and manufacturer names in this activity are provided in an effort to provide clarity. The use of brand or manufacturer names should not be viewed as an endorsement by Medscape of any specific product or manufacturer.

Release date: May 11, 2026; Expiration date: May 11, 2027

Learning Objectives

Upon completion of this activity, participants will be able to:

- Describe the clinical presentation of coccidioidomycosis
- Compare rates of delayed diagnosis of coccidioidomycosis based on clinical site
- Distinguish the mean delay in diagnosis of coccidioidomycosis among patients who experienced at least 1 missed diagnosis
- Evaluate risk factors for the delayed diagnosis of coccidioidomycosis

CME Editor

Jill Russell, BA, Technical Writer/Editor, Emerging Infectious Diseases. *Disclosure: Jill Russell, BA, has no relevant financial relationships.*

CME Author

Charles P. Vega, MD, Health Sciences Clinical Professor of Family Medicine, University of California, Irvine School of Medicine, Irvine, California. *Disclosure: Charles P. Vega, MD, has the following relevant financial relationships: served as consultant or advisor for Boehringer Ingelheim; Exact Sciences; GlaxoSmithKline.*

Authors

Desmond D. Barber, MD, MME; Alan T. Arakkal, PhD; George R. Thompson, MD; John W. Baddley, MD, MSPH; Joe E. Cavanaugh, PhD; Aaron C. Miller, PhD; Philip M. Polgreen, MD, MPH.

Diagnosis of coccidioidomycosis is challenging and requires a high index of clinical suspicion. We estimated the incidence and duration of, and risk factors associated with, diagnostic delays and missed opportunities in the diagnosis of coccidioidomycosis. We conducted a retrospective analysis of health insurance claims data in the United States during 2001–2022 included in the Merative MarketScan Databases. Using a case-crossover design and a bootstrapping approach, we estimated the number of excess visits for coccidioidomycosis-related symptoms before diagnosis. We also evaluated potential factors associated with delay. We estimated that almost 60% of patients experienced ≥1 missed opportunity for diagnosis; the average diagnostic delay was 29.69 (95% CI 28.25–31.18) days. Missed opportunities were predominantly observed in outpatient settings (73%) and were significantly associated with older age, rural residence, underlying pulmonary conditions, and prescriptions for antibiotics or inhalers. Diagnostic delays for coccidioidomycosis are common, and addressing such delays could improve clinical outcomes.

Coccidioidomycosis is an infectious disease caused by dimorphic fungi of the genus *Coccidioides* (*1*). Infections are caused by *C. immitis* and *C. posadasii,* and the clinical manifestations for both species are similar (*2*). In the United States, most cases occur in Arizona and California (*3*), but sporadic cases also occur in parts of Texas, New Mexico, Utah, and Nevada (*4*). The geographic range of infection might be more expansive than previously thought, and the range of the organisms might be increasing both northward and eastward within the continental United States (*5*). Furthermore, the incidence of coccidioidomycosis also appears to be increasing (*6*).

Coccidioides spp. grow as mold in the environment, and inhalation of airborne arthroconidia is the most common route of infection. Approximately 60% of cases are asymptomatic (*7*). Among symptomatic cases, common symptoms consist of cough, fever, chills, shortness of breath, chest discomfort, and fatigue, producing a clinical picture that closely mimics viral respiratory infection or pneumonia (*8*,*9*). Although primary pulmonary disease is most common, dissemination to extrapulmonary sites can occur through hematogenous or lymphatic spread, and the skin, bones, joints, and central nervous system are the most frequent targets (*10*). Overall, disseminated disease is rare (≈1% of cases) (*11*), but its risk is substantially elevated in immunocompromised persons (*12*).

Diagnosis of coccidioidomycosis is challenging and requires a high index of clinical suspicion, because the symptoms, physical examination findings, and radiographic findings for the disease are nonspecific. Given the clinical overlap of signs and symptoms with bacterial pneumonia or other respiratory symptoms, patients with coccidioidomycosis are frequently treated with multiple courses of antibiotics before diagnosis, even in regions where the disease is relatively common (*13*–*16*). Diagnosis is further complicated by the limitations of available testing modalities. Serologic testing for antibodies offers relatively high sensitivity (*17*) but can be negative early in the course of the disease, and ordering serologic testing requires suspicion of coccidioidomycosis on the part of the clinician. Understanding the timeliness of diagnosis is key not only for improving clinical care but also for public health response and disease surveillance. Delays in diagnosis can obscure the apparent timeline of infection, leading to bias in surveillance, outbreak detection, and source attribution.

Because of the potential of diagnostic delays for coccidioidomycosis, better characterization of the incidence and factors associated with those delays is urgently needed. Some studies of coccidioidomycosis-related diagnostic delays have been conducted (*15*,*18*,*19*), but larger studies that include risk factors for delays are needed. The purpose of this study was to use a large database of commercial insurance claims to estimate the incidence of delays in diagnosing coccidioidomycosis, estimate the average length of diagnostic delays, and identify potential factors associated with delayed diagnosis of coccidioidomycosis, including use of unnecessary antibiotics.

Methods

Data Source and Study Population

We conducted a retrospective study using longitudinal health insurance claims from the Merative MarketScan Research Databases, including the Commercial and Medicare databases from 2001–2022 and the Multi-State Medicaid databases from 2014–2021. Those data represent one of the largest databases of commercial insurance claims in the United States and contain records from inpatient, outpatient, and emergency department encounters, along with outpatient prescription medications. Over the study period, the Commercial and Medicare databases represented ≈29 million daily

Author affiliations: University of Iowa College of Medicine, Iowa City, Iowa, USA (D.D. Barber, A.T. Arakkal, J.E. Cavanaugh, A.C. Miller, P.M. Polgreen); University of California, Davis, California, USA (G.R. Thompson); Johns Hopkins University, Baltimore, Maryland, USA (J.W. Baddley)

DOI: https://doi.org/10.3201/eid3205.251421

enrollees, whereas the Medicaid database represented ≈11 million daily enrollees, on average.

We identified patients with coccidioidomycosis using diagnosis code 114.X from the International Classification of Diseases, 9th Revision, Clinical Modification (ICD-9-CM), and code B38.XX from the International Classification of Diseases, 10th Revision, Clinical Modification (ICD-10-CM). We identified the index coccidioidomycosis diagnosis as the first healthcare visit during which coccidioidomycosis was diagnosed. Patients were required to be continuously enrolled for ≥1 year before the index coccidioidomycosis diagnosis; thus, we excluded patients who received a diagnosis of coccidioidomycosis in the year 2001.

Statistical Analysis

We identified all potential missed diagnostic opportunities by evaluating healthcare visits before the index coccidioidomycosis diagnosis in which potential signs or symptoms of coccidioidomycosis were present. We reviewed all ICD-9-CM and ICD-10-CM diagnosis codes recorded during healthcare visits in the year before the index coccidioidomycosis diagnosis to identify visits in which the patient displayed signs or symptoms of coccidioidomycosis, visits in which tests were ordered for conditions with similar manifestations as coccidioidomycosis, or visits in which conditions were diagnosed that have similar manifestations to coccidioidomycosis. Codes meeting 1 of those criteria were deemed clinically plausible as potential evidence of underlying coccidioidomycosis and defined as symptomatically similar diagnoses (SSDs). We used the complete set of SSDs and corresponding ICD-9-CM and ICD-10-CM codes to identify potential missed diagnostic opportunities (Appendix Table 1, https://wwwnc.cdc.gov/EID/article/32/5/25-1421-App1.pdf).

Missed opportunities to diagnose coccidioidomycosis are not directly observable, because signs or symptoms occurring before diagnosis (e.g., cough, fever, fatigue) might be coincidental and caused by other diseases with similar symptomology (e.g., respiratory infection). Thus, to estimate the actual number of missed opportunities, we used the 2-step process described next, which has been used in multiple studies to evaluate diagnostic delays (*20*–*25*). Extensive details of this methodological approach can be found in Miller et al. (*26*).

Step 1—Estimating the Number of Missed Opportunities.

We began by implementing a type of case-crossover design to calculate the excess number of SSD visits each day before the coccidioidomycosis diagnosis. We specified a case period of 13 weeks (91 days) before the coccidioidomycosis diagnosis. That period is referred to as the diagnostic opportunity window, defined as the time before diagnosis when diagnostic opportunities might occur. The period from 92–365 days before the coccidioidomycosis diagnosis represents the crossover (control) period for each enrollee. We selected the 13-week cutoff as the point in time when the frequency of SSD-related visits began to increase (Appendix Figure 1). We also conducted a sensitivity analysis evaluating alternative crossover periods (Appendix Table 2).

To estimate the expected number of SSD visits each day before diagnosis, we computed the number of patients with an SSD-associated visit each day during the crossover period (92–365 days before diagnosis) and fit a quadratic time trend to those daily visit counts, including an additive effect for day of week to capture weekly periodicity. We then extrapolated that trend forward into the diagnostic opportunity window (i.e., 1–91 days before diagnosis) to estimate the expected number of SSD visits. Finally, we computed the number of missed diagnostic opportunities each day before diagnosis as the difference between the observed and expected number of SSD visits (i.e., the excess number of SSD visits) during the diagnostic opportunity window.

Step 2—Estimating Diagnostic Delay Metrics and Potential Risk Factors

We used a bootstrapping approach to estimate patient-level measures for the frequency and duration of and potential risk factors for diagnostic delays (*27*). First, we randomly draw individual patient visits representing a missed opportunity on a given day using the computed number of missed opportunities from the case-crossover analysis (described previously). Using those selected visits, we calculated the number of patients experiencing a missed opportunity, the number of missed opportunities per patient, the number of missed opportunities by healthcare setting, and duration of diagnostic delay, then evaluated the risk-factor models described next.

We implemented the bootstrapping procedure using the following 4-step process: draw a bootstrapped sample of patients with replacement, implement the case-crossover analysis computing the number of missed opportunities each day before diagnosis, randomly draw which individual patient visits represented a missed opportunity (using an uncorrelated algorithm [*27*]), and calculate delay

metrics and evaluate the risk-factor models (outlined next). We repeated steps 1–2 100 times, generating 100 bootstrapped samples. Then, for each bootstrapped sample, we repeated steps 3–4 100 times. That process resulted in a total of 10,000 trials. We aggregated results across all trials and reported the median of the bootstrapped estimates along with the 95% percentile-based CI.

Risk Factors for Experiencing a Missed Opportunity

We also conducted an exploratory analysis to identify possible risk factors associated with missed diagnostic opportunities. We evaluated a patient-level logistic regression model to estimate the odds of a patient experiencing a missed opportunity as a function of patient and clinical characteristics. For each simulation trial, we assigned patients selected as having a missed opportunity an outcome value of 1 (i.e., missed opportunity) and those not selected a value of 0 (i.e., no missed opportunity). Patient demographics evaluated included patient age group (categorized into <18, 18–34, 35–44, 45–54, 55–64, and ≥65 years), sex, and rurality. We created an indicator for rurality if the patient visited a rural health clinic (using the place of service variable on a claim record). In addition, we considered patients' clinical history of underlying pulmonary conditions that might induce cognitive bias into the diagnostic process. Specifically, we included indicators for underlying history of asthma, chronic obstructive pulmonary disease (COPD), and chest imaging (radiograph or computed tomography scan). Furthermore, we evaluated whether treatments for potential symptoms of coccidioidomycosis affected delays by including indicators for respiratory antibiotics and inhalers prescribed during the diagnostic opportunity window. We also included month and year of the index coccidioidomycosis diagnosis as categorical variables.

We conducted all statistical analyses using R version 3.5.1 (The R Project for Statistical Computing, https://www.r-project.org) and implemented the bootstrapping procedure using the delaySim package (https://github.com/aarmiller/delaySim), which we maintain. All of the code used for identifying cases, along with diagnosis, procedure, and medication codes, and for conducting all statistical analysis can be found at the GitHub repository (https://github.com/aarmiller/delay_diagnosis/publications/cocci). This study uses completely deidentified observational data and is thus classified as non–human subjects research according to the National Institutes of Health under category 4.

Secondary Analyses

We conducted 2 secondary analyses to evaluate geographic variability in delays and to evaluate potential excess antibiotic use as the result of delays. To evaluate differences in delay characteristics between patients residing in Arizona and those living elsewhere, we stratified the study population accordingly, repeated each analysis, and compared the resulting delay metrics of interest. To evaluate whether delays were potentially linked to excess antibiotic use, we identified all outpatient antibiotic prescriptions occurring in the year before diagnosis and compared that trend to SSD-associated visits.

Results

We identified 44,292 cases of coccidioidomycosis (43,210 from the Commercial and Medicare databases and 1,082 from the Medicaid database) during 2001–2022. Of those cases, 26,905 met the inclusion criteria of being continuously enrolled for ≥1 year before their index diagnosis (26,379 from Commercial and Medicare and 526 from Medicaid). The median age of patients in the cohort was 52.0 years; 51.5% of the cohort patients were female and 48.5% were male (Table 1). Most patients were identified in the Commercial claims database (80.2%), followed by the Medicare (17.9%) and Multi-State Medicaid (2.0%) databases.

In the year before the index coccidioidomycosis diagnosis, 26,398 (98.1%) patients had ≥1 healthcare visit for any reason, and 23,191 (86.2%) patients had ≥1 SSD visit. A total of 177,679 SSD-associated visit days were noted in the 365 days before the index diagnosis. The frequency of SSD-related visits increased substantially beginning ≈100 days before the index diagnosis (Figure 1, panel A).

During the 13-week diagnostic opportunity window, 88,130 total SSD visit days from 19,670 (73.1%) patients occurred, representing potential missed opportunities. We plotted the expected trend (in red) of SSD-related visits, estimated on the basis of visits during the crossover period from 92–365 days before diagnosis (Figure 1, panel B). We also plotted the distribution of the estimated number of missed diagnostic opportunities each day before the index diagnosis (Figure 2).

On the basis of the bootstrapping approach, we estimated that 43,338 (95% CI 40,566–46,125) of total SSD visit days during the diagnostic opportunity window represented actual missed diagnostic opportunities (Table 2). Approximately 73.2% (95% CI 72.4%–74.1%) of missed opportunities occurred in an outpatient setting, 18.6% (95% CI 17.8%–19.5%) in inpatient settings, 7.5% (95% CI 7.2%–7.7%) in

emergency department settings, and 0.7% (95% CI 0.6%–0.7%) in observational stay settings.

Approximately 59.7% (95% CI 58.3%–61.1%) of patients experienced ≥1 missed diagnostic opportunity (Table 3). Of the patients who experienced ≥1 missed opportunity, they experienced on average 2.70 (95% CI 2.58–2.81) visits representing missed opportunities and had an average diagnostic delay duration of 29.69 days (95% CI 28.25–31.18). An estimated 24.7% (95% CI 22.9%–26.7%) of patients experienced a diagnostic delay duration that lasted ≥30 days.

Patients with Medicare (odds ratio [OR] 0.61 [95% CI 0.47–0.78]) or Medicaid (OR 0.61 [95% CI 0.48–0.77]) were less likely to experience a delay (i.e., experience ≥1 missed diagnostic opportunity) than were patients with commercial insurance (Table 4; Appendix Table 3). Patients ≥65 years of age were more likely to experience a delay than were patients <18 years of age (OR 1.48 [95% CI 1.15–1.98]). Patients in rural locations were slightly more likely to experience a delay (OR 1.27 [95% CI 1.04–1.60]). Patients with underlying history of pulmonary conditions or related procedures were more likely to experience a diagnostic delay (i.e., asthma [OR 1.34 (95% CI 1.18–1.49)], COPD [OR 1.56 (95% CI 1.36–1.80)], chest computed tomography [OR 1.42 (95% CI 1.26–1.61)], and chest radiography [OR 1.21 (95% CI 1.12–1.30)]). Finally, receipt of medications to treat potential symptoms of coccidioidomycosis during the diagnostic opportunity window was positively associated with the likelihood of experiencing a diagnostic delay (i.e., antibiotics [OR 3.42 (95% CI 3.18–3.69)] and inhalers [OR 2.64 (95% CI 2.34–2.99)]).

Table 1. Baseline characteristics of study population in study of frequency and duration of diagnostic delays associated with coccidioidomycosis and risk factors for missed diagnoses, United States*

Characteristic	Value
Age at diagnosis, y	
<18	1,686 (6.3)
18–34	3,531 (13.1)
35–44	4,026 (15.0)
45–54	5,581 (20.7)
55–64	6,930 (25.8)
≥65	5,151 (19.1)
Mean (±SD)	50.1 (18.4)
Median (IQR)	52.0 (23.0)
Sex	
M	13,056 (48.5)
F	13,849 (51.5)
Database source	
Commercial	21,573 (80.2)
Medicare	4,806 (17.9)
Medicaid	526 (2.0)
Enrollment time before index diagnosis, y	
≤2	7,177 (26.7)
≤3	12,219 (45.4)
>3	14,686 (54.6)
Mean (±SD)	4.4 (3.4)
Median (IQR)	3.3 (3.9)

*Values are no. (%) patients except as indicated. IQR, interquartile range.

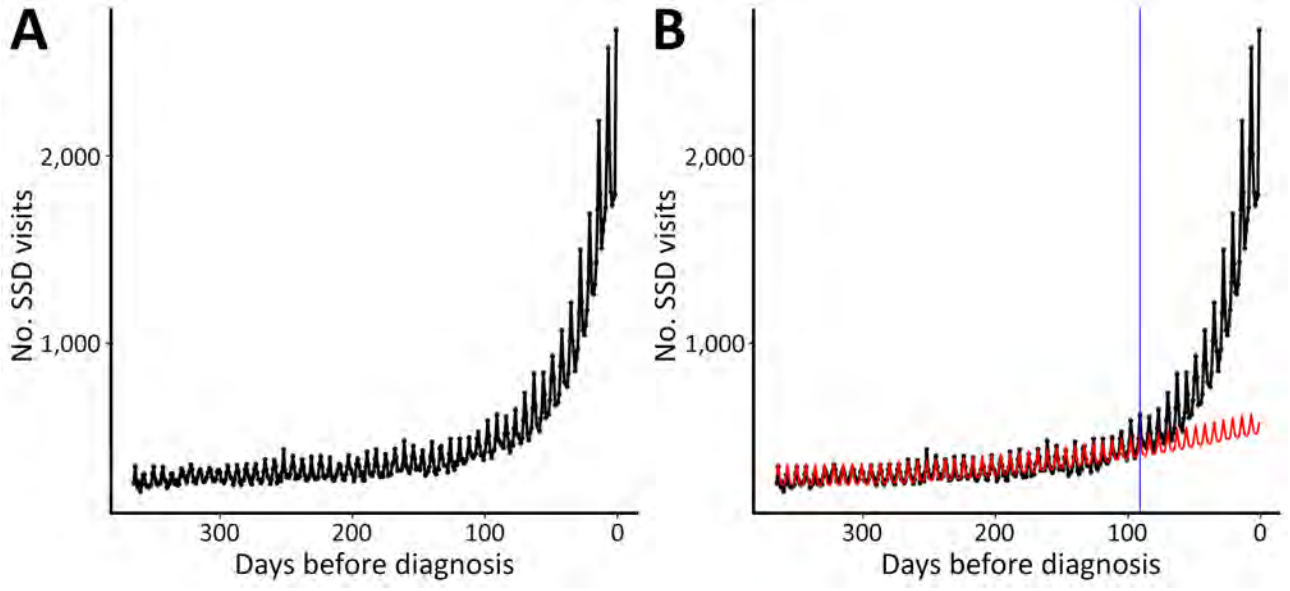

Figure 1. Trends in SSD-related healthcare visits in the 365 days before index coccidioidomycosis diagnosis in study of frequency and duration of diagnostic delays associated with coccidioidomycosis and risk factors for missed diagnoses, United States. A) Raw SSD visit counts for each day before the index coccidioidomycosis diagnosis. B) Expected trendline (in red) estimated from visits between 92–365 days before the index coccidioidomycosis diagnosis; vertical blue line indicates start of the diagnostic opportunity window, beginning 91 days before the index diagnosis. Estimated number of missed diagnostic opportunities is depicted as the area between the observed line (in black) and the expected trend (in red) during the diagnostic opportunity window (region to the right of the blue line). SSD, symptomatically similar diagnosis.

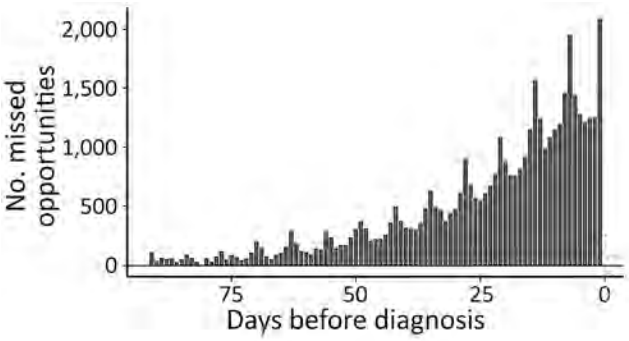

Figure 2. Estimated number of missed diagnostic opportunities each day before the index coccidioidomycosis diagnosis in study of frequency and duration of diagnostic delays associated with coccidioidomycosis and risk factors for missed diagnoses, United States. Estimates are based on the excess number of symptomatically similar diagnosis–associated healthcare visits, computed as the difference between the observed and expected values in Figure 1.

We observed similar patient-level delay metrics for patients residing in Arizona and patients not residing in Arizona (Appendix Table 4). However, a greater proportion of patients in the Arizona cohort experienced ≥1 missed diagnostic opportunity than did patients in the non-Arizona cohort (69.6% vs. 55.5%).

The number of outpatient antibiotic prescriptions increased substantially beginning nearly 90 days before diagnosis (Appendix Figure 2). The trend in antibiotic prescriptions mirrored the trend in SSD visits, suggesting that SSD visits attributable to diagnostic delays were associated with excess antibiotic prescriptions (Figure 3).

Discussion

We found that many patients who ultimately received a diagnosis of coccidioidomycosis experienced multiple healthcare encounters before diagnosis, and many of those visits represented potential missed opportunities for earlier diagnosis. Specifically, 60% of patients experienced ≥1 missed opportunity; among those persons, we estimated an average of 2.70 visits per patient to be potential missed opportunities, and ≈73% occurred in the outpatient setting. We estimated that the mean diagnostic delay was ≈30 days (median 24 days). In addition, elderly patients, patients living in rural areas, and those with underlying respiratory conditions were more likely to experience a delay in diagnosis. Furthermore, prescription of antibiotics or inhalers during the delay window increased the odds of experiencing a missed opportunity to diagnose coccidioidomycosis.

Coccidioidomycosis, similar to other endemic fungal infections, is an infectious disease that is commonly associated with diagnostic delays (*28*). Overall, our results largely align with previous studies reporting diagnostic delays for coccidioidomycosis. For example, a study of health claims for 139 patients in a large health system based in Phoenix, Arizona, found that 46% of patients had a diagnostic delay >1 month in length (*19*). A study in 14 US states found that among 339 patients, a median of 38 days passed between first seeking care and diagnosis (*29*). However, those studies might have described longer delays because determining when symptoms began is often difficult. For example, Benedict et al. (*29*) reported 1 case in their series with an extremely long interval of 1,654 days (*29*). Moreover, symptoms caused by other conditions have often been attributed to coccidioidomycosis in previous study designs of diagnostic delays (*29*,*30*). We included a much larger sample size than previous studies and used a case-crossover and bootstrapping approach, enabling us to distinguish attributable visits from background healthcare use, providing more accurate estimates of missed diagnostic opportunities. Indeed, our finding that 59.7% of patients experienced a diagnostic delay directly contrasts with a recent study (*30*) that used the

Table 2. Index diagnosis visits and simulation results for missed diagnostic opportunities by setting in study of frequency and duration of diagnostic delays associated with coccidioidomycosis and risk factors for missed diagnoses, United States*

		Index diagnosis visits†		Potential missed opportunities‡	
Setting	No. potential missed opportunity visit days	No. index visits	% Of all index visits	No. missed opportunities (95% CI)	% Of all missed opportunities (95% CI)
Outpatient	71,392	25,237	84.4%	35,435 (33,277–37,741)	73.2% (72.4%–74.1%)
Emergency department	6,985	1,230	4.1%	3,607 (3,330–3,838)	7.5% (7.2%–7.7%)
Observational stay	626	128	0.4%	318 (271–365)	0.7% (0.6%–0.7%)
Inpatient	18,897	3,314	11.1%	9,024 (8,280–9,834)	18.6% (17.8%–19.5%)
Inpatient visit§	3,169	3,314	11.1%	2,654 (2,532–2,784)	NC§

*NC, not calculated.
†Multiple settings may be associated with an index visit date (i.e., we are unable to order the timing of visits from claims on the same day); thus, the total number exceeds the number of individuals in the study population.
‡Multiple settings may occur on a given visit day (i.e., we are unable to order the timing of visits from claims on the same day); thus, the total number exceeds the total estimated potential missed diagnostic opportunities.
§Inpatient visits represent ≥1 days admitted to an inpatient facility. Our analysis of missed diagnostic opportunities is based on visit days in which the patient received a symptomatically similar diagnosis on a given day. We can aggregate potential missed opportunities, index diagnoses, and estimated missed opportunities from the bootstrapping approach into the overall inpatient stay in which they occurred. However, the denominator for computing the percent of missed opportunities that occurred in each setting represents the total number of visit days representing a missed opportunity; thus, a value for aggregate inpatient visits is not computed.

Table 3. Simulation results for number and duration of delayed visits per patient in study of frequency and duration of diagnostic delays associated with coccidioidomycosis and risk factors for missed diagnoses, United States*

Metric	Value	95% CI
No. (%) missed opportunities per patient		
≥1	16,061 (59.7%)	15,685–16,445 (58.3%–61.1%)
≥2	9,770 (36.3%)	9,312–10,238 (34.6%–38.1%)
≥3	5,824 (21.6%)	5,408–6,281 (20.1%–23.3%)
≥4	3,491 (13.0%)	3,159–3,849 (11.7%–14.3%)
≥5	2,183 (8.1%)	1,935–2,447 (7.2%–9.1%)
Mean	2.70	2.58–2.81
Median	2.00	2.00–2.00
Duration of delayed visits, d		
≥1	16,061 (59.7%)	15,685–16,445 (58.3%–61.1%)
≥3	15,113 (56.2%)	14,724–15,516 (54.7%–57.7%)
≥7	13,780 (51.2%)	13,376–14,213 (49.7%–52.8%)
≥10	12,453 (46.3%)	12,027–12,895 (44.7%–47.9%)
≥14	11,187 (41.6%)	10,738–11,625 (39.9%–43.2%)
≥21	9,050 (33.6%)	8,570–9,534 (31.9%–35.4%)
≥30	6,650 (24.7%)	6,169–7,177 (22.9%–26.7%)
≥45	3,930 (14.6%)	3,458–4,447 (12.9%–16.5%)
≥60	2,150 (8.0%)	1,781–2,580 (6.6%–9.6%)
≥90	153 (0.6%)	82–229 (0.3%–0.9%)
Mean delay duration, d	29.69	28.25–31.18
Median delay duration, d	24.05	23.00–26.00

*The distribution and mean number of potential missed diagnostic opportunities each patient experienced along with the distribution and mean and median duration of diagnostic delays (in days) are presented. Potential missed diagnostic opportunities represent healthcare visits in which sign/symptoms were present, but coccidioidomycosis was not diagnosed. Delay duration was defined as the time between the earliest potential missed diagnostic opportunity a patient experienced and their index diagnosis.

same data source and similar study population but reported that 71.3% of patients experienced a diagnostic delay. The difference in our findings is most likely attributable to the fact that the previous study did not account for an expected level of background healthcare utilization and, consequently, labeled every patient with potential signs or symptoms in the 90 days before diagnosis as a case of diagnostic delay.

We identified multiple factors associated with the odds of diagnostic delays for coccidioidomycosis. First, delays were more common in older patients (i.e., ≥65 years of age compared with persons <18 years of age), an unsurprising finding, given that older adults frequently demonstrate more vague or subtle signs and symptoms for infectious diseases (*31*,*32*). For example, older adults are substantially less likely to experience a fever than are younger patients (*33*). Second, patients living in rural areas were more likely to experience a missed opportunity to diagnose coccidioidomycosis. Diagnostic delays among rural populations might be partially attributed to lack of access to medical care. Rural patients are substantially less likely to have access to healthcare, especially specialty services, and might lack access to some diagnostic tests and services (*34*,*35*). Similarly, we found that most missed diagnostic opportunities occurred in outpatient settings where less diagnostic testing is available than in hospital settings. Previous reports have also indicated that a large proportion of cases are diagnosed during hospital stays rather than during outpatient visits (*36*).

Patients with previous lung disease (e.g., asthma, COPD) or pulmonary imaging were also more likely to experience a missed opportunity, which is likely secondary to attributing the signs and symptoms associated with coccidioidomycosis to the patient's previous lung disease. Indeed, missed opportunities

Table 4. Results of exploratory logistic regression model in study of frequency and duration of diagnostic delays associated with coccidioidomycosis and risk factors for missed diagnoses, United States*

Potential risk factor	Odds ratio (95% CI)
Database source	
Commercial	Referent
Medicare	0.61 (0.47–0.78)
Medicaid	0.61 (0.48–0.77)
Age group, y	
<18	Referent
18–34	0.89 (0.77–1.00)
35–44	0.94 (0.82–1.08)
45–54	0.94 (0.81–1.06)
55–64	0.93 (0.82–1.05)
>65	1.48 (1.15–1.98)
Female sex	0.99 (0.93–1.05)
Rural location	1.27 (1.04–1.60)
Asthma diagnosis before delay window	1.34 (1.18–1.49)
COPD diagnosis before delay window	1.56 (1.36–1.80)
Chest CT before delay window	1.42 (1.26–1.61)
Chest radiography before delay window	1.21 (1.12–1.30)
Respiratory antibiotic prescriptions filled during delay window	3.42 (3.18–3.69)
Inhaler prescriptions filled during delay window	2.64 (2.34–2.99)

*Odds ratios corresponding to the odds of a patient experiencing a diagnostic delay are aggregated across bootstrap trials. The mean odds ratio along with 95% CI are reported across trials for each potential risk factor. See Appendix Table 3 (https://wwwnc.cdc.gov/EID/article/32/5/25-1421-App1.pdf) for effects associated with month and year. COPD, chronic obstructive pulmonary disorder; CT, computed tomography.

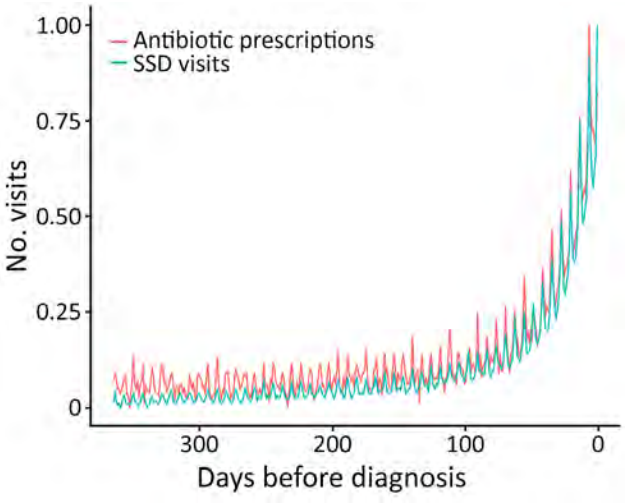

Figure 3. Number of patients with an outpatient antibiotic prescription or SSD visit each day before the index coccidioidomycosis diagnosis in study of frequency and duration of diagnostic delays associated with coccidioidomycosis and risk factors for missed diagnoses, United States**.** For comparison, both series have been minimum–maximum normalized between 0 and 1 to enable comparison of their trends; see Appendix Figure 2 (https://wwwnc.cdc.gov/EID/article/32/5/25-1421-App1.pdf) for raw counts of antibiotics before diagnosis. The trend in SSD visits and outpatient antibiotics exhibit a nearly identical pattern before diagnosis, with a similar increase occurring around 90 days before diagnosis. Those trends suggest an increase in unnecessary antibiotics prescribed in response to undiagnosed coccidioidomycosis symptoms before diagnosis. SSD, symptomatically similar diagnosis.

were associated with prescriptions for inhalers, suggesting that some missed opportunities were caused by clinicians attributing symptoms related to coccidioidomycosis to reactive or obstructive airway diseases. Comparable results have been reported for other lung infections, including tuberculosis (*25*) and histoplasmosis (*23*).

Surprisingly, patients living in Arizona were at higher risk of experiencing a missed diagnostic opportunity. We propose 2 possible reasons for this finding. First, in Arizona, the harder-to-diagnose cases (e.g., mild cases with subtle symptoms) might be diagnosed, but only after longer-than-average periods of time. However, in non–coccidioidomycosis-endemic regions, harder-to-diagnose cases might go undiagnosed altogether, leaving only the cases with classic symptoms, which are easier to diagnose. As a result, the time to diagnosis might appear shorter than it would otherwise in nonendemic regions. Second, although coccidioidomycosis is much more common in Arizona than in nonendemic regions, physicians in Arizona might not prioritize coccidioidomycosis as highly in their differential diagnosis because of a form of base-rate neglect. Indeed, physicians in nonendemic regions might consider coccidioidomycosis in their differential diagnosis as soon as history of travel to an endemic region is discovered. Rapid consideration of coccidioidomycosis is based on activation of a classical illness script rather than a consideration of the actual probability of disease risk. That overconsideration of coccidioidomycosis might help to reduce diagnosed delays for this disease outside of endemic regions.

Several studies have focused on the inappropriate use of antibiotics before the diagnosis of coccidioidomycosis (*13*–*16*,*37*,*38*); most patients receive an antibiotic before diagnosis, and a substantial proportion of patients receive multiple rounds of antibiotics (*38*). In a California study (*37*), 70% of patients testing positive for coccidioidomycosis received an antibiotic before diagnosis; the median number of antibiotic prescriptions for that population was 3. Our modeling framework enabled us to explore the potential association of antibiotic prescriptions and the likelihood of experiencing a missed opportunity before the coccidioidomycosis diagnosis. We found that persons who had been prescribed an antibiotic during the delay window had >3 times the odds of experiencing a missed opportunity. That finding might suggest that diagnostic delays are a potentially unappreciated harm with respect to inappropriate antibiotic use. Similar findings have been reported for tuberculosis (*25*), histoplasmosis (*23*), pertussis (*21*), herpes encephalitis (*24*), and sepsis (*20*). Current Infectious Diseases Society of America community-acquired pneumonia guidelines are silent on testing for endemic mycoses (*39*). Therefore, it might be useful for patients not improving on an initial course of antibiotics to be reevaluated for alternative diagnoses, including endemic mycoses, given their frequency in certain regions or after travel to high-risk areas.

The first limitation of this study is that we relied on administrative claims data that are routinely collected for billing purposes but might not capture key factors related to diagnostic delays. For example, we used diagnostic codes to identify cases of coccidioidomycosis and previous symptomatic visits. We did not have access to laboratory results or radiology reports to confirm cases of disease. We also did not have access to clinical notes that could have captured signs and symptoms not assigned to a diagnosis code. Thus, some patients with coccidioidomycosis might be misclassified, and symptoms that occurred before diagnosis might have been underidentified. In addition, although we have limited geographic data (i.e., enrollee state, metropolitan statistical area for

Commercial and Medicaid populations), details of travel history or localized exposures, which might be confounders in the diagnostic delay process, were unknown. Finally, the study population was restricted to commercially insured persons who were enrolled sometime during 2001–2022 and maintained continuous enrollment coverage for ≥1 year before diagnosis. That factor might limit generalizability to uninsured populations, persons who have frequent gaps in insurance coverage, or current and future patient populations outside the study period.

In conclusion, our study suggests that diagnostic delays in coccidioidomycosis are common and that multiple missed opportunities occur frequently. Raising clinician awareness and expanding access to timely diagnostic testing, particularly in outpatient settings, are critical steps toward improving outcomes for patients with coccidioidomycosis.

This work was supported in part by the Agency for Healthcare Research and Quality (grant no. R01HS027375 to P.M.P. and A.C.M.).

The data we used are not able to be shared. However, the data are available for purchase from Merative Marketscan. In addition, the bootstrapping procedure was implemented using the delaySim package (https:/github.com/aarmiller/delaySim), and the codes used for identifying cases along with diagnosis, procedure, and medication codes can be found at the GitHub repository (https://github.com/aarmiller/delay_diagnosis/publications/cocci).

P.M.P. has grant funding from Pfizer, Inc., and is a consultant for Eli Lilly, Inc. Neither are related to this article.

About the Author

Dr. Barber is an assistant professor of internal medicine in the Division of Pulmonary, Critical Care, and Occupational Medicine at the University of Iowa. His research involves medical education including work investigating diagnostic delays for pulmonary disorders.

References

1. Donovan FM, Ampel NM, Thompson GR III. Coccidioidomycosis. Infect Dis Clin North Am. 2025;39:183–97. https://doi.org/10.1016/j.idc.2024.11.012
2. Lockhart SR, Toda M, Benedict K, Caceres DH, Litvintseva AP. Endemic and other dimorphic mycoses in the Americas. J Fungi (Basel). 2021;7:151. https://doi.org/10.3390/jof7020151
3. Smith DJ, Williams SL, Benedict KM, Jackson BR, Toda M, Adame G, et al.; Endemic Mycoses State Partners Group. Surveillance for coccidioidomycosis, histoplasmosis, and blastomycosis—United States, 2019. MMWR Surveill Summ. 2022;71:1–14. https://doi.org/10.15585/mmwr.ss7107a1
4. Benedict K, McCotter OZ, Brady S, Komatsu K, Sondermeyer Cooksey GL, Nguyen A, et al. Surveillance for coccidioidomycosis—United States, 2011–2017. MMWR Surveill Summ. 2019;68:1–15. https://doi.org/10.15585/mmwr.ss6807a1
5. Engelthaler DM, Roe CC, Hepp CM, Teixeira M, Driebe EM, Schupp JM, et al. Local population structure and patterns of western hemisphere dispersal for *Coccidioides* spp., the fungal cause of Valley fever. MBio. 2016;7:e00550–16. https://doi.org/10.1128/mBio.00550-16
6. Williams SL, Chiller T. Update on the epidemiology, diagnosis, and treatment of coccidioidomycosis. J Fungi (Basel). 2022;8:666. https://doi.org/10.3390/jof8070666
7. Smith CE, Beard RR. Varieties of coccidioidal infection in relation to the epidemiology and control of the diseases. Am J Public Health Nations Health. 1946;36:1394–402. https://doi.org/10.2105/AJPH.36.12.1394
8. Valdivia L, Nix D, Wright M, Lindberg E, Fagan T, Lieberman D, et al. Coccidioidomycosis as a common cause of community-acquired pneumonia. Emerg Infect Dis. 2006;12:958–62. https://doi.org/10.3201/eid1206.060028
9. Dodge RR, Lebowitz MD, Barbee R, Burrows B. Estimates of *C. immitis* infection by skin test reactivity in an endemic community. Am J Public Health. 1985;75:863–5. https://doi.org/10.2105/AJPH.75.8.863
10. Adam RD, Elliott SP, Taljanovic MS. The spectrum and presentation of disseminated coccidioidomycosis. Am J Med. 2009;122:770–7. https://doi.org/10.1016/j.amjmed.2008.12.024
11. Odio CD, Marciano BE, Galgiani JN, Holland SM. Risk factors for disseminated coccidioidomycosis, United States. Emerg Infect Dis. 2017;23:308–11. https://doi.org/10.3201/eid2302.160505
12. Galgiani JN, Ampel NM, Blair JE, Catanzaro A, Geertsma F, Hoover SE, et al. 2016 Infectious Diseases Society of America (IDSA) clinical practice guideline for the treatment of coccidioidomycosis. Clin Infect Dis. 2016;63:e112–46. https://doi.org/10.1093/cid/ciw360
13. Chang DC, Anderson S, Wannemuehler K, Engelthaler DM, Erhart L, Sunenshine RH, et al. Testing for coccidioidomycosis among patients with community-acquired pneumonia. Emerg Infect Dis. 2008;14:1053–9. https://doi.org/10.3201/eid1407.070832
14. Khan MA, Brady S, Komatsu KK. Testing for coccidioidomycosis in emergency departments in Arizona. Med Mycol. 2018;56:900–2. https://doi.org/10.1093/mmy/myx112
15. Donovan FM, Wightman P, Zong Y, Gabe L, Majeed A, Ynosencio T, et al. Delays in coccidioidomycosis diagnosis and associated healthcare utilization, Tucson, Arizona, USA. Emerg Infect Dis. 2019;25:1745–7. https://doi.org/10.3201/eid2509.190023
16. Tartof SY, Benedict K, Xie F, Rieg GK, Yu KC, Contreras R, et al. Testing for coccidioidomycosis among community-acquired pneumonia patients, southern California, USA. Emerg Infect Dis. 2018;24:779–81. https://doi.org/10.3201/eid2404.161568
17. McHardy IH, Barker B, Thompson GR III. Review of clinical and laboratory diagnostics for coccidioidomycosis. J Clin Microbiol. 2023;61:e0158122. https://doi.org/10.1128/jcm.01581-22
18. Tsang CA, Anderson SM, Imholte SB, Erhart LM, Chen S, Park BJ, et al. Enhanced surveillance of coccidioidomycosis, Arizona, USA, 2007–2008. Emerg Infect Dis. 2010;16:1738–44. https://doi.org/10.3201/eid1611.100475
19. Ginn R, Mohty R, Bollmann K, Goodsell J, Mendez G, Bradley B, et al. Delays in coccidioidomycosis diagnosis and

relationship to healthcare utilization, Phoenix, Arizona, USA. Emerg Infect Dis. 2019;25:1742–4. https://doi.org/10.3201/eid2508.190019
20. Struble RD, Arakkal AT, Cavanaugh JE, Polgreen PM, Miller AC. Evaluating potential missed opportunities to prevent, treat, or diagnose sepsis: a population-based retrospective study of insurance claims. Crit Care Explor. 2025;7:e1240. https://doi.org/10.1097/CCE.0000000000001240
21. Evans NJ, Arakkal AT, Cavanaugh JE, Newland JG, Polgreen PM, Miller AC. The incidence, duration, risk factors, and age-based variation of missed opportunities to diagnose pertussis: a population-based cohort study. Infect Control Hosp Epidemiol. 2023;44:1629–36. https://doi.org/10.1017/ice.2023.31
22. Erickson BA, Miller AC, Warner HL, Drobish JN, Koeneman SH, Cavanaugh JE, et al. Understanding the prodromal period of necrotizing soft tissue infections of the genitalia (Fournier's gangrene) and the incidence, duration, and risk factors associated with potential missed opportunities for an earlier diagnosis: a population-based longitudinal study. J Urol. 2022;208:1259–67. https://doi.org/10.1097/JU.0000000000002920
23. Miller AC, Arakkal AT, Koeneman SH, Cavanaugh JE, Thompson GR, Baddley JW, et al. Frequency and duration of, and risk factors for, diagnostic delays associated with histoplasmosis. J Fungi (Basel). 2022;8:438. https://doi.org/10.3390/jof8050438
24. Miller AC, Koeneman SH, Arakkal AT, Cavanaugh JE, Polgreen PM. Incidence, duration, and risk factors associated with missed opportunities to diagnose herpes simplex encephalitis: a population-based longitudinal study. Open Forum Infect Dis. 2021;8:ofab400. https://doi.org/10.1093/ofid/ofab400
25. Miller AC, Arakkal AT, Koeneman S, Cavanaugh JE, Gerke AK, Hornick DB, et al. Incidence, duration and risk factors associated with delayed and missed diagnostic opportunities related to tuberculosis: a population-based longitudinal study. BMJ Open. 2021;11:e045605. https://doi.org/10.1136/bmjopen-2020-045605
26. Miller AC, Arakkal AT, Koeneman SH, Cavanaugh JE, Polgreen PM. A clinically-guided unsupervised clustering approach to recommend symptoms of disease associated with diagnostic opportunities. Diagnosis (Berl). 2022;10:43–53. https://doi.org/10.1515/dx-2022-0044
27. Miller AC, Cavanaugh JE, Arakkal AT, Koeneman SH, Polgreen PM. A comprehensive framework to estimate the frequency, duration, and risk factors for diagnostic delays using bootstrapping-based simulation methods. BMC Med Inform Decis Mak. 2023;23:68. https://doi.org/10.1186/s12911-023-02148-w
28. Suneja M, Beekmann SE, Dhaliwal G, Miller AC, Polgreen PM. Diagnostic delays in infectious diseases. Diagnosis (Berl). 2022;9:332–9. https://doi.org/10.1515/dx-2021-0092
29. Benedict K, Ireland M, Weinberg MP, Gruninger RJ, Weigand J, Chen L, et al. Enhanced surveillance for coccidioidomycosis, 14 US States, 2016. Emerg Infect Dis. 2018;24:1444–52. https://doi.org/10.3201/eid2408.171595
30. Benedict K, Hennessee I, Cooksey GS, Donovan FM, Thompson GR, Williamson T, et al. Comparison of patients with coccidioidomycosis in Arizona versus California: a commercial health insurance claims analysis. Open Forum Infect Dis. 2025;12:ofaf405. https://doi.org/10.1093/ofid/ofaf405
31. Mouton CP, Bazaldua OV, Pierce B, Espino DV. Common infections in older adults. Am Fam Physician. 2001;63:257–68.
32. Garibaldi RA, Nurse BA. Infections in the elderly. Am J Med. 1986;81(1a):53–8. https://doi.org/10.1016/0002-9343(86)90514-0
33. Miller AC, Koeneman SH, Suneja M, Cavanaugh JE, Polgreen PM. Diurnal temperature variation and the implications for diagnosis and infectious disease screening: a population-based study. Diagnosis (Berl). 2023;11:54–62. https://doi.org/10.1515/dx-2023-0074
34. Johnston KJ, Wen H, Joynt Maddox KE. Lack Of access to specialists associated with mortality and preventable hospitalizations of rural Medicare beneficiaries. Health Aff (Millwood). 2019;38:1993–2002. https://doi.org/10.1377/hlthaff.2019.00838
35. Douthit N, Kiv S, Dwolatzky T, Biswas S. Exposing some important barriers to health care access in the rural USA. Public Health. 2015;129:611–20. https://doi.org/10.1016/j.puhe.2015.04.001
36. Pu J, Donovan FM, Ellingson K, Leroy G, Stone J, Bedrick E, et al. Clinician practice patterns that result in the diagnosis of coccidioidomycosis before or during hospitalization. Clin Infect Dis. 2021;73:e1587–93. https://doi.org/10.1093/cid/ciaa739
37. Chi GC, Benedict K, Beer KD, Jackson BR, McCotter O, Xie F, et al. Antibiotic and antifungal treatment among persons with confirmed coccidioidomycosis—southern California, 2011. Med Mycol. 2020;58:411–3. https://doi.org/10.1093/mmy/myz073
38. Hayes JF, Nix DE. Challenges facing antimicrobial stewardship programs in the endemic region for coccidioidomycosis. Open Forum Infect Dis. 2024;11:ofae041. https://doi.org/10.1093/ofid/ofae041
39. Metlay JP, Waterer GW, Long AC, Anzueto A, Brozek J, Crothers K, et al. Diagnosis and treatment of adults with community-acquired pneumonia. an official clinical practice guideline of the American Thoracic Society and Infectious Diseases Society of America. Am J Respir Crit Care Med. 2019;200:e45–67. https://doi.org/10.1164/rccm.201908-1581ST

Address for correspondence: Philip M. Polgreen, University of Iowa, Department of Internal Medicine, Division of Infectious Diseases, 200 Hawkins Dr, Iowa City, IA 52242, USA; email: philip-polgreen@uiowa.edu

Zoonotic and Anthroponotic *Plasmodium* spp. Circulation between Wild Primates and Indigenous Community, Peruvian Amazon, 2007–2020

Gabriela M. Ulloa, Alex D. Greenwood, Omar E. Cornejo, Henar Alonso, Meddly L. Santolalla Robles, Stephanie Montero, Andres G. Lescano, Pedro Mayor

Malaria transmission at the human–wildlife interface remains poorly characterized in the Amazon. We conducted a molecular survey of *Plasmodium* spp. in an Indigenous community (n = 141) and sympatric nonhuman primates (NHPs) (n = 341; 10 species) in the Peruvian Amazon during 2007–2020. By using nested or quantitative PCR (targeting *cytb, cox3, and 18S rRNA genes*) and sequencing, we estimated prevalence, parasite load, and genetic similarity. We detected *Plasmodium* in 43.3% of humans and 51.9% of NHPs. *P. vivax*/*simium* predominated in humans (42.1%), whereas *P. brasilianum/malariae* predominated in NHPs (24.6%). *P. falciparum* was rare in both hosts. Children ≤8 years of age showed higher parasite load than older persons. Bayesian phylogenies revealed >99.9% identity among human and NHP lineages, supporting shared *Plasmodium* lineages. NHP lineages showed low interannual variation. One third of human infections were asymptomatic. Our findings reveal hidden reservoirs and support integrating wildlife surveillance into Amazon malaria elimination strategies.

Malaria parasites of nonhuman primates (NHPs) are increasingly recognized for their zoonotic potential and complicate malaria control efforts (*1*). The first report of a zoonotic malaria parasite capable of infecting humans was *Plasmodium knowlesi*, which emerged as a major cause of human malaria in Southeast Asia (*2*). In South America, *P. brasilianum* (morphologically, genetically, and immunologically indistinguishable from *P. malariae*) (*3*) and *P. simium* (closely related to *P. vivax*) (*4*) parasites have been detected in NHPs and implicated in zoonotic infections (*5*,*6*).

The Amazon basin harbors high biodiversity and dense human–wildlife overlap, particularly within Indigenous territories (*7*). Indigenous Peoples and local communities live in malaria-endemic areas with limited access to health systems and maintain close contact with wildlife (*8*), which creates favorable conditions for cross-species transmission of pathogens, including malaria parasites (*9*). This convergence of factors amplifies the risk for zoonotic and anthroponotic malaria transmission. Reports of natural infections with *P. vivax*, *P. simium*, *P. brasilianum*, *P. malariae*, and *P. falciparum* parasites in all neotropical NHP families underscore their potential reservoir role (*8*,*10*–*12*). Furthermore, experimental infections of neotropical NHPs with zoonotic malaria parasites from Asia raise concerns about the vulnerability of NHPs to emerging zoonoses (*13*).

Despite global declines in malaria incidence (*14*), progress in the Amazon is hindered by ecologic complexity, vector diversity, and high rates of subpatent infections (*15*). A recent study conducted in a remote

Author affiliations: Universidade Federal Rural da Amazônia, Belém-Pará, Brazil (G.M. Ulloa); Universidad Científica del Sur, Lima, Peru (G.M. Ulloa); Leibniz-Institute for Zoo and Wildlife Research, Berlin, Germany (A.D. Greenwood); Freie Universität Berlin, Berlin (A.D. Greenwood); University of California Santa Cruz, Santa Cruz, California, USA (O.E. Cornejo); University of Zaragoza, Zaragoza, Spain (H. Alonso); Universidad Peruana Cayetano Heredia, Lima (M.L. Santolalla Robles, S. Montero, A.G. Lescano); Universidad Peruana de Ciencias Aplicadas, Lima (S. Montero); Universitat Autònoma de Barcelona, Bellaterra-Barcelona, Spain (P. Mayor); Comunidad de Manejo de Fauna Silvestre en la Amazonía y en Latinoamérica, Iquitos, Peru (P. Mayor); Museo de Culturas Indígenas Amazónicas, Iquitos (P. Mayor)

DOI: https://doi.org/10.3201/eid3205.251695

community in the northeastern Peruvian Amazon reported a *P. vivax* prevalence of 56.0% based on quantitative PCR (qPCR) results; nearly half of the infections were submicroscopic, highlighting the persistence of hidden reservoirs despite ongoing control interventions (*16*). Subclinical and mixed infections, common in malaria-endemic areas, evade standard diagnostics and are rarely captured in surveillance systems (*17*). Despite this fact, malaria-control efforts remain focused on *P. falciparum* and *P. vivax* parasites, and little attention is given to NHP-associated species such as *P. brasilianum* or *P. malariae* (*18*).

Detecting hidden transmission dynamics requires highly sensitive, specific molecular tools and ethical field strategies (*19*,*20*). In remote forest settings, community-based methods, such as analyzing blood from legal subsistence hunting, can provide access to hard-to-reach wildlife populations while respecting Indigenous sovereignty (*21*). We investigated the molecular epidemiology of *Plasmodium* infections in sympatric humans and NHPs within a remote Indigenous territory in the Peruvian Amazon. By using blood samples from 141 Indigenous inhabitants and 341 neotropical NHPs (from 10 species) hunted for subsistence during an 11-year long-range wildlife collection program, we applied multigene molecular diagnostics and phylogenetic analysis to assess parasite prevalence, diversity, and evidence of cross-species transmission.

Methods

Study Area

We conducted this study in the Yavari-Mirin River basin, a remote upland forest region in the northeastern Peruvian Amazon. The area spans 107,000 hectares and includes a single Indigenous Yagua community, Nueva Esperanza, inhabited by 343 people in 2020. The community is located 302 km from the city of Iquitos and is surrounded by high biodiversity, including preserved populations of 14 NHP species (*22*). Malaria is endemic in the region; *P. vivax* is the most prevalent species. Villagers depend on subsistence activities (e.g., hunting, fishing, other forestry resources, and small-scale agriculture) and opportunistically trade wood, fish, wild meat, and agricultural products (Figure 1).

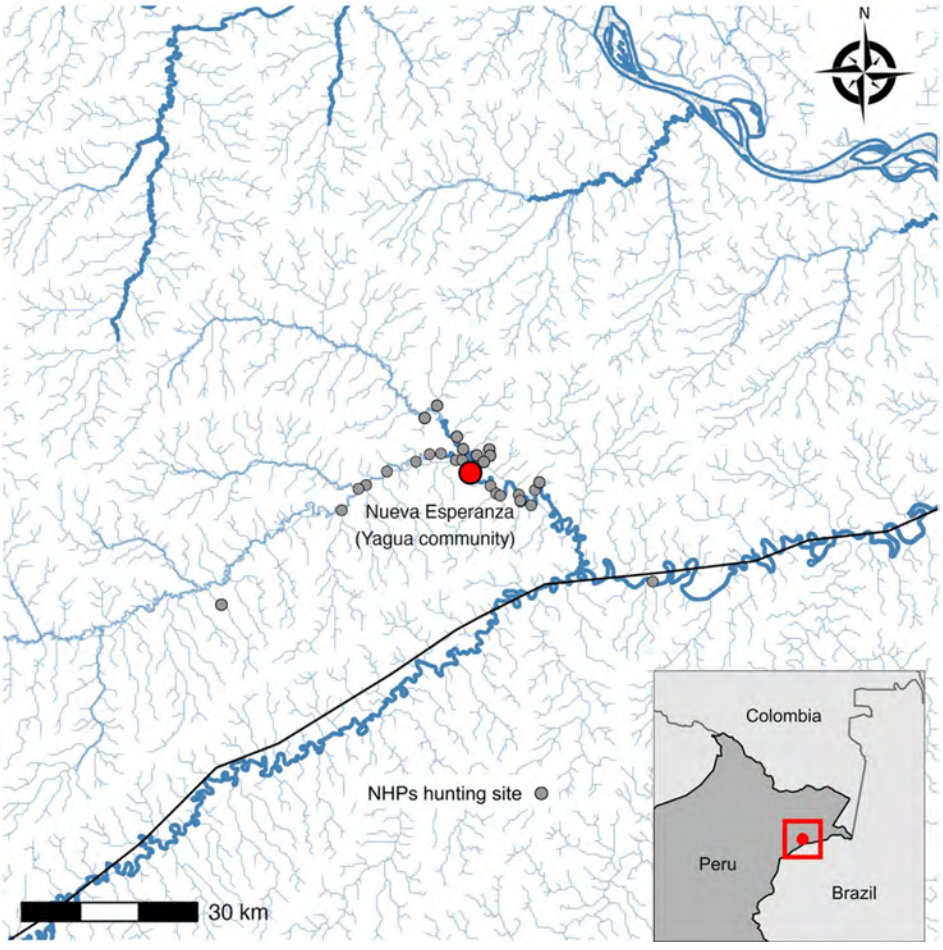

Figure 1. Geographic location of study of zoonotic and anthroponotic *Plasmodium* spp. circulation between wild primates and Indigenous community, Peruvian Amazon, 2007–2020. Red dot indicates Yagua Indigenous community of Nueva Esperanza, located along the Yavarí-Mirín River near the Peru–Brazil border. Gray dots represent locations of legally hunted nonhuman primates sampled during 2007–2020. Inset map indicates location of community (indicated by red dot in red square) at Peru–Brazil border.

Ethical Considerations

All human study procedures were approved by the Ethics Committees of Universidad Peruana Cayetano Heredia (approval no. 102142), Universitat Autònoma of Barcelona (Comisión de Ética en la Experimentación Animal y Humana approval no. 4829), and Hospital Clínic of Barcelona (approval no. HCB/2019/1107) and authorized by local and regional authorities of Nueva Esperanza (approval no. 267–2019-GRL-DRSL/30.09.01). NHP sampling was approved by the Peruvian Forest and Wildlife Service (approval no. 258–2019-MINAGRI-SERFOR-DGGSPFFS) and the Institutional Animal Use Ethics Committee of the Universidad Peruana Cayetano Heredia. We exported wildlife samples under Servicio Nacional Forestal y de Fauna Silvestre permits (nos. 003258/SP, 003260/SP, 003568-SERFOR, and 003579-SERFOR).

Study Design and Blood Samples

In February 2020, we conducted a cross-sectional survey in Nueva Esperanza. We obtained whole blood samples through venipuncture from 141 participants (41.1% of the population) with informed consent, assent, or both. We referred participants with microscopic or clinical suspicion of malaria during the study to the community health center and treated them according to malaria management guidelines of Peru's Ministry of Health (Supreme Decree no. 273–2025-MINSA).

In addition, we collected 17 samples from field workers; 5 were microscopically positive for *P. vivax* and had symptoms compatible with *P. vivax* infection; we molecularly analyzed samples of 3 of those workers and included results for sequence comparison only. Given the frequent malaria reports in Nueva Esperanza, field researchers received doxycycline as malaria chemoprophylaxis, in accordance with US Centers for Disease Control and Prevention (CDC) recommendations (*23*).

During 2007–2020, we collected dried blood spots (DBS) from 341 free-ranging NHPs (representing 10 species and 4 families) as part of a long-term wildlife monitoring program. Local hunters, trained in ethical sample collection, collected blood onto filter paper during postmortem handling of legally hunted animals. Species, sex, and date were recorded. The procedure was performed for all groups of mammals and birds (not only for wild NHPs) to avoid encouraging hunting of NHPs. The species sampled included 143 Poeppig's woolly monkeys (*Lagothrix lagothrica poeppigii*), 57 large-headed capuchin monkeys (*Sapajus macrocephalus*), 43 black spider monkeys (*Ateles chamek*), 29 Ucayali bald uakaris (*Cacajao calvus ucayalii*), 21 red howler monkeys (*Alouatta seniculus*), 19 Humboldt's white-fronted capuchin monkeys (*Cebus albifrons*), 16 monk saki (*Pithecia monachus*), 8 Ecuadorian squirrel monkeys (*Saimiri macrodon*), 4 coppery titi monkeys (*Plecturocebus cupreus*), and 1 brown-mantled tamarin (*Leontocebus fuscicollis*).

Microscopic Examination

We examined thick blood smears for 135 participants; 10 were positive and all confirmed by molecular assays. Because of low positivity and variable slide quality, we excluded microscopic examination results from analyses.

Molecular Diagnosis of *Plasmodium* Species

We extracted DNA from whole blood and DBS by using the AllPrep DNA/RNA Mini Kit (QIAGEN, https://www.qiagen.com). We collected all DBS from NHP in remote field conditions during 2007–2020, often with low DNA concentration and partial degradation. Therefore, we selected molecular targets to maximize sensitivity in cases of low parasitaemia and degraded material.

We detected parasites by using 2 nested PCRs and 2 commercial VIASURE qPCR diagnostic kits (Certest Biotec, https://www.certest.es) targeting mitochondrial cytochrome oxidase b (*cytb*), cytochrome c oxidase III (*cox3*), and *18S SSU rRNA* genes. For quantitative analyses, we generated a standard curve by using serial dilutions of the kit's Malaria Quantitative Standard (≈2×10^7 copies/μL) to estimate genome copy number. We converted cycle threshold values to DNA copies/μL and $\log_{10}$-transformed for statistical comparisons. Because of gene *18S rRNA* copy number variability among *Plasmodium* species, our estimates reflect relative (not absolute) parasitemia.

Partial Amplification of *cytb* Gene

We performed nested PCR (nPCR) for *cytb* to detect *Plasmodium* spp. parasites in both humans and NHP samples, as described previously (*24*). PCRs included appropriate positive and negative controls and were processed under protocols that prevented contamination. We sequenced amplicons for species confirmation.

Validation of *Plasmodium* spp. Detection

We validated a subset of 54 human and 81 NHPs samples at Leibniz Institute for Zoo and Wildlife Research (Berlin, Germany) (Figure 2) by using *cox3* nPCR and sequencing. The *cox3* nPCR uses genus-specific primers for the primary PCR, whereas the

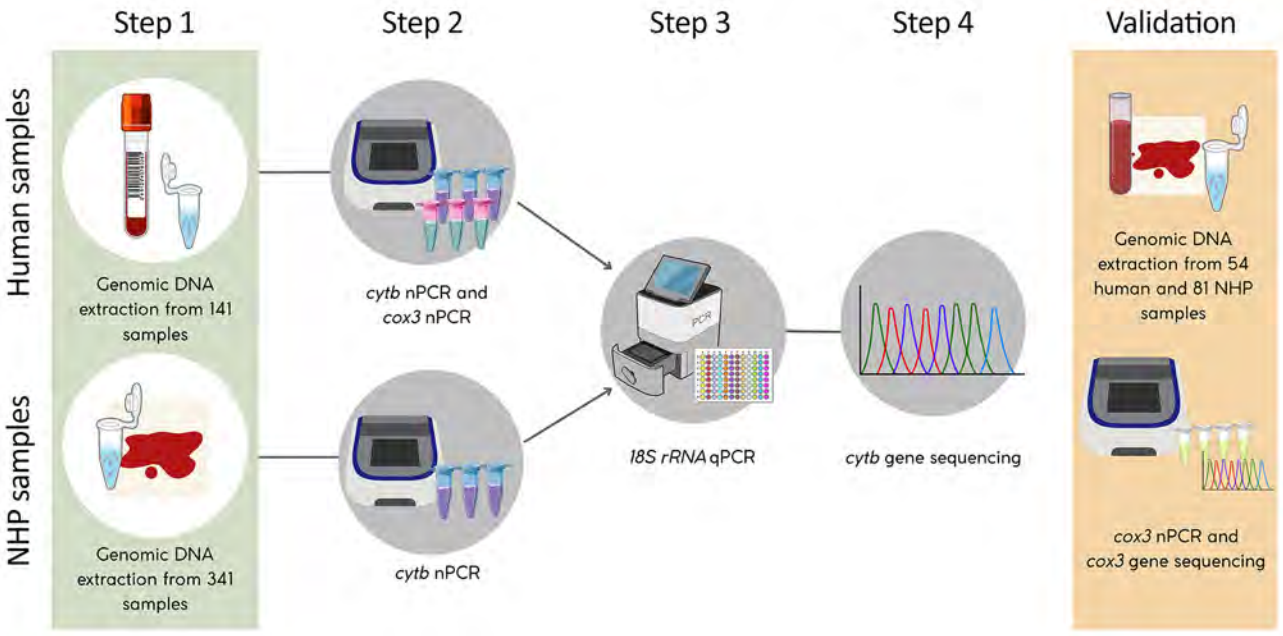

Figure 2. Workflow for molecular detection and validation of *Plasmodium* spp. infections in study of zoonotic and anthroponotic *Plasmodium* spp. circulation between wild primates and Indigenous community, Peruvian Amazon, 2007–2020. Schematic of laboratory procedures show DNA extraction and detection of *Plasmodium* spp. in human and NHP blood samples using qPCR (targeting *18S rRNA* gene) and nPCR targeting mitochondrial genes (*cytb* and *cox3*). Selected samples underwent sequencing for species confirmation and external validation. *cytb*, cytochrome oxidase b; *cox3*, cytochrome c oxidase III; NHP, nonhuman primate; nPCR, nested PCR; qPCR, quantitative PCR.

secondary PCR uses species-specific primers. The genus-specific primers were designed to avoid regions of high sequence similarity to human mitochondrial DNA, and each species-specific primer pair differs by ≥7 nucleotides at the 3′ end, which is critical for specificity. We used the oligonucleotides 5′-CTC GCC ATT TGA TAG CGG TTA ACC-3′ (forward) and 5′-CCT GTT ATC CCC GGC GAA CCT TC-3′ (reverse) as primers, as previously described (*25*), with some modifications: we performed first-round PCR in 25-µL reactions with 2 µM of each primer, 12.5 µL 2X MyTaq Mix (Meridian Bioscience, https://www.meridianbioscience.com), and 5 µL of template DNA. We conducted thermocycling: 96°C for 1 minute, followed by 40 cycles of 96°C for 10 seconds, 63°C for 1 minute, 72°C for 1 minute, and a final extension at 72°C for 10 minutes.

Nested reactions used 2.5 µL of 1:50-diluted PCR product, 4 µM primers, and 10 µL of 2X MyTaq Mix. We conducted cycling on *P. falciparum* and *P. vivax*/*P. simium* samples: 96°C for 1 minute; 30 cycles of 96°C for 10 seconds, 54°C for 1.5 minute, 72°C for 1 minute; and final extension at 72°C for 10 minutes. We applied the same protocol for *P. brasilianum*/*P. malariae* with 58 °C annealing. We gel-purified and sequenced amplicons for species confirmation. We performed nPCR separately for *P. falciparum*, *P. vivax*/*P. simium*, and *P. brasilianum*/*P. malariae* to generate sequences (Appendix Table 1, https://wwwnc.cdc.gov/EID/article/32/5/25-1695-App1.pdf).

Statistical Analysis

We analyzed data in R version 4.4.2 (The R Project for Statistical Computing, https://www.r-project.org). We estimated associations between symptoms and *Plasmodium* infection by using prevalence ratios and 95% CIs. We inferred parasite load from cycle threshold values converted to genome copy number (DNA copies/µL) by using a standard curve based on *Plasmodium 18S rRNA* qPCR and expressed these values as $\log_{10}$(DNA/µL + 1).

We assessed differences by age (≤8 years vs. >8 years) and symptom status using Welch's t-tests or Wilcoxon tests. We used linear regression models (Gaussian family, identity link) to evaluate age–symptom interactions.

We analyzed interannual NHPs prevalence by using a generalized linear model (binomial family, logit link) with host species and year as predictors. We assessed temporal stability by using coefficients of variation (CV), which we calculated as the SD divided by the mean prevalence per host–parasite pair; lower CV values indicated more stable infection patterns.

We compared patristic distances by using Kruskal-Wallis test and used pairwise Wilcoxon tests with Holm correction for multiple comparisons. We evaluated diagnostic agreement by using positive percent agreement (PPA), negative percent agreement (NPA), Cohen kappa coefficient, and percent concordance, using *cytb* nPCR sequencing as the reference standard. We defined statistical significance at $\alpha = 0.05$.

Phylogenetic Analysis

We manually inspected chromatograms and corrected them for base-calling errors. We assembled consensus sequences in Geneious Prime version 2025.0.3 (Geneious, https://www.geneious.com) (*26*). We performed multiple sequence alignment in Geneious using the Clustal-Omega algorithm and visually trimmed ambiguous regions, resulting in final alignments of ≈776 bp of the mitochondrial *cytb* gene.

We inferred preliminary phylogenies by using the neighbor-joining method with 1,000 bootstrap replicates. We selected the best-fit nucleotide substitution model according to the Akaike information criterion in MEGA version 11.0.13 (*27*). We reconstructed final trees by using maximum-likelihood in FastTree version 2.1.11 (*28*) and Bayesian inference in MrBayes version 3.2.6 (*29*), applying the selected substitution model in both. Bayesian inference analyses consisted of 2 independent runs of 3 million generations, sampling every 1,000 generations, and a 25% burn-in.

We included reference *Plasmodium* sequences from GenBank and PlasmoDB to contextualize the evolutionary placement of lineages detected in humans and NHPs. Those sequences were *P. falciparum*, *P. vivax* (Sal-I, P01, PAM), *P. simium*, *P. malariae*, *P. brasilianum*, and rodent (*P. chabaudi*, *P. vinckei*, *P. berghei*, and *P. yoelii*) and avian (*P. gallinaceum* and *P. relictum*) *Plasmodium* species. The Apicomplexa parasite *Toxoplasma gondii* served as the outgroup. In addition, we incorporated 3 sequences from symptomatic field researchers, confirmed as *P. vivax* infections by microscopic examination and qPCR to assess their phylogenetic relationship with community-derived human and NHP infections.

Data Availability

Anonymized metadata will be available upon reasonable request. Sequence data are in GenBank (accession nos. PV769906–68 and PV786447–592) (Appendix Table 2). Protocols are available at https://www.protocols.io (Appendix).

Results

Prevalence of *Plasmodium* spp. in Humans and NHPs

Among 141 human participants, we detected *Plasmodium* parasites in 35.5% (50/141) by qPCR and in 43.3% (61/141) by *cytb* nPCR. In 341 NHPs, prevalence reached 31.2% (69/221) by qPCR) and 51.9% (177/341) by *cytb* nPCR. Species-specific qPCR revealed *P. vivax*/*P. simium* in 30.5% (43/141) of samples, including 2 *P. falciparum* co-infections (1.4% [2/141]). Five samples were positive only at genus-level by qPCR. *cytb* nPCR sequencing confirmed *P. vivax*/*P. simium* in 42.1% (58/141) of participants, with single cases of *P. falciparum* and *P. brasilianum*/*P. malariae* (0.7% [1/141 each]). Species-level identification was successful in 98.4% (60/61) of nPCR-positive samples.

Among 110 persons for whom data were complete, 38 (34.6%) reported malaria-like symptoms (e.g., fever, headache, vomiting, nausea, pallor, or diarrhea). Of qPCR-positive patients, 16 (37.2%) were asymptomatic. Symptomatic persons were 3.8 times more likely to test positive (prevalence ratio 3.82 [95% CI 2.13–6.88]) (Table 1).

In NHPs, qPCR detected *P. brasilianum*/*P. malariae* in 25.8% (57/221), *P. vivax*/*P. simium* in 3.2% (7/221), and *P. falciparum* in 0.5% (1/221). *cytb* nPCR sequencing confirmed *P. brasilianum*/*P. malariae* in 24.6% (84/341), *P. vivax*/*P. simium* in 17.9% (61/341), and *P. falciparum* in 0.3% (1/341) (Table 2). Sequencing success was 82.5% (146/177).

We observed no statistically significant interannual trend for *P. brasilianum*/*P. malariae* in NHPs ($p = 0.414$). However, host-specific variation emerged. Ucayali bald uakaris showed low interannual variation (CV 0.20, n = 29), suggesting stable *P. brasilianum*/*P. malariae* transmission. Poeppig's woolly monkeys also showed sustained *P. brasilianum*/*P. malariae* prevalence (CV 0.26, n = 143). For *P. vivax*/*P. simium*, Humboldt's white-fronted capuchin monkeys had the most consistent pattern (CV 0.36, n = 19), whereas black spider monkeys and large-headed capuchin monkeys showed more fluctuation (Figure 3; Appendix Table 3).

Parasite Load

Participants (n = 141) included 84 women (59.6%) and 57 men (40.4%). Median age was 21 years (interquartile range 11–35, range 3–79 years); 9 participants (6.4%) were ≤8 years of age. Children <8 years of age had significantly higher relative parasite DNA levels inferred from qPCR (mean +SD $\log_{10}$ 2.4 ±1.1 vs. 0.9 ±0.8; $p = 0.005$) than older persons (Figure 4). We

Table 1. Association between clinical symptoms and *Plasmodium* spp. quantitative PCR results in 110 members of Indigenous Yagua community, Nueva Esperanza, Loreto region, Peru, 2020*

Result	No. (%) asymptomatic persons, n = 72	No. (%) symptomatic persons, n = 38†	Prevalence ratio (95% CI)‡	p value§
Negative	56 (77.8)	11 (28.9)	Referent	<0.001
Positive	16 (22.2)	27 (71.1)	3.82 (2.13–6.88)	

*Prevalence ratios and 95% CIs estimated by using the cohort.count method in epiR (The R Project for Statistical Computing, https://www.r-project.org).
†Defined as persons reporting ≥1 malaria-related symptom (e.g., fever, headache, vomiting, nausea, pallor, or diarrhea) at the time of sampling.
‡Calculated by using asymptomatic persons as reference.
§By Fisher exact test.

found no significant differences in parasite load between symptomatic and asymptomatic participants. Linear modeling showed higher relative parasite loads in young children (β = 1.28, p = 0.020), independent of symptoms. We found no interaction between age and symptom status (p = 0.750).

In NHPs, *P. brasilianum*/*P. malariae* infections had higher relative parasite DNA levels than *P. vivax*/*P. simium* (1.2 ± 0.8 vs. 0.6 ± 0.3; p<0.001). *P. vivax* in humans showed higher relative loads than *P. vivax*/*P. simium* in NHPs (p = 0.044), whereas *P. vivax* in humans and *P. brasilianum*/*P. malariae* in NHPs had similar densities (p = 0.851) (Table 3; Appendix Figure 2). Among NHPs, Ucayali bald uakaris exhibited significantly higher *P. brasilianum*/*P. malariae* relative loads than did Poeppig's woolly monkeys (1.4 ±0.9 vs. 0.8 ±0.6; p = 0.020) (Figure 5).

Sequence and Phylogenetic Analysis

We analyzed a total of 209 partial *cytb* sequences, consisting of 60 human sequences, 3 sequences from fieldworkers, and 146 sequences from NHPs. Intraspecific and interspecific patristic distances based on *cytb* sequences revealed marked differences in genetic divergence among *Plasmodium* species across host groups (χ^2 = 11.18 by Kruskal-Wallis test; degrees of freedom = 4, p<0.001). Human sequences had lower genetic divergence (mean 0.007) than did NHPs (mean 0.03; p<0.001). *P. vivax*/*P. simium* sequences from both hosts had very low divergence (mean 0.0007); *P. brasilianum*/*P. malariae* sequences showed even lower divergence (mean 0.0005, p<0.001). We found *P. falciparum* in 1 human and 1 NHP, with 99.6% identity.

Bayesian phylogenetics revealed 3 clades: *P. vivax*/*P. simium*, *P. brasilianum*/*P. malariae*, and *P. falciparum*. Most (96.7% [58/60]) human sequences and 41.8% (61/146) of NHP sequences clustered within the *P. vivax*/*P. simium* clade (Figure 6). All fieldworkers' sequences also clustered within *P. vivax*/*P. simium*. Sequences clustering within the *P. brasilianum*/*P. malariae*clade comprised 57.5% (84/146) of NHP and 1.7% (1/60) of human sequences. *P. falciparum* appeared in 1 human and 1 NHP. FastTree and neighbor-joining trees matched the Bayesian results, showing consistent clustering and no host-specific structuring (Appendix Figures 3, 4).

Validation of *Plasmodium* Detection

We reanalyzed a subset of 54 human and 81 NHP samples at Leibniz Institute for Zoo and Wildlife Research by using *cox3* nPCR. In humans, we confirmed *P. vivax*/*P. simium* in 31.5% (17/54) and mixed infections in 11.1% (6/54). Laboratory concordance

Table 2. Prevalence of *Plasmodium* spp. detected by nested PCR targeting *cytb* gene in 341 nonhuman primates from 10 species sampled in Yavarí-Mirín River basin, Loreto region, Peru, 2007–2020*

Host species	Total no. samples	*Plasmodium* spp., no. (%)	*P. brasilianum* or *P. malariae*, no. (%)	*P. vivax* or *P. simium*, no. (%)	*P. falciparum*, no (%)
Atelidae	207	92 (44.44)	43 (22.75)	31 (16.40)	0
Lagothrix lagothrica poeppigii	143	57 (39.86)	32 (24.24)	14 (10.61)	0
Ateles chamek	43	18 (41.86)	5 (12.82)	9 (23.08)	0
Alouatta seniculus	21	17 (80.95)	6 (33.33)	8 (44.44)	0
Cebidae	84	48 (57.14)	15 (20.27)	23 (31.08)	0
Sapajus macrocephalus	57	26 (45.61)	5 (9.80)	15 (29.41)	0
Cebus albifrons	19	14 (73.68)	7 (41.18)	5 (29.41)	0
Saimiri macrodon	8	8 (100)	3 (50.00)	3 (50.00)	0
Pitheciidae	49	36 (73.47)	24 (53.33)	7 (15.56)	1 (2.22)
Cacajao calvus ucayalii	29	22 (75.86)	18 (66.67)	2 (7.41)	0
Pithecia monachus	16	10 (62.50)	6 (40.00)	2 (13.33)	1 (6.67)
Plecturocebus cupreus	4	4 (100)	1 (25.00)	3 (75.00)	0
Callitrichidae	1	1 (100)	1 (100)	0	0
Leontocebus fuscicollis	1	1 (100)	1 (100)	0	0
Total	341	177 (51.91)	84 (24.63)	61 (17.89)	1 (0.29)

*Data presented by taxonomic group and species. Percentages reflect proportion of positive persons for each parasite species within sampled group. Prevalence values calculated relative to total persons per host species.

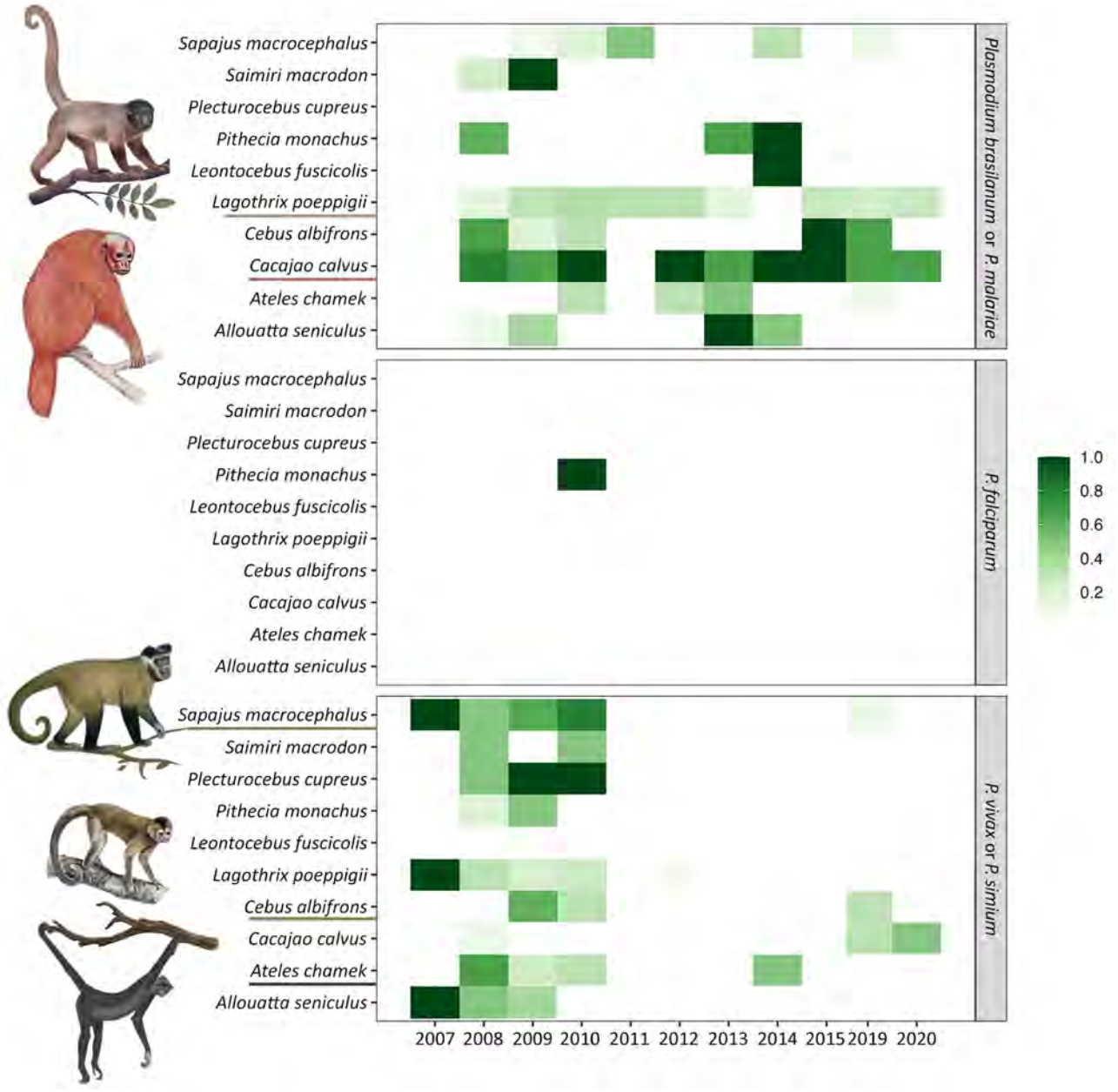

Figure 3. Annual prevalence of *Plasmodium* spp. infections in wild nonhuman primate species detected in study of zoonotic and anthroponotic *Plasmodium* spp. circulation between wild primates and Indigenous community, Peruvian Amazon, 2007–2020. Prevalence of cytochrome oxidase b nested PCR–detected infections are shown for 10 nonhuman primate species sampled during 2007–2015, 2019, and 2020 in the Yavarí-Mirín River basin, Loreto region, Peru. Each tile indicates the proportion of infected persons for a given host–parasite pair, by year (shading intensity reflects prevalence). Illustrations and underlining highlight taxa with more stable or recurrent infection patterns.

was 83.3% (kappa 0.66). In NHPs, we confirmed *P. brasilianum*/*P. malariae* in 19.8% (16/81) and *P. vivax*/*P. simium* in 16.1% (13/81). Agreement metrics were as follows: PPA 25.4%, NPA 95.2%, kappa 0.08. For *P. brasilianum*/*P. malariae* only, agreement metrics were PPA 44.0%, NPA 100.0%, and kappa 0.40. We consistently recovered major parasite lineages across laboratories and markers, indicating the robustness of detecting dominant parasite lineages despite low interlaboratory concordance for wildlife samples attributable to low DNA concentration and partial degradation (Appendix Figure 5).

Discussion

The challenge facing infectious disease studies in free-ranging wild animals lies in the accessibility

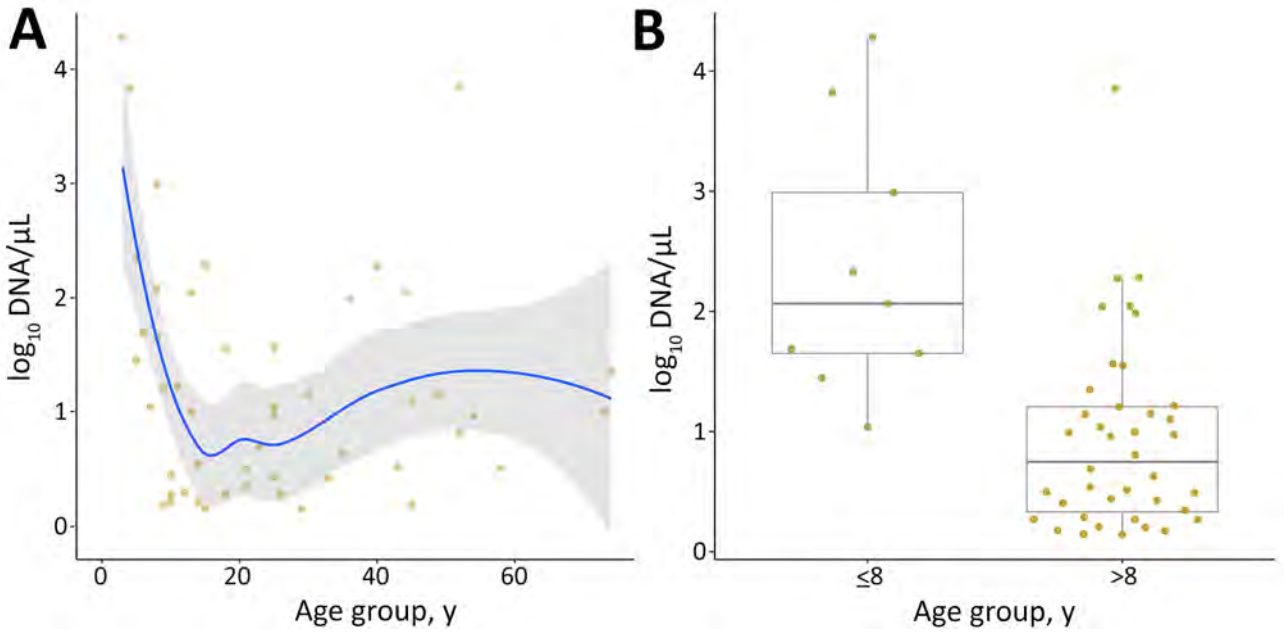

Figure 4. Age-specific parasite load in humans based on quantitative PCR targeting for *Plasmodium* spp. *18S rRNA* genes in study of zoonotic and anthroponotic *Plasmodium* spp. circulation between wild primates and Indigenous community, Peruvian Amazon, 2007–2020. A) Smoothed regression of log-transformed parasite DNA concentration, by age, in 49 persons. B) Boxplot comparing parasite loads between children ≤8 years and older persons. Higher parasite loads occurred in younger age groups. Horizontal lines within boxes indicate medians; box tops and bottoms indicate interquartile range (25th–75th percentiles); error bars indicate 1.5 × interquartile range.

of biological material. Therefore, we implemented a culturally sensitive and sustainable surveillance approach on the basis of blood samples from discarded byproducts of legal subsistence hunting by Indigenous Peoples, respecting national laws and local practices and enabling long-term access to remote, well-preserved ecosystems, regions that are typically underrepresented in public health and zoonotic research (*20*).

Our results revealed a high prevalence of *Plasmodium* spp. in both humans and NHPs. *P. vivax* and *P. simium* were dominant in humans, whereas *P. brasilianum* and *P. malariae* predominated in NHPs and included sporadic *P. falciparum* co-infections. Parasite load decreased with age in humans, suggesting development of partial immunity from around 8 years of age, consistent with previous evidence of early adaptive immune response to *P. vivax* (*30*).

Nonetheless, one third of infections were asymptomatic, highlighting the role of subclinical carriage in sustaining silent transmission (*31*). In addition, similar findings in the remote community of Santa Emilia, in the northeastern Peruvian Amazon, indicated 44.0% submicroscopic *P. vivax* infections, underscoring the widespread presence of low-parasitemia reservoirs across the Peruvian Amazon (*16*). However, our study extends this evidence to sympatric wild primates, revealing a broader eco-epidemiologic interface of *Plasmodium* spp. circulation.

Assay performance varied by host and sample type, particularly in cases of low parasitaemia and long-term stored DBS from NHPs. Differences between qPCR (targeting the *18S rRNA* gene) and nPCR (targeting the *cytb* gene) probably reflect gene copy number variation (*32*). Incorporating an independent *cox3* nPCR improved confirmation of infection and detection of coinfections, enhancing resolution for subpatent infections in both hosts. However, large-scale implementation remains challenging because of structural barriers, limited access to healthcare, and reliance on suboptimal diagnostic tools, which contribute to underreporting of malaria

Table 3. Comparison of parasite load, by host and *Plasmodium* species, based on quantitative PCR targeting *18S rRNA* gene in humans and NHPs from the Yavarí-Mirín River basin, Loreto region, Peru*

Host	Parasite species	log_{10} DNA/µL, mean ±SD	Comparison	p value
NHP, n = 57	*P. brasilianum*/*P. malariae*	1.2 ±0.8	vs. *P. vivax*/*P. simium* (NHP)	0.023
NHP, n =7	*P. vivax*/*P. simium*	0.6 ±0.3	vs. *P. vivax*/*P. simium* (human)	0.044
Human, n = 43	*P. vivax*/*P. simium*	1.2 ±1.0	vs. *P. brasilianum*/*P. malariae* (NHP)	0.851

*Parasite load expressed as log_{10}-transformed DNA concentration per µL. Statistical comparisons performed using pairwise tests between groups. NHP, nonhuman primate.

cases and are critical obstacles to effective surveillance and control (*33*).

Molecular and phylogenetic analyses confirmed *P. vivax*/*P. simium* and *P. brasilianum*/*P. malariae* in both hosts. Although human sampling occurred in 2020 and NHP samples spanned 2007–2020, several human sequences matched NHP sequences collected more than a decade earlier, suggesting long-term maintenance of shared *Plasmodium* lineages across hosts, rather than recent spillover. Human *P. vivax*/*P. simium* sequences showed high mitochondrial similarity, consistent localized outbreaks, whereas greater diversity in NHPs indicates their role as long-term reservoirs.

Plasmodium spp. prevalence in NHPs ranged from 33% to 52% and exhibited species-specific variation. Ucayali bald uakaris (*C. c. ucayalii*), Poeppig's woolly monkeys (*L. l. poeppigii*), Humboldt's white-fronted capuchin monkeys (*C. albifrons*), black spider monkeys (*A. chamek*), and large-headed capuchin monkeys (*S. macrocephalus*) showed higher relative parasite DNA levels and stable infections, potentially reflecting differences in host susceptibility, immune tolerance, ecologic exposure, and evolutionary history (*34*). Low-grade chronic infections in NHPs might parallel asymptomatic infections in humans (*35*). Of note, the uakari (*C. c. ucayalii*) of Peru is classified as a vulnerable species because of its restricted distribution (*36*). This species has distinctive red facial vasculature and shows consistently higher relative parasitaemia than animals from sympatric taxa (*37*). Although the biologic basis of this pattern remains unclear, it may reflect species-specific ecologic or physiologic traits rather than host–parasite coevolution.

The single *P. falciparum* detection in a wild NHP (monk saki [*P. monachus*]), confirmed by 2 independent molecular assays, probably represents anthroponotic spillover. This finding underscores the permeability between human and animal malaria cycles and the need to monitor bidirectional transmission (*10*,*11*).

Our study provides longitudinal molecular evidence of *Plasmodium* spp. circulation in wild Amazonian NHPs (from 10 species) and 341 humans over an 11-year period. This approach, which integrated wildlife and human screening in parallel, provided a unique ecologic and temporal view of malaria dynamics in a remote Indigenous territory. Endemic *P. brasilianum*/*P. malariae* maintenance in wildlife contrasts with sporadic, low-parasitaemia *P. vivax*/*P. simium* detection. This pattern might reflect a complex eco-immunologic balance (*34*,*35*) in which *P. vivax*/*P. simium* circulates at undetectable levels in adapted NHP hosts, whereas *P. brasilianum*/*P. malariae* persists more overtly. Relative parasite DNA levels inferred from qPCR in *P. vivax*/*P. simium*–infected NHPs were ≈4 times lower than in local humans with low parasitaemia, reinforcing the need for sensitive and specific surveillance tools to detect cryptic reservoirs. However, that result should be interpreted cautiously, given that molecular estimates do not replace measurements acquired through microscopic examination.

Our findings carry important implications for malaria elimination. In Amazonian contexts, where humans and wildlife are closely linked through ecology and culture, traditional surveillance might miss important sources of transmission. Asymptomatic human infections and cryptic wildlife reservoirs add complexity to malaria ecology, reinforcing the need for One Health approaches that integrate wildlife monitoring and sensitive diagnostics.

One limitation of our study is that NHP samples were obtained opportunistically, taking advantage of waste materials from subsistence hunting; therefore, species representation reflects ecologic, behavioral,

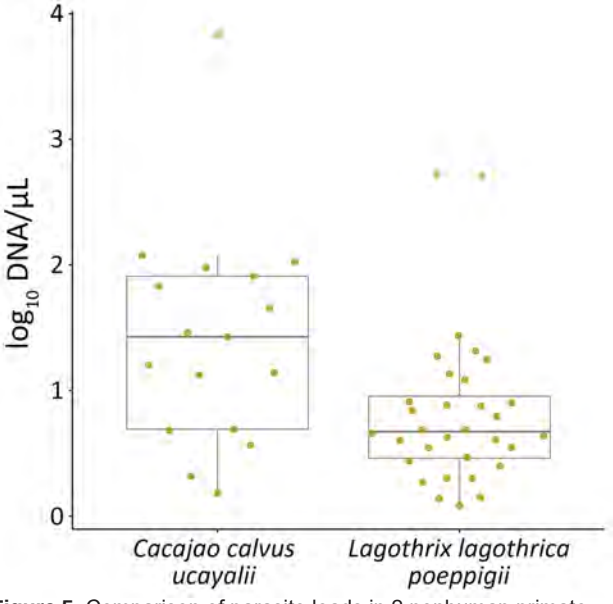

Figure 5. Comparison of parasite loads in 2 nonhuman primate species with *Plasmodium brasilianum* or *P. malariae* infections in study of zoonotic and anthroponotic *Plasmodium* spp. circulation between wild primates and Indigenous community, Peruvian Amazon, 2007–2020. Relationship boxplots of log-transformed *P. brasilianum* or *P. malariae* DNA concentration in 17 Ucayali bald uakaris (*Cacajao calvus ucayalii*) and 31 Poeppig's woolly monkeys (*Lagothrix lagothrica poeppigii*), highlighting species-specific differences in parasitaemia. Horizontal lines within boxes indicate medians; box tops and bottoms indicate interquartile range (25th–75th percentiles); error bars indicate 1.5 × interquartile range.

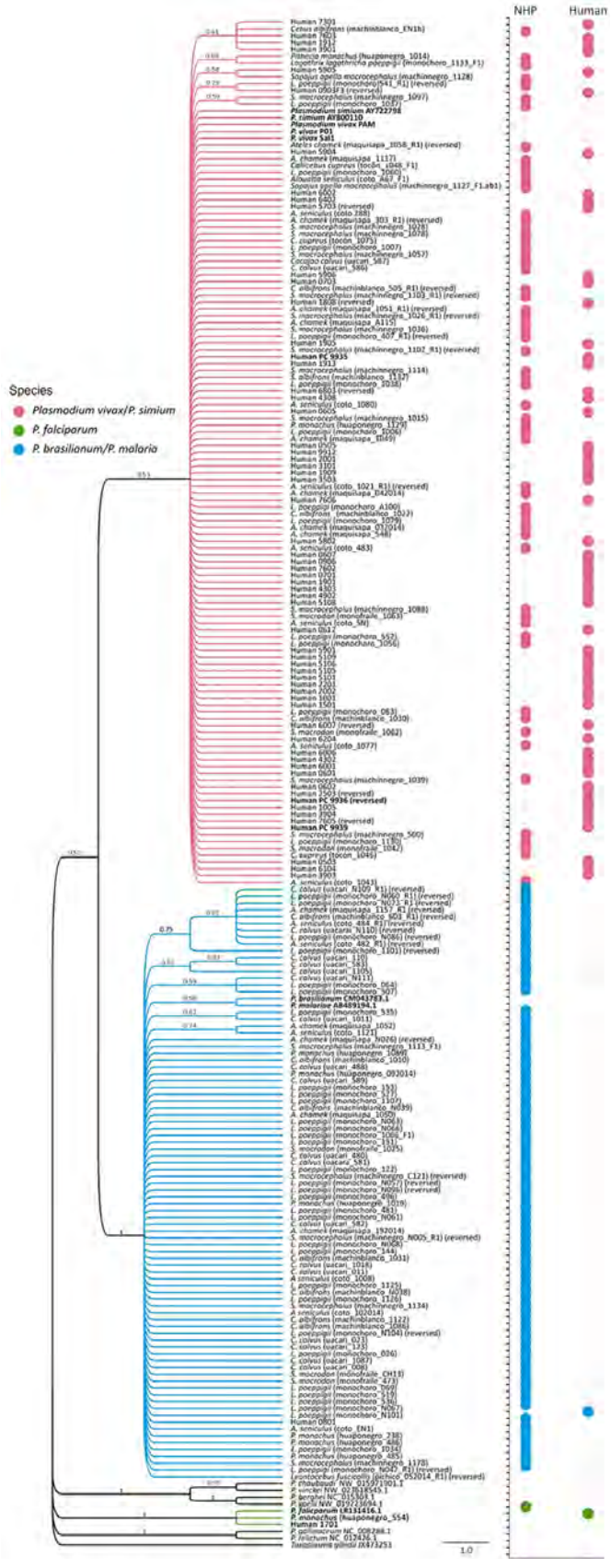

Figure 6. Bayesian phylogeny of *Plasmodium* spp. from humans and nonhuman primates in study of zoonotic and anthroponotic *Plasmodium* spp. circulation between wild primates and Indigenous community, Peruvian Amazon, 2007–2020. Phylogenetic tree shows cytochrome oxidase b gene sequences (≈776 bp) obtained from 60 humans and 146 wild nonhuman primates sampled in the Yavarí-Mirín River basin, Loreto region, Peru. Tree reconstructed by using Bayesian inference (209 sequences). Tip symbols denote host origin (human or nonhuman primates) and are color-coded by species: pink, *P. vivax* or *P. simium*; blue, *P. brasilianum* or *P. malariae*; and green, *P. falciparum*; black, reference sequences. Bold type indicates sequences from fieldworkers with confirmed *P. vivax* infection.

and seasonal factors, as well as hunter preferences influencing hunting practices, rather than the full primate community (*38*). Prevalence estimates thus should be interpreted carefully. We inferred parasite load from molecular data, and relative parasite DNA levels derived from qPCR should be interpreted cautiously because they do not replace parasitaemia measurements acquired through microscopic examination. We selected mitochondrial markers to optimize amplification from long-term storage DBS, low-parasitaemia samples, prioritizing sensitivity over fine-scale taxonomic resolution, but their limited resolution constrains discrimination between closely related parasites such as *P. vivax* and *P. simium*.

In conclusion, this study demonstrates that *Plasmodium* spp. transmission in the Peruvian Amazon involves overlapping human and NHPs reservoirs and that distinct parasite species predominate in each host. We show high prevalence of *P. vivax*/*P. simium* in humans and sustained circulation of *P. brasilianum*/*P. malariae* across multiple NHP species over more than a decade, confirming long-term maintenance of malaria parasites in wildlife. Detection of asymptomatic human infections and low-parasitaemia infections in NHPs highlights a hidden transmission layer that is largely missed by routine surveillance. Those findings indicate that malaria elimination efforts in Amazonian forest settings face additional challenges from cryptic reservoirs at the human–wildlife interface. Integrating sensitive molecular diagnostics and wildlife-informed surveillance within a One Health framework will be essential to reduce the risk for persistent transmission and reemergence in remote Indigenous territories.

Acknowledgments

We are very grateful to the people of Nueva Esperanza for their hospitality and their support in collecting biologic samples. We thank the Regional Directorate of Health and Management of Indigenous Affairs of the Regional Government of Loreto, the Iquitos Air Wing No. 5 of the Peruvian Air Force, the Municipality and the Health Medical Center of Islandia, the Comité Permanente de Atención Integral en Salud of the Scientific Society of San Fernando (Universidad Nacional Mayor de San Marcos), Campamento Universitario Multidisciplinario de Investigación y Servicio, volunteer students of human medicine and biology from the National University of the Peruvian Amazon, Winnie Michelle Contreras-Marmolejo, Arturo Mamani-Salce and the team of the Research Unit in Emerging Diseases and Climate Change of the Peruvian University Cayetano Heredia, Ricardo Gamboa, Katherina Alicia Viscaychipi, Milagritos Fernández Larrauri, and the team of physicians including Janet Cordori Carpio, Jackeline Magaly Tinoco Figueroa, Cristian Hipólito Andonaire Munaico, Augusto Gavino Escalante Candía, Saúl Javier Santiváñez Salazar, Sabina Mendivil Tuchia, and José Antonio Salinas Morales. We thank Karin Hönig for technical support. We thank Andree Valle-Campos for his advice on data analysis and graphics in R. We thank Alfredo Mayor and members of the Malaria Group of ISGlobal Barcelona of the Hospital Clinic of the University of Barcelona for their hospitality and support in carrying out the sample analysis.

This work was supported by ERANet-LAC (project no. ERANet17/HLH-0271), research projects (contract nos. 136-2018-FONDECYT, AC18/00054 Instituto de Salud Carlos, and Conselho Nacional de Desenvolvimento Científico e Tecnológico–400800/2019-5), and a training grant (no 2D43 TW007393) awarded to A.G.L. by the Fogarty International Center of the US National Institutes of Health. G.M.U. had 2 fellowships from Programa de Pós-graduação em Saúde e Produção Animal na Amazônia by Conselho Nacional de Desenvolvimento Científico e Tecnológico: a doctoral fellowship (GD modality; fellowship no. 140312/2020-0) and a doctoral sandwich fellowship (SWE modality; fellowship no. 201546/2020-5).

About the Author

Dr. Ulloa is a molecular eco-epidemiologist specializing in *Plasmodium* parasites at the human–wildlife interface. Her work integrates molecular diagnostics, population genomics, and evolutionary ecology to investigate zoonotic malaria transmission and host–parasite adaptation in the Amazon Basin.

References

1. Grigg MJ, Snounou G. *Plasmodium simium*: a Brazilian focus of anthropozoonotic vivax malaria? Lancet Glob Health. 2017;5:e961–2. https://doi.org/10.1016/S2214-109X(17)30343-1
2. Barber BE, Rajahram GS, Grigg MJ, William T, Anstey NM. World malaria report: time to acknowledge *Plasmodium knowlesi* malaria. Malar J. 2017;16:135. https://doi.org/10.1186/s12936-017-1787-y
3. Bajic M, Ravishankar S, Sheth M, Rowe LA, Pacheco MA, Patel DS, et al. The first complete genome of the simian malaria parasite *Plasmodium brasilianum*. Sci Rep. 2022; 12:19802. https://doi.org/10.1038/s41598-022-20706-6
4. Brasil P, Zalis MG, de Pina-Costa A, Siqueira AM, Júnior CB, Silva S, et al. Outbreak of human malaria caused by *Plasmodium simium* in the Atlantic Forest in Rio de Janeiro: a molecular epidemiological investigation. Lancet Glob Health. 2017;5:e1038–46. https://doi.org/10.1016/S2214-109X(17)30333-9
5. Lalremruata A, Magris M, Vivas-Martínez S, Koehler M, Esen M, Kempaiah P, et al. Natural infection of *Plasmodium*

brasilianum in humans: man and monkey share quartan malaria parasites in the Venezuelan Amazon. EBioMedicine. 2015;2:1186–92. https://doi.org/10.1016/j.ebiom.2015.07.033
6. de Alvarenga DAM, Culleton R, de Pina-Costa A, Rodrigues DF, Bianco C Jr, Silva S, et al. An assay for the identification of *Plasmodium simium* infection for diagnosis of zoonotic malaria in the Brazilian Atlantic Forest. Sci Rep. 2018;8:86. https://doi.org/10.1038/s41598-017-18216-x
7. Pimm SL, Jenkins CN, Abell R, Brooks TM, Gittleman JL, Joppa LN, et al. The biodiversity of species and their rates of extinction, distribution, and protection. Science. 2014;344:1246752. https://doi.org/10.1126/science.1246752
8. de Abreu FVS, dos Santos E, Mello ARL, Gomes LR, de Alvarenga DAM, Gomes MQ, et al. Howler monkeys are the reservoir of malarial parasites causing zoonotic infections in the Atlantic forest of Rio de Janeiro. Fuehrer HP, editor. PLoS Negl Trop Dis. 2019;13:e0007906.
9. Ferreira LM, Rezende HR, Fux B, De Alencar FEC, Loss AC, Buery JC, et al. *Anopheles* (*Kerteszia*) *cruzii* infected by *Plasmodium* in the Atlantic Forest indicates that the malaria transmission cycle is maintained even after howler monkeys' population decline. Parasitol Res. 2022;121:3627–34. https://doi.org/10.1007/s00436-022-07689-z
10. Chaves A, Dolz G, Ibarra-Cerdeña CN, Núñez G, Ortiz-Malavasi E E, Bernal-Valle S, et al. Presence and potential distribution of malaria-infected New World primates of Costa Rica. Malar J. 2022;21:17. https://doi.org/10.1186/s12936-021-04036-y
11. Silva TRM, Barros FNL, Bahia M, Sampaio Junior FD, Santos SSF, Inoue LS, et al. *Plasmodium vivax* and *Plasmodium falciparum* infection in neotropical primates in the western Amazon, Brazil. Zoonoses Public Health. 2019;66:798–804. https://doi.org/10.1111/zph.12626
12. Fuehrer HP, Campino S, Sutherland CJ. The primate malaria parasites *Plasmodium malariae*, *Plasmodium brasilianum* and *Plasmodium ovale* spp.: genomic insights into distribution, dispersal and host transitions. Malar J. 2022;21:138. https://doi.org/10.1186/s12936-022-04151-4
13. Hang JW, Tukijan F, Lee EQH, Abdeen SR, Aniweh Y, Malleret B. Zoonotic malaria: non–*Laverania Plasmodium* biology and invasion mechanisms. Pathogens. 2021;10:889. https://doi.org/10.3390/pathogens10070889
14. WHO. World malaria report 2022 [cited 2023 Mar 28]. https://www.who.int/teams/global-malaria-programme/reports/world-malaria-report-2022
15. Recht J, Siqueira AM, Monteiro WM, Herrera SM, Herrera S, Lacerda MVG. Malaria in Brazil, Colombia, Peru and Venezuela: current challenges in malaria control and elimination. Malar J. 2017;16:273. https://doi.org/10.1186/s12936-017-1925-6
16. Ramirez R, Torres K, Rodríguez P, Acosta C, Guzmán-Guzmán M, Llanos-Cuentas A, et al. High prevalence, genetic diversity and temporal differentiation of *Plasmodium vivax* in a remote hard-to-reach community from the Peruvian Amazon region. Am J Trop Med Hyg. 2025;113:990–6. https://doi.org/10.4269/ajtmh.24-0662
17. Almeida GG, Costa PAC, Araujo MS, Gomes GR, Carvalho AF, Figueiredo MM, et al. Asymptomatic *Plasmodium vivax* malaria in the Brazilian Amazon: submicroscopic parasitemic blood infects *Nyssorhynchus darlingi*. PLoS Negl Trop Dis. 2021;15:e0009077.
18. Cunha MG, Santos CS, Raiol M, Costa SPT, Ventura AMR, Póvoa MM, et al. Mixed *Plasmodium malariae* infections were underdetected in a malaria endemic area in the Amazon region, Brazil. Am J Trop Med Hyg. 2021;105:1184–6. https://doi.org/10.4269/ajtmh.21-0296
19. Estrada A, Garber PA, Rylands AB, Roos C, Fernandez-Duque E, Di Fiore A, et al. Impending extinction crisis of the world's primates: why primates matter. Sci Adv. 2017;3:e1600946. https://doi.org/10.1126/sciadv.1600946
20. Cáceres L, Calzada JE, Gabster A, Young J, Márquez R, Torres R, et al. Social representations of malaria in the Guna indigenous population of Comarca Guna de Madungandi, Panama. Malar J. 2017;16:256. https://doi.org/10.1186/s12936-017-1899-4
21. Jacob M, Medeiros Souza A, Martins de Carvalho A, Alves de Vasconcelos Neto CF, Tregidgo D, Hunter D, et al. Food biodiversity as an opportunity to address the challenge of improving human diets and food security. Ethnobiology and Conservation. 2023;12. https://doi.org/10.15451/ec2023-02-12.05-1-14
22. Mayor P, Pérez-Peña P, Bowler M, Puertas PE, Kirkland M, Bodmer R. Effects of selective logging on large mammal populations in a remote indigenous territory in the northern Peruvian Amazon. Ecol Soc. 2015;20:art36. https://doi.org/10.5751/ES-08023-200436
23. Centers for Disease Control and Prevention. Malaria. In: Brunette GW, Nemhauser JB, editors. CDC Yellow Book 2020: health information for international travel. New York: Oxford University Press; 2019.
24. Ulloa GM, Greenwood AD, Cornejo OE, Monteiro FOB, Scofield A, Santolalla Robles ML, et al. Phylogenetic congruence of *Plasmodium* spp. and wild ungulate hosts in the Peruvian Amazon. Infect Genet Evol. 2024;118:105554. https://doi.org/10.1016/j.meegid.2024.105554
25. Isozumi R, Fukui M, Kaneko A, Chan CW, Kawamoto F, Kimura M. Improved detection of malaria cases in island settings of Vanuatu and Kenya by PCR that targets the *Plasmodium* mitochondrial cytochrome c oxidase III (*cox3*) gene. Parasitol Int. 2015;64:304–8. https://doi.org/10.1016/j.parint.2014.09.006
26. Kearse M, Moir R, Wilson A, Stones-Havas S, Cheung M, Sturrock S, et al. Geneious Basic: an integrated and extendable desktop software platform for the organization and analysis of sequence data. Bioinformatics. 2012;28:1647–9. https://doi.org/10.1093/bioinformatics/bts199
27. Kumar S, Stecher G, Tamura K. MEGA7: Molecular Evolutionary Genetics Analysis version 7.0 for bigger datasets. Mol Biol Evol. 2016;33:1870–4. https://doi.org/10.1093/molbev/msw054
28. Price MN, Dehal PS, Arkin AP. FastTree: computing large minimum evolution trees with profiles instead of a distance matrix. Mol Biol Evol. 2009;26:1641–50. https://doi.org/10.1093/molbev/msp077
29. Huelsenbeck JP, Ronquist F. MRBAYES: Bayesian inference of phylogenetic trees. Bioinformatics. 2001;17:754–5. https://doi.org/10.1093/bioinformatics/17.8.754
30. Ome-Kaius M, Kattenberg JH, Zaloumis S, Siba M, Kiniboro B, Jally S, et al. Differential impact of malaria control interventions on *P. falciparum* and *P. vivax* infections in young Papua New Guinean children. BMC Med. 2019;17:220. https://doi.org/10.1186/s12916-019-1456-9
31. Villasis E, Garcia Castillo SS, Guzman M, Torres J, Gomez J, Garro K, et al. Epidemiological characteristics of *P. vivax* asymptomatic infections in the Peruvian Amazon. Front Cell Infect Microbiol. 2022;12:901423. https://doi.org/10.3389/fcimb.2022.901423
32. Echeverry DF, Deason NA, Davidson J, Makuru V, Xiao H, Niedbalski J, et al. Human malaria diagnosis using a single-step direct-PCR based on the *Plasmodium* cytochrome oxidase III gene. Malar J. 2016;15:128. https://doi.org/10.1186/s12936-016-1185-x

33. Ministerio de Salud del Perú. Análisis de situación de salud de los pueblos indígenas de la Amazonía, viviendo en el ámbito de las cuatro cuencas y el Río Chambira. 2020 Dec 1 [cited 2025 May 24]. https://www.gob.pe/institucion/minsa/informes-publicaciones/1893891-analisis-de-situacion-de-salud-de-los-pueblos-indigenas-de-la-amazonia-viviendo-en-el-ambito-de-las-cuatro-cuencas-y-el-rio-chambira
34. Monteiro EF, Fernandez-Becerra C, Araujo MDS, Messias MR, Ozaki LS, Duarte AMRC, et al. Naturally acquired humoral immunity against malaria parasites in non-human primates from the Brazilian Amazon, Cerrado and Atlantic Forest. Pathogens. 2020;9:525. https://doi.org/10.3390/pathogens9070525
35. de Assis GMP, de Alvarenga DAM, Costa Pereira MO, Sánchez-Arcila JC, de Pina Costa A, de Souza Junior JC, et al. Profiling humoral immune response against pre-erythrocytic and erythrocytic antigens of malaria parasites among neotropical primates in the Brazilian Atlantic Forest. Front Cell Infect Microbiol. 2021;11:678996. https://doi.org/10.3389/fcimb.2021.678996
36. Ennes Silva F, Valsecchi do Amaral J, Roos C, Bowler M, Röhe F, Sampaio R, et al. Molecular phylogeny and systematics of bald uakaris, genus *Cacajao* (Primates: Pitheciidae), with the description of a new species. Mol Phylogenet Evol. 2022;173:107509. https://doi.org/10.1016/j.ympev.2022.107509
37. Mayor P, Mamani J, Montes D, González-Crespo C, Sebastián MA, Bowler M. Proximate causes of the red face of the bald uakari monkey (*Cacajao calvus*). R Soc Open Sci. 2015;2:150145. https://doi.org/10.1098/rsos.150145
38. Rosin C, Swamy V. Variable density responses of primate communities to hunting pressure in a western Amazonian River Basin. Neotrop Primates. 2013;20:25–31. https://doi.org/10.1896/044.020.0105

Address for correspondence: Gabriela M. Ulloa, Grupo de Enfermedades Infecciosas Re-emergentes, Universidad Científica del Sur, Crta. Panamericana sur km 19, Lima 15067, Peru; email: gulloau92@gmail.com

Investigation of and Response to Autochthonous Dengue, Los Angeles County, California, USA, August–November 2024

Aisling M. Vaughan, Claire Park, Van P. Ngo, Zuelma A. Contreras, Jordan John Lee, Phoebe Danza, Meredith Haddix, Olivia Moir, Nicole Green, Michael Brown, Taylor Burleson, Amy Marutani, Ashley Nicholas, Tristan Hallum, Steve Vetrone, Liza Ortiz, Gladys Fernandez, Eric El-Tobgy, Jose Escobar, Tricia-Nicole Gandela, Cristin Mondy, Jan King, Brandon Dean, Elizabeth Rubin, Pablo Valadez, Stella Fogleman, Dawn Terashita, Sharon Balter, Umme-Aiman Halai

Dengue is not endemic in the continental United States; most cases occur in returning travelers. During August–November 2024, a total of 14 locally acquired cases of dengue were identified in Los Angeles County, California, USA. Epidemiologic evidence indicates that locally acquired cases occurred in several neighborhoods, suggesting short transmission chains after introductions from returning travelers. In one neighborhood, evidence supported ongoing transmission for up to 7 weeks. Median patient age was 54 (range 5–79) years; 8 (57%) patients were female and 6 (43%) male, and 6 (43%) required hospitalization. Delays in healthcare seeking and diagnoses were noted; median time from symptom onset to specimen collection for dengue testing was 9 (range 2–34) days. Local dengue transmission in Los Angeles County highlights the emerging threat of mosquitoborne disease transmission in nonendemic areas and the need for rapid and coordinated public health and vector control responses to interrupt transmission.

Dengue, a mosquitoborne disease caused by 4 dengue virus types (DENV-1–4), is transmitted mainly by *Aedes aegypti* and *Ae. albopictus* mosquitoes. Symptoms usually appear 2–7 days after infection and can include fever, headache, retro-orbital pain, joint and muscle pain, and rash. Most cases are mild, but severe dengue can cause bleeding, shock, and death. Dengue causes substantial global illness and death. In 2024, global incidence reached record levels (*1*); ≈13 million cases were reported in the Americas, far surpassing previous years (*2*). Dengue is not endemic in the continental United States; most cases occur in returning travelers, but sporadic local transmission has been documented, including in California (*3*).

Dengue is reportable in Los Angeles County (LAC), California, where a marked increase in travel-associated cases has been observed. In 2024, a total of 222 travel-associated cases were reported in the LAC Department of Public Health (LACDPH) jurisdiction, compared with 35 during 2022 and 75 during 2023, closely mirroring global increases in dengue activity. In addition, sporadic locally acquired dengue cases were reported by the Pasadena and Long Beach Public Health Departments in LAC in 2023; however, no evidence of sustained transmission was identified (*4*,*5*).

On August 30, 2024, LACDPH was notified of a positive dengue laboratory result for a person with no recent travel history. Subsequently, several additional autochthonous dengue cases were identified across LAC. We describe the public health and vector control measures implemented during August–November 2024 to rapidly identify cases and prevent further local transmission.

Author affiliations: Epidemic Intelligence Service, Centers for Disease Control and Prevention, Atlanta, Georgia, USA (A.M. Vaughan); Los Angeles County Department of Public Health, Los Angeles, California, USA (A.M. Vaughan, C. Park, V.P. Ngo, Z.A. Contreras, J.J. Lee, P. Danza, M. Haddix, O. Moir, L. Ortiz, G. Fernandez, E. El-Tobgy, J. Escobar, T.-N. Gandela, C. Mondy, J. King, B. Dean, E. Rubin, P. Valadez, S. Fogleman, D. Terashita, S. Balter, U.-A. Halai); Public Health Laboratory, Los Angeles (N. Green, M. Brown, T. Burleson, A. Marutani, A. Nicholas); San Gabriel Valley Mosquito and Vector Control District, Los Angeles (T. Hallum); Greater Los Angeles County Vector Control District, Los Angeles (S. Vetrone)

DOI: https://doi.org/10.3201/eid3205.251812

Methods

Case and Outbreak Identification

Healthcare providers or laboratories are mandated to report dengue cases to LACDPH, which coordinates laboratory confirmation; interviews patients to collect symptom onset, type and duration of symptoms, hospitalization, exposure and travel history; and reviews household composition and medical records. Cases are classified according to the Council of State and Territorial Epidemiologists definition (*6*). Locally acquired (autochthonous) dengue refers to infections acquired through local mosquito transmission, as distinguished from travel-associated cases, in which infections are acquired elsewhere. A case is classified as locally acquired if the patient had no travel to dengue-risk areas during the 2 weeks before symptom onset. An outbreak was considered when ≥2 locally acquired cases occurred in patients with symptom onset dates 2–8 weeks apart and primary exposure sites located <1 mile apart, suggesting sustained local transmission. That timeframe accounts for the combined human incubation period (5–7 days) and mosquito extrinsic incubation period (8–12 days); the 1-mile radius reflects the limited flight range of *Aedes* mosquitoes (≈150 meters).

Public Health Response

LACDPH had initiated an intradepartmental planning effort between principals in the Disease Control and Health Protection bureaus in anticipation of a local outbreak, using Centers for Disease Control and Prevention (CDC) Public Health Emergency Preparedness funding to develop, train, and exercise response plans. CDC guidance (*7*) was also used to inform the Dengue Response Plan.

Response operations targeted a 150-meter radius around the patient residence (i.e., the flight span of an *Aedes* mosquito). A field command post was established to coordinate the deployment of LACDPH staff, including providing just-in-time training, safety instructions, and logistical support such as water, mosquito repellant, and radio communications. An overview of the outreach population was produced by linking census-level data from the 2002 Population Estimates Program (*8*) with parcels and addresses from the 2023 County Tax Assessors Parcels dataset and census tract–level demographic characteristics from the 2020 American Community Survey. Metrics included the number of residential and nonresidential buildings, primary languages spoken, race, ethnicity, age distribution, and household size. New cases identified from enhanced surveillance expanded the operational fields. Enhanced surveillance included offering testing to all household members, attempts to contact nearby households, and reviewing emergency department visit data in the affected area (Appendix, https://wwwnc.cdc.gov/EID/article/32/5/25-1812-App1.pdf).

Vector Control Response

Five independent vector control districts (VCDs) serve the LACDPH jurisdiction. When a locally acquired dengue case is identified, LACDPH notifies the relevant VCD, which implements enhanced, targeted mosquito control activities within the 150-meter radius around the patient's residence. Activities include door-to-door property inspections, education, increased mosquito trapping and testing, and larvicidal and adulticidal mosquito abatement.

Laboratory Testing

Healthcare providers and laboratories report positive results to LACDPH. Specimens were sent to the public health laboratory (PHL) for confirmatory PCR and nonstructural protein (NS) 1 testing, following CDC guidelines (*9*). If PCR and NS1 results were negative or PCR serotyping was not available, samples were referred to the California Department of Public Health's Viral and Rickettsial Disease Laboratory (VRDL) for plaque reduction neutralization testing (PRNT) or to CDC for PRNT and serotyping.

Samples from patients with compatible symptoms and equivocal DENV-specific IgM or positive IgG results also underwent additional IgM and PCR testing, per CDC guidance. In addition, because of the potential for cross-reactivity with other flaviviruses, febrile patients without neuroinvasive disease who tested positive for West Nile virus (WNV) were also tested for dengue by IgM, PCR, and NS1. Household members and neighbors of confirmed patients were tested by dengue NS1 and IgM assays, and PCR was performed on positive specimens.

Results

Initial Case Detection

On August 30, 2024, LACDPH was notified of a positive IgM dengue laboratory result in a resident of neighborhood A, located in the central San Gabriel Valley region of LAC (patient 1) (Figure). The patient, who sought emergency department care in mid-August, had fever, leukopenia, and thrombocytopenia and tested positive for dengue IgM. Medical record review and patient interview confirmed no recent travel. LACDPH notified the San Gabriel Valley Mosquito

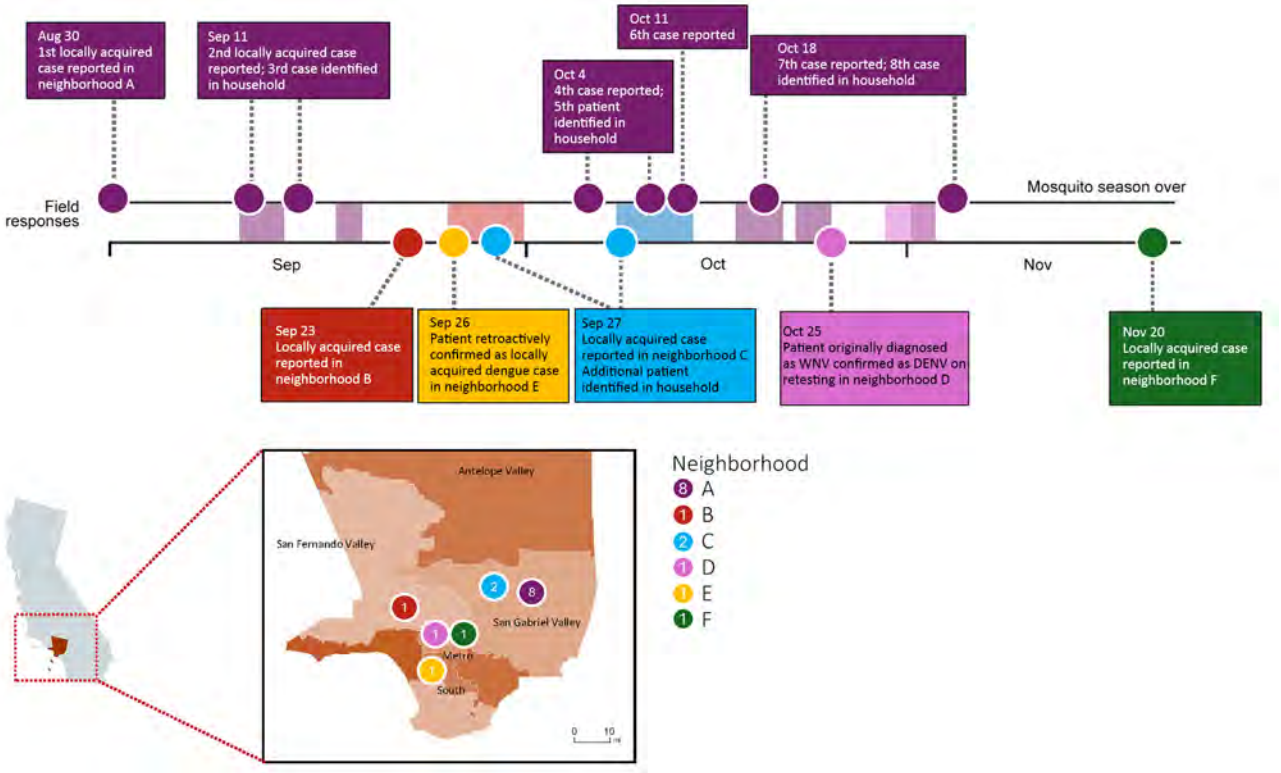

Figure. Timeline and geographic distribution of autochthonous dengue cases and public health response, Los Angeles County, California, USA, 2024. A) Timeline of cases (circles) by date of report, or date of confirmation (positive laboratory result) for a household member. Colors indicate residential neighborhood (see key in panel B); shaded bars indicate vector control and public health response activities in each neighborhood after identification of a locally acquired case. B) Map of Los Angeles County. Circles indicate cases identified by neighborhood; numbers indicate total cases per neighborhood. Case identified in neighborhood E was initially classified as a travel-related case; however, retrospective review revealed travel only to areas without ongoing DENV transmission. Based on that information, the case was reclassified as locally acquired. Inset shows location of Los Angeles County within California. DENV, dengue virus; WNV, West Nile virus.

and Vector Control District, which initiated mosquito control activities within a 150-meter radius of the patient's residence. PHL performed additional testing for dengue NS1 antigen and PCR; both results were positive, confirming DENV-3 infection. Confirmatory PRNT testing performed at the California Department of Public Health's VRDL also yielded a positive result.

Outbreak Detection

Active case finding was launched within a 150-meter radius of the patient's residence using an established response plan. All household members and neighbors reached within the radius were offered testing and provided guidance on dengue prevention, mosquito breeding reduction, and healthcare seeking. During the field response, a healthcare provider reported a case in a person residing near the first patient (patient 2). In response, testing was offered to household members, and the outreach radius was expanded to incorporate households within 150 meters of the new case; the household testing identified a third case (patient 3). Shortly thereafter, another case was reported in a person who lived <1 mile from the initial cluster (patient 4); testing of household members identified a fifth case in a child (patient 5). Patients 4 and 5 attended a place of worship with an adjoining school, identified as a potential secondary exposure site; we conducted outreach and testing at that location. A sixth case (patient 6), reported to LACDPH by a laboratory, lived near patient 1 outside the 150-meter response area and was not identified during the field response. All 6 cases were identified within a 1-mile radius over a 7-week period, consistent with an outbreak involving ongoing local transmission. Finally, another case (patient 7) was reported by a laboratory after an 11-day hospital stay during which dengue was not suspected. Subsequent household testing identified an additional case (patient 8). Those cases were farther from the original cluster (3 miles) but closer to the place of worship and school (1.7 miles). Overall, 8 locally acquired dengue cases were identified in neighborhood A.

Additional Introductions

During September–November, 6 additional dengue cases were identified across 5 distinct areas in LAC; none had relevant travel history. The first patient, reported to LACDPH by a healthcare provider, resided in neighborhood B, ≈37 miles from neighborhood A in the San Fernando Valley. During the field response, 2 workplaces were identified within the operation radius, and LACDPH deployed a mobile response unit to offer testing to all employees; no additional cases were identified. The second patient resided in neighborhood C, 5 miles from neighborhood A in the San Gabriel Valley, and sought testing for dengue after multiple unsuccessful attempts at a diagnosis; a laboratory notified LACDPH of that case. A symptomatic household member also tested positive for DENV, but no further cases were identified in the surrounding areas. Additional patients were identified in multiple different areas >20 miles from neighborhood A. The fourth patient, in neighborhood D in the city of Los Angeles, was initially misdiagnosed with WNV; however, subsequent testing by PCR and PRNT requested by LACDPH confirmed DENV infection. Public health and vector control activities were promptly implemented in response to those cases to mitigate further spread. Finally, 2 patients were identified in neighborhood E in Los Angeles and neighborhood F in South Los Angeles and reported to LACDPH by laboratories. However, because of low mosquito activity at that time of year, no door-to-door field responses were mounted in response to those cases.

Enhanced Surveillance

In total, 9 field responses were conducted in LAC in response to case detections for locally acquired dengue. Public health responses were extensive, requiring 16 field operations (1 field operation per day); 866 households, 2 worksites, and 1 place of worship and school were reached during the emergency response, resulting in 318 completed household surveys. Overall, 245 (28%) households declined participation, and 303 (35%) households could not be reached (reasons included properties were determined as unsafe to access, marked as vacant after 2 visits, or no response was received during outreach).

A total of 224 persons were tested for dengue during the response; 2 were IgM-positive for DENV. One sample from an IgM-positive person also had confirmatory PRNT testing performed at CDC, which was positive for DENV-1; that person did not report symptoms and did not meet the case definition. The second IgM-positive case-patient was also positive for NS1 and reported compatible symptoms but had traveled recently to an area with ongoing dengue transmission. Therefore, neither patient met the criteria for locally acquired dengue.

Of 314 households surveyed, 44% reported that household members had experienced mosquito bites during the previous 2 months. Twenty-three (8%) of 301 households reported that a resident was symptomatic; however, only 1 of those noted as symptomatic was successfully reached for testing during field responses. One in 5 households (18%; 57/313) reported that a household member had traveled internationally or out of state during the previous 2 months. Many households were taking measures to prevent mosquitoes on their properties and mosquito bites: eliminating standing water on the property (59%; 188/318), wearing mosquito repellent (44%; 140/318), checking screens and windows for holes or tears (43%; 138/318), and removing mosquito resting sites (40%; 126/318). However, 11% (34/318) households reported that they do not do anything to prevent mosquitoes. At the time of the survey, 46% (143/314) of households reported that they were already aware of a local case of dengue in LAC, primarily from the news (45%; 65/143), a notice from LACDPH (27%; 39/143), or social media (13%; 18/143).

Syndromic surveillance for dengue in LAC was conducted during September–December, continuing for ≥45 days after the last reported locally acquired case. During that period, 81 dengue-compatible detections were identified across 4 postal (ZIP) codes and surrounding areas. After review, LACDPH requested medical records for 12 patients who exhibited compatible clinical symptoms without an alternative diagnosis. Specimens were unavailable for 11 (92%) of those patients, and medical record review did not indicate sufficient clinical suspicion of dengue to warrant new specimen collection. One patient's specimen was tested at PHL and VRDL, with negative results for DENV. No additional locally acquired dengue cases were identified through syndromic surveillance.

Patient Characteristics

For 14 locally acquired dengue cases, median patient age was 54 (range 5–79) years; 8 (57%) patients were female and 6 (43%) male (Table). Four (29%) cases were identified through patient household testing by public health; the remainder were detected through healthcare providers. Eight (57%) patients, including 3 household cases, lived in the same neighborhood (neighborhood A); 6 (43%) of those resided within 1 mile of another patient.

Six (42.9%) patients reported known mosquito exposure, whereas 4 (28.6%) patients reported no history of mosquito bites before symptom onset. All patients reported fever; 8 (57%) had headache, and 8 (57%) had nausea and vomiting. Six (43%) patients required hospitalization. No patients met criteria for severe dengue or dengue hemorrhagic fever, and none died. Infection history was unknown for all patients.

All 14 patients were tested for DENV IgM; 12 were positive, 1 was equivocal, and 1 was negative. PHL performed confirmatory testing on all specimens using reverse transcription PCR and NS1 testing. Nine (64%) patients tested positive by NS1 testing, reverse transcription PCR, or both. Additional confirmatory testing using PRNT was performed for 8 (57%) patients, 5 whose specimens were negative by both PCR and NS1 testing and 3 who had positive PCR or NS1 testing but no available serotype information. DENV serotypes were available for 11 (79%) patients; DENV-3 was confirmed for 8, DENV-1 for 1, and indeterminant for 2 (DENV-1 or DENV-3). Sequencing results were available for only 1 patient and confirmed DENV-3 infection.

Table. Characteristics of patients with locally acquired dengue cases, Los Angeles County, California, USA, August–November 2024*

Characteristic	Value
Total	14 (100)
Median age, y (range)	54 (5–79)
Age group, y	
0–19	1 (7)
20–39	2 (14)
40–59	8 (57)
≥60	3 (21)
Sex	
F	8 (57)
M	6 (43)
Location	
Neighborhood A	8 (57)
Neighborhood B	2 (14)
Neighborhood C	1 (7)
Neighborhood D	1 (7)
Neighborhood E	1 (7)
Neighborhood F	1 (7)
Epidemiologic link	
Household	4 (29)
Neighborhood†	6 (43)
None	4 (29)
Mosquito exposure	
Y	6 (43)
N	4 (29)
Unknown	4 (29)
Symptoms	
Fever	14 (100)
Headache	8 (57)
Nausea and vomiting	8 (57)
Chills	7 (50)
Rash	6 (43)
Muscle pain	5 (36)
Joint pain	4 (29)
Diarrhea	2 (14)
Eye pain	1 (7)
Hospitalization	
Y	6 (43)
N	8 (57)
Serotype	
DENV-3	8 (57)
DENV-1 or −3‡	2 (14)
DENV-1	1 (7)
Unknown	3 (21)

*Values are no. (%) except as indicated. Percentages are rounded to the nearest whole number and may not sum to 100%. DENV, dengue virus.
†Resided within 1 mile of a case (includes index patient; includes 2 patients identified through household testing).
‡Indeterminant.

Median time from symptom onset to seeking medical care was 2 (range 1–14) days. The median interval from healthcare encounter to specimen collection was 3.5 (range 0–27) days. Overall, median time from symptom onset to specimen collection was 10 (range 4–34) days, and median interval from specimen collection to reporting to LACDPH was 5 (range 1–17) days. Once a case was reported to LACDPH, most case interviews were completed ≤2 days after notification. Four (31%) cases were first identified through public health investigation rather than clinical diagnosis. All 4 patients reported symptoms compatible with dengue; 2 had previously sought medical care but were not tested for dengue at that time, and 1 was identified through retrospective testing of residual clinical specimens.

Vector Control Response

Adult mosquito surveillance using traps placed within a 150-meter radius of case residences collected a mixture of *Culex*, *Aedes*, and *Culiseta* spp. mosquitoes; *Cx. quinquefasciatus* mosquitoes were most abundant. Among *Aedes* mosquitoes, *Ae. aegypti* was the dominant species detected near case households; *Ae. albopictus* was detected in low abundance. During property inspections, breeding sources near the case households were documented; however, formal larval indices were not calculated because they are not considered informative for risk assessment (*10*). Female *Ae. aegypti* mosquitoes collected at each trapping site within the response areas were tested for DENV, chikungunya virus, and Zika virus; however, no mosquitoes tested positive for DENV.

Public and Healthcare Provider Outreach

To raise public awareness and promote dengue prevention, LACDPH implemented messaging campaigns focused on persons who work or reside within a 150-meter radius of confirmed locally acquired cases. Educational materials were made available in multiple languages on the basis of population needs to ensure broad accessibility. During the response, LACDPH issued 6 press re-

leases and held a press conference in neighborhood A to enhance public awareness and deliver timely risk communication. A dedicated dengue webpage provided real-time updates and served as a central resource for prevention and control resources for the public. LACDPH issued 2 health advisories to alert healthcare providers about the risks of local DENV transmission in LAC, emphasizing the need to consider dengue in patients with consistent symptoms, regardless of travel history, in the absence of an alternative diagnosis; order appropriate diagnostic testing for suspected dengue infection; counsel patients and travelers on prevention strategies; and promptly report dengue cases to LACDPH to enable timely public health response (*11*).

Discussion

In 2024, LACDPH identified 14 locally acquired dengue cases in LAC, likely from multiple introductions by infected returning travelers. Epidemiologic evidence suggests that ≥1 introduction resulted in sustained local transmission, demonstrating the potential for dengue to emerge in nonendemic areas of the United States that have competent *Aedes* mosquito vectors and suitable environmental conditions. In response, LACDPH and partners rapidly implemented intensive public health and vector control measures, including active case finding, mosquito control, and community outreach around patient residences, to mitigate spread, raise awareness, and promote prevention. The ability to mobilize quickly and coordinate across sectors was aided by the existing LAC Dengue Response Plan, which provided a structured multisectoral response framework and established communication channels to coordinate efforts across VCDs, laboratories, and state and federal partners. In addition to dengue preparedness planning, LAC maintains response plans for other arboviruses, including Zika virus; a chikungunya response plan is under development.

Vector control was central to mitigating DENV spread in areas at risk for local transmission. Unlike many other jurisdictions, LAC is served by multiple independent VCDs, each with its own governance, operational protocols, and resource levels. This decentralized system means that vector surveillance, outbreak response, and mosquito control activities depended on the capacity and expertise of the individual districts. During this investigation, local vector control districts identified established *Ae. aegypti* mosquito populations near case households; however, no DENV-positive mosquitoes were detected. The absence of positive mosquito pools during localized outbreaks should be interpreted with caution because mosquito infection prevalence can be very low. Studies from Puerto Rico reported very low mosquito infection rates even during periods of active dengue transmission, indicating that the absence of DENV-positive mosquito pools does not exclude ongoing transmission (*12*,*13*).

During this outbreak, enhanced surveillance played a crucial role in identifying dengue infections that might otherwise have gone undetected, improving understanding of the extent of local transmission and enabling more tailored public health responses to interrupt transmission. Of the 6 dengue infections identified, 4 were household members of previously confirmed patients, highlighting the importance of household testing. Dengue virus infections often cluster within households and nearby areas, making household testing an effective strategy to identify cases and interrupt transmission chains. However, neighborhood-level door-to-door testing, although valuable for understanding the extent of local transmission, was resource-intensive and required substantial staffing and logistical coordination, making it unsustainable in the long term. Overall participation rates in door-to-door outreach were modest because of declined participation or lack of reach (vacancy or nonresponse), which might have resulted in underascertainment of cases and limited our ability to fully characterize the extent of local transmission. Although persons reported symptoms during neighborhood outreach, testing proved challenging because many declined or were unavailable during the field response and did not follow up with their healthcare provider or attend mobile health clinics. Workplace testing was also challenging, in part because of lack of communication with staff and barriers to scheduling during work hours. In contrast, a community testing event at a place of worship and school, organized in collaboration with trusted community partners, achieved a high turnout; 68 persons were tested for dengue. Future responses should prioritize more resource-efficient strategies, including patient household testing and community events, while enhancing provider and public awareness.

Another limitation of this investigation is that surveillance relied primarily on identifying symptomatic cases consistent with the Council of State and Territorial Epidemiologists dengue case definition. Because dengue infections are frequently asymptomatic or mildly symptomatic, a substantial number might have gone undetected. As a result, the number of infections identified during this investigation might underestimate the true extent of transmission. Future serologic studies could clarify

the extent of transmission and inform prevention and control activities.

For this outbreak, health information was disseminated via press releases, social media campaigns, press conferences, and in-person outreach during field activities. Messaging was delivered in multiple languages to ensure accessibility across diverse communities. Those efforts informed residents about dengue risk and encouraged measures to reduce mosquito breeding and avoid bites. Going forward, proactive risk communication will be delivered ahead of the mosquito season in LAC, aiming to raise awareness of vectorborne disease risk and provide the public with tools to prevent infection.

Despite efforts to raise awareness among healthcare providers, clinical recognition of locally acquired dengue remained limited, and several cases were not initially suspected as dengue. That challenge is heightened in nonendemic settings because symptoms during the acute phase overlap with those of other viral illnesses, and clinical suspicion is often low in the absence of travel history. That issue was evident in the delays in diagnosis of the local cases. In this investigation, the median time from symptom onset to specimen collection was 10 (range 4–34) days, often exceeding the optimal diagnostic window for PCR and NS1 detection during the first week of illness (*9*), and PRNT confirmatory testing was required for several patients. Those delays likely reflected both delayed healthcare seeking and missed opportunities for DENV testing during clinical encounters, highlighting the need for increased awareness of locally acquired dengue among the public and clinicians. Given the potential for dengue to emerge in nonendemic areas, clinicians should maintain a high index of suspicion for dengue in febrile patients with compatible symptoms, regardless of travel history, and prioritize timely testing to aid in early detection, prevent further transmission, and ensure prompt recognition and management of severe disease.

In addition to clinical challenges, laboratory testing practices contributed to diagnostic delays. In several cases, CDC-recommended testing (*9*) was not consistently performed by providers, requiring follow-up confirmatory testing at PHL and state or federal laboratories, extending the time to confirm diagnosis. Once testing was performed, reporting and public health response occurred relatively rapidly. Delayed specimen collection and low viral loads also limited the availability of specimens suitable for genomic sequencing, restricting ability to assess genetic relationships between DENV genomes and determine whether cases represented localized spread or independent introductions. Despite those limitations, the spatial and temporal distribution of the cases suggests that multiple introductions across geographically distinct areas of LAC might have occurred during August–November 2024. Fourteen locally acquired cases were identified across 6 geographically distinct areas, separated by ≥5 miles and up to 37 miles, and no epidemiologic links were identified. In addition, no recent travel-associated dengue cases were reported within the postal code of the initial locally acquired cases during the outbreak period.

In conclusion, local DENV transmission occurred in LAC during a time of record global dengue incidence, active outbreaks in US territories, and ongoing travel to endemic areas (*14*,*15*), highlighting the need for heightened vigilance in nonendemic areas where *Aedes* mosquitos are established. Effective preparedness depends on coordinated partnerships and multisectoral response plans, improved clinical recognition for timely detection, and robust entomologic and epidemiologic surveillance.

Acknowledgments

We thank the LAC Acute Communicable Disease Control Epidemiology & Data Unit (Lauren Finn, Monica Jimenez, Tae Hee Koo, Darien Pasigan, Harry Persaud, Omesh Ranasinghe); the Public Health Laboratory molecular epidemiology, serology, bioinformatics, and sequencing units (Heran Berhanu, Lee Borenstein, Monique Sanchez, Ayla Quraishi, Isabel Mendoza, Alen Karamian, Sophia Serrano, Hector Rivas, Jacob Garrigues, Kathryn Siemers); the LACDPH Geographic Information System Unit (Jake Campbell, Margaret Carlin, Victoria Elmore, Deborah Hernandez, Nicole Richardson, Benjamin Stone); the Emergency Preparedness and Response Division (EPRD) Policy and Planning, Emergency Planning and Analysis Unit (Dee Ann Bagwell, Hazel Escusa, Caitlin Harvey, Samir Patel, Kristina Rattnanak); the EPRD Emergency Operations Program (Christineh Aivazian, John Allen, Linda Aragon, Amoriz Castillon, Louis Jasper, John Opalski, Mike Rogers, Josue Rosas); the Community and Field Services Outreach and District teams; the Office of Worker Health and Safety (Alice Berliner, Lisa Patrick-Mudd); the VCDs (Greater Los Angeles County Vector Control Operations, Scientific-Technical, and Communications staff); the LACDPH Communications team (Becky Schlikerman Sernik, Nancy Rodriguez); the CDC Dengue Branch (National Center for Emerging and Zoonotic Infectious Diseases, Division of Vector-Borne Pathogens); and the California Department of Public Health Viral and Rickettsial Disease Laboratory for assistance in performing plaque reduction neutralization testing, and the California Department of Public Health.

This project was funded by CDC as part of a financial assistance award totaling $8,448,660.

This activity was reviewed by the Los Angeles County Department of Public Health Institutional Review Board and CDC, was deemed not research, and was conducted consistent with applicable federal law and CDC policy (§45 C.F.R. part 46, 21 C.F.R. part 56; 42 U.S.C. Sect. 241(d); 5 U.S.C. Sect. 552a; 44 U.S.C. Sect. 3501 et seq.).

About the Author

Dr. Vaughan is a CDC Epidemic Intelligence Service officer based in the Los Angeles County Department of Public Health. Her interests include emerging and zoonotic infectious diseases, outbreak response, and pandemic preparedness.

References

1. Centers for Disease Control and Prevention. Dengue data, 2024 [cited 2025 Feb 4]. https://www.cdc.gov/dengue/data-research/facts-stats/historic-data.html
2. Pan American Health Organization/World Health Organization. Dengue epidemiological situation in the Region of the Americas—epidemiological week 17, 2025 [cited 2025 May 20]. https://www.paho.org/en/arbo-portal/dengue-data-and-analysis
3. Centers for Disease Control and Prevention. Data and statistics on dengue in the United States. 2025 [cited 2025 Nov 13]. https://www.cdc.gov/dengue/data-research/facts-stats/index.html
4. Feaster M, Patrick R, Oshiro M, Kuan M, Goh YY, Carmona M, et al. Notes from the field: first locally acquired dengue virus infections—Pasadena, California, October–December 2023. MMWR Morb Mortal Wkly Rep. 2024;73:955–6. https://doi.org/10.15585/mmw.mm7342a4
5. City of Long Beach. Long Beach Health Department confirms case of locally acquired dengue. 2023 Nov 1 [cited 2025 May 21]. https://longbeach.gov/press-releases/long-beach-health-department-confirms-case-of-locally-acquired-dengue
6. Centers for Disease Control and Prevention. Dengue virus infections 2015 case definition. 2021 Jun 11 [cited 2025 Feb 7]. https://ndc.services.cdc.gov/case-definitions/dengue-virus-infections-2015
7. Centers for Disease Control and Prevention. Response to dengue cases in non-endemic areas of the United States. 2024 [cited 2025 Aug 29]. https://www.cdc.gov/dengue/media/pdfs/2024/08/response_to_dengue.pdf
8. County of Los Angeles Internal Services Department, Information Technology Service, Geographic Information Systems Section. Population estimates of Los Angeles County tract-city and countywide statistical area splits by age, sex, and race/ethnicity for 2022. Los Angeles, CA: Hedderson Demographic Services; 2023.
9. Centers for Disease Control and Prevention. Clinical testing guidance for dengue. 2025 [cited 2025 May 21]. https://www.cdc.gov/dengue/hcp/diagnosis-testing/index.html
10. Bowman LR, Runge-Ranzinger S, McCall PJ. Assessing the relationship between vector indices and dengue transmission: a systematic review of the evidence. PLoS Negl Trop Dis. 2014;8:e2848. https://doi.org/10.1371/journal.pntd.0002848
11. Los Angeles County Department of Public Health. LAC DPH alert: locally acquired case of dengue in Los Angeles County [cited 2025 Feb 4]. https://t.e2ma.net/webview/zf62nz/bb8a8592ee3adabe7519e4d898e6632b
12. Barrera R, Acevedo-Soto V, Ruiz-Valcarcel J, Medina J, Rivera R, Otero L, et al. Defining *Aedes aegypti* density thresholds for preventing human arboviral infections. Acta Trop. 2025;267:107688. https://doi.org/10.1016/j.actatropica.2025.107688
13. Otero LM, Medina J, Ruiz-Valcarcel J, Rivera R, Maldonado Y, Torres J, et al. Monitoring dengue virus in *Aedes aegypti* to improve dengue surveillance and control in Puerto Rico. Viruses. 2025;17:1539. https://doi.org/10.3390/v17121539
14. Centers for Disease Control and Prevention. Public health considerations for dengue. 2025 [cited 2025 May 2]. https://www.cdc.gov/dengue/php/public-health-considerations/index.html
15. Centers for Disease Control and Prevention. CDC health advisory: increased risk of dengue virus infections in the United States [cited 2025 May 20]. https://t.e2ma.net/webview/zf6mzy/fa56fa575dfaecc6d437cc532872ace3

Address for correspondence: Aisling Vaughan, Centers for Disease Control and Prevention, 1600 Clifton Rd NE, Mailstop US10-1, Atlanta, GA 30329-4018, USA; email: avaughan2@cdc.gov

Updated Genomic Epidemiologic Description of *Candida* (*Candidozyma*) *auris*, United States

Lindsay A. Parnell, Amanda Ribeiro Dos Santos, Kaitlin Forsberg, Meghan Lyman, Elizabeth Misas, Lalitha Gade, D. Joseph Sexton, Anastasia P. Litvintseva, Nancy A. Chow

The multidrug-resistant yeast *Candida* (*Candidozyma*) *auris* has caused several healthcare-associated outbreaks in the United States. We provide a genomic epidemiologic description of 1,535 *C. auris* isolates collected in the United States during 2013–2022. We identified clades I, II, III, and IV but not clades V or VI. Median pairwise single-nucleotide polymorphism distances indicated lower intraclade relatedness for clades I (91), III (43), and IV (43), compared with clade II (1,455). Phylogenetic analysis showed regional clusters with varying predominant clades. Of 809 isolates that underwent antifungal susceptibility testing, 53 were echinocandin resistant, distributed across 3 clades; 92% (49/53) had *FKS1* hotspot mutations, which varied regionally. Our findings corroborate ongoing transmission and clonal expansion of *C. auris*, likely propagated by multiple introductions within and between geographic regions. Echinocandin resistance in multiple clades highlights the need to increase awareness, improve treatment practices, and engage in rapid public health response.

Candida auris, reclassified as *Candidozyma auris* to reflect its updated phylogenetic position (*1*), is a fungal pathogen characterized by high rates of multidrug resistance and high transmissibility in healthcare settings. More than 40 countries have reported cases; many experienced outbreaks of invasive infection associated with high mortality rates (*2*). The World Health Organization has categorized *C. auris* as a critical-priority fungal pathogen, driven by the need to mitigate spread by scaling up research, scientific development, and public health response efforts (*3*).

Author affiliation: Centers for Disease Control and Prevention, Atlanta, Georgia, USA

DOI: https://doi.org/10.3201/eid3205.250760

Genomic sequencing has been pivotal for understanding global *C. auris* emergence and transmission. Early phylogenetic studies revealed a genetically diverse species that could be classified into 4 major clades hypothesized to have emerged independently and simultaneously from South Asia (clade I), East Asia (clade II), Africa (clade III), and South America (clade IV) (*4*). Clade V was identified later in Iran, and clade VI was reported in Singapore and Bangladesh (*5*–*7*). Some countries have reported the circulation of multiple clades, underscoring the role of travel-related healthcare as an important driver of introductions into new geographic areas (*8*–*11*). An early US study demonstrated the presence of clades I–IV and occurrence of multiple introductions, some of which were linked to seeking healthcare abroad (*8*). Rapid local transmission driven by patient colonization and persistence in the healthcare environment has also been widely reported; low intraclade genetic diversity identified in our study supported those findings (*12*).

C. auris clade typing has enabled further characterization of strains of public health and clinical importance, highlighting clade-specific microbiologic and epidemiologic properties. Clades I, III, and IV have primarily been associated with outbreaks, invasive infections, and antifungal resistance; clade II has not (*8*,*13*–*17*). In an early international genomic epidemiologic study, clade I exhibited the highest levels of multidrug resistance to 3 major antifungal drug classes: triazoles (fluconazole), polyenes (amphotericin B), and echinocandins (anidulafungin, caspofungin, and micafungin) (*12*). High fluconazole resistance has consistently been reported in clades I and III (*12*,*16*,*18*,*19*). Clade IV resistance is commonly characterized as variable, both geographically and by drug class (*19*). For example, azole and amphotericin

B resistance is reportedly low in the midwestern United States, where clade IV is common (*20*). However, increased resistance has been observed in Colombia among clade IV isolates; resistance patterns varied by region (*21*–*23*). There have been fewer reports of clades II, V, and VI and, among those reported, the strains have generally exhibited low antifungal resistance (*24*–*26*).

Although echinocandin resistance remains low in the United States, increasing pan-resistance and echinocandin resistance remains a concern because echinocandins are the recommended first-line therapy for *C. auris* infection. Researchers hypothesize that patients acquire resistance through antifungal pressure from exposure to echinocandin medications; strains develop substitutions in hotspot regions of *FKS1,* encoding a fungal cell wall protein and an echinocandin target (*27*). Echinocandin resistance has also been documented in drug-naive patients, suggesting the potential for resistant strain transmission (*20*,*28*). Of note, the Clinical and Laboratory Standards Institute gives precedence to *FKS1* hotspot mutations over phenotypic resistance for predicting clinical failure (*29*).

C. auris is nationally notifiable in the United States, but reporting of cases varies by jurisdiction. The US Centers for Disease Control and Prevention (CDC) Antimicrobial Resistance Laboratory Network (AR Lab Network), which provides nationwide testing to detect and respond to cases, supporting public health response efforts, conducts complementary laboratory-based testing (*30*). We provide an update on the genomic epidemiology of *C. auris* in the United States, integrating a convenience sample of sequenced cases collected during 2013–2022 with previously reported US sequences. We highlight phylogeographic, phylotemporal, and antifungal resistance patterns observed within each *C. auris* clade.

Methods

Cases

AR Lab Network regional laboratories forwarded isolates representing clinical and screening cases from 32 states and jurisdictions to CDC. Each regional laboratory provides antimicrobial resistance testing, including for *C. auris* detection and drug susceptibility. CDC prioritized 1,162 isolates for whole-genome sequencing (WGS) to support public health response efforts. WGS selection criteria included cases with recent healthcare exposures outside of the region; that had unique epidemiology; that were from new facilities or regions; whose isolates exhibited resistant MICs (particularly pan- or echinocandin resistance); that were associated with high-priority outbreaks or donor-derived infection investigations; and that were from areas with known cases where no prior WGS data existed. Some cases were sequenced from high-prevalence areas. We confirmed all unique isolates received for this study were *C. auris* by matrix-assisted laser desorption/ionization time-of-flight mass spectrometry, Sanger sequencing, or both. We used a MALDI Biotyper (Bruker Daltonik, https://www.bruker.com) with the MicrobeNet MALDI database (https://microbenet.cdc.gov). We Sanger sequenced the internal transcribed spacer of the isolates.

Case Metadata

We extracted case metadata for 1,535 US isolates, using a combination of laboratory submissions and case-based surveillance reporting systems (Table). Specimen collection dates and geographic areas were available for all cases in the study. We included all other epidemiologic data (case type, specimen type, age, and sex) as available from the reporting streams. We classified specimens into 8 categories: colonization screening sites, blood, ear, fluid and drainage, indwelling device, respiratory, urine, and wound. We categorized isolates that could not be classified into those 8 groups as other and isolates for which collection site was unavailable as unknown.

We categorized all US cases as clinical or screening on the basis of available case-based or laboratory-based surveillance data. When that information was unavailable, we used case definitions from the Council of State and Territorial Epidemiologists (*31*). We considered cases that could not be classified as clinical or screening to be unknown.

DNA Extraction and WGS

We performed DNA extraction and WGS as described previously (*8*), with the following exceptions. We constructed genomic libraries using the NEBNext Ultra DNA Library Prep Kit for Illumina (New England Biolabs, https://www.neb.com) or the DNA Prep Kit (Illumina, https://www.illumina.com), and we sequenced libraries using the HiSeq Rapid SBS Kit v2 (500 cycles), the NovaSeq 6000 SP Reagent Kit, or the MiSeq Reagent Kit v2 (500 cycles) (all Illumina).

Quality Control, Single-Nucleotide Polymorphism Calling, Phylogenetic Analysis, and Temporal Analysis

We performed quality control, whole-genome single-nucleotide polymorphism (SNP) variant calling, and phylogenetic reconstruction by using the reference-

Table. Patient demographic data and clinical information for isolates sequenced in study of genomic epidemiologic description of *Candida (Candidozyma) auris*, United States

Characteristic	All, n = 1,535	Central, n = 9	Mid-Atlantic, n = 188	Midwest, n = 234	Mountain, n = 87	Northeast, n = 560	Southeast, n = 181	West, n = 276
	No. (%) cases							
Case type								
Clinical	736 (48)	8 (89)	55 (29)	101 (43)	29 (33)	250 (45)	156 (86)	137 (50)
Screening*	728 (47)	1 (11)	120 (64)	132 (56)	58 (67)	266 (48)	16 (9)	135 (49)
Unknown	71 (5)	0	13 (7)	1 (0.43)	0	44 (8)	9 (5)	4 (1)
Specimen type								
Colonization screening sites	727 (47)	1 (11)	120 (64)	132 (56)	58 (67)	265 (47)	16 (9)	135 (49)
Blood	293 (19)	3 (33)	18 (10)	34 (15)	13 (15)	94 (17)	70 (39)	61 (22)
Ear	9 (1)	1 (11)	0	1 (0.43)	0	5 (1)*	1 (1)	1
Fluid and drainage	20 (1)	0	3 (2)	3 (1)	0	9 (2)	1 (1)	4 (1)
Indwelling device	10 (1)	0	0	4 (2)	0	3 (1)	0	3 (1)
Respiratory	80 (5)	0	4 (2)	8 (3)	5 (6)	28 (5)	24 (13)	11 (4)
Urine	210 (14)	2 (22)	21 (11)	35 (15)	8 (9)	75 (13)	34 (19)	35 (13)
Wound	55 (4)	0	8 (4)	7 (3)	2 (2)	16 (3)	17 (9)	5 (2)
Other	89 (6)	2 (22)	1 (1)	9 (4)	1 (1)	48 (9)	9 (5)	19 (7)
Unknown	42 (3)	0	13 (7)	1 (0.43)	0	17 (3)	9 (5)	2 (1)
Age, y								
<21	10 (1)	0	1 (1)	1 (0.43)	0	2	2 (1)	4 (1)
≥21 to <64	629 (41)	5 (56)	97 (52)	127 (54)	46 (53)	183 (33)	70 (39)	101 (37)
≥65	793 (52)	2 (22)	78 (41)	83 (35)	41 (47)	316 (56)	104 (57)	169 (61)
Unknown	103 (7)	2 (22)	12 (6)	23 (10)	0	59 (11)	5 (3)	2 (1)
Sex								
F	519 (34)	0	72 (38)	72 (31)	31 (36)	199 (36)	54 (30)	91 (33)
M	687 (45)	7 (78)	87 (46)	100 (43)	42 (48)	255 (46)	63 (35)	133 (48)
Unknown	329 (21)	2 (22)	29 (15)	62 (26)	14 (16)	106 (19)	64 (35)	52 (19)
Year of collection								
2013	1 (0.07)	0	0	0	0	1 (0.18)	0	0
2014	0	0	0	0	0	0	0	0
2015	1 (0.07)	0	0	0	0	1 (0.18)	0	0
2016	100 (7)	0	6 (3)	22 (9)	0	72 (13)	0	0
2017	350 (23)	2 (22)	3 (2)	22 (9)	0	317 (57)	5 (3)	1 (0.36)
2018	123 (8)	1 (11)	3 (2)	54 (23)	1 (1)	59 (11)	4 (2)	1 (0.36)
2019	134 (9)	1 (11)	21 (11)	5 (2)	8 (9)	7 (1)	39 (22)	53 (19)
2020	295 (19)	2 (22)	61 (32)	32 (14)	2 (2)	17 (3)	84 (46)	97 (35)
2021	386 (25)	2 (22)	93 (49)	82 (35)	62 (71)	37 (7)	43 (24)	67 (24)
2022	145 (9)	1 (11)	1 (1)	17 (7)	14 (16)	49 (9)	6 (3)	57 (21)

*One early ear case in the Northeast was counted as a screening case because of circumstances of collection and case definition at the time.

based pipeline MycoSNP-nf version 1.4 (https://github.com/CDCgov/mycosnp-nf). All sequences subjected to variant calling, phylogenetic analysis, and querying for antifungal resistance mechanisms had a minimum mean coverage depth of 20×, a guanine-cytosine content of 42.5%–47%, and a minimum Phred score of 28. For all MycoSNP-nf analyses, we applied downsampling to a coverage of 70 (rate = 0) and used the default haploid parameter. We generated maximum-likelihood phylogenetic trees using the IQ-TREE version 2.1.4 module (https://iqtree.github.io) with Shimodaira-Hasegawa–like approximate likelihood ratio test and ultrafast bootstrap approximation methods.

For the global tree, we aligned 1,162 US sequences and previously reported US (n = 373) and global contextual comparators from Africa, the Americas, Asia, Europe, and Oceania (n = 75) to the clade I reference genome, B11205 (GenBank accession no. GCA_016772135.1), and subjected them to quality control, variant calling, and phylogenetic analysis. For regional trees, we aligned isolates to a clade-specific reference on the basis of the predominant clade in the region. We performed phylogenetic visualizations using Interactive Tree of Life version 7.1 (https://itol.embl.de). We performed temporal clade analyses in R version 4.4.0 (The R Project for Statistical Computing, https://www.r-project.org).

Intraclade SNP Diversity

We aligned US sequences to their clade-specific references, including B11205 (GenBank accession no. GCA_016772135.1) for sequences identified as clade I, B11220 (GenBank accession no. GCA_003013715.2) for clade II, B11221 (GenBank accession no. GCF_002775015.1) for clade III, and B11243 (GenBank accession no. GCA_003014415.1) for clade IV. We then subjected them to quality control and variant calling using MycoSNP-nf. We used pairwise SNP distance matrices, generated from the SnpDist version

0.8.2 MycoSNP-nf module, for intraclade SNP diversity analysis. To compare intraclade SNP diversity, we calculated the mean SNP distance per isolate within each clade, excluding the reference from comparisons. We visualized distances in clade-specific boxplots using R version 4.4.0.

Identification of Mutations Associated with Antifungal Resistance

We annotated SNPs obtained with MycoSNP-nf workflow using SnpEff version 5.0 (https://pcingola.github.io/SnpEff) (*32*) and a local SnpEff database for the *C. auris* reference B11205. To identify mutations or polymorphisms only in coding regions, we used the parameters -no-downstream -no-upstream -no-intergenic. We applied filters to the annotated VCF using SnpEffR (https://github.com/CDCgov/snpeffr) to identify mutations and polymorphisms present in the well-known hotspots, including hotspot 1 (F635 to P643), hotspot 2 (D1350 to L1357), and a presumptive hotspot 3 (L686 to N696) as reported previously (*33*,*34*). We annotated regional phylogenetic trees with cases harboring *FKS1* hotspot mutations.

Antifungal Susceptibility Testing Analysis

The AR Lab Network prioritizes isolates for antifungal susceptibility testing (AFST) as described previously (*20*). In this dataset, AFST was performed on 55% (n = 843/1,535) of the US cases sequenced in this study. The submitting laboratories performed testing using the reference broth microdilution method as described previously (*20*), except for amphotericin B, which was tested by Etest (bioMérieux, https://www.biomerieux.com). We interpreted MICs for fluconazole (n = 836/1,535), amphotericin B (n = 834/1,535), anidulafungin (n = 841/1,535), caspofungin (n = 840/1,535), micafungin (n = 810/1,535), and all echinocandins (n = 809/1,535) as resistant on the basis of CDC-established tentative breakpoints (*35*). We considered echinocandin interpretations not tested if MIC results were unavailable for all 3 echinocandin drugs at the time of the analysis.

Statistical Analyses

We performed Kruskal-Wallis test with posthoc Dunn test to determine whether pairwise SNP distances differed significantly between clade pairs. We performed χ^2 tests with standardized Pearson residuals to analyze the associations between clade and various clinical specimen types. We performed all statistical analyses using R version 4.4.0.

Data Sharing

We submitted reads for newly sequenced cases (n = 1,162), 69 of which were also included in a recently published benchmark dataset (*36*), to the National Center for Biotechnology Information Sequence Read Archive (https://www.ncbi.nlm.nih.gov/sra) under BioProject PRJNA638416 as part of genomic surveillance efforts. Other previously reported US comparators used in this study were deposited under BioProject PRJNA328792 (*4*,*37*), PRJNA796037 (*38*), and PRJNA493622 (*8*).

This activity was reviewed by CDC and determined by a CDC Human Subjects Advisor to be public health surveillance and not human subjects research. Therefore, institutional review board review was not required.

Results

Demographics

We performed WGS for 1,535 *C. auris* isolates from 32 states and jurisdictions within 7 AR Lab Network–defined US regions (Table). We classified 728 (47%) of the sequenced isolates as screening cases and 736 (48%) as clinical cases. Among the clinical cases, common specimen types were blood (293 [40%]), urine (210 [29%]), and respiratory sites (80 [11%]). Among 1,432 cases with reported patient age, the median age was 67 (range 0–99) years. Of 1,206 cases with reported sex, 519 (43%) were female and 687 (57%) were male.

Phylogenetic and Phylotemporal Characterization

Phylogenetic analysis classified sequenced US cases within clade I (n = 860), II (n = 8), III (n = 451), and IV (n = 216) (Figure 1; Figure 2, panel A). Clade V or VI were not identified (Phylogeny of US and Global Isolates, https://itol.embl.de/tree/15811123643432441764620795). Cases identified from 2013–2016 belonged to clades I, II, and IV. We identified no clade III cases before 2017, then an increase in sequenced clade III cases starting in 2019. By 2017, we identified cases from all 4 clades and ≥1 clade I, III, and IV case every year thereafter. Clade II appeared infrequently: in 2016 (n = 4), 2018 (n = 1), 2019 (n = 1), and 2021 (n = 2) (Figure 2, panel B).

We calculated mean pairwise SNP distances for each case within a clade and found distances between all clade pairs differed significantly (Figure 3). Clades III and IV both exhibited a median pairwise SNP distance of 43 (clade III range 32–97; clade IV range 33–225), and clade I had a median pairwise SNP distance of 91 (range 53–1,083). We observed greater SNP

diversity in clade II than in any other clade (median 1,455, range 1,201–1,788).

Resistance

Of 843 cases with AFST, 801 were tested for all 3 antifungal drug classes. Of those, 738 were resistant to ≥1 antifungal drug. The proportion of resistant cases varied by clade. Clade I and III cases were most frequently resistant; 479/479 isolates of clade I, 1/6 isolates of clade II, 211/212 isolates of clade III, and 47/104 isolates of clade IV were resistant (Appendix Figure 1, panel A). Of the isolates tested for resistance to individual antifungal drugs, 764/836 (91%) were fluconazole-resistant, 97/834 (12%) were amphotericin B–resistant, and 53/809 (7%) were echinocandin-resistant (Appendix Figure 1, panels B–D). For each drug, resistance patterns varied by clade. Of the 809 isolates tested against echinocandins, 49/53 (92%) of echinocandin-resistant isolates had an *FKS1* mutation (Appendix Figure 2), including F635C/Y, S639F/P/Y, and D642Y within hotspot 1; R1354S within hotspot 2; and M690I and W691L within a presumptive hotspot 3. *FKS1* hotspot mutations in echinocandin-susceptible strains were infrequent. We detected mutations in 13/756 (2%) of such cases: in hotspot 1, L638F, S639Y, D642Y; in hotspot 2, L1357F; in hotspot 3, D687V and M690I. In addition, 8 cases without reported AFST harbored an *FKS1* hotspot mutation, including L638F, S639P/Y, L1357F, and D642Y.

Regional Analysis

We observed regional geographic clustering in all clades (Figure 1). Although all regions had multiple clades, most regions had a predominant clade (Figure 4). We identified clade I primarily in the Mid-Atlantic, Mountain, and Northeast regions and clade III primarily in the Southeast and West regions. The Midwest was the only region where clade IV was primarily identified. We sequenced fewer isolates from the Central region (n = 9), and no clade predominated. Within each region, the number of clades sequenced varied over time (Figure 5). We generated phylogenetic trees displaying results by state, clade, and drug resistance findings (Figure 6).

We detected an *FKS1* mutation in 100% of echinocandin-resistant cases sequenced in 4 regions: in the Mid-Atlantic, D642Y, S639F, and W691L; in the Midwest, M690I, S639F, and S639P; in the Mountain, F635C and S639Y; and in the West, S639F, S639P, and S639Y (Figure 7). We detected an *FKS1* mutation in 23/26 (88%) of Northeast echinocandin-resistant cases sequenced (F635C, F635Y, R1354S, S639F, S639P, and S639Y). We detected no *FKS1* mutation in the 1 echinocandin-resistant case in the Central region. Detected *FKS1* genotypes varied regionally; the Northeast region exhibited more unique mutations than did other regions.

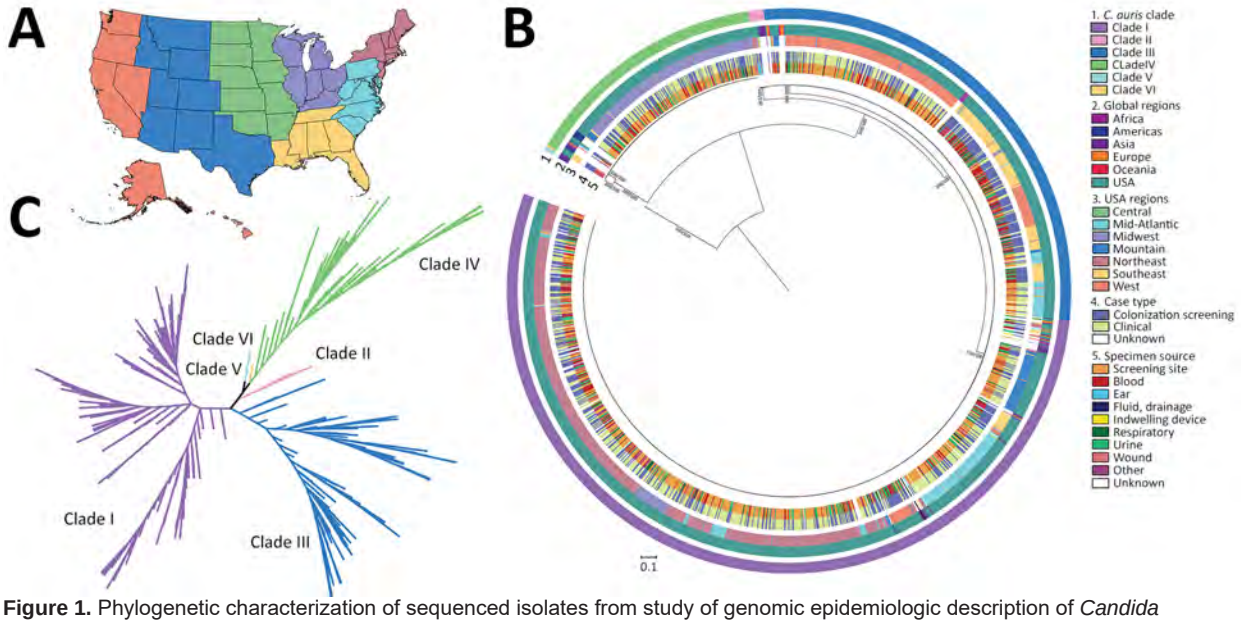

Figure 1. Phylogenetic characterization of sequenced isolates from study of genomic epidemiologic description of *Candida (Candidozyma) auris* in the United States. A) US map showing regions where sequenced cases originated, as defined by the Centers for Disease Control and Prevention Antimicrobial Resistance Laboratory Network (colors defined in section 3 of key at right). B) Maximum-likelihood phylogenetic tree, rooted at the midpoint, represents cases sequenced from the United States (n = 1,535) and various global regions (n = 75). C) Genetic relationships among cases represented as an unrooted phylogenetic tree colored by clade. All US cases cluster within clades I–IV. The phylogenetic trees were inferred from 421,678 whole-genome single nucleotide polymorphisms. Bootstrap support values between major clades were 100, as determined by the IQ-TREE SH-aLRT/UFboot methods.

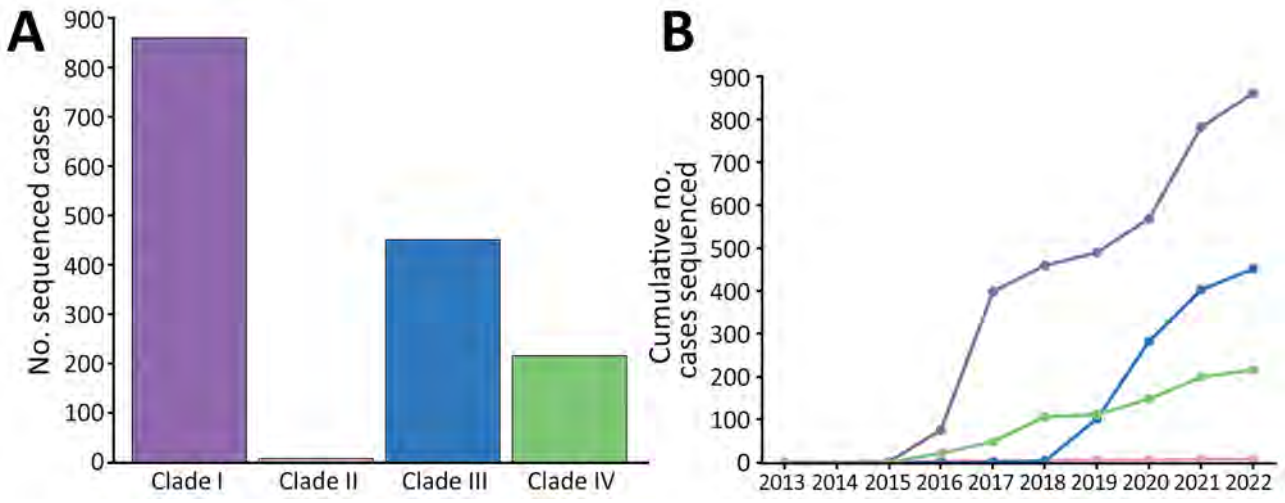

Figure 2. Sequenced isolates by clade and over time from study of genomic epidemiologic description of *Candida (Candidozyma) auris*, United States. A) Isolates by clade: clade I, n = 860; clade II, n = 8; clade III, n = 451; clade IV, n = 216. B) Cumulative number of sequenced US cases of *C. auris* collected from 2013–2022. Colors match clade colors in panel A.

Discussion

We present an updated genomic epidemiologic picture of *C. auris* cases from 7 US regions. Consistent with previous genomic epidemiologic survey reporting (*8*), sequenced cases revealed the presence of 4 major clades (I, II, III, and IV). Clades V and VI were absent within the timeframe; clade V has not been reported outside of Iran, and clade VI is a recently reported clade that has been identified in Bangladesh and Singapore (*6*,*7*). However, a likely introduction to Singapore from Bangladesh suggests potential transmission to new areas through travel-related healthcare.

Clades I, III, and IV exhibited relatively low intraclade diversity; median pairwise SNP distances were <100. Even with that level of diversity within

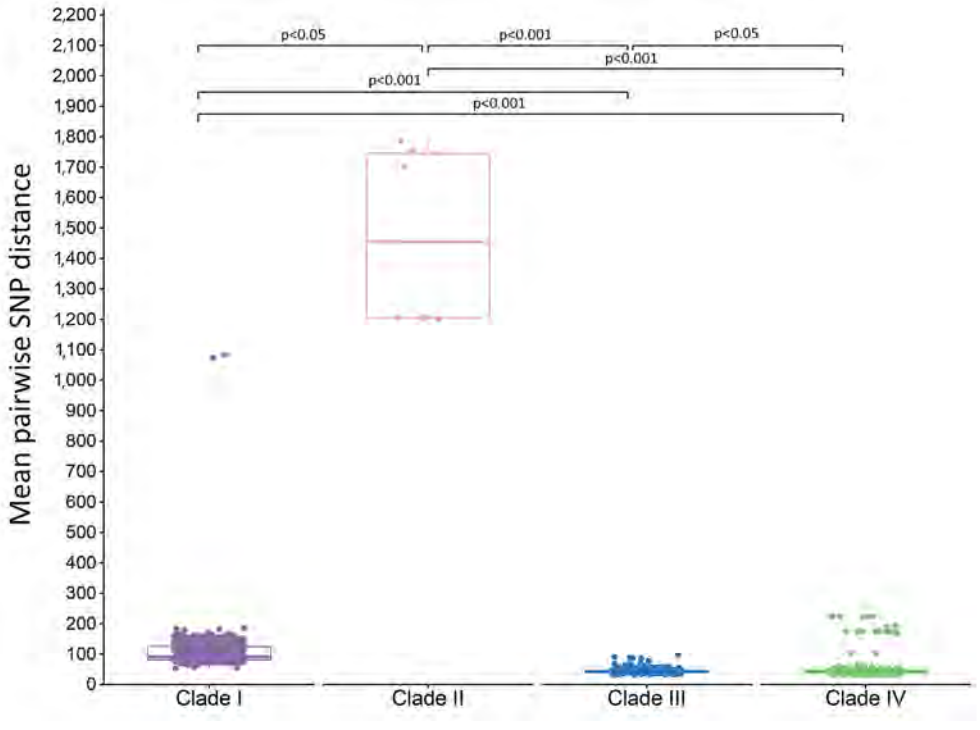

Figure 3. Pairwise SNP distances from study of genomic epidemiologic description of *Candida (Candidozyma) auris* isolates, by clade, United States. Tukey boxplots summarize pairwise SNP distances within each clade; horizontal line within box indicates the median, upper and lower boundaries indicate interquartile range); whiskers indicate largest and smallest distance value within 1.5 times the interquartile range. Dots correspond to each isolate's mean pairwise SNP distance within its clade. The Kruskal-Wallis test with posthoc Dunn test indicated significant differences in pairwise SNP distances between all clade pairs. Reference strains used were as follows: clade I, B11205 (GenBank accession no. GCA_016772135.1); clade II, B11220 (GenBank accession no. GCA_003013715.2); clade III, B11221 (GenBank accession no. GCF_002775015.1); clade IV, B11243 (GenBank accession no. GCA_003014415.1). SNP, single-nucleotide polymorphism.

the clades, we observed clustering patterns that correlated with the regions and states of collection. That finding suggests that the main transmission patterns of *C. auris* lie within and between healthcare facilities in similar geographic areas. Although most cases observed are likely a consequence of clonal spread, maximum pairwise distances reached 1,083 SNPs for clade I, 97 SNPs for clade III, and 225 SNPs for clade IV, suggesting more divergent strains in these areas. For example, 2 clade I cases identified in the Central region in 2017 were genetically distinct from all other clade I cases sequenced; their mean pairwise SNP distances were 1,073 and 1,083. We did not sequence genetically similar strains to those 2 in this study. It is possible that the strains were not transmitted after their initial introductions or related strains remained undetected, based on our testing strategy.

Clade II exhibited greater intraclade diversity compared with others, despite its early initial introduction into the United States. Temporal analysis revealed sporadic identification of clade II cases throughout the years. Of >700 clinical cases sequenced, 6 were of clade II and demonstrated a strong association with the ear (Appendix Figure 3). That observation is consistent with a study demonstrating a propensity for this clade in ear specimens among 61 cases collected over 20 years (*25*). We saw no evidence of transmission of clade II in our study; that underrepresentation might be rooted in clinical testing practices that limit fungal detection in the ear and other nonsterile sites, unique genetic or

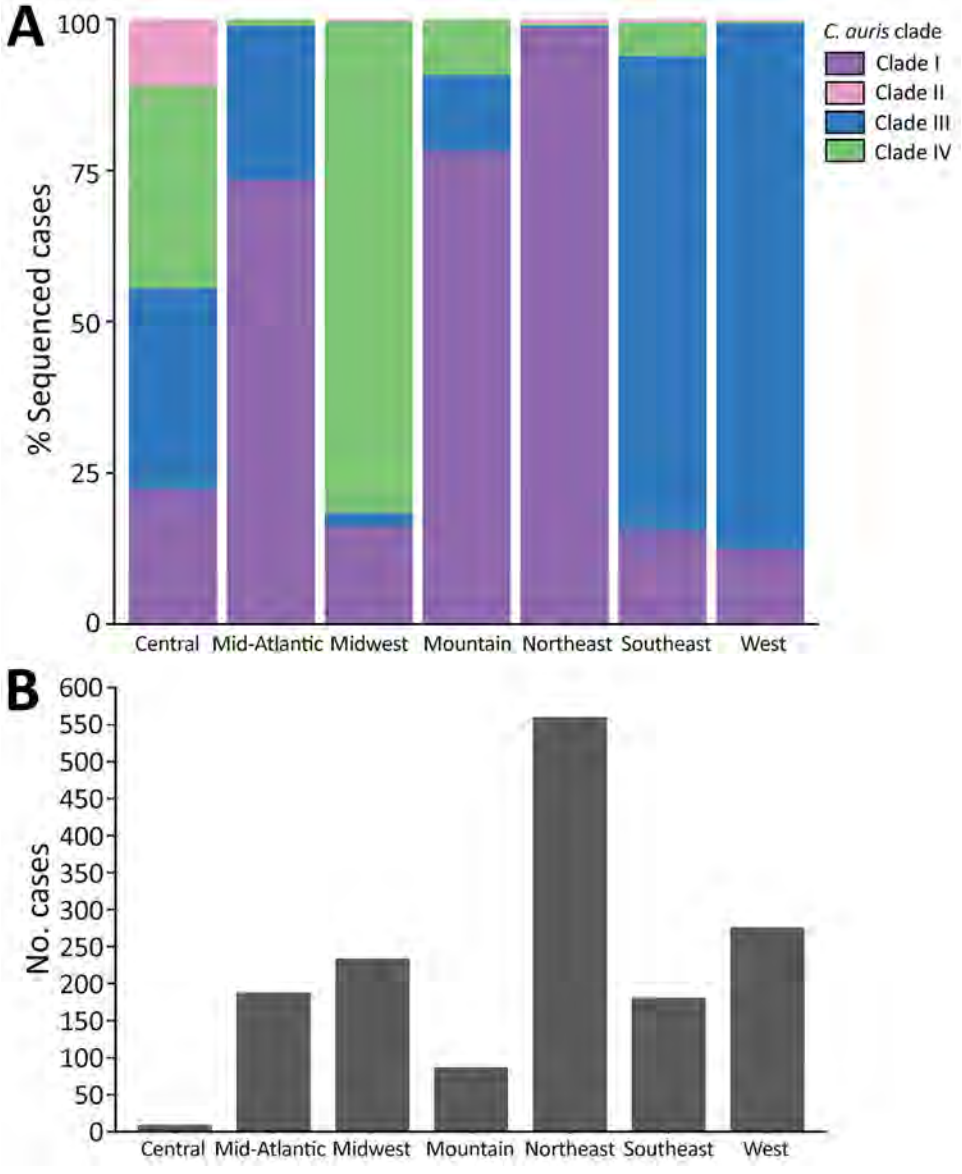

Figure 4. Clades by geographic region from study of genomic epidemiologic description of *Candida (Candidozyma) auris*, United States. A) Percentage of isolates belonging to each clade for each region. B) Total number of cases sequenced in each region.

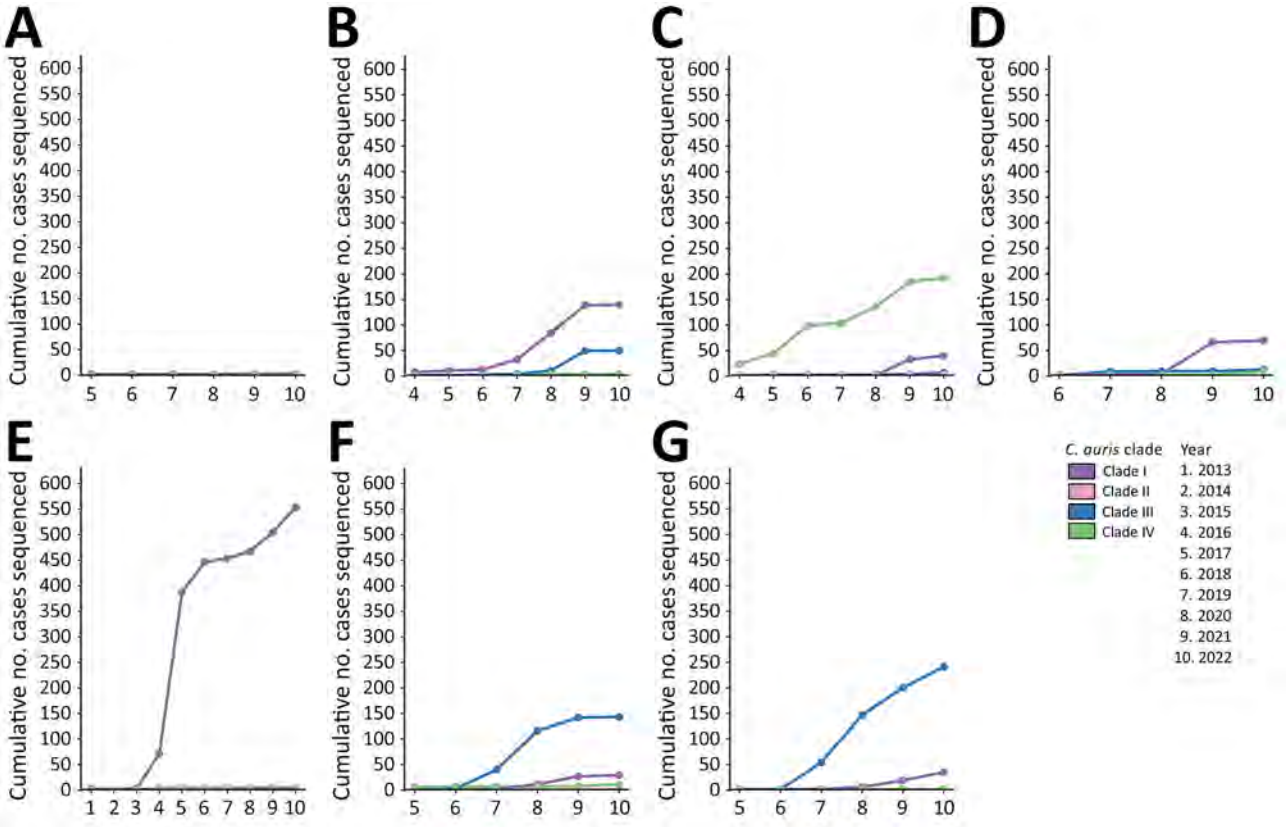

Figure 5. Cumulative number of isolates sequenced per clade, by year and by geographic region, from study of genomic epidemiologic description of *Candida (Candidozyma) auris*, United States. (A) Central; (B) Mid-Atlantic; (C) Midwest; (D) Mountain; (E) Northeast; (F) Southeast; (G) West.

biochemical features that make it less virulent and transmissible, or a combination of those factors (*39*). Furthermore, we sequenced cases on the basis of predetermined priorities, which might have limited our ability to capture clade II cases.

We also observed phylogeographic patterns of specific strains found in different states or regions. We identified ≥2 clades in all regions, but 1 specific clade was more frequently sequenced in most regions. Testing priorities and targeted sequencing strategy likely affect those observed patterns. Nonetheless, the pattern suggests that a clade initially established in an area is sustained through ongoing transmission and is not displaced by other clades. Whether competition between clades plays a role in those observations is unknown.

In some instances, we observed relatedness among strains collected in different regions and states (Figures 1, 6). Interregional and interstate clustering likely stemmed from patient movement or transfers, in which patients sought and received healthcare in other areas. Those data reinforce the role of both local spread and travel-related introductions as important drivers of *C. auris* geographic expansion. Further genomic characterization of phylogeographic patterns is needed to resolve local strain differences and understand how they reflect transmission.

Previous studies have demonstrated the circulation of multiple clades, even within the same facility and patient (*40*); that study described the coexistence of clade I and III in 5 patients in southern Nevada, an area that has experienced large clade I and III outbreaks. However, the clinical implications of multiple clades within a single person are not known. It has been hypothesized that coexisting clades within a single host or geographic area, even those of opposite mating types, might provide conditions for mating and genetic exchanges that lead to more virulent clades and strains. Evidence of recombination signatures among clades is lacking; rather, the high intraclade relatedness observed in our study and population genomic studies suggests clonal expansion (*41*).

We observed drug resistance frequently among clade I and III cases, largely driven by fluconazole resistance (Appendix Figure 1). That finding is consistent with reported susceptibility profiles in areas

experiencing clade I and III transmission (*11*,*16*,*42*). We observed echinocandin resistance in multiple clades. Regions where clade I predominated (Mid-Atlantic, Mountain, and Northeast) collectively had 44/53 (83%) of such strains.

As expected, *FKS1* mutations differed across regions (Figure 7). Most likely, those mutations arose independently as a result of antifungal pressure following treatment. However, the mutations do not preclude the possibility of echinocandin-resistant transmission, particularly in highly related strains with common *FKS1* mutations. We could not distinguish between those possibilities because treatment history was unavailable. In addition, some clade I cases in the Central and Northeast regions exhibited echinocandin resistance without an identified *FKS1* mutation, which could warrant further investigation for potential novel non-*FKS1* mutations driving resistance.

Our dataset does not represent overall reported US *C. auris* cases. Although the AR Lab Network

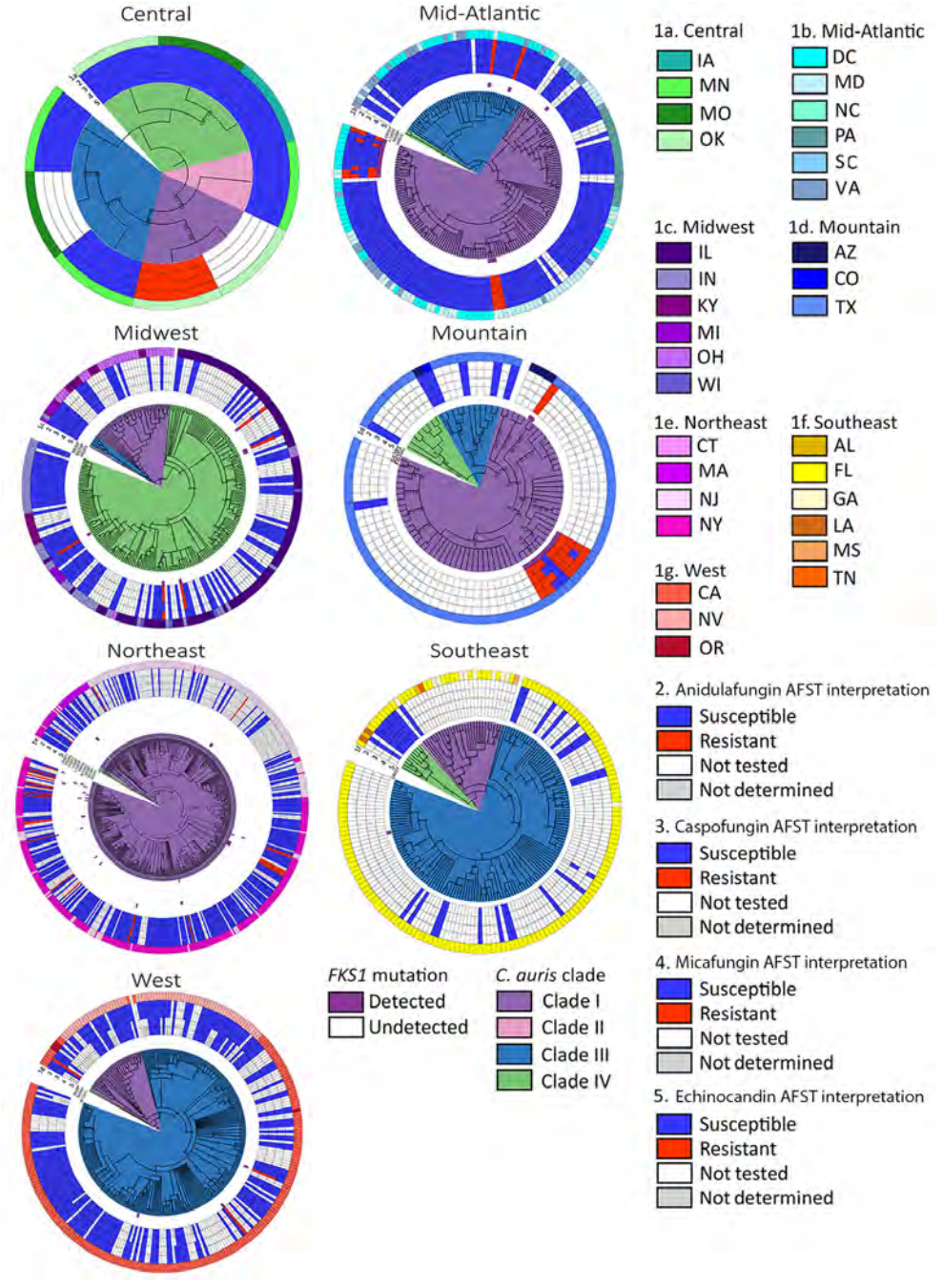

Figure 6. Midpoint-rooted maximum-likelihood phylogenetic trees of sequenced isolates, by region, from study of genomic epidemiologic description of *Candida (Candidozyma) auris*, United States, using clade-specific references. Clades are distinguished on the phylogenetic trees. Branch lengths are annotated with bootstrap support values (Shimodaira-Hasegawa–like approximate likelihood ratio test//ultrafast bootstrap approximation), where Shimodaira-Hasegawa–like approximate likelihood ratio test is ≥80 and ultrafast bootstrap approximation is ≥95. AFST, antifungal susceptibility testing.

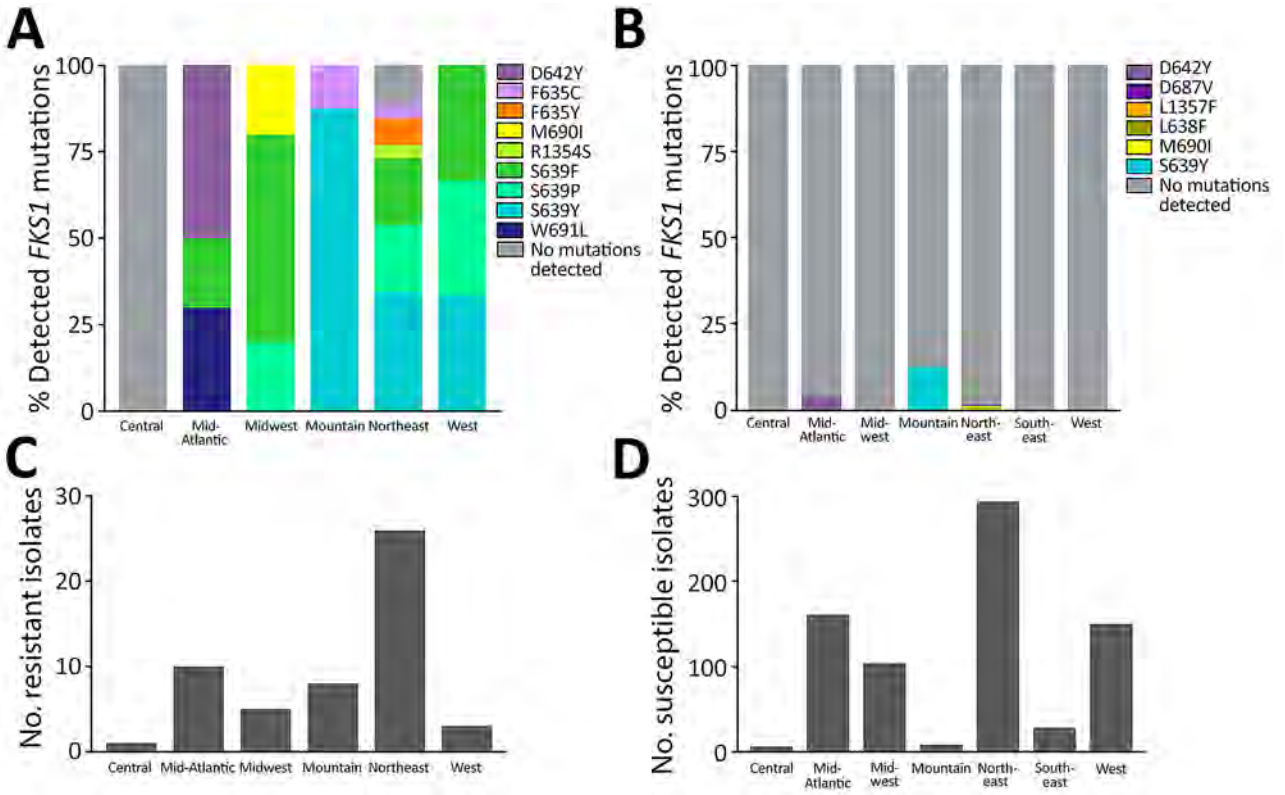

Figure 7. Echinocandin susceptibility by region for isolates from study of genomic epidemiologic description of *Candida (Candidozyma) auris*, United States. A, B) Percentages of isolates with detected *FKS1* mutations among resistant (A) and susceptible (B) isolates. C, D) Total numbers of resistant (C; n = 53) and susceptible (D; n = 756) isolates detected.

tests a substantial volume of cases nationally, some are tested independently by commercial, clinical, and public health laboratories. Therefore, this dataset reflects isolates available through the network based on established testing priorities, which were driven by epidemiologic need and logistical factors. Sequencing of the available isolates focused primarily on cases from new and emerging areas and other topics of interest and was intended to inform public health response. For example, we targeted pan- and echinocandin-resistant isolates, which may result in overrepresentation of such strains in the dataset. Although most isolates in this study represent unique cases, there were exceptions. For example, we sequenced isolates from the same patient on a few occasions to confirm the development of echinocandin resistance following treatment. Overall, because of circumstances surrounding priorities for isolate testing and data availability, phylogeographic and clade-related resistance patterns we described here are not generalizable to the entire *C. auris* population in the United States.

Approximately 55% of isolates in this dataset had accompanying AFST results. Because data availability varies regionally based on the laboratory's testing strategy and resources, AFST results may be overrepresented or underrepresented in certain jurisdictions. Certain AFST patterns might also be overrepresented in areas experiencing high transmission. For example, *C. auris* strains sequenced in areas in the Midwest, which had frequent clade IV transmission (*43*), likely exhibit similar AFST patterns. Therefore, the resistance frequencies we reported are not intended to be representative of the AFST patterns across the United States.

In conclusion, our data provide a national and regional perspective of *C. auris* clades in the United States and their resistance profiles. A multilevel approach to monitoring clades and echinocandin resistance will inform the targeting of public health resources to mitigate transmission and treat infections.

Acknowledgments

We thank the CDC AR Lab Network for providing testing for *C. auris* detection and drug susceptibility and isolates for whole-genome sequencing. We thank Malavika Rajeev for providing methodology for data linkages. We thank CDC's Office of Advanced Molecular Detection, Division of High-Consequence Pathogens, National Center for Emerging and Zoonotic Infectious Diseases, and the

Biotechnology Core Facility Branch, Division of Core Laboratory Services and Response, Office of Laboratory Systems and Response, for their continued support.

CDC and the US National Action Plan for Combatting Antibiotic-Resistant Bacteria provided funding for this work. The Oak Ridge Institute for Science and Education funded research fellowships for E.M. and A.S.

About the Author

Dr. Parnell is a biologist with the Mycotic Diseases Branch, Division of Foodborne, Waterborne, and Environmental Diseases, National Center for Emerging and Zoonotic Infectious Diseases, CDC, Atlanta, Georgia, USA. Her research interests include genomic surveillance and epidemiology of infectious diseases and antimicrobial resistance.

References

1. Liu F, Hu Z-D, Zhao X-M, Zhao W-N, Feng Z-X, Yurkov A, et al. Phylogenomic analysis of the *Candida auris-Candida haemuli* clade and related taxa in the *Metschnikowiaceae,* and proposal of thirteen new genera, fifty-five new combinations and nine new species. Persoonia. 2024;52:22–43.
2. Du H, Bing J, Hu T, Ennis CL, Nobile CJ, Huang G. *Candida auris*: epidemiology, biology, antifungal resistance, and virulence. PLoS Pathog. 2020;16:e1008921. https://doi.org/10.1371/journal.ppat.1008921
3. World Health Organization. WHO fungal priority pathogens list to guide research, development and public health action. Geneva: The Organization; 2022.
4. Lockhart SR, Etienne KA, Vallabhaneni S, Farooqi J, Chowdhary A, Govender NP, et al. Simultaneous emergence of multidrug-resistant *Candida auris* on 3 continents confirmed by whole-genome sequencing and epidemiological analyses. Clin Infect Dis. 2017;64:134–40. https://doi.org/10.1093/cid/ciw691
5. Chow NA, de Groot T, Badali H, Abastabar M, Chiller TM, Meis JF. Potential fifth clade of *Candida auris*, Iran, 2018. Emerg Infect Dis. 2019;25:1780–1. https://doi.org/10.3201/eid2509.190686
6. Khan T, Faysal NI, Hossain MM, Mah-E-Muneer S, Haider A, Moon SB, et al. Emergence of the novel sixth *Candida auris* clade VI in Bangladesh. Microbiol Spectr. 2024;12:e0354023. https://doi.org/10.1128/spectrum.03540-23
7. Suphavilai C, Ko KKK, Lim KM, Tan MG, Boonsimma P, Chu JJK, et al. Detection and characterisation of a sixth *Candida auris* clade in Singapore: a genomic and phenotypic study. Lancet Microbe. 2024;5:100878. https://doi.org/10.1016/S2666-5247(24)00101-0
8. Chow NA, Gade L, Tsay SV, Forsberg K, Greenko JA, Southwick KL, et al.; US Candida auris Investigation Team. Multiple introductions and subsequent transmission of multidrug-resistant *Candida auris* in the USA: a molecular epidemiological survey. Lancet Infect Dis. 2018;18:1377–84. https://doi.org/10.1016/S1473-3099(18)30597-8
9. De Luca DG, Alexander DC, Dingle TC, Dufresne PJ, Hoang LM, Kus JV, et al. Four genomic clades of *Candida auris* identified in Canada, 2012–2019. Med Mycol. 2022;60:myab079. https://doi.org/10.1093/mmy/myab079
10. Borman AM, Johnson EM. *Candida auris* in the UK: Introduction, dissemination, and control. PLoS Pathog. 2020;16:e1008563. https://doi.org/10.1371/journal.ppat.1008563
11. Kekana D, Naicker SD, Shuping L, Velaphi S, Nakwa FL, Wadula J, et al.; for GERMS-SA1. *Candida auris* clinical isolates associated with outbreak in neonatal unit of tertiary academic hospital, South Africa. Emerg Infect Dis. 2023;29:2044–53. https://doi.org/10.3201/eid2910.230181
12. Chow NA, Muñoz JF, Gade L, Berkow EL, Li X, Welsh RM, et al. Tracing the evolutionary history and global expansion of *Candida auris* using population genomic analyses. mBio. 2020;11:e03364-19. https://doi.org/10.1128/mBio.03364-19
13. Gorzalski A, Ambrosio FJ III, Massic L, Scribner MR, Siao DD, Hua C, et al. The use of whole-genome sequencing and development of bioinformatics to monitor overlapping outbreaks of *Candida auris* in southern Nevada. Front Public Health. 2023;11:1198189. https://doi.org/10.3389/fpubh.2023.1198189
14. Rhodes J, Abdolrasouli A, Farrer RA, Cuomo CA, Aanensen DM, Armstrong-James D, et al. Author correction: genomic epidemiology of the UK outbreak of the emerging human fungal pathogen *Candida auris.* Emerg Microbes Infect. 2018;7:104. https://doi.org/10.1038/s41426-018-0098-x
15. Spruijtenburg B, Nobrega de Almeida Júnior J, Ribeiro FC, Kemmerich KK, Baeta K, Meijer EFJ, et al.; Brazilian Candida auris collaborative network. Multicenter *Candida auris* outbreak caused by azole-susceptible clade IV in Pernambuco, Brazil. Mycoses. 2024;67:e13752. https://doi.org/10.1111/myc.13752
16. Price TK, Mirasol R, Ward KW, Dayo AJ, Hilt EE, Chandrasekaran S, et al. Genomic characterizations of clade III lineage of *Candida auris*, California, USA. Emerg Infect Dis. 2021;27:1223–7. https://doi.org/10.3201/eid2704.204361
17. Barbian HJ, Lie L, Kittner A, Harrington A, Carson J, Frias M, et al. *Candida auris* outbreak and epidemiologic response in burn intensive care unit, Illinois, USA, 2021–2023. Emerg Infect Dis. 2025;31:438–47. https://doi.org/10.3201/eid3103.241195
18. Cancino-Muñoz I, Mulet-Bayona JV, Salvador-García C, Tormo-Palop N, Guna R, Gimeno-Cardona C, et al. Short-term evolution and dispersal patterns of fluconazole-resistance in *Candida auris* clade III. mBio. 2025;16:e0316424. https://doi.org/10.1128/mbio.03164-24
19. da Silva KJG, Lucini F, Dos Santos RAC, Santos DA, Meis JF, Melhem MSC, et al. How does antifungal resistance vary in *Candida (Candidozyma) auris* and its clades? Quantitative and qualitative analyses and their clinical implications. Clin Microbiol Infect. 2025;31:1146–56. https://doi.org/10.1016/j.cmi.2025.04.003
20. Lyman M, Forsberg K, Sexton DJ, Chow NA, Lockhart SR, Jackson BR, et al. Worsening spread of *Candida auris* in the United States, 2019 to 2021. Ann Intern Med. 2023;176:489–95. https://doi.org/10.7326/M22-3469
21. Misas E, Escandón PL, Gade L, Caceres DH, Hurst S, Le N, et al. Genomic epidemiology and antifungal-resistant characterization of *Candida auris*, Colombia, 2016–2021. mSphere. 2024;9:e0057723. https://doi.org/10.1128/msphere.00577-23
22. Escandón P, Chow NA, Caceres DH, Gade L, Berkow EL, Armstrong P, et al. Molecular epidemiology of *Candida auris* in Colombia reveals a highly related, countrywide colonization with regional patterns in amphotericin B resistance. Clin Infect Dis. 2019;68:15–21. https://doi.org/10.1093/cid/ciy411

23. Escandón P, Cáceres DH, Lizarazo D, Lockhart SR, Lyman M, Duarte C. Laboratory-based surveillance of *Candida auris* in Colombia, 2016–2020. Mycoses. 2022;65:222–5. https://doi.org/10.1111/myc.13390
24. Sekizuka T, Iguchi S, Umeyama T, Inamine Y, Makimura K, Kuroda M, et al. Clade II *Candida auris* possess genomic structural variations related to an ancestral strain. PLoS One. 2019;14:e0223433. https://doi.org/10.1371/journal.pone.0223433
25. Kwon YJ, Shin JH, Byun SA, Choi MJ, Won EJ, Lee D, et al. *Candida auris* clinical isolates from South Korea: identification, antifungal susceptibility, and genotyping. J Clin Microbiol. 2019;57:e01624-18. https://doi.org/10.1128/JCM.01624-18
26. Spruijtenburg B, Badali H, Abastabar M, Mirhendi H, Khodavaisy S, Sharifisooraki J, et al. Confirmation of fifth *Candida auris* clade by whole genome sequencing. Emerg Microbes Infect. 2022;11:2405–11. https://doi.org/10.1080/22221751.2022.2125349
27. Gow NAR, Latge JP, Munro CA. The fungal cell wall: structure, biosynthesis, and function. Microbiol Spectr. 2017;5:5.3.01. https://doi.org/10.1128/microbiolspec.FUNK-0035-2016
28. Lyman M, Forsberg K, Reuben J, Dang T, Free R, Seagle EE, et al. Notes from the field: transmission of pan-resistant and echinocandin-resistant *Candida auris* in health care facilities—Texas and the District of Columbia, January–April 2021. MMWR Morb Mortal Wkly Rep. 2021;70:1022–3. https://doi.org/10.15585/mmwr.mm7029a2
29. Pfaller MA, Diekema DJ, Andes D, Arendrup MC, Brown SD, Lockhart SR, et al.; CLSI Subcommittee for Antifungal Testing. Clinical breakpoints for the echinocandins and *Candida* revisited: integration of molecular, clinical, and microbiological data to arrive at species-specific interpretive criteria. Drug Resist Updat. 2011;14:164–76. https://doi.org/10.1016/j.drup.2011.01.004
30. Centers for Disease Control and Prevention. Antimicrobial Resistance Laboratory Network. [cited 2024 Jun 4]. https://www.cdc.gov/antimicrobial-resistance-laboratory-networks/php/about/domestic.html
31. Council of State and Territorial Epidemiologists. Standardized case definition for *Candida auris* clinical and colonization/screening cases and national notification of *C. auris* case, clinical. 2018 [cited Jun 4]. https://cdn.ymaws.com/www.cste.org/resource/resmgr/ps/2018ps/18-ID-05_Dec2018_Update.pdf
32. Cingolani P, Platts A, Wang L, Coon M, Nguyen T, Wang L, et al. A program for annotating and predicting the effects of single nucleotide polymorphisms, SnpEff: SNPs in the genome of *Drosophila melanogaster* strain w1118; iso-2; iso-3. Fly (Austin). 2012;6:80–92. https://doi.org/10.4161/fly.19695
33. Carolus H, Pierson S, Muñoz JF, Subotić A, Cruz RB, Cuomo CA, et al. Genome-wide analysis of experimentally evolved *Candida auris* reveals multiple novel mechanisms of multidrug resistance. mBio. 2021;12:e03333-20. https://doi.org/10.1128/mBio.03333-20
34. Kordalewska M, Cancino-Prado G, Nobrega de Almeida Júnior J, Brasil Brandão I, Tigulini de Souza Peral R, Colombo AL, et al. Novel non–hot spot modification in *FKS1* of *Candida auris* confers echinocandin resistance. Antimicrob Agents Chemother. 2023;67:e0042323. https://doi.org/10.1128/aac.00423-23
35. Centers for Disease Control and Prevention. Antifungal susceptibility testing for *C. auris*. [cited June 4, 2024]. https://www.cdc.gov/candida-auris/hcp/laboratories/antifungal-susceptibility-testing.html
36. Misas E, Parnell LA, Rajeev M, López LF, Santos AR, Mudge ZB, et al. A benchmark dataset for validating *FKS1* mutations in *Candida auris*. Microbiol Spectr. 2025;13:e0314724. https://doi.org/10.1128/spectrum.03147-24
37. Muñoz JF, Gade L, Chow NA, Loparev VN, Juieng P, Berkow EL, et al. Genomic insights into multidrug-resistance, mating and virulence in *Candida auris* and related emerging species. Nat Commun. 2018;9:5346. https://doi.org/10.1038/s41467-018-07779-6
38. Karmarkar EN, O'Donnell K, Prestel C, Forsberg K, Gade L, Jain S, et al. Rapid assessment and containment of *Candida auris* transmission in postacute care settings—Orange County, California, 2019. Ann Intern Med. 2021;174:1554–62. https://doi.org/10.7326/M21-2013
39. Welsh RM, Sexton DJ, Forsberg K, Vallabhaneni S, Litvintseva A. Insights into the unique nature of the East Asian clade of the emerging pathogenic yeast *Candida auris*. J Clin Microbiol. 2019;57:e00007–00019. https://doi.org/10.1128/JCM.00007-19
40. Massic L, Gorzalski A, Siao DD, Dykema P, Hua C, Schneider E, et al. Detection of five instances of dual-clade infections of *Candida auris* with opposite mating types in southern Nevada, USA. Lancet Infect Dis. 2023;23:e328–9. https://doi.org/10.1016/S1473-3099(23)00434-6
41. Wang Y, Xu J. Population genomic analyses reveal evidence for limited recombination in the superbug *Candida auris* in nature. Comput Struct Biotechnol J. 2022;20:3030–40. https://doi.org/10.1016/j.csbj.2022.06.030
42. Ostrowsky B, Greenko J, Adams E, Quinn M, O'Brien B, Chaturvedi V, et al.; C. auris Investigation Work Group. *Candida auris* isolates resistant to three classes of antifungal medications—New York, 2019. MMWR Morb Mortal Wkly Rep. 2020;69:6–9. https://doi.org/10.15585/mmwr.mm6901a2
43. Barbian HJ, Walblay KA, Kittner A, Zelinski C, Newcomer EP, Adil H, et al. Genomic analysis of *Candida auris* transmission within an urban region. Microb Genom. 2025;11:001478. https://doi.org/10.1099/mgen.0.001478

Address for correspondence: Lindsay A. Parnell, Centers for Disease Control and Prevention, 1600 Clifton Rd NE, Mailstop H17-2, Atlanta, GA 30329-4018, USA; email: lparnell@cdc.gov

Retrospective Phylogenetic Analysis of Mayaro Virus, French Guiana, 1996–2024

Alisé Lagrave,[1] Antoine Enfissi,[1] Sourakhata Tirera, Loïc Epelboin, Jean-Bernard Duchemin, Tiphanie Succo, Anne Lavergne, Dominique Rousset

We conducted a retrospective phylogenetic analysis of Mayaro virus (MAYV) detected in French Guiana during 1996–2024. Analysis revealed circulation of MAYV genotype D sublineage 2 and suggested introduction from Brazil and spread to Haiti and Venezuela. Phylogenetic findings support endemic circulation and reinforce the need for MAYV surveillance in the region.

Mayaro virus (MAYV), a mosquitoborne RNA virus of the genus *Alphavirus* (family Togaviridae), causes acute febrile illness, often accompanied by prolonged arthralgia (*1*). Identified in 1954 in Trinidad and Tobago, MAYV has caused sporadic outbreaks throughout Central and South America (*2*–*5*). Clinical manifestations of MAYV infection include fever, headache, myalgia, nausea, and persistent joint pain, sometimes lasting more than a year (*6*,*7*).

Among arboviruses in the Amazon region, MAYV and emerging Oropouche virus are considered to have the highest epidemic potential (*1*,*2*). Phylogenetic analyses have identified 3 MAYV genotypes, D, L, and N (*8*–*10*). Genotype D is widely distributed, L is restricted to Brazil, and N has only been described from Peru, but evidence suggests recombination among MAYVs, as for other alphaviruses (*8*–*10*).

MAYV is primarily maintained in a sylvatic cycle involving *Haemagogus janthinomys* mosquitoes and nonhuman primates, with occasional spillover to humans (*2*). However, experimental studies with urban vectors *Aedes aegypti* and *Ae. albopictus* mosquitoes have shown them to be competent MAYV vectors, raising concerns about urban emergence (*11*).

In French Guiana, serologic studies support endemic sylvatic MAYV transmission, but an increase in urban and periurban cases in 2020 suggested a possible epidemiologic shift, reminiscent of adaptations observed in chikungunya virus (*7*,*12*,*13*). However, MAYV remains a neglected pathogen, and genomic data are scarce. By 2024, only 2 complete genomes were publicly available, and no comprehensive evolutionary analyses had been conducted for French Guiana. To address those gaps, we conducted a retrospective genomic analysis of virologically confirmed MAYV infections to explore potential genetic markers that could be associated with shifting transmission patterns and potential adaptation to new ecologic niches.

The Study

In French Guiana, the National Reference Center for Arboviruses collects serum samples for diagnostic and surveillance purposes (Appendix, https://wwwnc.cdc.gov/EID/article/32/5/25-1435-App1.pdf). During 1996–2024, French Guiana reported 38 cases of MAYV infection, including 2 exported cases, 1 to Germany and 1 to mainland France, and 4 cases that seroconverted without PCR confirmation. Cases were sporadic during 1996–2019, especially during 2005–2016, when specific surveillance was lacking. In 2020, a cluster of 14 cases occurred within 3 months, mainly in Cayenne and surrounding areas, most without identified epidemiologic links. In 2024, four additional PCR-confirmed cases were detected, 2 linked to the Nouragues Nature Reserve and 2 from the western and central coastal regions.

Author affiliations: Institut Pasteur de la Guyane, Arbovirus National Reference Center, Virology Unit, Cayenne, French Guiana (A. Lagrave, A. Enfissi, S. Tirera, A. Lavergne, D. Rousset); CHU de Guyane, Unité des Maladies Infectieuses et Tropicales, Cayenne (L. Epelboin); CHU de Guyane, CIC Inserm, Santé des Populations Amazoniennes, Cayenne (L. Epelboin); Institut Pasteur de la Guyane, Unité Entomologie médicale, Cayenne (J.-B. Duchemin); Santé Publique France, Cellule Guyane, Cayenne (T. Succo)

DOI: https://doi.org/10.3201/eid3205.251435

[1]These first authors contributed equally to this article.

Overall, French Guiana confirmed 34 infections by quantitative reverse-transcription PCR (qRT-PCR) or viral isolation in C6/36 cells; 32 were diagnosed locally (Appendix Figure). From those cases, we obtained 25 complete genomes, including 24 sequences we generated (Appendix Table 1). We performed whole-genome sequencing by using an amplicon-based MinION protocol (Oxford Nanopore Technologies, https://nanoporetech.com) and in-house primers (Appendix Table 2). We generated consensus genomes by using the ARTIC pipeline (ARTIC Network, https://artic.network) with Medaka polishing and completed missing regions by using Sanger sequencing (Appendix).

For phylogenetic analyses, we retrieved 76 complete coding sequences from GenBank and combined those with the 24 newly generated genomes for a total of 100 sequences. Using the Recombination Detection Program 4 (https://web.cbio.uct.ac.za/~darren/rdp.html), we detected no recombination events among French Guiana strains. We used a dataset of 45 genotype D sublineage 2 sequences to refine evolutionary inferences. We reconstructed Bayesian time-scaled phylogenies under a general time-reversible plus gamma distribution plus invariable site model with a strict molecular clock and Bayesian skyline prior plots; all parameters showed adequate convergence (effective sample size >200).

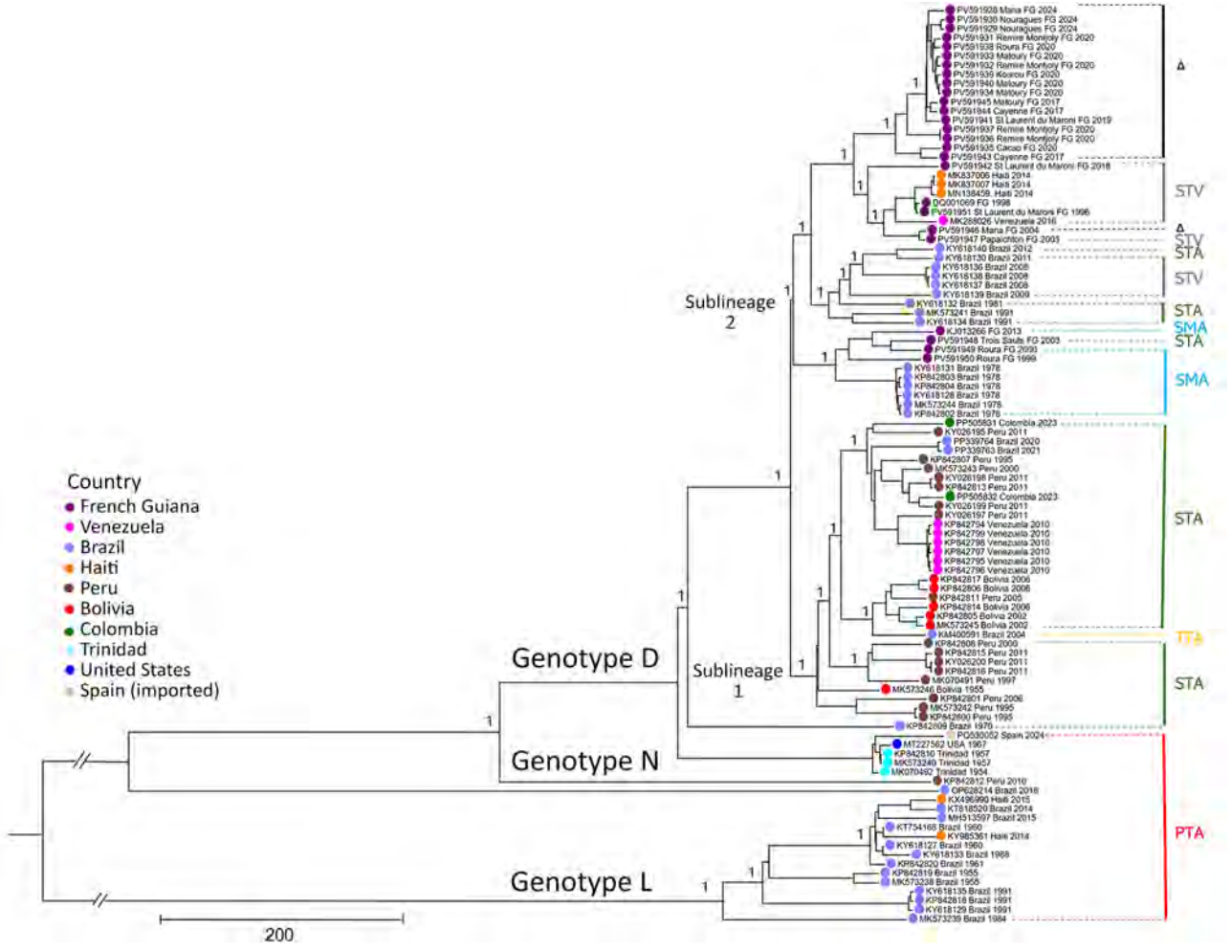

Figure 1. Bayesian phylogeny of 100 coding sequences from a retrospective phylogenetic analysis of Mayaro virus, French Guiana, 1996–2024. Maximum clade credibility tree inferred by using the general time-reversible with gamma distribution and invariant site substitution model, under a strict clock and Bayesian skyline coalescent prior. The tree was generated by using TreeAnnotator version 1.10.4 (BEAST Developers, https://beast.community/treeannotator), and the resulting time-scaled phylogenies were visualized with FigTree version 1.4.3 (http://tree.bio.ed.ac.uk/software/figtree). The tree includes major genotypes L, N, and D, and sublineages 1 and 2. The amino acid motifs at positions 1714–1716 are shown in color on the right side of the figure; triangles indicate strains with STV deletions. Bootstrap support values are indicated on the corresponding branches; a value of 1 corresponds to 100% bootstrap support. GenBank accession numbers are provided. Scale bar indicates nucleotide substitutions per site.

Our analyses showed that all French Guiana MAYV strains identified during 1996–2024 belonged to genotype D, and local strains shared high (97.58%–99.98%) nucleotide identity (Figure 1). Within global genotype D sequences, we identified 2 major sublineages: sublineage 1, which included sequences from Peru, Brazil, Bolivia, and Venezuela; and sublineage 2, which included sequences from French Guiana, Brazil, Haiti, and Venezuela. French Guiana sequences within sublineage 2 formed 2 clades that had a time to most recent common ancestor (tMRCA) of 1928 (95% highest posterior density [HPD] 1900–1956) (Figure 2).

Sublineage 2 clade 1 included sequences from Brazil from 1978 and French Guiana strains from 1999–2013 (tMRCA 1951, 95% HPD 1934–1968). Sublineage 2 clade 2 comprised sequences from Brazil from 1981–2012, and most French Guiana strains collected during 1996–2024; in addition, strains from Haiti from 2014 and from Venezuela from 2016 grouped within the French Guiana subclade. We estimated the sublineage 2 clade 2 tMRCA at 1942 (95% HPD 1928–1956).

Amino acid analyses revealed variability in nonstructural protein 3 at positions 1714–1716. Of note, sublineage 1 predominantly exhibited an STA motif, but sublineage 2 showed greater diversity, including SMA, STV, and a deletion shared French Guiana strains since 2004, consistent with ongoing local diversification.

All strains circulating in French Guiana belonged exclusively to genotype D, consistent with its broad distribution in South and Central America (*3*–*5*,*8*,*14*). The presence of Brazil sequences in both clades supports historical introductions from Brazil followed by sustained local transmission. Conversely, clustering of sequences from Haiti and Venezuela within a French Guiana subclade suggests possible secondary exportations, although we cannot exclude sampling bias given the limited number of recent genomes available (*3*–*5*).

High nucleotide identity among French Guiana strains and across sublineage 2, combined with relatively recent estimates of tMRCA, support long-term endemic circulation with limited genetic divergence.

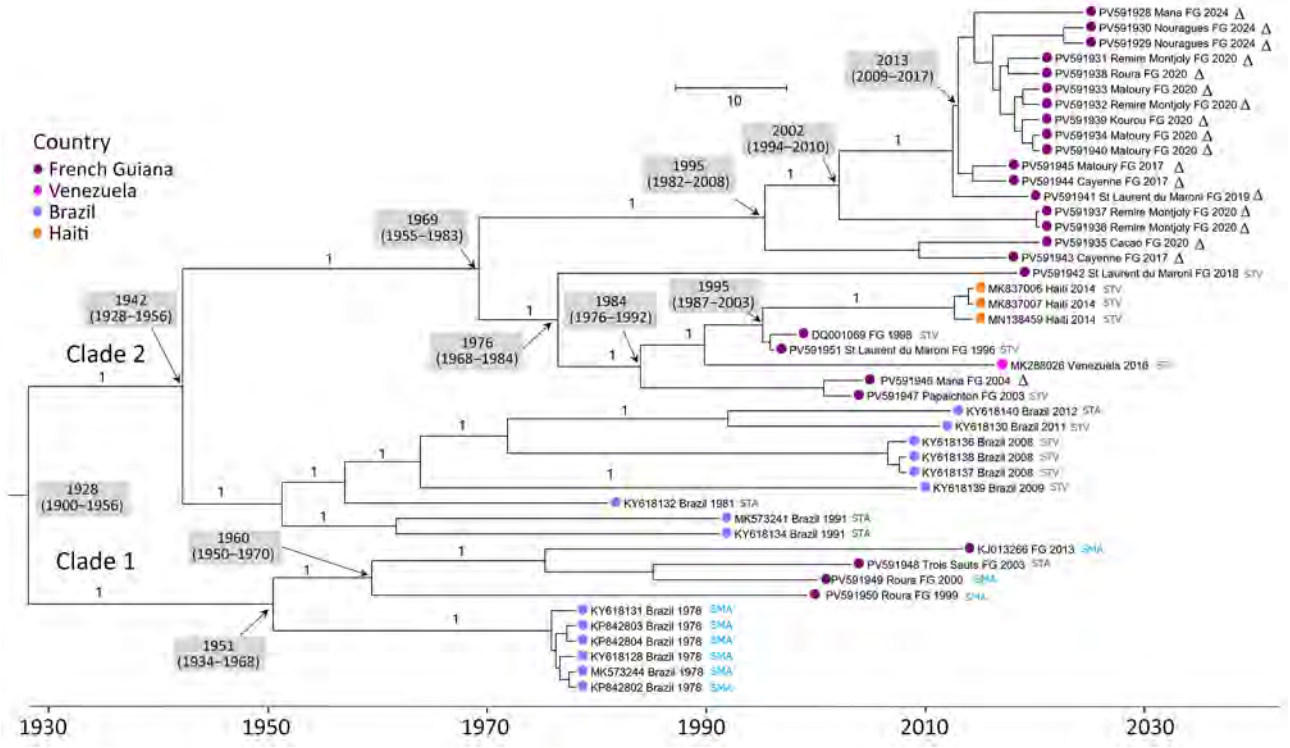

Figure 2. Bayesian phylogeny of 45 selected genotype D sublineage 2 coding sequences from a retrospective phylogenetic analysis of Mayaro virus, French Guiana, 1996–2024. Maximum clade credibility tree inferred by using the general time-reversible with gamma distribution and invariant site substitution model, under a strict clock and Bayesian skyline coalescent prior. The tree was generated by using TreeAnnotator version 1.10.4 (BEAST Developers, https://beast.community/treeannotator), and the resulting time-scaled phylogenies were visualized with FigTree version 1.4.3 (http://tree.bio.ed.ac.uk/software/figtree). Amino acid motifs at positions 1714–1716 are indicated by color at the terminal nodes of each sequence. Gray shaded boxes indicate dates of time to most recent common ancestor (95% highest posterior density). Bootstrap support values are indicated on the corresponding branches; a value of 1 corresponds to 100% bootstrap support. GenBank accession numbers are provided. Scale bar indicates nucleotide substitutions per site.

Phylogeographic patterns further indicate progressive spatial expansion: early clade 1 strains were mainly confined to inland and eastern areas, whereas clade 2 strains spread from western regions eastward and toward urban coastal centers, including Cayenne and surrounding municipalities. That distribution is consistent with persistent local transmission within a relatively stable ecologic niche, punctuated by episodic emergence.

The unusual cluster of 14 urban and periurban cases in 2020 raised concerns about a potential epidemiologic shift from a predominantly sylvatic cycle toward increased urban transmission (*11*,*15*). However, we detected no recombination events among French Guiana genomes and did not identify any mutation specifically associated with the 2020 cases. Enhanced diagnostic efforts, particularly during the COVID-19 pandemic and concurrent dengue outbreaks, likely improved case detection and could partly explain the 2020 case increase.

Amino acid analyses revealed variability at positions 1714–1716 in nonstructural protein 3, including a recurrent STV deletion in clade 2 strains sharing a common ancestor around 1995. Of note, we observed that deletion in strains from both urban and remote forest areas, arguing against a clear association with ecologic shift or vector change. Thus, alternative explanations must be considered, including spillover enabled by increasing overlap between forest fragments and expanding urban areas or competence of urban vectors such as *Ae. aegypti* and *Ae. albopictus* mosquitoes (although absent in French Guiana), which experimental studies demonstrated as viable vectors (*11*,*13*,*15*).

Conclusions

Genomic studies of MAYV remain limited, reflecting the continued neglect of this virus despite its broad distribution in the Amazon Basin and outbreaks in South America and the Caribbean (*3*–*5*). Few complete genomes are publicly available, restricting robust phylogeographic analyses and assessment of emergence potential. This study provides insights into the long-term evolutionary dynamics of MAYV in French Guiana and increases the total number of publicly available sequences. However, historical surveillance gaps and underdiagnosis suggest that current genomic data underestimate MAYV diversity.

Overall, our findings support longstanding endemic circulation of genotype D in French Guiana, characterized by geographic structuring and limited diversification, underscoring the need for integrated genomic, ecologic, and entomologic surveillance strategies. Expanded, sustained genomic surveillance across South America is essential to improving phylogenetic resolution, monitoring viral evolution, and assessing urbanization risk.

Acknowledgments

We thank the working group members of the arbovirus genomics diagnostic laboratories for their valuable contributions. We also thank the technicians of the National Research Center for Arboviruses of French Guiana for their input.

This work was financed by the National Research Center for Arboviruses of French Guiana. The activity of the National Reference Centers is supported by Santé publique France.

About the Authors

Dr. Lagrave is a research engineer at the Pasteur Institute of French Guiana. Her research interests focus on arboviruses circulating in the region. Dr. Enfissi is a research engineer and deputy head of the National Reference Center of the Pasteur Institute for arboviruses in French Guiana. Her research interests focus on surveillance of emerging and reemerging viruses in the French territories of the Americas.

References

1. Caicedo EY, Charniga K, Rueda A, Dorigatti I, Mendez Y, Hamlet A, et al. The epidemiology of Mayaro virus in the Americas: a systematic review and key parameter estimates for outbreak modelling. PLoS Negl Trop Dis. 2021;15:e0009418. https://doi.org/10.1371/journal.pntd.0009418
2. Wei LLL, Tom R, Kim YC. Mayaro virus: an emerging alphavirus in the Americas. Viruses. 2024;16:1297. https://doi.org/10.3390/v16081297
3. Forato J, Meira CA, Claro IM, Amorim MR, de Souza GF, Muraro SP, et al. Molecular epidemiology of Mayaro virus among febrile patients, Roraima State, Brazil, 2018–2021. Emerg Infect Dis. 2024;30:1013–6. https://doi.org/10.3201/eid3005.231406
4. Halsey ES, Siles C, Guevara C, Vilcarromero S, Jhonston EJ, Ramal C, et al. Mayaro virus infection, Amazon Basin region, Peru, 2010–2013. Emerg Infect Dis. 2013;19:1839–42. https://doi.org/10.3201/eid1911.130777
5. Lednicky J, De Rochars VMB, Elbadry M, Loeb J, Telisma T, Chavannes S, et al. Mayaro virus in child with acute febrile illness, Haiti, 2015. Emerg Infect Dis. 2016;22:2000–2. https://doi.org/10.3201/eid2211.161015
6. Acosta-Ampudia Y, Monsalve DM, Rodríguez Y, Pacheco Y, Anaya JM, Ramírez-Santana C. Mayaro: an emerging viral threat? Emerg Microbes Infect. 2018;7:1–11. https://doi.org/10.1038/s41426-018-0163-5
7. Mutricy R, Matheus S, Mosnier É, Martinez-Lorenzi E, De Laval F, Nacher M, et al. Mayaro virus infection in French Guiana, a cross sectional study 2003–2019.

Infect Genet Evol. 2022;99:105243. https://doi.org/10.1016/j.meegid.2022.105243
8. Auguste AJ, Liria J, Forrester NL, Giambalvo D, Moncada M, Long KC, et al. Evolutionary and ecological characterization of Mayaro virus strains isolated during an outbreak, Venezuela, 2010. Emerg Infect Dis. 2015;21:1742–50. https://doi.org/10.3201/eid2110.141660
9. Mavian C, Rife BD, Dollar JJ, Cella E, Ciccozzi M, Prosperi MCF, et al. Emergence of recombinant Mayaro virus strains from the Amazon basin. Sci Rep. 2017;7:8718. https://doi.org/10.1038/s41598-017-07152-5
10. Marinho MDS, Ferreira GM, Grosche VR, Nicolau-Junior N, Campos TL, Santos IA, et al. Evolutionary profile of Mayaro virus in the Americas: an update into genome variability. Viruses. 2024;16:809. https://doi.org/10.3390/v16050809
11. Long KC, Ziegler SA, Thangamani S, Hausser NL, Kochel TJ, Higgs S, et al. Experimental transmission of Mayaro virus by *Aedes aegypti*. Am J Trop Med Hyg. 2011;85:750–7. https://doi.org/10.4269/ajtmh.2011.11-0359
12. Bonifay T, Le Turnier P, Epelboin Y, Carvalho L, De Thoisy B, Djossou F, et al. Review on main arboviruses circulating on French Guiana, an ultra-peripheric European region in South America. Viruses. 2023;15:1268. https://doi.org/10.3390/v15061268
13. Hozé N, Salje H, Rousset D, Fritzell C, Vanhomwegen J, Bailly S, et al. Reconstructing Mayaro virus circulation in French Guiana shows frequent spillovers. Nat Commun. 2020;11:2842. https://doi.org/10.1038/s41467-020-16516-x
14. Powers AM, Aguilar PV, Chandler LJ, Brault AC, Meakins TA, Watts D, et al. Genetic relationships among Mayaro and Una viruses suggest distinct patterns of transmission. Am J Trop Med Hyg. 2006;75:461–9. https://doi.org/10.4269/ajtmh.2006.75.461
15. Mackay IM, Arden KE. Mayaro virus: a forest virus primed for a trip to the city? Microbes Infect. 2016;18:724–34. https://doi.org/10.1016/j.micinf.2016.10.007

Address for correspondence: Alisé Lagrave, Institut Pasteur de la Guyane, Arbovirus National Reference Center, Virology Unit, 23 Ave Pasteur, Cayenne 97306, French Guiana; email: alagrave@pasteur-cayenne.fr

Development and Validation of Real-Time PCR for Detecting *Anaplasma bovis*–Like Agent in *Dermacentor* spp. Ticks

Rachel C. Smith, Daniel F. Barrantes Murillo, Aryanna Carr, Kathryn T. Duncan, Lindsay A. Starkey

We developed and validated a real-time PCR to detect an *Anaplasma bovis*–like agent. We applied that assay to 672 *Dermacentor* spp. ticks collected from across the United States and found 0.1% *A. bovis*–like agent prevalence. This assay could enhance epidemiologic surveys for this *A. bovis*–like agent in ticks and humans.

An *Anaplasma bovis*–like agent was detected in humans in the United States in 2020 and was further described from 4 patients and a few *Dermacentor* spp. ticks in 2023 (*1*,*2*). Clinical data from human cases was not available, although patient samples were submitted for suspicion of tickborne illness (*1*,*2*). A subsequent regional survey detected the *A. bovis*–like agent in 10.1% (4/38) of *D. variabilis* ticks from Oklahoma but not in 93 Kansas *D. variabilis* ticks or 140 Oklahoma beef cattle (*3*).

Human illness caused by *A. bovis* has been described in China, where infection of ruminants is common (*4*,*5*). Epidemiologic investigation of the *A. bovis*–like agent is obstructed by lack of a specific, rapid molecular assay. Previous studies have relied on conventional PCRs (*2*,*3*), which are suitable for genetic characterization but cumbersome for screening large sample sets. To improve diagnostic methods, we developed and optimized a real-time probe-based PCR assay specifically for the *A. bovis*–like agent.

The Study

We retrieved from GenBank heat shock chaperon gene (*gro*EL) sequences from the *A. bovis*–like agent and related *Anaplasma* spp. bacteria, including *A. bovis*, *A. capra*, *A. centrale*, *A. marginale*, *A. ovis*, *A. phagocytophilum*, and *A. platys* (Appendix Table, https://wwwnc.cdc.gov/EID/article/32/5/25-1750-App1.pdf). We aligned sequences and generated potential primers and probes in Geneious Prime version 2025.2.2 (https://www.geneious.com) by using the primer design tool. We generated 1 assay (AboviTM) targeting a 125-bp fragment of the *gro*EL gene. AboviTM satisfied the design parameters, and we expected it to be specific to *A. bovis*–like agent because of base mismatches with nontarget sequences within the oligo binding sites.

We had custom AboviTM oligos synthesized in TaqMan assays (Thermo Fisher Scientific, https://www.thermofisher.com), then further interrogated the oligos (Table 1). We performed PCR reactions in MicroAmp EnduraPlate Optical 96-Well Clear Reaction Plates on an Applied Biosystems QuantStudio 3 Real-Time PCR instrument (both Thermo Fisher Scientific) and included nontemplate controls for every run.

We initially verified AboviTM by amplifying (×3) four *A. bovis*–like DNA samples previously extracted from *D. variabilis* ticks, then confirming by conventional PCR (*3*). Each 20-µL PCR re action contained 10 µL TaqMan Fast Advanced Master Mix (Thermo Fisher Scientific), 900 nmol of each primer, 250 nmol probe, 2 µL DNA template, and molecular grade water. Thermocycling conditions were enzyme activation at 95°C for 60 seconds, followed by 45× cycles of denaturation at 95°C for 3 seconds, and annealing/extension at 60°C for 30 seconds. To confirm appropriate amplicon size and identity, we performed gel electrophoresis in 2.0% agarose gel, followed by PCR product purification using the Wizard SV Gel and PCR Clean-up Kit (Promega, https://www.promega.com). Oklahoma State University (OSU) Molecular Core Facility performed Sanger sequencing (unidirectional), and we confirmed sequence identity by BLAST analysis (https://blast.ncbi.nlm.nih.gov).

For further assay optimization, we used a gBlocks synthetic double-stranded DNA standard (Integrated DNA Technologies, https://www.idtdna.com) of

Author affiliation: Oklahoma State University College of Veterinary Medicine, Stillwater, Oklahoma, USA

DOI: https://doi.org/10.3201/eid3205.251750

Table 1. Oligo sequences used to develop and validate real-time PCR for detecting *Anaplasma bovis*–like agent in *Dermacentor* spp. ticks, United States*

Type	Oligo name	Sequence, 5′ → 3′
Primer	AboviTMF	TGC GCA GTG TGT TAA GGA AG
Primer	AboviTMR	ACG GAG AAA GAT ATC CAC GAT CA
Probe	AboviTMPro	FAM-TCG GAA GAG ACG GAG TAA-MGB

*Oligos devised from heat shock chaperon gene (*gro*EL) sequences from *A. bovis*–like agent and related *Anaplasma* spp. bacteria retrieved from GenBank (Appendix Table, https://wwwnc.cdc.gov/EID/article/32/5/25-1750-App1.pdf).

the target sequence. We prepared a series of 10-fold dilutions to attain a range of 1–100,000,000 copies of target DNA per reaction. We evaluated combinations of varying primer (75–900 nmol) and probe (100–250 nmol) concentrations by using 100 copies/reaction. We considered assay performance to be optimal when the amplification curve demonstrated concurrently high baseline-corrected normalized reporter and low cycle threshold value (*6*). Assay performance was optimal at primer concentrations of 900 nmol each and probe concentration of 250 nmol. We performed subsequent PCR reactions with those concentrations and the thermocycling protocol described above.

We conducted standard curve analyses to evaluate the AboviTM assay efficiency and sensitivity by using 2 sample sets: the 10-fold dilution series containing synthetic target DNA only and the same dilution series with ≈54 ng of noninfected *D. variabilis* tick DNA added per reaction. We used tick samples to assess assay performance in the tick DNA matrix and obtained noninfected adult ticks from the OSU Tick Rearing Facility.

We amplified both dilution series in triplicate and repeated that experiment over 5 independent runs. We checked raw PCR data for quality, then used Applied Biosystems Design & Analysis Software version 2.8.0 (Thermo Fisher Scientific) to analyze data and exported data into Excel Version 1808 (Microsoft, https://www.microsoft.com). We calculated standard curve regression, amplification efficiency, and correlation by using the qPCRtools package in R Studio 2024.09.1 (*7*). We used the ggplot2 package in R Studio to visualize statistical and cycle threshold data (Figure 1).

The assay's limit of detection was 10 target copies. AboviTM detected as low as 1 target copy; however, limit of detection <3 copies is considered invalid because of stochastic limitations of quantitative PCR (*8*). We interrogated specificity by running AboviTM in triplicate with genetically similar agents that might be detected in ticks or mammals and observed no cross-amplification against *Anaplasma phagocytophilum*, *A. marginale*, *A. platys*, *Ehrlichia ewingii*, *E. chaffeensis*, *Rickettsia bellii*, or *R. montanensis*. Those

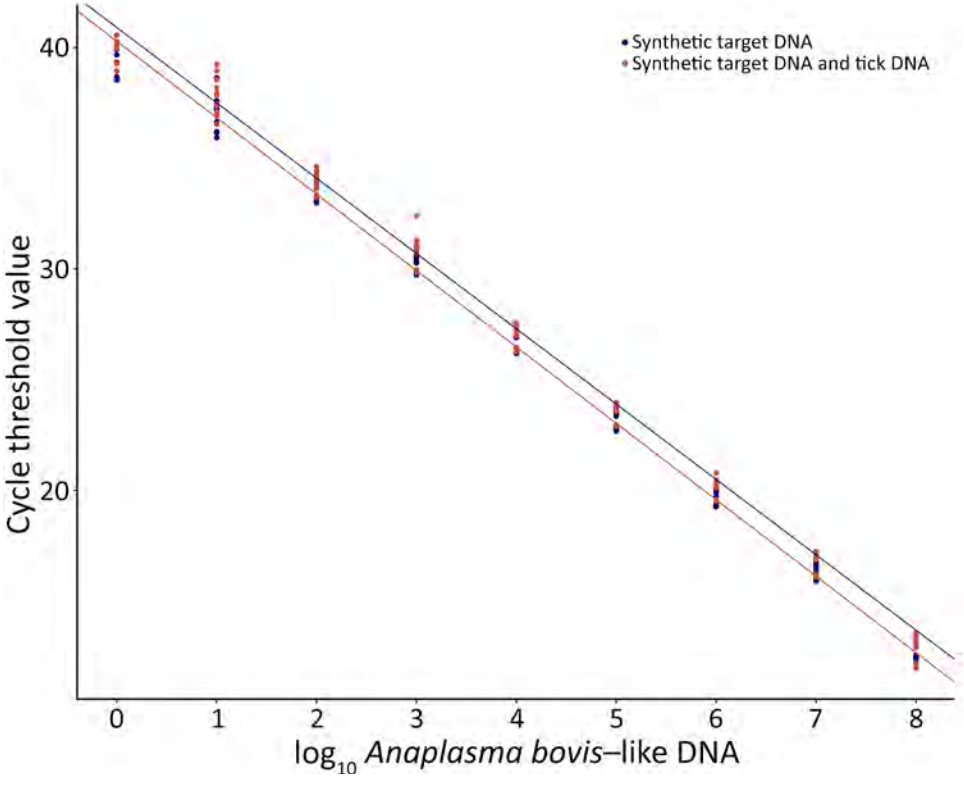

Figure 1. Results of the standard curve analyses, correlation, and amplification efficiency of real-time PCR for detecting *Anaplasma bovis*–like agent in *Dermacentor* spp. ticks, United States. We conducted standard curve analyses to evaluate assay efficiency and sensitivity by using 2 sets of samples: a 10-fold dilution series containing synthetic *A. bovis*–like DNA only and the same dilution series with ≈54 ng of noninfected *D. variabilis* tick DNA added per reaction. We used tick samples to assess assay performance in the tick DNA matrix. Graph shows standard curve lines for each sample set, with cycle threshold value graphed as a function of target copy number.

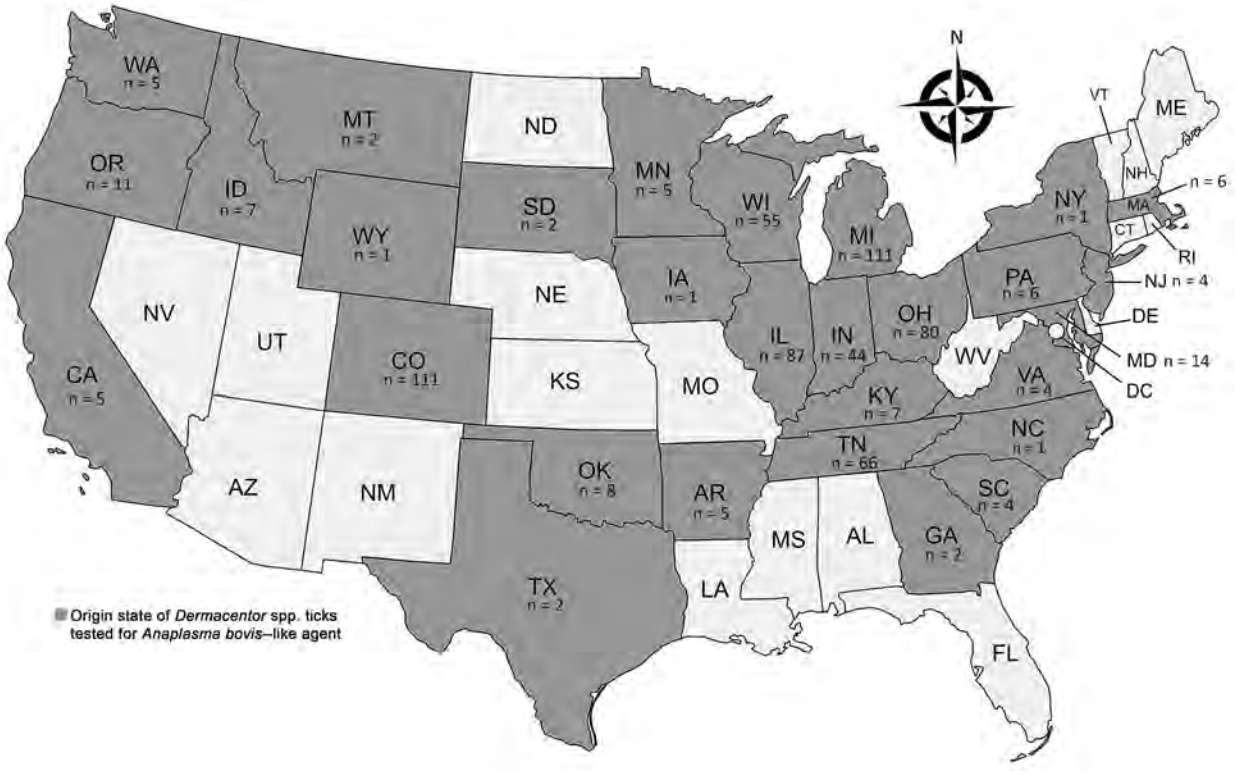

Figure 2. Number and geographic distribution of *Dermacentor* spp. ticks collected from dogs and cats and tested by real-time PCR (AboviTM assay) for *Anaplasma bovis*–like agent, United States. Ticks were collected at veterinary clinics across the country during 2021–2023 and shipped to the Oklahoma State University College of Veterinary Medicine Show Us Your Ticks program (https://www.showusyourticks.org), where staff morphologically identified ticks and stored in 70% ethanol at −20°C until dissection and DNA extraction in this study.

nontarget DNA samples were previously extracted from ticks or mammalian whole blood and confirmed by PCR and Sanger sequencing (data not shown).

We then applied the optimized AboviTM assay to 672 *Dermacentor* spp. ticks collected from dogs and cats across the United States during 2021–2023 (Figure 2). Veterinary clinics shipped ticks to the OSU College of Veterinary Medicine (https://www.showusyourticks.org), where staff morphologically identified ticks and stored in 70% ethanol at −20°C until dissection and DNA extraction.

We performed dissection by adhering ticks, ventral side down, on glass slides using double-sided adhesive tape. We used sterile no. 11 scalpels to open each tick along the coronal plane and to scrape out internal contents, which we transferred to sterile 1.5 mL microfuge tubes. We discarded tick exoskeletons. We used Cytiva Blood Genomic Prep Mini Spin Kit (Cytiva, https://www.cytivalifesciences.com) to extract total genomic DNA from tick samples, according to manufacturer recommendations. We tested ≤1 female and ≤1 male tick per species from an individual host. We detected *A. bovis*–like agent from only 1 (0.1%) tick (Table 2): a male *D. variabilis* tick collected from a dog in Blaine, Minnesota. We further verified that positive sample by using conventional PCRs targeting the 16S (*rrs*), citrate synthetase (*glt*A), and *gro*EL genes, as previously described (*2*,*9*,*10*). We resolved amplicons by gel

Table 2. Results from survey of ticks tested with real-time PCR for detecting *Anaplasma bovis*–like agent in *Dermacentor* spp. ticks, United States*

Tick species	Tick host		Tick sex		No. ticks tested	No. PCR positive (% [95% CI])
	Dog	Cat	F	M		
D. variabilis	592	39	394	237	631	1 (0.2 [0–0.9])
D. andersoni	35	2	30	7	37	0 (0 [0–9.5])
D. albipictus	2	2	3	1	4	0 (0 [0–60.2])
Total	629	43	427	245	672	1 (0.1 [0–0.8])

*Ticks were collected at veterinary clinics across the United States during 2021–2023 and shipped to the Oklahoma State University College of Veterinary Medicine Show Us Your Ticks program (https://www.showusyourticks.org), where staff morphologically identified ticks and stored in 70% ethanol at −20°C until dissection and DNA extraction in this study.

electrophoresis, then purified, performed Sanger sequencing (unidirectional), and analyzed as described. All sequences were 100% identical to previously reported sequences from *Dermacentor* spp. ticks and humans in the United States (GenBank accession nos. OQ772255, OQ772257.1, OQ693619, and PQ166304–7).

Conclusions

Few cases of human *A. bovis*–like infection have been reported in the United States (*1*,*2*). Some data suggest *Dermacentor* spp. tick transmission, although we detected *A. bovis*–like DNA in only 0.1% of *Dermacentor* spp. ticks tested. In our previous survey, we detected *A. bovis*–like DNA in 10.1% (4/38) of *D. variabilis* ticks from Oklahoma, 3 (75%) of which originated from the same collection site (*3*). Distribution of *A. bovis* might be highly focalized because, including findings from this study, *A. bovis*–like DNA has only been detected in humans and *D. variabilis* ticks from central US states, including Minnesota, Oklahoma, Missouri, Iowa, and Nebraska, and in *D. andersoni* ticks from Saskatchewan, Canada (*2*,*3*). Other possible tick and mammal species involved in transmission are currently unknown.

Because *A. bovis*–like agent has been detected in few *Dermacentor* spp. ticks and humans and few studies have investigated its epidemiology, broad conclusions cannot yet be drawn about its complete geographic distribution. AboviTM enables rapid, specific detection for *A. bovis*–like agent with high efficiency, dramatically improving methods for screening samples. Application of AboviTM to future studies could enable further largescale screening of humans, potential vectors, and animal hosts, which could greatly improve epidemiologic understanding of *A. bovis*–like agent in the United States.

Acknowledgments

We thank Susan Little, Kellee Sundstrom, and all other past and present OSU College of Veterinary Medicine personnel who have supported the Show Us Your Ticks Project, the source of ticks used for this study. We also thank Wade Burton and Ruth Scimeca for providing DNA-positive controls for *A. platys* and *A. marginale*, respectively. We thank the National Center for Veterinary Parasitology, who provided research grant funding in support of this study (primary investigator R.C.S.).

R.C.S. designed the study, performed and supervised most of the laboratory work described, wrote the first draft of the manuscript, and was responsible for funding acquisition. A.C. and D.F.B.M. performed DNA extraction from tick specimens. K.T.D. provided insight on experimental design of qPCR optimization and instrument use. L.A.S. assisted with funding acquisition. All authors reviewed and approved the final version of this article.

About the Author

Dr. Smith is a recent graduate of the Oklahoma State College of Veterinary Medicine Comparative Biomedical Sciences graduate program. Her research interests include epidemiology and diagnosis of emerging vectorborne infections of zoonotic and veterinary importance and clinical diagnostic parasitology.

References

1. Kingry L, Sheldon S, Oatman S, Pritt B, Anacker M, Bjork J, et al. Targeted metagenomics for clinical detection and discovery of bacterial tick-borne pathogens. J Clin Microbiol. 2020;58:e00147-20. https://doi.org/10.1128/JCM.00147-20
2. Karpathy SE, Kingry L, Pritt BS, Berry JC, Chilton NB, Dergousoff SJ, et al. *Anaplasma bovis*–like infections in humans, United States, 2015–2017. Emerg Infect Dis. 2023;29:1904–7. https://doi.org/10.3201/eid2909.230559
3. Smith RC, Myers S, Sundstrom KD, Wilson R, Scimeca RC, Starkey LA, et al. Detection of *Anaplasma bovis*–like agent in the southcentral United States. Ticks Tick Borne Dis. 2024;15:102411. https://doi.org/10.1016/j.ttbdis.2024.102411
4. Lu M, Chen Q, Qin X, Lyu Y, Teng Z, Li K, et al. Outbreak reports: *Anaplasma bovis* infection in fever and thrombocytopenia patients—Anhui Province, China, 2021. China CDC Wkly. 2022;4:249–53. https://doi.org/10.46234/ccdcw2022.053
5. Liu Z, Ma M, Wang Z, Wang J, Peng Y, Li Y, et al. Molecular survey and genetic identification of *Anaplasma* species in goats from central and southern China. Appl Environ Microbiol. 2012;78:464–70. https://doi.org/10.1128/AEM.06848-11
6. Raymaekers M, Smets R, Maes B, Cartuyvels R. Checklist for optimization and validation of real-time PCR assays. J Clin Lab Anal. 2009;23:145–51. https://doi.org/10.1002/jcla.20307
7. Li X, Wang Y, Li J, Mei X, Liu Y, Huang H. qPCRtools: an R package for qPCR data processing and visualization. Front Genet. 2022;13:1002704. https://doi.org/10.3389/fgene.2022.1002704
8. Bustin SA, Benes V, Garson JA, Hellemans J, Huggett J, Kubista M, et al. The MIQE guidelines: minimum information for publication of quantitative real-time PCR experiments. Clin Chem. 2009;55:611–22. https://doi.org/10.1373/clinchem.2008.112797
9. Sumner JW, Nicholson WL, Massung RF. PCR amplification and comparison of nucleotide sequences from the *gro*ESL heat shock operon of *Ehrlichia* species. J Clin Microbiol. 1997;35:2087–92. https://doi.org/10.1128/jcm.35.8.2087-2092.1997
10. Zhuang L, Du J, Cui XM, Li H, Tang F, Zhang PH, et al. Identification of tick-borne pathogen diversity by metagenomic analysis in *Haemaphysalis longicornis* from Xinyang, China. Infect Dis Poverty. 2018;7:45. https://doi.org/10.1186/s40249-018-0417-4

Address for correspondence: Rachel C. Smith, Oklahoma State University College of Veterinary Medicine, 250 McElroy Hall, 208 N McFarland St, Stillwater, OK 74078, USA; email: rachel.c.smith@okstate.edu

Exposure in Horses to Human Tick-Borne Relapsing Fever Agent *Borrelia persica*, Israel, 2025

Dor Shwartz, Lior Haras, Yaarit Nachum-Biala, Sharon Tirosh-Levy, Amir Steinman, Gad Baneth

Human tick-borne relapsing fever caused by *Borrelia persica* is common in western Asia. A survey of 301 horses in Israel revealed 9.96% seropositivity toward *B. persica* antigens; 1 horse (0.33%) was also PCR positive for *B. persica* DNA. Phylogenetic analysis supported a transmission cycle involving ticks, humans, and horses.

Tick-borne relapsing fever (TBRF) is a human and veterinary illness caused by spirochetes of the genus *Borrelia* (*1*). *Borrelia persica*, transmitted by the argasid tick *Ornithodoros tholozani*, is the primary cause of TBRF in Israel and affects persons in other parts of the eastern Mediterranean basin and Asia (*2*–*4*). Relapsing fever in humans is characterized by episodes of recurrent fever, lethargy, and headache; an up to 10% mortality rate in untreated patients has been documented (*5*). TBRF caused by *B. persica* in dogs and cats is associated with fever, lethargy, anorexia, anemia, and thrombocytopenia and can be fatal (*6*). Several species of wild animals are known potential reservoirs for *B. persica* spirochetes, including the red fox (*Vulpes vulpes*), golden jackal (*Canis aureus*), European badger (*Meles meles*), and some rodent species (*7*–*9*). In contrast to *Borrelia* spp. that cause Lyme disease in horses, for which high seroprevalence has been reported in several countries (*10*), equine TBRF is poorly documented. One case of equine abortion has been reported in a mare from California infected with either *B. parkeri* or *B. turicatae*, which could not be distinguished (*10*,*11*). We tested samples from horses from throughout Israel for *B. persica* seroreactivity.

The Study

We collected samples from 301 clinically unremarkable horses from 27 stables throughout Israel, representing the geographic distribution of the equine population, and from 12 horses living in a nonendemic area for TBRF in southern Israel, where *O. tholozani* ticks have not been reported (*7*), which served as negative controls. Of the 301 horses, 1 (0.33%) was positive for *B. persica* DNA by using real-time PCR amplification, confirmed by sequencing of the *flaB* and *glpQ* genes, as described previously (*9*). Thirty (9.96%) horses were seroreactive against *B. persica* antigen by ELISA testing.

The ELISA assay was developed and performed as previously described for dogs and cats (*8*) with adaptation to horses. We extracted crude antigen from 1 L of *B. persica* culture containing 10^7 spirochetes/mL and lysed by sonication. We coated each well with 0.7 μg of antigen. We performed blocking by using 5% skimmed milk powder dissolved in phosphate-buffered saline (PBS) (Merck KGaA, https://www.emdgroup.com) and incubated the plates overnight at 4°C. We diluted the tested serum 1:500 in PBS with 0.1% Tween 20 (PBS-T) and 2% fetal bovine serum. We incubated serum bound antibodies for 1 hour at 37°C with horseradish peroxide-conjugated goat anti-horse IgG (ABCAM, https://www.abcam.com) diluted 1:50,000 in PBS-T and 2% fetal bovine serum. We read each plate when the absorbance (λ = 405 nm) of the positive reference serum reached an optical density (OD) value of 1.1. We determined a cutoff value of 0.35 OD by adding 3 SEs to the mean absorbance of serum from the negative control group. Serum from the horse found positive for *B. persica* by real-time PCR and sequencing was used as a positive control.

The median serologic OD was 0.472 for the seropositive, 0.145 for the seronegative, and 0.138 for the negative control horses (Figure 1). We found significant differences between the 3 groups (Kruskal-Wallis H = 64.72; p<0.0001). Posthoc Dunn tests demonstrated that seropositive horses had a higher OD than both seronegative (adjusted p<0.0001; mean rank difference = 156.98) and negative control (adjusted p<0.0001; mean rank difference = 182.00) groups. We

Author affiliation: Hebrew University of Jerusalem, Koret School of Veterinary Medicine, Rehovot, Israel

DOI: https://doi.org/10.3201/eid3205.251283

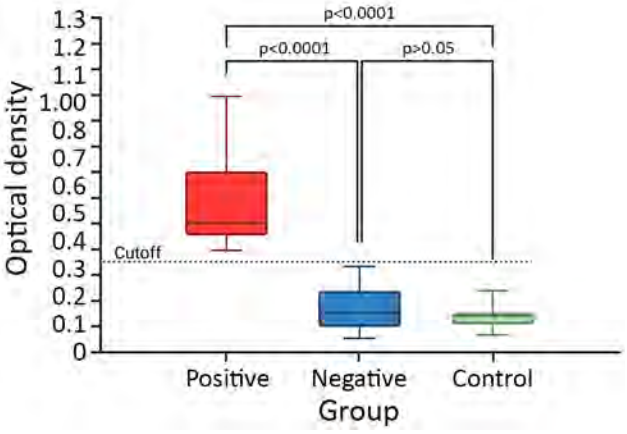

Figure 1. Comparative analysis of serologic responses of horses exposed to human tick-borne relapsing fever agent *Borrelia persica*, Israel, 2025. Box-and-whisker plot demonstrates optical density measurements from seropositive (blue), seronegative (red), and negative control (green) horses. The dashed line represents the established cutoff value (optical density = 0.35). Statistical significance was determined using a Kruskal–Wallis test followed by Dunn multiple comparison test. Results significantly distinguish between the seropositive horses compared with the seronegative and control groups, whereas the seronegative group did not significantly differ from the negative control. Horizontal lines within boxes represent median values; box tops and bottoms indicate the upper and lower quartiles; error bars represent ranges. p values are indicated.

did not observe a significant difference between seronegative and negative control groups (adjusted p = 1.000; mean rank difference = 25.02) (Figure 1). Seropositive horses were significantly older than seronegative ones (mean ±SD 13.8 ±6.3 years for seropositive vs. 10.8 ±5.4 years for seronegative; Mann-Whitney U = 2,633, p = 0.009). Furthermore, we found age was a significant independent predictor of TBRF seropositivity with an odds ratio (OR) of 1.09 per year (95% CI 1.03–1.17; p = 0.007). Seropositivity did not significantly differ according to sex (χ^2 = 2.32; p = 0.313) or housing type (χ^2 = 2.01; p = 0.367).

The PCR-positive horse was also found to be seropositive (OD 1.04). It was a 10-year-old gelding from a stall in the city of Ramat Gan, Israel. Sequencing analysis of a 272-bp segment of the *flaB* and a 224-bp segment of the *glpQ* gene fragments from the positive horse revealed 100% identity and coverage to a *B. persica* amplified from a human (GenBank accession no. DQ679907.1 [*flaB*]) and from an *O. tholozani* tick (GenBank accession no. HM161658.1 [*glpQ*]). Seropositive horses resided in 15 different locations (Figure 2). All positive horses were adults with a median age of 13 years (range 3–38 years); there were 18 geldings and 12 mares.

Phylogenetic analysis on the basis of a 272-bp segment of the *flaB* gene sequence (Figure 3) revealed that the *B. persica* sequence from the positive horse clustered together with a *B. persica* genotype II sequence previously amplified from a human in Israel (GenBank DQ679907.1) (*12*). All *B. persica* sequences clustered separately from other Old World relapsing fever *Borrelia* spp. that are transmitted by ixodid ticks, including *B. lonestari* and *B. theileri*, which clustered together, but separately from *B. miyamotoi*, which clustered with *B. hermsii*. Phylogenetic analysis on the basis of a 224-bp segment of the *glpQ* gene (Figure 4) also revealed that the sequence from the *B. persica*–positive horse clustered with other *B. persica* sequences from a human, a cat, a European badger, and an *O. tholozani* tick and with the corresponding sequence of the only published whole-genome reference of *B. persica* from an *Ornithodoros papillipes* tick in Uzbekistan (GenBank accession no. AYOT00000000).

Conclusions

This study describes a survey of TBRF *Borrelia* spp. in horses. Furthermore, it introduces a new ELISA

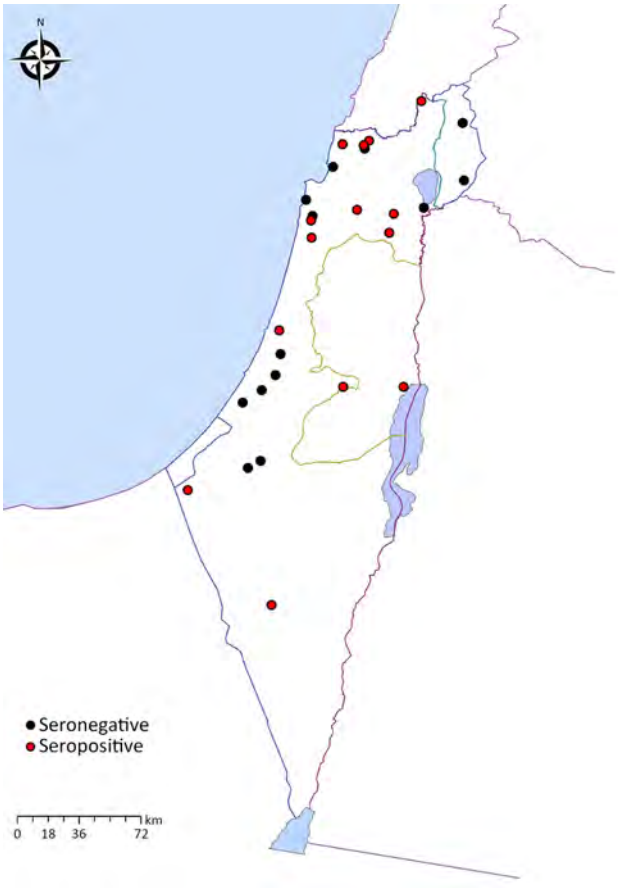

Figure 2. Geographic distribution of sampled horses in study of horses exposed to human tick-borne relapsing fever agent *Borrelia persica* in Israel that indicates the seroprevalence. Red circles represent the locations of seropositive horses; black circles denote seronegative horse locations.

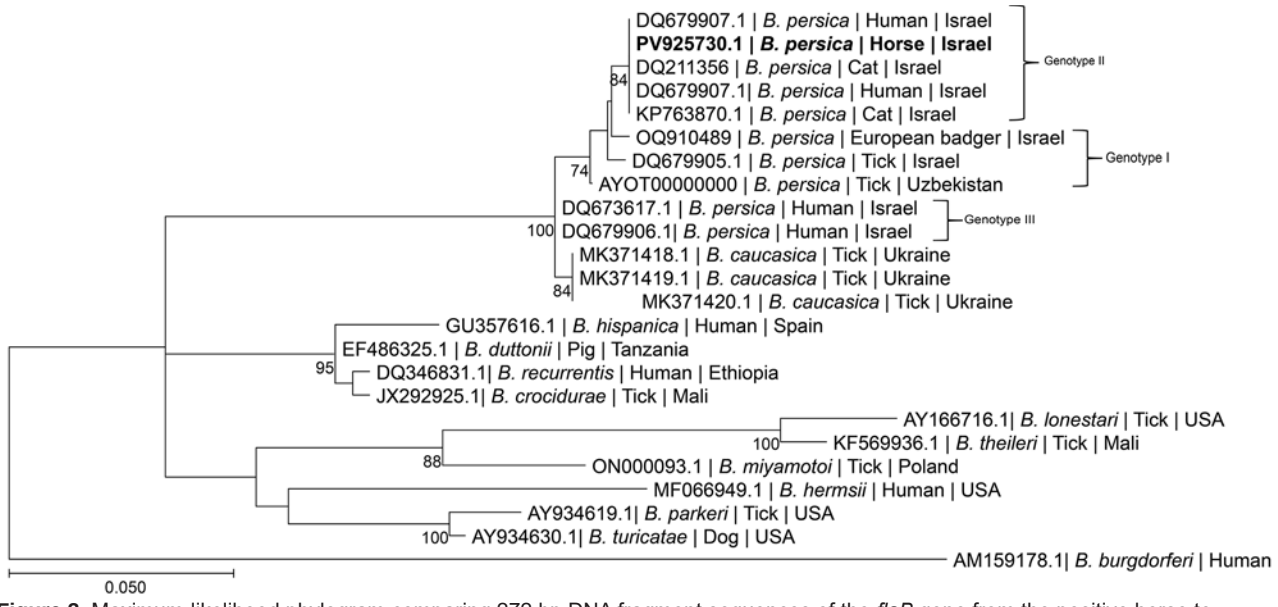

Figure 3. Maximum-likelihood phylogram comparing 272 bp DNA fragment sequences of the *flaB* gene from the positive horse to sequences from other *Borrelia persica* and other *Borrelia* spp. GenBank accession numbers in a study of *B. persica* exposed horses in Israel. Bold indicates new sequence derived from this study. *B. persica* genotypes are noted at right. GenBank accession number, species of infected host, and country of origin is provided for each sequence. The Tamura 3-parameter model was used in the construction of this phylogram with bootstrap performed on 1,000 replicates; values >70% are indicated. Scale bar represents the number of nucleotide substitutions per site; branch numbers indicate bootstrap support values, expressed as percentages.

optimized for horse serum to detect antibodies against *B. persica*, enabling seroepidemiologic investigations. Our findings indicate an unexpectedly high seroprevalence (9.96%) among clinically healthy horses, suggesting high exposure to *B. persica* and to infected *O. tholozani* ticks. *B. persica* DNA was detectable in 1 of the seropositive horses, which indicates that horses are not only exposed to this spirochete but also might develop a circulating infection. The horses included in the study were all apparently healthy, but, as is the case for humans, dogs, and cats, illness might develop after infection. Furthermore, horses might serve as potential reservoir hosts for TBRF, which could then be transmitted to humans and other animals.

Israel and the surrounding region are not endemic for Lyme borreliosis, and no autochthonous infections have been reported in humans or animals in Israel to our knowledge. Therefore, serologic cross-reactivity with a Lyme borreliosis agent is unlikely in the studied horses. Nevertheless, the potential occurrence of other relapsing fever species besides *B. persica* in Israel is possible (*13*). The *glpQ* phylogram displays

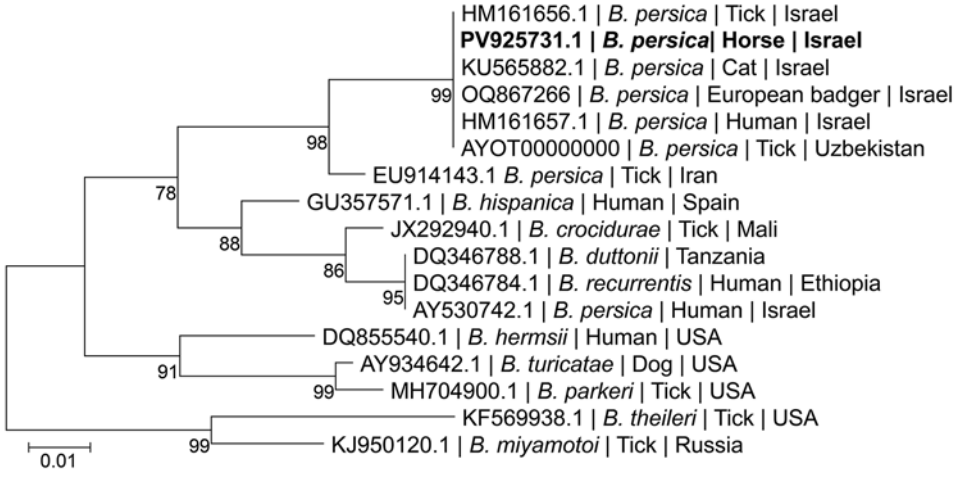

Figure 4. Maximum-likelihood phylogram comparing 224 bp DNA fragment sequences of the *glpQ* gene from the positive horse sequences from other *B. persica* and other *Borrelia* spp. GenBank accessions. Bold indicates new sequence derived from this study . GenBank accession number, species of infected host, and country of origin is provided for each sequence. The Tamura 3-parameter model was used in the construction of this phylogram with bootstrap performed on 1,000 replicates; values >70% are indicated. Scale bar represents the number of nucleotide substitutions per site; branch numbers indicate bootstrap support values, expressed as percentages.

variation in 2 *B. persica* sequences (GenBank accession nos. EU914143.1 [tick] and AY530742.1 [human]) that were amplified in Israel. Those sequences share <95% identity with other *B. persica glpQ* sequences deposited into GenBank and could possibly belong to different species.

Increasing age was associated with seropositivity, which aligns with prolonged or cumulative exposure to tick vectors during the horse lifespan. Neither horse sex nor housing conditions was associated with seropositivity, indicating exposure regardless of management practices.

The phylogenetic analyses we report support a potential shared transmission cycle of *B. persica* involving horses, humans, and *O. tholozani* ticks, and suggesting a potential zoonotic risk associated with infected equine populations. Horses might serve as reservoirs and sentinels for human infection with *B. persica*, and One Health approach strategies should be implemented to monitor and manage risks posed by this pathogen.

This study was approved by the Internal Research Committee of the Koret School of Veterinary Medicine Veterinary Teaching Hospital at the Hebrew University (approval no. KSVM-VTH/23_2014).

All data generated or analyzed during this study are included in this manuscript. Sequences obtained in this study were deposited in GenBank (accession nos. PV925730.1 [*flaB*] and PV925731.1 [*glpQ*]).

About the Author

Dr. Shwartz is a veterinary doctor and a PhD candidate in the Koret School of Veterinary Medicine, Hebrew University of Jerusalem, Israel. His research interests focus on vector-borne zoonotic diseases.

References

1. Dworkin MS, Schwan TG, Anderson DE Jr, Borchardt SM. Tick-borne relapsing fever. Infect Dis Clin North Am. 2008;22:449–68, viii. https://doi.org/10.1016/j.idc.2008.03.006
2. Safdie G, Farrah IY, Yahia R, Marva E, Wilamowski A, Sawalha SS, et al. Molecular characterization of *Borrelia persica*, the agent of tickborne relapsing fever in Israel and the Palestinian Authority. PLoS One. 2010;5:e14105. https://doi.org/10.1371/journal.pone.0014105
3. Muigg V, Seth-Smith HMB, Goldenberger D, Egli A, Nickel B, Dürig R, et al. Tick-borne relapsing fever caused by *Borrelia persica* in traveler to Central Asia, 2019. Emerg Infect Dis. 2020;26:824–6. https://doi.org/10.3201/2604.191771
4. Davis GE, Hoogstraal H. Biology of the spirochete *Borrelia persica*, found in the tick Ornithodorus tholazani (Argasinae) collected in the governorat of the Western Egyptian Desert; comments on the distribution and ecology of the vector tick [in French]. Ann Parasitol Hum Comp. 1956;31:147–54. https://doi.org/10.1051/parasite/1956311147
5. Barbour AG. Relapsing fever and Borrelia miyamotoi disease. In: Loscalzo J, Fauci A, Kasper D, Hauser S, Longo D, Jameson JL, editors. Harrison's principles of internal medicine. 21st ed. New York: McGraw-Hill Education; 2022.
6. Baneth G, Nachum-Biala Y, Halperin T, Hershko Y, Kleinerman G, Anug Y, et al. *Borrelia persica* infection in dogs and cats: clinical manifestations, clinicopathological findings and genetic characterization. Parasit Vectors. 2016;9:244. https://doi.org/10.1186/s13071-016-1530-5
7. Kleinerman G, Eshed T, Nachum-Biala Y, King R, Baneth G. Transmission of the human relapsing fever spirochete *Borrelia persica* by the argasid tick Ornithodoros tholozani involves blood meals from wildlife animal reservoirs and mainly transstadial transfer. Appl Environ Microbiol. 2021;87:e03117–20. https://doi.org/10.1128/AEM.03117-20
8. Baneth G, Dvorkin A, Ben-Shitrit B, Kleinerman G, Salant H, Straubinger RK, et al. Infection and seroprevalence of *Borrelia persica* in domestic cats and dogs in Israel. Parasit Vectors. 2022;15:102. https://doi.org/10.1186/s13071-022-05223-9
9. Shwartz D, Nachum-Biala Y, Oren S, Aharoni K, Edery N, Moss L, et al. *Borrelia persica* infection in wild carnivores in Israel: molecular characterization and new potential reservoirs. Parasit Vectors. 2023;16:337. https://doi.org/10.1186/s13071-023-05953-4
10. Divers TJ, Gardner RB, Madigan JE, Witonsky SG, Bertone JJ, Swinebroad EL, et al. Borrelia burgdorferi infection and Lyme disease in North American horses: a consensus statement. J Vet Intern Med. 2018;32:617–32. https://doi.org/10.1111/jvim.15042
11. Walker RL, Read DH, Hayes DC, Nordhausen RW. Equine abortion associated with the Borrelia parkeri-B. turicatae tick-borne relapsing fever spirochete group. J Clin Microbiol. 2002;40:1558–62. https://doi.org/10.1128/JCM.40.4.1558-1562.2002
12. Assous MV, Wilamowski A, Bercovier H, Marva E. Characterization of relapsing fever. Emerg Infect Dis. 2006;12:1740–3. https://doi.org/10.3201/eid1211.060715
13. Halperin T, Orr N, Cohen R, Hasin T, Davidovitch N, Klement E, et al. Detection of relapsing fever in human blood samples from Israel using PCR targeting the glycerophosphodiester phosphodiesterase (GlpQ) gene. Acta Trop. 2006;98:189–95. https://doi.org/10.1016/j.actatropica.2006.04.004

Address for correspondence: Dor Shwartz, The Koret School of Veterinary Medicine, P.O. Box 12, Rheovot 7610001, Israel; email: dor.shwartz@mail.huji.ac.il

One Health Investigation into Fatal Encephalitis Caused by Pigeon Paramyxovirus Type 1, France

Nicolas Veyrenche, Susana Boluda,[1] Philippe Pérot,[1] Isabelle Malissin, Marianne Leruez-Ville, Anne Jamet, Agnès Ferroni, Béatrice Regnault, Maud Salmona, Linda Feghoul, Laurine Robert-Capraro, Aurélie Leroux, Béatrice Grasland, Eric Niqueux, François-Xavier Briand, Isabelle Plu, Danielle Seilhean,[2] Bruno Megarbane,[2] Jacques Fourgeaud,[2] Nolwenn M. Dheilly[2]

Pigeon paramyxovirus type 1 (PPMV-1) is a genotype of avian paramyxovirus type 1 that uses species of the family Columbidae as reservoir species. We report fatal PPMV-1 encephalitis in a human without immunosuppression or travel history outside metropolitan France. Postmortem analyses revealed PPMV-1 in tissues, underscoring that physicians should consider this potential diagnosis.

Paramyxoviridae is a family of enveloped, negative-sense single-stranded RNA viruses that includes many human pathogens. Paramyxoviruses have a broad host range and high risk for spillover events to humans (*1*). Newcastle disease virus, classified as Avian orthoavulavirus (AOAV-1; formerly avian paramyxovirus type 1 [APMV-1]), is divided into class I and II, which are further subdivided into genotypes and subgenotypes (*2*–*4*). Pigeon paramyxovirus type 1 (PPMV-1) refers to class II genotype VI strains that circulate in pigeons and doves (*5*,*6*). The first well-documented human PPMV-1 infections were reported in the late 1990–2000s as fatal pneumonia in immunosuppressed transplant recipients (*7*–*9*). During the past few years, 2 fatal cases of PPMV-1–associated encephalitis were reported in immunodeficient patients (*10*,*11*). We report an autochthonous case of fatal encephalitis caused by PPMV-1 in France.

The Study

A 69-year-old man was admitted to an emergency department after repeated falls at home. A week earlier, he attended a shamanism workshop in the Ardèche forest (France). Four days before hospitalization, marked asthenia, diarrhea, diplopia, and dizziness developed in the patient, resulting in falls without loss of consciousness. His family reported a cough for the past year and fatigue and weight loss for several months. The patient had never traveled outside metropolitan (mainland) France.

At admission, the patient was confused and unable to stand or walk and had a fever of 39°C, right-ear hearing loss, right peripheral facial paralysis, left upper limb ataxia, and multidirectional nystagmus. Deep tendon and plantar reflexes were unremarkable. Routine laboratory tests revealed mild inflammation (hyperleukocytosis at 15 G/L [reference range 4–10 G/L]) and C-reactive protein of 25 mg/L (reference range <5 mg/L). Two cerebrospinal fluid (CSF) analyses revealed no pleocytosis, negative viral and bacterial PCR testing, and negative cultures. We noted isolated hyperproteinorachia of 0.72 g/L (reference range 0.15–0.45 g/L). An electroencephalogram revealed nonspecific encephalopathy (Figure 1, panel A). Brain magnetic resonance imaging revealed no hemorrhage or recent ischemia but showed mild

Author affiliations: Hôpital Necker-Enfants malades, Paris, France (N. Veyrenche, M. Leruez-Ville, A. Jamet, A. Ferroni, J. Fourgeaud); Université Paris Cité, FETUS, Paris (N. Veyrenche, M. Leruez-Ville, J. Fourgeaud); APHP-Hôpital de la Pitié-Salpêtrière, Sorbonne Université, Paris (S. Boluda, I. Plu, D. Seilhean); Institut Pasteur, Université de Paris, Paris (P. Pérot, B. Regnault, L. Robert-Capraro, N.M. Dheilly); Lariboisière Hospital, Paris Cité University, INSERM UMRS-1144, Paris (I. Malissin, L. Feghoul, B. Megarbane); Saint-Louis Hospital, APHP, Paris (M. Salmona); Biology and Pathogenesis of Viral Infection team, INSERM UMR 1342, Saint Louis Research Institute, Université Paris-Cité, Paris (M. Salmona); Anses, Ploufragan-Plouzané-Niort Laboratory, Ploufragan, France (A. Leroux, B. Grasland, E. Niqueux, F.-X. Briand)

DOI: https://doi.org/10.3201/eid3205.251576

[1]These authors contributed equally to this article.

[2]These senior authors contributed equally to this article.

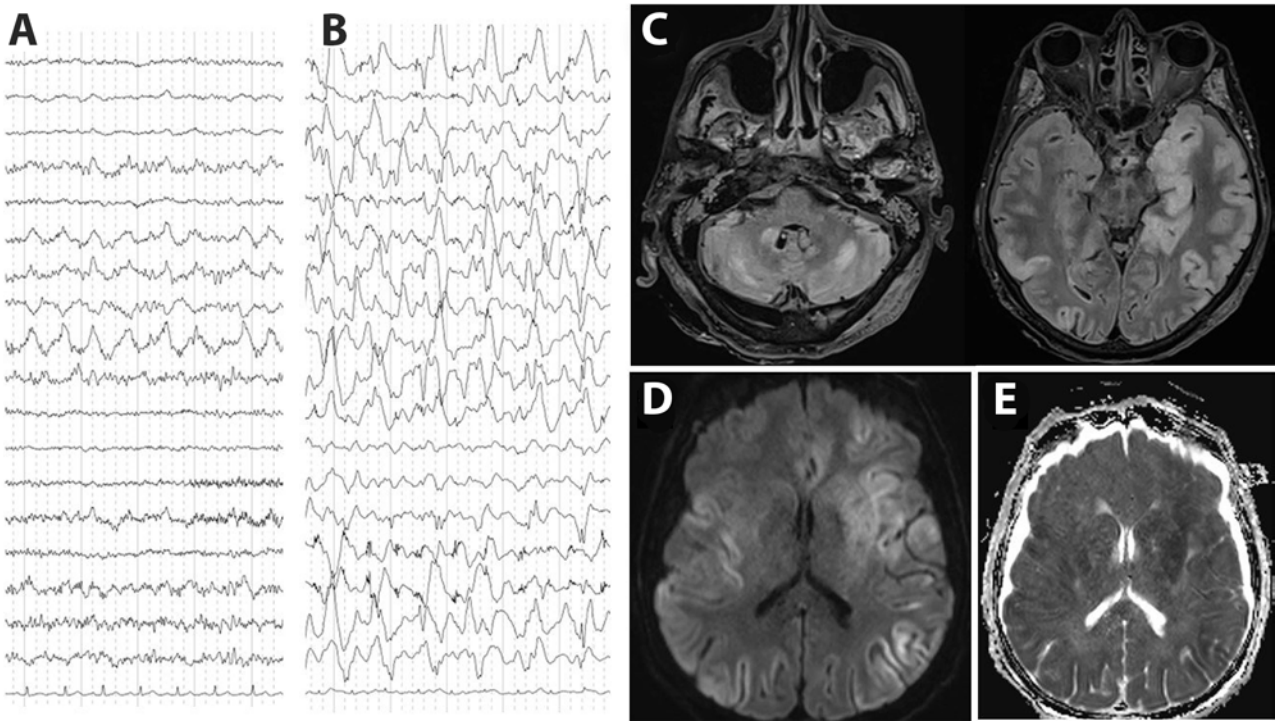

Figure 1. Electroencephalogram (EEG) and brain magnetic resonance imaging (MRI) testing of a patient with encephalitis caused by pigeon paramyxovirus type 1, France. A) The first EEG (day 5 after hospitalization) revealed nonspecific encephalopathy consisting of disorganized theta background rhythm and right temporal rhythmic delta focalization without seizure. B) A later EEG (day 23 after hospitalization) confirmed severe encephalitis with continuous, diffuse, nonreactive, high-amplitude, delta rhythm background of pseudo-periodic delta biphasic and triphasic waves, suggestive of cortical necrosis. C) MRI revealed diffuse bilateral fluid-attenuated inversion recovery hyperintensities, primarily cortical, with subcortical extensions, particularly to the temporal and insular regions, involving the pulvinar nuclei of the thalami, the basal ganglia, the internal capsule, the limbic system, and cerebellum. D, E) Hypersignals in diffusion-weighted images (D) and with reduced apparent diffusion coefficient (E) suggested diffuse cytotoxic brain edema in relation to severe necrotic encephalitis.

white matter hyperintense lesions at the junction of the mesencephalon and pons on T2 or fluid-attenuated inversion recovery.

Five days after admission, the patient was transferred to the intensive care unit for coma, respiratory failure, and aspiration pneumonia. His neurologic condition deteriorated, and dysarthria, diplopia, deafness, ataxia, swallowing disorders, and quadriparesis developed. He was promptly intubated and mechanically ventilated. Repeat electroencephalogram (Figure 1, panel B) and brain magnetic resonance imaging (Figure 1, panels C–E) confirmed severe encephalitis. A third CSF analysis confirmed hyperproteinorachia of 1.5 g/L and no pleocytosis. Routine laboratory test results were unremarkable, including investigations for rare etiologies of encephalitis (Appendix, http://wwwnc.cdc.gov/EID/article/32/5/25-1576-App1.pdf). Electroneuromyography revealed severe motor and sensory axonal neuropathy of all 4 limbs. A full-body computed tomography scan revealed enlarged centimetric mediastinal and hilar lymphadenopathies and widespread colitis from the sigmoid to the cecum. Despite supportive care and intensive medical management (Appendix), the patient died 26 days after admission from progressively worsening, life-threatening encephalitis and polyradiculoneuropathy of unknown etiology.

To investigate the origin of the encephalitis, we performed metagenomic next-generation sequencing on postmortem midbrain and cervical spinal cord tissues obtained at autopsy, generating 82.5 million midbrain reads and 67.3 million cervical spinal cord reads. We assembled the complete PPMV-1/Human/France/2023 genome from 3,245 reads (0.48%, sequencing depth 28×) from the midbrain and 3,790 reads (0.68%, sequencing depth 34×) from the cervical spinal cord samples. We did not detect any additional pathogens.

Phylogenetic analyses revealed that PPMV-1/Human/France/2023 belongs to APMV-1 class II, genotype VI, sub-genotype 2.1.1.2.2. The predicted fusion protein contained the polybasic cleavage motif ^{112}RRQKRF^{117} associated with virulence in birds (*10,12*). PPMV-1/Human/France/2023 was related to

PPMV-1 strains from China, Egypt, Belgium, and Ukraine but also APMV-1/pigeon/France/172784/2017 from France (Haute-Garonne department). The sequence from France was obtained through a surveillance program in wild birds: the original sample was collected from a wild pigeon in November 2017, ≈250 km away from Ardèche (Appendix Table 1). PPMV-1/Human/France/2023 is more

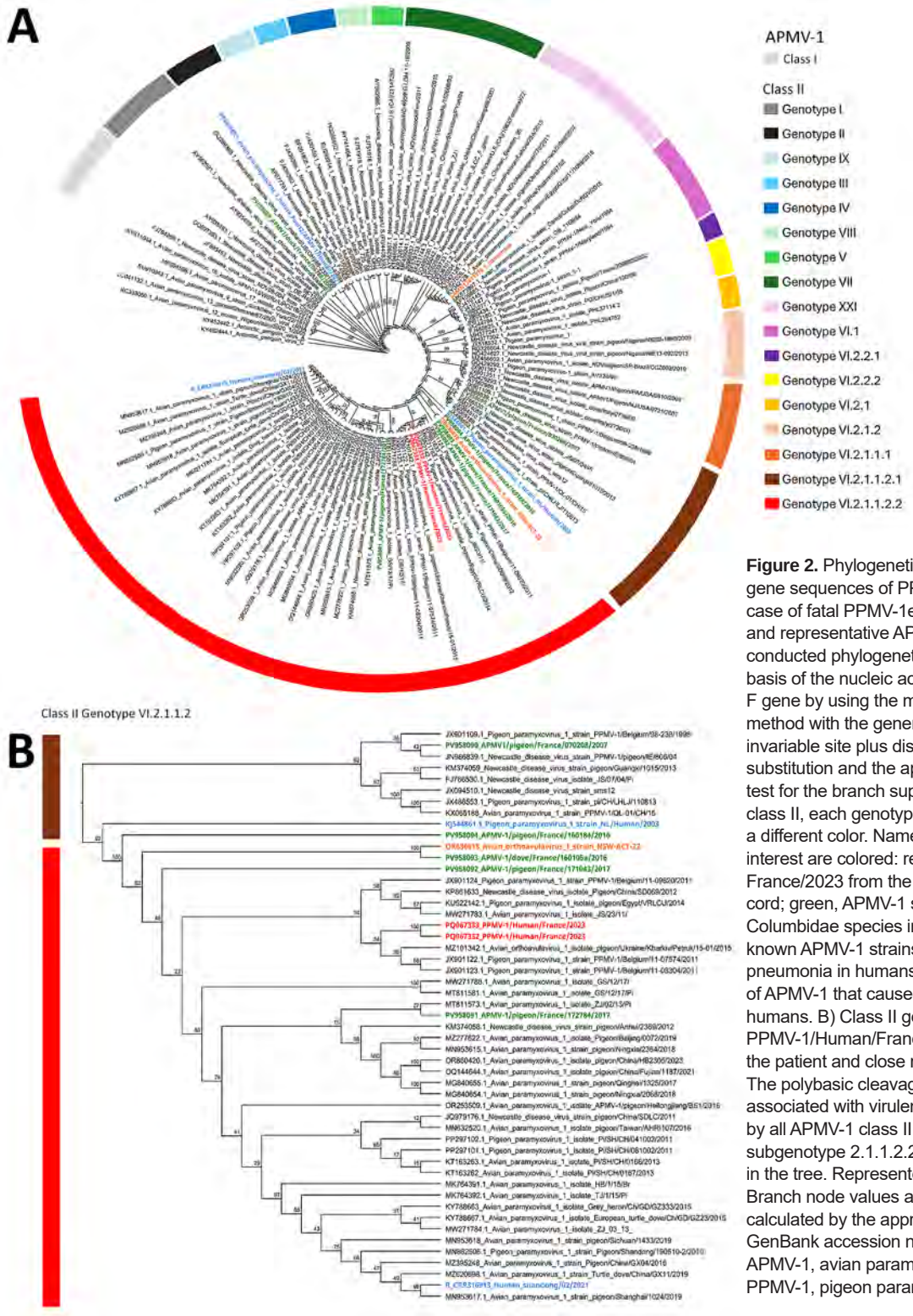

Figure 2. Phylogenetic analysis of fusion gene sequences of PPMV-1from a human case of fatal PPMV-1encephalitis in France and representative APMV-1 strains. A) We conducted phylogenetic analysis on the basis of the nucleic acid sequence of the F gene by using the maximum-likelihood method with the general time reversible with invariable site plus discrete gamma model substitution and the approximate Bayes test for the branch support analysis. Within class II, each genotype is represented by a different color. Names of sequences of interest are colored: red, PPMV-1/Human/France/2023 from the midbrain and cervical cord; green, APMV-1 strains identified in Columbidae species in France n; blue, known APMV-1 strains that caused fatal pneumonia in humans; orange, 2 strains of APMV-1 that caused encephalitis in humans. B) Class II genotype VI.2.1.1.2 PPMV-1/Human/France/2023 isolate from the patient and close reference sequences. The polybasic cleavage motif ^{112}RRQKRF^{117} associated with virulent strains is exhibited by all APMV-1 class II, genotype VI, subgenotype 2.1.1.2.2 strains represented in the tree. Represented as a cladogram. Branch node values are branch support as calculated by the approximate Bayes test. GenBank accession numbers are provided. APMV-1, avian paramyxovirus type 1; PPMV-1, pigeon paramyxovirus type 1.

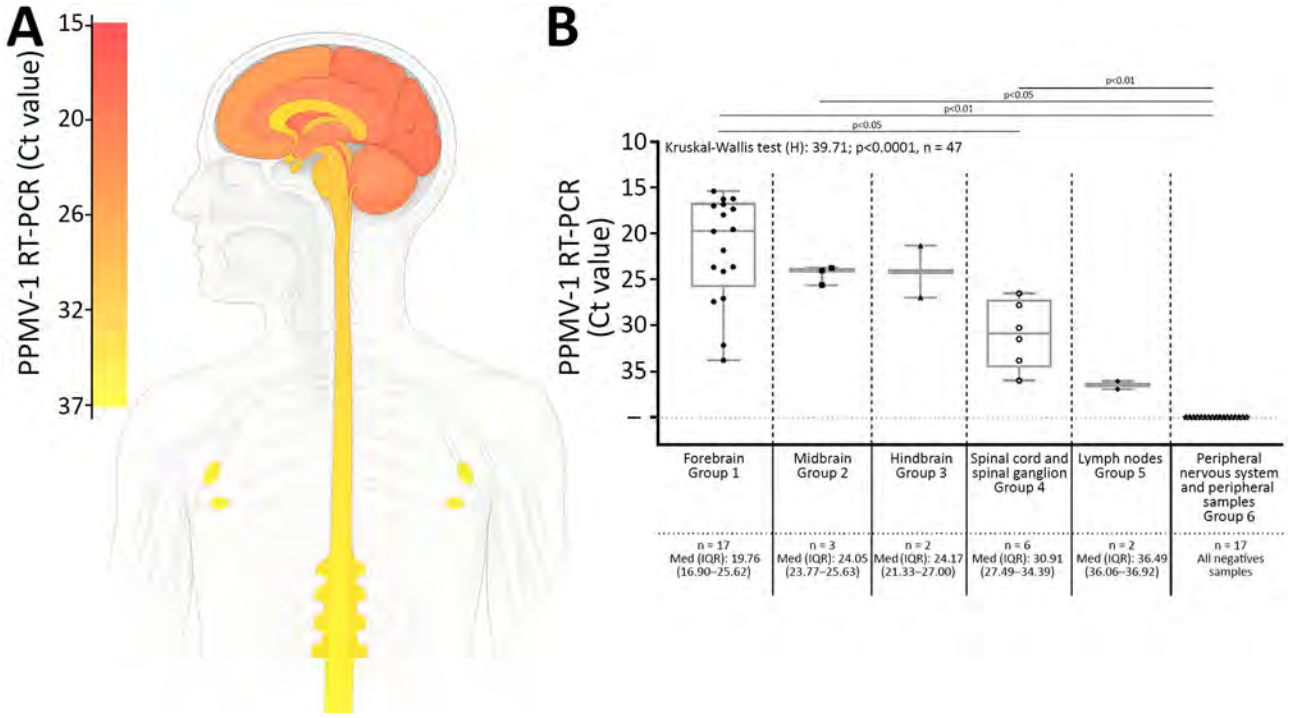

Figure 3. PPMV-1 dissemination in the central and peripheral nervous systems and in axillary lymph nodes in a patient with fatal PPMV-1 encephalitis in France. A) Schematic representation of PPMV-1 viral load in 30 postmortem tissue samples; complete list of all samples is provided (Appendix Table 3, https://wwwnc.cdc.gov/EID/article/32/5/25-1576-App1.pdf). Viral loads were estimated at 5.2×10^5–2.6×10^6 genome copies/gram of tissue in the midbrain and 1.1–5.5×10^5 genome copies/gram of tissue in the cervical spinal cord. B) PPMV-1 viral burden in different anatomic compartments. Samples were classified into 6 groups: group 1, forebrain (including telencephalon and diencephalon); group 2, midbrain; group 3, hindbrain (including metencephalon and myelencephalon); group 4, spinal cord and spinal ganglion; group 5, lymph nodes; group 6, peripheral nervous system and peripheral samples. For the 17 forebrain samples (group 1), the PPMV-1 Ct values were the lowest (median 19.76 [IQR 16.90–25.62]), reflecting the highest viral burden. A Ct value >30 was observed in only 2 forebrain samples, the choroid plexus (Ct = 32.2) and the pituitary gland (Ct = 33.85). The 3 midbrain samples (group 2) and the 2 hindbrain samples (group 3) had higher Ct values: medians 24.05 (IQR 23.77–25.63) and 24.17 (IQR 21.33–27.00). Ct value further increased in the subsequent groups: medians 30.91 (IQR 27.49–34.39) in the 4 spinal cord and 2 spinal ganglion samples (group 4) and 36.49 (IQR 36.06–36.92) in the 2 axillary lymph node samples (group 5), indicating a progressive decrease in viral burden. The last group, consisting of 17 samples (group 6) including peripheral nervous system samples and 5 peripheral samples were all negative. We conducted a nonparametric Kruskal-Wallis test that indicated differences among groups ($p<0.0001$). Posthoc tests revealed an increasing trend in PPMV-1 Ct value from the brain to the peripheral samples. Pairwise Wilcoxon tests (2-tailed) for differences in means between groups adjusted with Bonferroni correction are displayed. Nonsignificant p values (>0.05) are not shown. Horizontal line within boxes indicate medians, box tops and bottoms represent IQRs, and whiskers indicate minimum and maximum values. Ct, cycle threshold; IQR, interquartile range; PPMV-1, pigeon paramyxovirus type 1.

closely related to Pi/SH/CH/041002/2011 (GenBank accession no. PP297102.1), which was discovered in pigeons from China in 2011 (Figure 2; Appendix Table 2).

To investigate the dissemination of PPMV-1 in the patient, we conducted semiquantitative real-time PCR on all clinical samples (Appendix Table 3). PPMV-1 was detected in the CNS, thoracic spinal ganglia, and axillary lymph nodes. We identified the highest viral burdens in the brain, specifically localized to the forebrain. Posthoc tests revealed an increasing trend in PPMV-1 cycle threshold values from the brain to the peripheral samples (Figure 3).

Postmortem examination of the CNS revealed brain edema, friable midbrain tissue, and gray matter discoloration of the spinal cord (Appendix). Histopathologic testing (Appendix Table 4) revealed a diffuse inflammatory infiltrate of activated macrophages, microglia, and CD3+ and CD8+ T lymphocytes, with severe neuronal loss in the spinal cord, brainstem, and cerebellum. Neuronophagia and microglial nodules were frequent. We did not observe cytopathic effect. The choroid plexus and ependymal cells appeared unremarkable. We found perivascular inflammatory infiltrates in peripheral nerves (Figure 4). Newcastle disease virus immunostaining was positive in the spinal cord, midbrain, cerebellum, hypothalamus, and lymph nodes (Figure 4).

Conclusions

We report a case of fatal encephalitis associated with PPMV-1 in France that belonged to virulent class II, genotype VI, subgenotype 2.1.1.2.2, with polybasic F cleavage motif RRQKRF, in a patient with no known immunosuppression. That motif is associated with high intracerebral pathogenicity in birds (*13*) and was reported in another fatal encephalitis case (*10*). PPMV-1 belongs to the velogenic pathotype of AOAV-1 (Appendix).

The patient had never traveled outside France, indicating autochthonous infection. Although the source of infection is undetermined, the temporal association with a shamanism workshop in the Ardèche forest suggests environmental exposure to avian pathogens, potentially through contact with avian feces. PPMV-1 is shed orally and cloacally, remains stable in pigeon feces, and can spread by windborne dust, extending risk beyond localized environments (*8*).

Two previously reported human APMV-1 encephalitis cases occurred in severely immunosuppressed patients, suggesting that immune status might modulate APMV-1 neuropathogenicity (*10*,*11*). However, the patient we report had no known

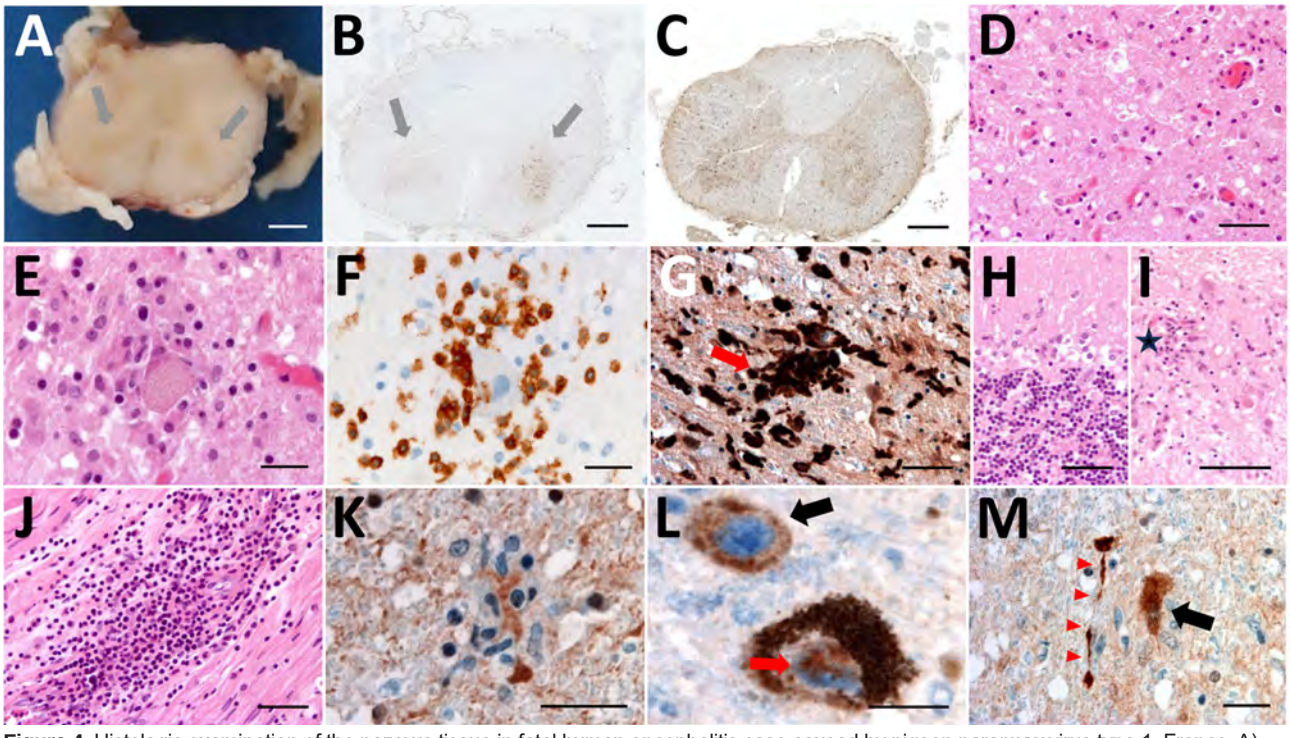

Figure 4. Histologic examination of the nervous tissue in fatal human encephalitis case caused by pigeon paramyxovirus type 1, France. A) Brown discoloration of the anterior horns (gray arrows) of the spinal cord at macroscopic examination. We evaluated the tissue microscopically by using hematoxylin and eosin staining, which highlighted a diffuse inflammatory infiltrate consisting of activated macrophages and microglia in the anterior horns of the spinal cord (throughout its entire length), the brainstem (including medulla oblongata, pons and midbrain), the thalamus, and the cerebellum. Scale bar = 2 mm. B) Anti-CD163 staining revealed marked infiltration of the anterior horns of the spinal cord by activated macrophages (gray arrows). Scale bar = 1.5 mm. C) Anti-Iba1 staining revealed activated microglia involving the anterior horns and the lateral cords of the spinal cord. This inflammatory infiltrate was associated with severe neuronal loss, particularly in the anterior horns of the spinal cord and the dentate nucleus and the Purkinje cell layer of the cerebellum. Scale bar = 1.5 mm. D, E) H&E staining revealed massive loss of motor neurons of the anterior horn (D; scale bar = 50 µm) associated with foci of neuronophagia (E; scale bar = 25 µm). F) Anti-CD3 staining revealed microglial activation was associated with T-cytotoxic lymphocyte (CD3+/CD8+) infiltration of the brain parenchyma in the most severely affected regions, the T lymphocytes surrounding a motor neuron in the gray matter of the spinal cord. Scale bar = 25 µm. G) Anti-Iba1 staining revealed multiple foci of neuronophagia and microglial nodules were observed, indicating high activity of the cellular immune response involving mainly neurons as seen in microglial nodule (red arrow) in the substantia nigra. Scale bar = 50 µm. H) H&E staining revealed that this inflammatory infiltrate was associated with severe neuronal loss, particularly in the Purkinje cell layer of the cerebellum. Scale bar = 50 µm. I) H&E staining revealed massive loss of Purkinje cells associated with Bergmann astrogliosis in the cerebellar cortex and in the anterior horns of the spinal cord and the dentate nucleus, loss of neurons in the dentate nucleus of the cerebellum associated with the presence of microglial nodules (star). Scale bar = 50 µm. J) H&E staining revealed a subtle lymphocytic infiltrate surrounding some of the vessels and a perivascular lymphocytic inflammatory infiltrate of the endoneurium of peripheral nerves. Scale bar = 50 µm. K–M) Anti-NVD staining revealed positivity in a microglial nodule in the anterior horn of the spinal cord (K), in the soma (black arrow) and in the nucleus (red arrow) of neurons in the *substantia* nigra (L), and (in the soma of a neuron (black arrow) and in neurites (red arrowheads) in the dentate nucleus of the cerebellum M). Scale bars = 25 µm). No cytopathic effects were noted. Immunohistochemistry testing with for herpes simplex virus 1, cytomegalovirus, polyomavirus, papovavirus, and rabies virus were negative. H&E, hematoxylin and eosin.

underlying disease or immunosuppressive treatment. His family reported a deterioration in his general condition, including severe weight loss, in the year before death, without medical evaluation. No laboratory markers of immunosuppression were found. We quantified blood torque teno virus loads to further assess immunosuppression, but results were inconclusive regarding immune status at the time of PPMV-1 infection (*14*). Detecting unusual pathogens in seemingly immunocompetent patients should prompt immune status investigation.

Real-time PCR of postmortem and peripheral samples exhibited strong neurotropism of PPMV-1 without meningitis or systemic infection at the time of neurologic manifestations. PPMV-1 was not detected in the CSF by PCR or metagenomics. PCR of bronchoalveolar lavage was negative 10 days after symptom onset, suggesting weak and transient respiratory replication despite the respiratory tract being the usual entry route. Negative blood PCR results on days 16 and 24 might reflect a brief early viremia.

The patient's clinical manifestations included severe polyradiculoneuropathy with inflammatory infiltrates in the spinal cord and peripheral nerves, which were not described previously (*10*,*11*). The patient also exhibited enlarged lymphadenopathies, and PPMV-1 was detected at low burden in the right and left axillary lymph nodes; immunostaining confirmed viral tropism in those nodes. Lymph node aspiration could provide a minimally invasive alternative to brain biopsy for diagnosing PPMV-1 encephalitis.

In summary, in the case we report and 2 other reported encephalitis cases, class II APMV-1 with a virulence-associated F-protein cleavage site was identified. APMV-1 infection might be underdiagnosed and should be considered in neurologic disease of unknown etiology, particularly among patients who report exposure to Columbidae fauna.

Written informed consent for publication was obtained from the patient's next of kin.

About the Author

Dr. Veyrenche is a clinical virologist working in the clinical microbiology department at Necker-Enfants Malades University Hospital in Paris, France. His research interests include the detection of emerging viral infection and clinical metagenomics.

References

1. Thibault PA, Watkinson RE, Moreira-Soto A, Drexler JF, Lee B. Zoonotic potential of emerging paramyxoviruses: knowns and unknowns. Adv Virus Res. 2017;98:1–55. https://doi.org/10.1016/bs.aivir.2016.12.001
2. Diel DG, da Silva LHA, Liu H, Wang Z, Miller PJ, Afonso CL. Genetic diversity of avian paramyxovirus type 1: proposal for a unified nomenclature and classification system of Newcastle disease virus genotypes. Infect Genet Evol. 2012;12:1770–9. https://doi.org/10.1016/j.meegid.2012.07.012
3. Lu X, Wang X, Zhan T, Sun Y, Wang X, Xu N, et al. Surveillance of class I Newcastle disease virus at live bird markets and commercial poultry farms in eastern China reveals the epidemic characteristics. Virol Sin. 2021;36:818–22. https://doi.org/10.1007/s12250-021-00357-z
4. Dimitrov KM, Abolnik C, Afonso CL, Albina E, Bahl J, Berg M, et al. Updated unified phylogenetic classification system and revised nomenclature for Newcastle disease virus. Infect Genet Evol. 2019;74:103917. https://doi.org/10.1016/j.meegid.2019.103917
5. Chong YL, Lam TTY, Kim O, Lu H, Dunn P, Poss M. Successful establishment and global dispersal of genotype VI avian paramyxovirus serotype 1 after cross species transmission. Infect Genet Evol. 2013;17:260–8. https://doi.org/10.1016/j.meegid.2013.04.025
6. Pestka D, Stenzel T, Koncicki A. Occurrence, characteristics and control of pigeon paramyxovirus type 1 in pigeons. Pol J Vet Sci. 2014;17:379–84. https://doi.org/10.2478/pjvs-2014-0056
7. Goebel SJ, Taylor J, Barr BC, Kiehn TE, Castro-Malaspina HR, Hedvat CV, et al. Isolation of avian paramyxovirus 1 from a patient with a lethal case of pneumonia. J Virol. 2007;81:12709–14. https://doi.org/10.1128/JVI.01406-07
8. Kuiken T, Breitbart M, Beer M, Grund C, Höper D, van den Hoogen B, et al. Zoonotic infection with pigeon paramyxovirus type 1 linked to fatal pneumonia. J Infect Dis. 2018;218:1037–44. https://doi.org/10.1093/infdis/jiy036
9. Zou X, Suo L, Wang Y, Cao H, Mu S, Wu C, et al. Concurrent pigeon paramyxovirus-1 and *Acinetobacter baumannii* infection in a fatal case of pneumonia. Emerg Microbes Infect. 2022;11:968–77. https://doi.org/10.1080/22221751.2022.2054366
10. Hurley S, Eden JS, Bingham J, Rodriguez M, Neave MJ, Johnson A, et al. Fatal human neurologic infection caused by pigeon avian paramyxovirus-1, Australia. Emerg Infect Dis. 2023;29:2482–7. https://doi.org/10.3201/eid2912.230250
11. Winter S, Lechapt E, Gricourt G, N'debi M, Boddaert N, Moshous D, et al. Fatal encephalitis caused by Newcastle disease virus in a child. Acta Neuropathol. 2021;142:605–8. https://doi.org/10.1007/s00401-021-02344-w
12. Cui S, Xiong H, Feng Z, Chu Y, Que C, Qin J, et al. Severe pigeon paramyxovirus 1 infection in a human case with probable post-COVID-19 condition. Emerg Microbes Infect. 2023;12:2251600. https://doi.org/10.1080/22221751.2023.2251600
13. World Organisation for Animal Health. Newcastle disease (infection with Newcastle disease virus). Chapter 3.3.10. In: Manual of diagnostic tests and vaccines for terrestrial animals. Paris : The Organisation; 2021 [cited 2026 Apr 27]. https://www.woah.org/fileadmin/Home/eng/Health_standards/tahm/3.03.10_NEWCASTLE_DIS.pdf
14. Mallet F, Diouf L, Meunier B, Perret M, Reynier F, Leissner P, et al. Herpes DNAemia and TTV viraemia in intensive care unit critically ill patients: a single-centre prospective longitudinal study. Front Immunol. 2021;12:698808. https://doi.org/10.3389/fimmu.2021.698808

Address for correspondence: Nolwenn M Dheilly, Institut Pasteur, Pathogen Discovery Laboratory, 25-28 rue du Dr. Roux, 75015, Paris, France; email: nolwenn.dheilly@pasteur.fr

Yezo Virus Diversity in Tick Bite Patients and Ticks, Russia

Yulia O. Epik, Kseniia A. Sycheva, Lyudmila S. Karan, Evgenia V. Mokretsova, Anna G. Dragomeretskaya, Olga E. Trotsenko, Anna R. Efimova, Yulia M. Spirina, Olga M. Drozdova, Tatyana E. Bondarenko, Ekaterina A. Blinova, Vasiliy G. Akimkin, Evgeny S. Morozkin

Yezo virus is an emerging tickborne orthonairovirus. We detected Yezo virus RNA in tick bite patients and in *Ixodes persulcatus* ticks in west Siberia and Far East, Russia. Clinicians should consider the expanded area of Yezo virus identification and the *I. persulcatus* tick habitat when evaluating patients after tick bites in Russia.

Tickborne orthonairoviruses (Nairoviridae, *Orthonairovirus*) are a recognized global health threat to humans. In Russia, the most common pathogenic agent to humans within the genus *Orthonairovirus* is Crimean-Congo hemorrhagic fever virus, transmitted by ticks belonging to the family Ixodidae. Crimean-Congo hemorrhagic fever virus is endemic to southern regions in Russia and causes >100 annual severe fever cases in humans (*1*).

In recent years several novel orthonairoviruses have been discovered in China and Japan. Songling virus (*2*), Tacheng tick virus 1 (*3*), and Beiji nairovirus (*4*) are associated with human febrile illness in northeastern and northwestern China. Yezo virus (YEZV) (*Orthonairovirus yezoense*), a newly described tickborne orthonairovirus, was identified in Japan in 2021 and causes acute febrile illness accompanied by thrombocytopenia and leukopenia. YEZV was detected in blood samples from 7 patients in Hokkaido, Japan (*5*), and 1 patient in northeastern China (*6*) after tick bites. Afterward, 18 tick bite patients with YEZV infection were identified in northeastern China (*7*). Furthermore, YEZV was identified in ixodid ticks in both countries. We report detection of YEZV in *Ixodes persulcatus* ticks and the serum of tick bite patients in Russia.

The Study

We retrospectively investigated the presence of YEZV RNA in 310 blood samples from tick bite patients. The samples included 144 samples from patients hospitalized in the Kemerovo region of Russia during 2024 and 2 sets of samples from the Khabarovsk region, 60 samples from patients hospitalized in 2015 and 106 samples from patients hospitalized in 2023–2024. We used an in-house real-time reverse transcription PCR (qRT-PCR) for YEZV RNA detection (Appendix Table 1, http://wwwnc.cdc.gov/EID/article/32/5/25-1620-App1.pdf). We identified 2 positive samples: 1 from the Kemerovo region of Russia and 1 from the Khabarovsk region of Russia.

The patient from the Khabarovsk region, Far East, Russia, was a 68-year-old woman who was bitten by a tick in 2015; the species of tick was not determined. Five days after the bite, tick bite fever developed, accompanied by headache, malaise, myalgia, lumbago, and nausea. Two days after fever onset, the patient was hospitalized. A physical examination at admission revealed no meningeal symptoms or rash (Table 1). An eschar, ≈4 mm in diameter and consistent with a tick bite site, was observed. Laboratory testing did not detect thrombocytopenia or leukopenia. Serum levels of liver aminotransferases were unremarkable. While hospitalized, the patient received unidox solutab (100 mg 2×/d for 8 d) (Appendix Table 2). The patient fully recovered on day 9 of hospitalization and was discharged. Molecular investigation of the patient's blood samples revealed negative results for common tickborne pathogens. However, positive

Author affiliations: Central Research Institute of Epidemiology, Moscow, Russia (Y.O. Epik, K.A Sycheva, E.A. Blinova, V.G. Akimkin, E.S. Morozkin); Russian Center of Neurology and Neurosciences, Moscow (L.S. Karan); Far Eastern State Medical University, Khabarovsk, Russia (E.V. Mokretsova); Khabarovsk Research Institute of Epidemiology and Microbiology, Khabarovsk (E.V. Mokretsova, A.G. Dragomeretskaya, O.E. Trotsenko), Centre of Hygiene and Epidemiology in the Kemerovo region–Kuzbass, Kemerovo, Russia (A.R. Efimova, Y.M. Spirina); Kemerovo State Medical University, Kemerovo (O.M. Drozdova); Kuzbass Clinical Infectious Diseases Hospital, Kemerovo (T.E. Bondarenko).

DOI: https://doi.org/10.3201/eid3205.251620

Table 1. Characteristics of 2 Yezo virus–infected patients with history of tick bites from Khabarovsk and Kemerovo regions, Russia

Epidemiologic characteristics	Patient 1	Patient 2
Age, y	68	69
Sex	F	M
Geographic region	Khabarovsk	Kemerovo
Days from tick bite to symptom onset	5	3
Days from symptom onset to hospital admission	2	0
Tick bite identification method	Self-reported	Self-reported
Clinical manifestations		
Fever	Yes	Yes
Headache	Yes	No
Malaise	Yes	Yes
Nausea	Yes	No
Myalgia	Yes	Yes
Lumbago	Yes	No
Rash	No	No
Meningeal symptoms	No	No
Bacterial co-infection	Yes	No
Tickborne pathogen detection		
Tickborne encephalitis virus	No	No
Borrelia spp.	No	No
Anaplasma spp.	No	No
Ehrlichia chaffeensis	No	No
Ehrlichia muris	No	No
Rickettsia heilongjiangensis	Yes	No
Yezo virus	Yes	Yes

results were obtained for *Rickettsia heilongjiangensis* and YEZV (Table 1). qRT-PCR analysis detected YEZV RNA at a concentration of 10^6 copies/mL in the patient's serum collected on day 1 after fever onset.

The second clinical case occurred in the Kemerovo region, West Siberia, Russia, in 2024. The patient, a 69-year-old man, was admitted to the hospital with a diagnosis of tickborne fever of moderate severity. His clinical manifestation included fever, malaise, and myalgia (Table 1). The patient reported a tick bite 3 days earlier; however, the tick was not available for examination. Platelet and leukocyte counts and serum levels of liver aminotransferases were unremarkable. While hospitalized, the patient received prophylactic intramuscular ceftriaxone (1 g 2×/d for 9 d) (Appendix Table 2). He was discharged on day 9 after a full recovery. Molecular analysis of his blood sample for tickborne pathogens yielded negative results (Table 1). qRT-PCR analysis detected YEZV RNA at a concentration of 5×10^5 copies/mL in serum collected on the first day after fever onset.

To assess the epidemiologic situation in Russia, we tested a total of 2,497 ticks, consisting of 3 species (*I. persulcatus*, *Haemaphysalis concinna*, and *H. japonica*), collected during 2006–2023 in the Kemerovo region and during 2023 from the Khabarovsk region of Russia (Table 2). We tested for YEZV RNA testing by using qRT-PCR. We amplified positive samples by using in-house primer pairs (Appendix Table 3) and then performed sequencing.

We detected YEZV RNA exclusively in *I. persulcatus* ticks from both the Kemerovo and Khabarovsk regions of Russia (Figure). The prevalence of YEZV infection in ticks was determined to be 0.5% in the Khabarovsk region and ranged from 0.3% to 0.9% in the Kemerovo region in different sampling years (Table 2).

We obtained 12 nucleoprotein 12 glycoprotein precursor, and 10 RNA-dependent RNA polymerase gene segment sequences of YEZV. In addition to the obtained sequences, we included sequences from China, Japan, and Russia, accessed from GenBank, in the analysis. We selected Sulina virus, the closest known relative of YEZV, as the outgroup. Our analysis revealed the obtained sequences formed 3 distinct clades across all 3 genome segments: 1 from the Khabarovsk region (clade A) and 2 from the Kemerovo region (clades B and C) (Appendix Figure 1). Khabarovsk variants exhibited close phylogenetic proximity to sequences from China and Japan. Nucleotide differences between sequences from clades B and C (Kemerovo region) were 7.8% for the nucleoprotein gene segments, 9.0% for the glycoprotein precursor gene segments, and 9.7% for the RNA-dependent RNA polymerase gene segments (Appendix Figure 2). Of note, the division of viruses from Kemerovo sequence into 2 distinct clades correlated with their specific tick sampling locations. All viral genome sequences from this study have been deposited into GenBank (accession nos. PV770287–98, PX898217–28, PX904390–9).

Conclusions

We identified 3 genomic variants of YEZV within Russia. The variant from Khabarovsk is closely related to viruses previously reported in China and

Table 2. Detection of Yezo virus RNA in ixodid ticks from Khabarovsk and Kemerovo regions, Russia*

Region	Sampling year	Tick species	No. ticks	No. pools	No. positive pools	Prevalence	SE
Kemerovo	2006	*Ixodes persulcatus*	700	70	6	0.9%	0.0036
	2023	*I. persulcatus*	648	216	2	0.3%	0.0022
Khabarovsk	2023	*I. persulcatus*	816	272	4	0.5%	0.0025
	2023	*Haemaphysalis concinna*	159	53	0	NA	NA
	2023	*H. japonica*	168	56	0	NA	NA
Total			2,491	667	12		

*We calculated the prevalence by using Epitools (https://epitools.ausvet.com.au). NA, not available.

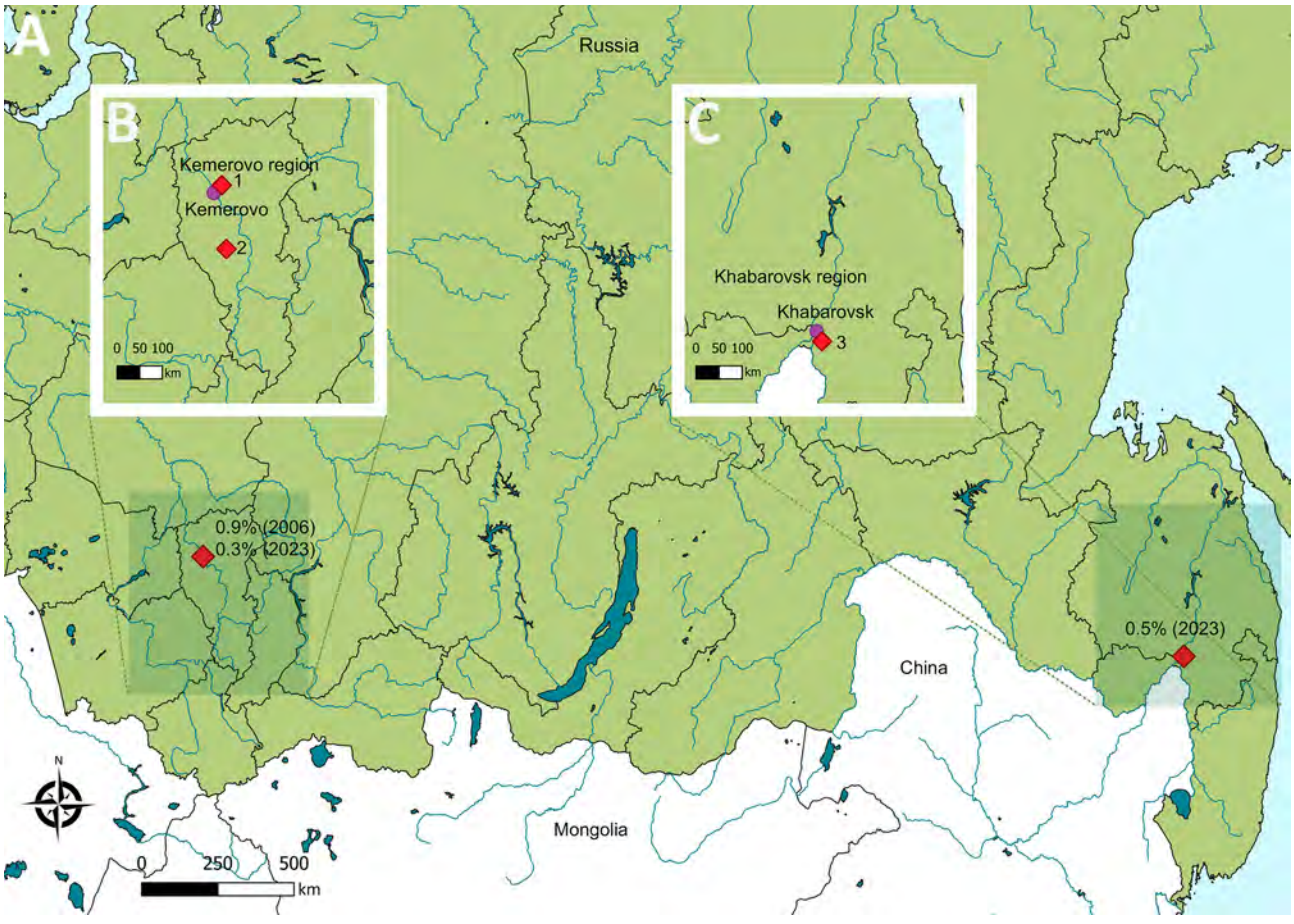

Figure. Geographic distribution of Yezo virus (YEZV) detection in ticks from Russia. Red diamonds indicate sampling locations of YEZV-positive *Ixodes persulcatus* ticks. A) Distribution across Russia. YEZV prevalence (%) and sampling year are indicated adjacent to symbols. B) Distribution within the Kemerovo region. Samples of isolates 143 (GenBank accession nos. PV770292, PX898221, and PX904396), 24-4 (accession nos. PV770294, PX898220, and PX904395), 6-1 (accession nos. PV770295 and PX898217), 6-4 (accession nos. PV770296 and PX898218), and 6-5 (accession nos. PV770297, PX898219, and PX904394) were derived from ticks collected in location 1. The sample of isolate 165 (accession nos. PV770293, PX898222, and PX904397) was derived from a tick collected in location 2. C) Distribution within the Khabarovsk region. Samples of isolates 560 (accession nos. PV770287, PX898225, and PX904391), 576 (accession nos. PV770288, PX898226, and PX904392), 649 (accession nos. PV770289, PX898227, and PX904390), and 662 (accession nos. PV770290, PX898228, and PX904393) were derived from ticks collected in location 3.

Japan. We detected 2 genomic variants in the Kemerovo region. This genetic diversity, which correlates with sampling location, might indicate an association between different YEZV variants and distinct *I. persulcatus* tick populations (*8*). Reassortment events in the YEZV genome have previously been reported (strains BT-2135 and T-HLJ02) (Appendix Figure 1 (*9*); however, we did not detect reassortant strains among the obtained sequences. Further investigation is needed to determine the causes of high diversity of YEZV in West Siberia, Russia, compared with Japan and China, and to identify possible novel genetic variants of the YEZV by studying more western regions of the *I. persulcatus* tick habitat.

We identified 2 patients with YEZV infection after tick bites: 1 from the Kemerovo region with monoinfection and the other from the Khabarovsk region with co-infection with *R. heilongjiangensis*. Both patients' clinical manifestations included nonspecific symptoms common to many infections. Because neither patient had traveled abroad, the cases represent autochthonous YEZV transmission within Russia. All blood samples were tested for the presence of YEZV RNA retrospectively, preventing the investigation of blood parameter dynamics. Previous studies have reported that, in addition to general clinical manifestations such as fever and malaise, YEZV infection might be accompanied by elevated serum levels of liver aminotransferases (alanine aminotransferase and aspartate aminotransferase), thrombocytopenia, and leukopenia (*5*–*7*,*10*). In both cases we identified, platelet and leukocyte counts

and liver aminotransferase levels were unremarkable (Appendix Table 2).

Specific clinical manifestations of YEZV infection that would enable reliable clinical diagnosis are difficult to define. Other common tickborne diseases, such as tick-borne encephalitis, borreliosis, and rickettsiosis, do not always occur with specific symptoms, which can lead to misdiagnosis. In those cases, qPCR or qRT-PCR is used to confirm the etiologic agent. The emergence of YEZV as a novel tickborne pathogen highlights the need to update diagnostic panels for routine testing of patients with unclear clinical manifestations after tick bites.

Acknowledgments

We thank Anna Valdokhina, Victoria Bulanenko, and Kamil Khafizov for sequencing implementation and German Roev for assistance with data analysis.

About the author

Ms. Epik is a junior researcher at the Central Research Institute of Epidemiology, Moscow, Russia. Her research interests focus on genetic diversity, evolution, and epidemiology of Yezo virus and other members of the genus *Orthonairovirus*.

References

1. Volynkina A, Lisitskaya Y, Kolosov A, Shaposhnikova L, Pisarenko S, Dedkov V, et al. Molecular epidemiology of Crimean-Congo hemorrhagic fever virus in Russia. PLoS One. 2022;17:e0266177. https://doi.org/10.1371/journal.pone.0266177
2. Ma J, Lv XL, Zhang X, Han SZ, Wang ZD, Li L, et al. Identification of a new orthonairovirus associated with human febrile illness in China. Nat Med. 2021;27:434–9. https://doi.org/10.1038/s41591-020-01228-y
3. Liu X, Zhang X, Wang Z, Dong Z, Xie S, Jiang M, et al. A tentative Tamdy orthonairovirus related to febrile illness in northwestern China. Clin Infect Dis. 2020;70:2155–60. https://doi.org/10.1093/cid/ciz602
4. Wang YC, Wei Z, Lv X, Han S, Wang Z, Fan C, et al. A new Nairo-like virus associated with human febrile illness in China. Emerg Microbes Infect. 2021;10:1200–8. https://doi.org/10.1080/22221751.2021.1936197
5. Kodama F, Yamaguchi H, Park E, Tatemoto K, Sashika M, Nakao R, et al. A novel nairovirus associated with acute febrile illness in Hokkaido, Japan. Nat Commun. 2021;12:5539. https://doi.org/10.1038/s41467-021-25857-0
6. Lv X, Liu Z, Li L, Xu W, Yuan Y, Liang X, et al. Yezo virus infection in tick-bitten patient and ticks, northeastern China. Emerg Infect Dis. 2023;29:797–800. https://doi.org/10.3201/eid2904.220885
7. Zhang MZ, Bian C, Ye RZ, Cui XM, Yao NN, Yang JH, et al. A series of patients infected with the emerging tick-borne Yezo virus in China: an active surveillance and genomic analysis. Lancet Infect Dis. 2025;25:390–8. https://doi.org/10.1016/S1473-3099(24)00616-9
8. Liebig K, Boelke M, Grund D, Schicht S, Springer A, Strube C, et al. Tick populations from endemic and non-endemic areas in Germany show differential susceptibility to TBEV. Sci Rep. 2020;10:15478. https://doi.org/10.1038/s41598-020-71920-z
9. Nishino A, Tatemoto K, Ishijima K, Inoue Y, Park ES, Yamamoto T, et al. Transboundary movement of Yezo virus via ticks on migratory birds, Japan, 2020–2021. Emerg Infect Dis. 2024;30:2674–8. https://doi.org/10.3201/eid3012.240539
10. Ogata Y, Sato T, Kato K, Kikuchi K, Mitsuhashi K, Watari K, et al. A case of tick-borne Yezo virus infection: concurrent detection in the patient and tick. Int J Infect Dis. 2024;143:107038. https://doi.org/10.1016/j.ijid.2024.107038

Address for correspondence: Yulia O. Epik, Central Research Institute of Epidemiology, 3a Novogireevskaya St., Moscow 111123, Russia; email: yulia.epik719@gmail.com

Orthopoxvirus Antibodies in Feral Mammals in Mpox Outbreak Areas, Nigeria, 2021–2022

Adeyinka Jeremy Adedeji, Clement Adebajo Meseko, Ismaila Ademola Shittu, Nanven Maurice, Suleiman Ladan, Emmanuel Obishakin, Dennis Kabantiyok, Rimfa Amos Gambo, Masdooq Aliyu, Odianosen Ehiakhamen, Ifeanyi Abali, Kwada Asunduwa Chagwa, Bitrus Vandi, Seyi Oyetunde, Nicodemus Mkpuma, Dorcas Gado, Besong Mathias Ayuk, Obadua Adegboyega, Akinbamidele Akinsorotan, Saleh Muhammad, Audrey Matheny, Clint N. Morgan, Yoshinori Nakazawa, Jeffrey B. Doty

We analyzed tissue and serum samples from 124 wild animals from communities with confirmed mpox cases in Nigeria. Tissue samples were PCR-negative, but serum samples from 8 animals (6.45%)—3 feral cats, 4 giant pouched rats, and 1 shrew—revealed *Orthopoxvirus* antibodies, suggesting these species as probable reservoirs.

Members of the genus *Orthopoxvirus* are zoonotic pathogens belonging to the family Poxviridae (*1*–*3*). Orthopoxviruses (OPXVs) are capable of infecting a broad range of mammalian hosts via multiple routes, which could result in widespread infections and deaths in humans and animals (*1*,*2*). Monkeypox virus (MPXV) is a member of the genus *Orthopoxvirus* (*2*). OPXV infections are typically diagnosed by viral isolation and molecular assays, such as real-time PCR (*4*,*5*). Research has implicated rodents and small mammals as MPXV putative reservoirs (*6*–*9*). MPXV is endemic in animal reservoirs in West and Central Africa rainforest, and habitat encroachment and wildlife hunting are cited as likely factors associated with zoonotic spillover events (*8*,*10*).

The first reported human mpox cases in Nigeria occurred in 1971 and then again in 1978; the disease reemerged in 2017 and has increased to endemic levels since then (*11*,*12*). During 2017–2025, the Nigeria Centre for Disease Control and Prevention (Abuja, Nigeria) reported 1,491 confirmed human cases of mpox in Nigeria, with 21 associated deaths. We conducted this study as part of a One Health investigation of the likely role of animal reservoirs in the transmission and maintenance of MPXV following reported human mpox cases in 2 states of Nigeria.

The Study

In 2021–2022, Ondo State in Nigeria reported 40 confirmed human mpox cases (World Health Organization External Situation Report 8, October 2022, https://www.who.int/emergencies/situation-reports). Similarly, in 2022, Adamawa State (Figure 1), reported its index human mpox case in a serving soldier in Nigeria, followed by 28 mpox cases among inmates at a correctional facility in March 2022 (*13*). The correctional facility held inmates who were involved in terrorist activities and may have shared the same forest region with military personnel (*13*). Hence, in 2021–2022, health officials deployed a One Health mpox animal surveillance team (veterinarians, a physician, a microbiologist, and environmentalists) to investigate the role of animals in the upsurge of mpox cases in Ondo and Adamawa States.

Author affiliations: National Veterinary Research Institute, Vom, Nigeria (A.J. Adedeji, C.A. Meseko, I.A. Shittu, N. Maurice, E. Obishakin, D. Kabantiyok, R.A. Gambo, M. Aliyu, S. Oyetunde, N. Mkpuma, D. Gado); Federal Ministry of Agriculture and Food Security, Abuja, Nigeria (S. Ladan, B.M. Ayuk); Nigeria Centre for Disease Control and Prevention, Abuja (O. Ehiakhamen, I. Abali); Adamawa State Ministry of Livestock and Aquaculture, Yola, Nigeria (K.A. Chagwa); Adamawa State Ministry of Environment, Yola (B. Vandi); Ondo State Ministry of Agriculture, Akure, Nigeria (O. Adegboyega, A. Akinsorotan); Nigeria Centre for Disease Control and Prevention, Abuja (S. Muhammad); US Centers for Disease Control and Prevention, Atlanta, Georgia, USA (A. Matheny, C.N. Morgan, Y. Nakazawa, J.B. Doty)

DOI: http://doi.org/10.3201/eid3205.251565

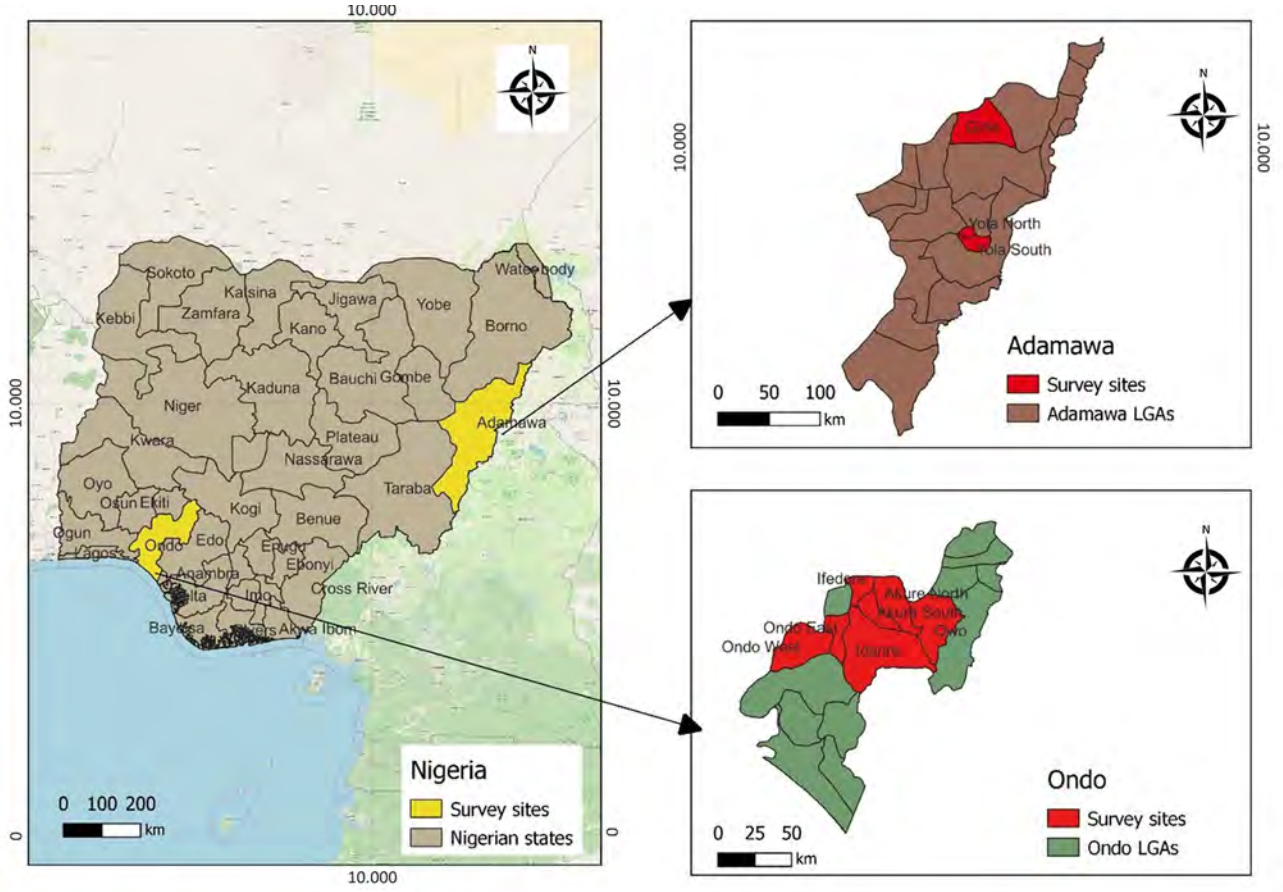

Figure 1. Sites of mpox animal surveillance activities for investigation of *Orthopoxvirus* antibodies in feral mammals in mpox outbreak areas, Adamawa and Ondo states, Nigeria, 2021–2022. LGA, Local Government Area.

Study locations in Ondo State included Idanre Forest Reserve, Owena Forest Reserve, Abule Oluketa, Oba-Ile/Araromi, Oya, Emure, Igbara-Oke, and Akure metropolis (Figure 1). Our team also collected samples from wildlife purchased at bushmeat market stalls at Owena and Emure forest zones. Trapping sites in Adamawa State included a correctional facility, 2 public markets, and households with confirmed mpox cases (Figure 1). The animal surveillance team set Tomahawk live traps (https://tomahawklivetrap.org), Sherman live traps (https://shermantraps.com), and Victor snap traps (https://www.victorpest.com).

Before necropsy, we humanely euthanized trapped animals following standard operating procedures (*14*). We followed protocols approved by the National Veterinary Research Institute Animal Ethics

Table. Geographic distribution of animals trapped or purchased from bushmeat markets in states of Ondo and Adamawa in study of *Orthopoxvirus* antibodies in feral mammals in mpox outbreak areas, Nigeria, 2021–2022

Scientific name	Common name	Adamawa	Ondo	Total
Animals trapped				
Feral cat	Cat	6	0	6
Crocidura spp.	Shrew	19	12	31
Rattus rattus	Black rat	21	0	21
Mus spp.	House mouse	6	5	11
Cricetomys	Giant pouched rat	50	5	55
Subtotal		102	22	124
Animals harvested from bushmeat markets				
Dendrohyrax	Tree hyrax	0	1	1
Xerus erythropus	Stripped ground squirrel	0	13	12
Atilax paludinosus	Marsh mongoose	0	1	1
Atherurus africanus	Brush-tailed porcupine	0	6	6
Thryonomys swinderianus	Marsh cane rat; grasscutter	0	30	30
Subtotal		0	50	50
Total		102	72	174

Committee, Vom, Nigeria (AEC/03/53/18), and the US Centers for Disease Control and Prevention Institutional Animal Care and Use Committee, Atlanta, Georgia, USA (3183DOTMULX), in trapping and sampling rodents and small mammals. We collected blood samples by cardiac puncture and dropped samples onto Nobuto filter paper, allowing droplets to air dry before storing samples in a pouch with silica gel. We centrifuged the blood remaining in microtubes and aliquoted serum samples for storage in liquid nitrogen. We recorded age, species, and sex of each animal and took morphometric measurements as previously described to aid phenotypic species identification (*14*). We also examined each animal for pox-like lesions. We shipped the samples, collected in duplicate, to the National Veterinary Research Institute and the US Centers for Disease Control and Prevention for analysis.

We extracted DNA from tissue samples (liver, spleen, lungs, kidney, skin) collected from all 124 animals by using a MagMAX magnetic processor (Thermo Fisher Scientific, https://www.thermofisher.com) and conducted real-time PCR on all available samples by using OPXV-generic and MPXV-specific assays as previously described (*5*,*7*). To detect the presence of OPXV IgG, we tested all serum samples and dried blood spots using an in-house–developed ELISA, used in previous studies, at dilutions of 1:100, 1:200, and 1:400 (*6*–*8*). We used Western reserve vaccinia virus as the antigen to coat the plates (*7*). We considered serum samples that were reactive at 1:100 and 1:200 dilutions to be positive (*7*).

The survey team trapped 124 rodents and small mammals (Table). The identified species consisted of house mice (*Mus* spp.), black rats (*Rattus rattus*), white-toothed shrews (*Crocidura spp.*), giant pouched rats

Figure 2. Animals collected for an investigation of *Orthopoxvirus* antibodies in feral mammals in mpox outbreak areas, Nigeria, 2021–2022. A) Freshly hunted giant pouched rat and stripped ground squirrel at bushmeat market in Ondo State. B) Trapped giant pouched rat in Yola in northern Adamawa state. C) Feral cats that inadvertently entered a Tomahawk live trap. D) Marsh mongoose bought at a wildlife market in Idanre Ondo state.

(*Cricetomys* spp.), and feral cats that were inadvertently caught in the live traps (Table; Figure 2). We also collected tissue samples (liver, spleen, lungs, skin) from 5 species of freshly hunted wild rodents and small mammals at bushmeat markets (Table, Figure 2). We observed no pox-like lesions on animals sampled.

Laboratory results revealed no OPXV or MPXV DNA in tissue samples collected from the 174 rodents and other small mammals we studied. All blood samples on the Nobuto dry spots tested negative as well. However, we detected OPXV IgG in 8 (6.45%) of 124 serum samples collected from the trapped animals, specifically feral cats (3/6 [50%]), giant pouched rats, (4/55 [7.27%]), and a shrew (1/31 [3.23%]). All detected OPXV antibodies were in animals trapped in 2 local government areas in Adamawa State: Girei (shrew) and Yola North (feral cats, giant pouched rat), where confirmed human mpox cases were recently reported.

Conclusion

In this study, we detected OPXV IgG in serum samples collected in 3 animal species in communities where human mpox cases were confirmed, suggesting that MPXV or other OPXVs may be circulating in animal populations. In our previous study, we found OPXV antibodies in rodents, namely *Praomys* spp. rodents and *R. rattus* rats, in a community with confirmed human mpox cases in Nigeria, further validating the hypothesis that rodents may be likely reservoirs of OPXV, such as MPXV or taterapox virus (*6*,*7*). We also detected OPXV antibodies in *Cricetomys* spp. rats, *Crocidura* spp. shrews, and feral or stray domestic cats. Other studies have demonstrated the presence of OPXV antibodies in *Cricetomys* spp. rats and *Crocidura* spp. shrews in some countries in African (*6*,*15*). Although our findings do not definitively confirm *Cricetomys* spp. rats or *Crocidura* spp. shrews as a sylvatic reservoir for OPVX or MPXV, this research does provide additional evidence of the possible role of those species in maintaining the viruses within the ecology. Of interest, the only positive sample associated with *Crocidura* spp. shrews was from an animal trapped in a household with no prior history of mpox. However, all locations in this study had reported nearby human mpox cases.

It is possible that the IgG-positive animals we reported were exposed to OPXV or MPXV via human-to-animal transmission or reverse spillover. The proportion of stray cats in the study with OPXV antibodies was high (50%). All sampled stray cats were inadvertently captured at sites near confirmed human mpox cases. It is reasonable to hypothesize that the antibodies in those cats may have come from consuming potentially OPXV-infected rodents or from exposure to contaminated environments. A major limitation of this study was the inability of the serologic assay used to differentiate the OPXVs. It is likely that the animals may have been exposed to MPXV, but we cannot completely rule out the possibility of exposures to other OPXVs, including taterapox virus or an unidentified OPXV.

In summary, our study demonstrates the presence of OPXV antibodies in *Cricetomys* spp. rats, *Crocidura* spp. shrews, and feral cats in communities with confirmed human mpox cases in Nigeria. Our research offers further evidence of the possible role of small mammals as likely hosts of zoonotic OPXVs in nature.

Acknowledgments

The authors acknowledge the support of Muhammad Shakir Balogun and the staff of the African Field Epidemiology Network, Nigeria, during the field study. We also acknowledge the support of the laboratory staff of the National Veterinary Research Institute, including Seyi Oyetunde, who died before publication of this paper.

This study was funded by the US Centers for Disease Control and Prevention.

About the Author

Dr. Adedeji is a veterinarian and a researcher with the National Veterinary Research Institute, Vom, Nigeria. His research focuses on zoonotic and economically important poxviruses.

References

1. Essbauer S, Pfeffer M, Meyer H. Zoonotic poxviruses. Vet Microbiol. 2010;140:229–36. https://doi.org/10.1016/j.vetmic.2009.08.026
2. Bonwitt J, Doty JB, McCollum AM, Nakazawa Y. Zoonotic *Orthopoxviruses*: innocuous rash or global public health threat? In: Sing A, editor. Zoonoses: infections affecting humans and animals. Cham, Switzerland; Springer International Publishing; 2022: p. 1–24.
3. Douglass N. Borealpox (Alaskapox) virus: will there be more emerging zoonotic orthopoxviruses? Lancet Microbe. 2024; 5:100883. https://doi.org/10.1016/S2666-5247(24)00106-X
4. Li Y, Ropp SL, Zhao H, Damon IK, Esposito JJ. *Orthopoxvirus* pan-genomic DNA assay. J Virol Methods. 2007;141:154–65. https://doi.org/10.1016/j.jviromet.2006.12.005
5. Li Y, Olson VA, Laue T, Laker MT, Damon IK. Detection of monkeypox virus with real-time PCR assays. J Clin Virol. 2006;36:194–203. https://doi.org/10.1016/j.jcv.2006.03.012
6. Meseko C, Adedeji A, Shittu I, Obishakin E, Nanven M, Suleiman L, et al. Orthopoxvirus infections in rodents, Nigeria, 2018–2019. Emerg Infect Dis. 2023;29:433–4. https://doi.org/10.3201/eid2902.221411

7. Doty JB, Malekani JM, Kalemba LN, Stanley WT, Monroe BP, Nakazawa YU, et al. Assessing monkeypox virus prevalence in small mammals at the human-animal interface in the Democratic Republic of the Congo. Viruses. 2017;9:283. https://doi.org/10.3390/v9100283
8. Hutson CL, Nakazawa YJ, Self J, Olson VA, Regnery RL, Braden Z, et al. Laboratory investigations of African pouched rats (*Cricetomys gambianus*) as a potential reservoir host species for monkeypox virus. PLoS Negl Trop Dis. 2015; 9:e0004013. https://doi.org/10.1371/journal.pntd.0004013
9. Khodakevich L, Szczeniowski M, Manbu-ma-Disu, Jezek Z, Marennikova S, Nakano J, et al. The role of squirrels in sustaining monkeypox virus transmission. Trop Geogr Med. 1987a;39:115–22.
10. Reynolds MG, Doty JB, McCollum AM, Olson VA, Nakazawa Y. Monkeypox re-emergence in Africa: a call to expand the concept and practice of One Health. Expert Rev Anti Infect Ther. 2019;17:129–39. https://doi.org/10.1080/14787210.2019.1567330
11. Yinka-Ogunleye A, Aruna O, Dalhat M, Ogoina D, McCollum A, Disu Y, et al.; CDC Monkeypox Outbreak Team. Outbreak of human monkeypox in Nigeria in 2017–18: a clinical and epidemiological report. Lancet Infect Dis. 2019;19:872–9. https://doi.org/10.1016/S1473-3099(19)30294-4
12. Meseko CA, Maurice N, Shittu I, Onoja BA, Kabantiyok D, Oguche M, et al. The hunter and the hunted: mpox in the Mkpot rainforest community of Nigeria. Trans R Soc Trop Med Hyg. 2025;119:1313–5. https://doi.org/10.1093/trstmh/traf085
13. Pembi E, Omoleke S, Paul H, Augustine T, Cuevas LE. Monkeypox outbreak in a correctional center in North Eastern Nigeria. J Infect. 2022b;85:702–69. https://doi.org/10.1016/j.jinf.2022.09.010
14. Mills JN. Methods for trapping and sampling small mammals for virologic testing. Atlanta: US Department of Health & Human Services; 1995.
15. Orba Y, Sasaki M, Yamaguchi H, Ishii A, Thomas Y, Ogawa H, et al. *Orthopoxvirus* infection among wildlife in Zambia. J Gen Virol. 2015;96:390–4. https://doi.org/10.1099/vir.0.070219-0

Address for correspondence: Adeyinka Adedeji, National Veterinary Research Institute, P.B.M. 01 Vom Plateau, Nigeria; email: yinkadeji2017@gmail.com

etymologia

Borealpox [bōr′-ē-əl-poks]

JJ L. Miranda

The emerging borealpox virus causes zoonotic borealpox disease, characterized by dermal lesions, in humans. From the Latin adjective *borealis*, which refers to Boreas (βορέας), the Greek god of the north wind, boreal has indicated northern origin since the 15th Century.

The orthopoxvirus isolate AK2015_poxvirus was isolated from a resident of Fairbanks, Alaska, USA, in 2015, and initially dubbed Alaskapox virus after complete genome sequence analysis revealed a novel species similar to Old World orthopoxviruses. Seven human cases, including 1 fatal case, preceded renaming to borealpox virus. Boreal references the taiga, a subarctic coniferous forest ecosystem where case-patients and likely small mammal virus reservoirs resided.

Sources

1. Gigante CM, Gao J, Tang S, McCollum AM, Wilkins K, Reynolds MG, et al. Genome of Alaskapox virus, a novel orthopoxvirus isolated from Alaska. Viruses. 2019;11:708. https://doi.org/10.3390/v11080708
2. Mooring EQ, Rogers J, Whitehill F, Werle Z, Gigante CM, Matheny A, et al. Six cases of borealpox and evidence of a zoonotic source—Alaska, 2020–2023. Clin Infect Dis. 2025 Sep 8 [Epub ahead of print]. https://doi.org/10.1093/cid/ciaf497
3. Oxford English Dictionary. Boreal [cited 2024 Sept 12]. https://doi.org/10.1093/OED/2781119121
4. Rogers JH, Westley B, Mego T, Newell KG, Laurance J, Smith L, et al. Fatal borealpox in an immunosuppressed patient treated with antivirals and vaccinia immunoglobulin—Alaska, 2023. Clin Infect Dis. 2025;80:1053–9. https://doi.org/10.1093/cid/ciae536
5. Springer YP, Hsu CH, Werle ZR, Olson LE, Cooper MP, Castrodale LJ, et al. Novel orthopoxvirus infection in an Alaska resident. Clin Infect Dis. 2017;64:1737–41. https://doi.org/10.1093/cid/cix219

Author affiliation: Barnard College, Columbia University, New York, New York, USA

DOI: https://doi.org/10.3201/eid3205.241377

Address for correspondence: JJ L. Miranda, Department of Biology, Barnard College, 3009 Broadway, New York, NY 10027, USA; email: jj@jjmirandalab.org and jmiranda@barnard.edu

Severe Respiratory Illness and Death Associated with Outbreak of Human Rhinovirus B14 among Older Adults, France, 2024

Julien Andreani, Céline Boschi, Anne Decoppet, Jeremy Delerce, Gwilherm Penant, Aylin Karadeniz, Clio Grimaldier, Priscilla Jardot, Laure Zangoli, Maud Mandy, Nicole Vigroux, Florent Polesso, Sophie Edouard, Philippe Cano, Jean-Christophe Lagier, Bernard La Scola, Philippe Colson

We investigated an outbreak of unknown respiratory disease and 8 deaths among older adults in a long-term care facility in France. We identified human rhinovirus (HRV) by quantitative PCR and HRV-B14 by metagenomics. We obtained 5 HRV-B14 genomes that diverged from 5 publicly available genomes. Real-time metagenomics could enable rapid clinical diagnoses.

Viral respiratory infections can be particularly severe in fragile persons, especially older adults (*1*). Influenza virus and respiratory syncytial virus (RSV) are known to be associated with high mortality rates among persons ≥65 years of age (*2*). However, other respiratory viruses, such as human rhinovirus (HRV), also can lead to hospitalization and death (*3*). HRV could become a predominant viral etiology now that effective vaccines are available to prevent severe outcomes from influenza and RSV among older adults (*4*).

During late fall 2024, a total of 18 of 66 older adult residents of a long-term care facility (LTCF) in southeastern France developed severe respiratory illnesses. Five patients had rapid onset cardiorespiratory decompensation and died (Figure 1), which prompted notification to health authorities at the Agence Régionale de la Santé Provence-Alpes Côte d'Azur (Marseille, France). Results of quantitative PCR (qPCR) for SARS-CoV-2, influenza viruses, and RSV were negative.

Health authorities sent residue nasopharyngeal swab samples to the microbiological and virological diagnostic laboratory of the University Hospital Institute (IHU) Méditerranée Infection in Marseille for retrospective testing. We report the rapid multiplex qPCR and metagenomic investigation of that cluster of severe and fatal respiratory infections.

The Study

At IHU, we initially received 11 nasopharyngeal samples collected 3–10 days earlier from 11 of the LTCF patients. We first attempted virus isolation in a Biosafety Level 3 laboratory, as previously described (*5*). Within 3 hours of receipt, we tested samples by FilmArray Respiratory Panel 2 multiplex qPCR (BioFire Diagnostics, https://www.biofiredx.com); 4 samples tested HRV RNA–positive. All attempted cultures were negative.

The next day, we extracted DNA and RNA for next-generation sequencing (NGS) (Appendix, https://wwwnc.cdc.gov/EID/article/32/5/25-0981-App1.pdf). We performed qPCR on nucleic acid extracts by using the FTD Respiratory Pathogens 21 Assay (Fast Track Diagnostics/Siemens Healthineers, https://www.siemens-healthineers.com) and in-house designed qPCR (Appendix). Results of qPCR targeting 46 pathogens were negative for all but 1 sample, which was *Staphylococcus aureus* DNA–positive.

Author affiliations: Institut hospitalo-universitaire Méditerranée Infection, Marseille, France (J. Andreani, C. Boschi, J. Delerce, G. Penant, A. Karadeniz, C. Grimaldier, P. Jardot, S. Edouard, J.-C. Lagier, B. La Scola, P. Colson); Aix-Marseille University, Marseille (J. Andreani, C. Boschi, J. Delerce, S. Edouard, J.-C. Lagier, B. La Scola, P. Colson); Assistance Publique-Hôpitaux de Marseille, Marseille (J. Andreani, C. Boschi, G. Penant, A. Karadeniz, C. Grimaldier, P. Jardot, J.-C. Lagier, B. La Scola, P. Colson); Agence Régionale de la Santé Provence-Alpes Côte d'Azur, Marseille (A. Decoppet, P. Cano); Centre Hospitalier Intercommunal de Brignoles–Le Luc, Brignoles, France (L. Zangoli, M. Mandy, F. Polesso); Laboratoire de Biologie Médicale Eurofins, Garéoult, France (N. Vigroux)

DOI: https://doi.org/10.3201/eid3205.250981

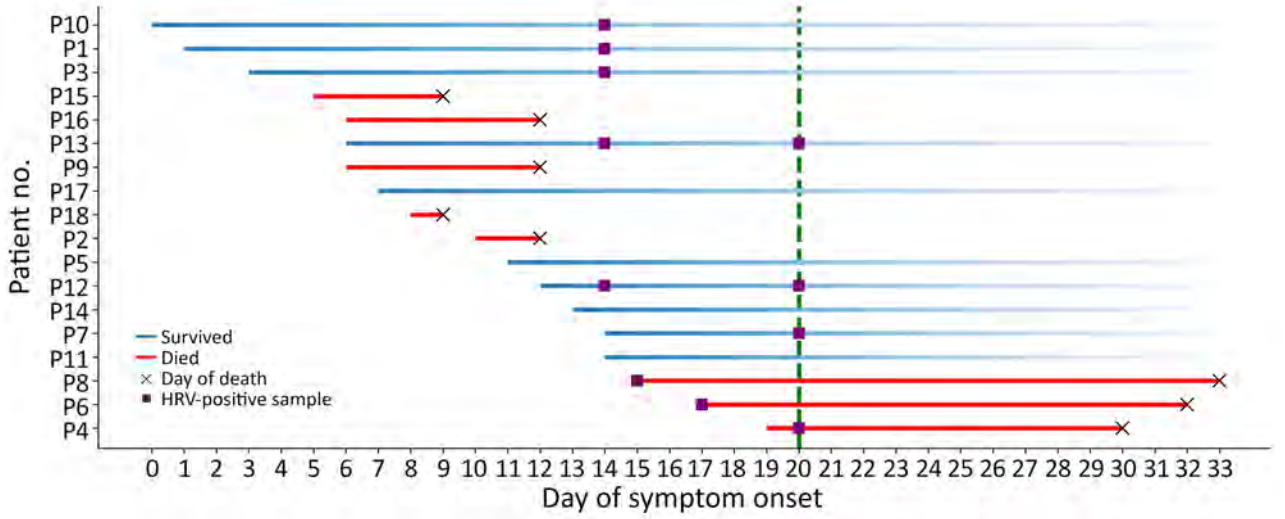

Figure 1. Timeline of severe respiratory illness and death associated with outbreak of HRV-B14 among older adults, France, 2024. Each row represents 1 case and starts on the day of symptom onset, on the basis of retrospectively collected information. Crosses indicate timeline for death. Purple squares indicate HRV RNA–positive samples. The green vertical dotted line indicates transfer of clinical samples to the Marseille laboratory for more extensive diagnosis and metagenomic analyses. Patient 9 had 2 additional HRV-positive postmortem samples (data not shown). No tests were performed for cases P15–P18. No nasopharyngeal swab sample was available for P2. HRV, human rhinovirus.

We then performed NGS on DNA and RNA from the 4 HRV-positive, 2 additional HRV-negative samples, and a negative, sample-free control by using the Ligation Sequencing Kit for library preparation and sequencing on GridION (Oxford Nanopore Technologies, https://nanoporetech.com). Next, we sequenced on the MiSeq platform using MiSeq Reagent version 2 kit (Illumina Inc., https://www.illumina.com), according to manufacturer's protocol (Appendix).

Table. Clinical outcomes and results of molecular testing of nasopharyngeal swab samples collected in a study of severe respiratory illness and death associated with outbreak of HRV-B14 among older adults, France, 2024*

Pt. no.	Sample no.	Biofire qPCR†	FTD multiplex qPCR (Ct)‡	Shotgun mNGS		Probe-based mNGS; % coverage§	VP1 genotype	Hospitalized; clinical outcome
				First batch	Second batch			
1	1	HRV	–	HRV-B14; 2 reads	ND	HRV-B14; 73	HRV-B14	N; recovered
2	NS	ND	ND	ND	ND	ND	ND	Y; died
3	3	HRV	HRV (31)	HRV-B14; 13 reads	ND	HRV-B14; 81	HRV-B14	N; recovered
4	7	HRV	–	ND	No HRV detected	ND	ND	N; died
5	8	–	–	ND	No HRV detected	ND	–	N; recovered
6#	9	HRV	–	ND	No HRV detected	HRV-B14; 13	–	Y; died
7	14	HRV	ND	ND	No HRV detected	ND	ND	N; recovered
8	15	HRV	HRV (31)	No HRV detected	ND	HRV-B14; 43	HRV-B14	Y; died
9**	18	HRV	–	No HRV detected	ND	ND	–	Y; recovered
	22	–	–	ND	No HRV detected	ND	ND	
	23	HRV	–	ND	ND	ND	ND	
10	24	HRV	–	ND	No HRV detected	ND	–	N; recovered
	28	–	–	ND	No HRV detected	ND	ND	
11††	29	–	–	No HRV detected	ND	ND	–	N; recovered
12	30	HRV	HRV (33)	No HRV detected	ND	HRV-B14; 32	HRV-B14	N; recovered
	34	HRV	HRV (34)	ND	No HRV detected	ND	ND	
13	35	HRV	–	ND	No HRV detected	ND	–	N; recovered
	39	HRV	–	ND	No HRV detected	ND	ND	
	40	–	–	ND	ND	ND	ND	
14	42	–	–	ND	No HRV detected	ND	–	Y; recovered

*Ct, cycle threshold; HRV, human rhinovirus; mNGS, metagenomic next-generation sequencing; ND, not done; NS, no sample; Pt., patient; qPCR, quantitative PCR; VP1, viral capsid-encoding gene; –, negative.
†FilmArray Respiratory Panel 2 multiplex qPCR assay (BioFire Diagnostics, https://www.biofiredx.com).
‡FTD Respiratory Pathogens 21 (Fast Track Diagnostics/Siemens Healthineers, https://www.siemens-healthineers.com).
§Probe-based ± ARTIC-like viral enrichment, then mNGS.
#Patient had a history of oxygen requirement and metastatic bladder cancer.
**Patient was anorexic and on an intravenous drip.
††Patient had recent anorexia and cough develop.

We conducted bioinformatic analyses of generated NGS reads by using various commercial and freely available tools, as well as in-house pipelines (Appendix). Six hours after starting NGS, 15 NGS reads generated from the samples of 2 patients (13 reads from 1 patient and 2 reads from the other), ranging from 468 to 2,024 nt in length, were found to be best matches with an HRV-B14 genome (GenBank accession no. NC_001490.1) (Tables; Appendix Tables 1, 2). We used those reads

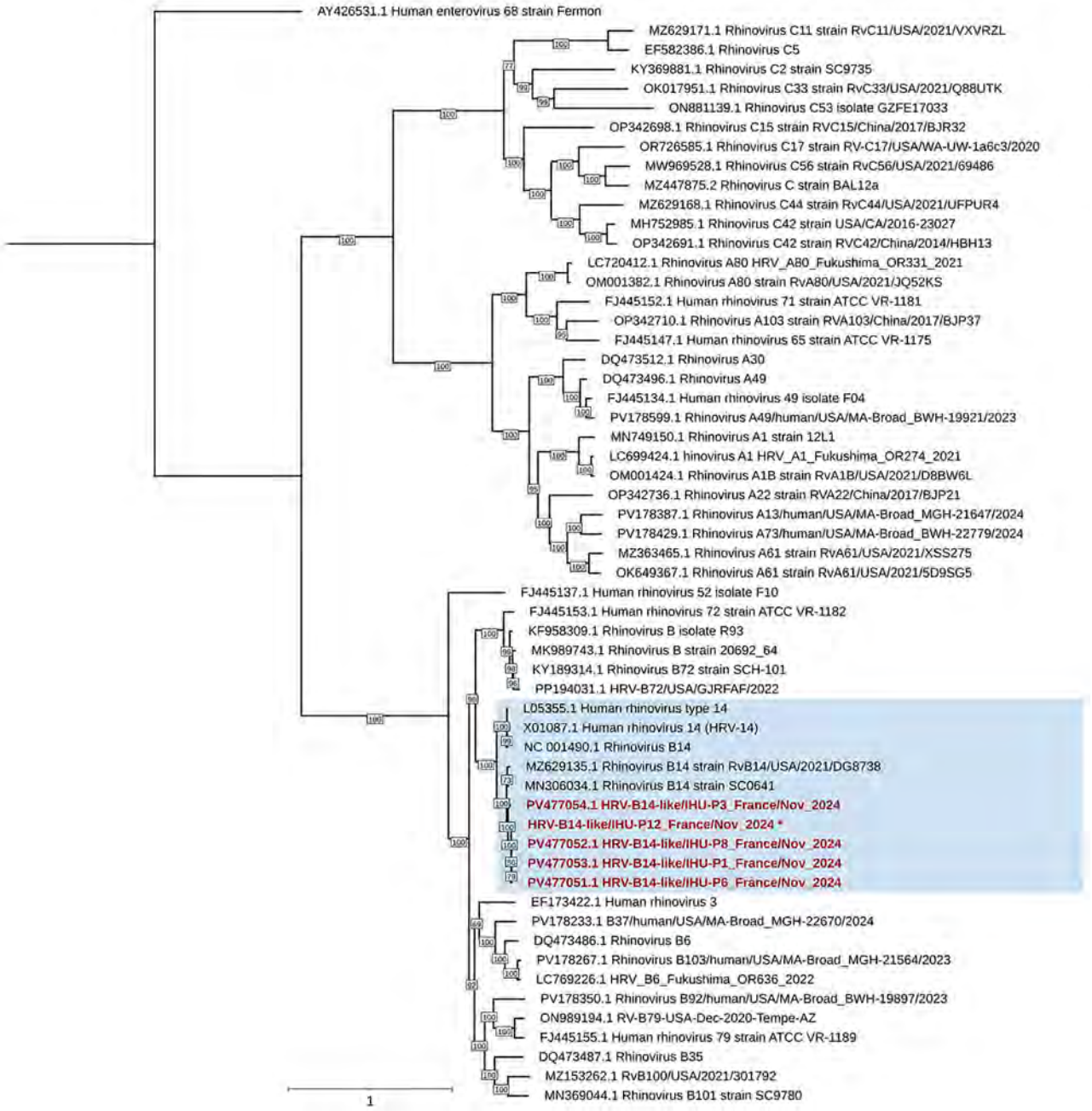

Figure 2. Phylogenetic tree of HRV-B14 from outbreak of severe respiratory illness and death among older adults, France, 2024. Tree includes HRV genomes downloaded from GenBank; accession numbers are indicated. Red font indicates genomes obtained in this study; blue background indicates HRV-B14 genomes. Asterisk (*) indicates that the genome is fragmented (multiple GenBank accession numbers available). Genome alignment was performed by using MUSCLE (https://www.ebi.ac.uk/Tools/msa/muscle) with standard parameters for nucleotide sequences. Tree was built by using IQ-TREE (http://www.iqtree.org) with the transitional model 2 plus empirical base frequencies plus proportion of invariable site plus gamma-distributed rate variation with 4 categories model identified as the most suitable by the best-fit model research module according to the Bayesian information criterion. A total of 10,000 ultra-fast bootstrap replicates were performed. Scale bar indicates nucleotide substitutions per site. HRV, human rhinovirus.

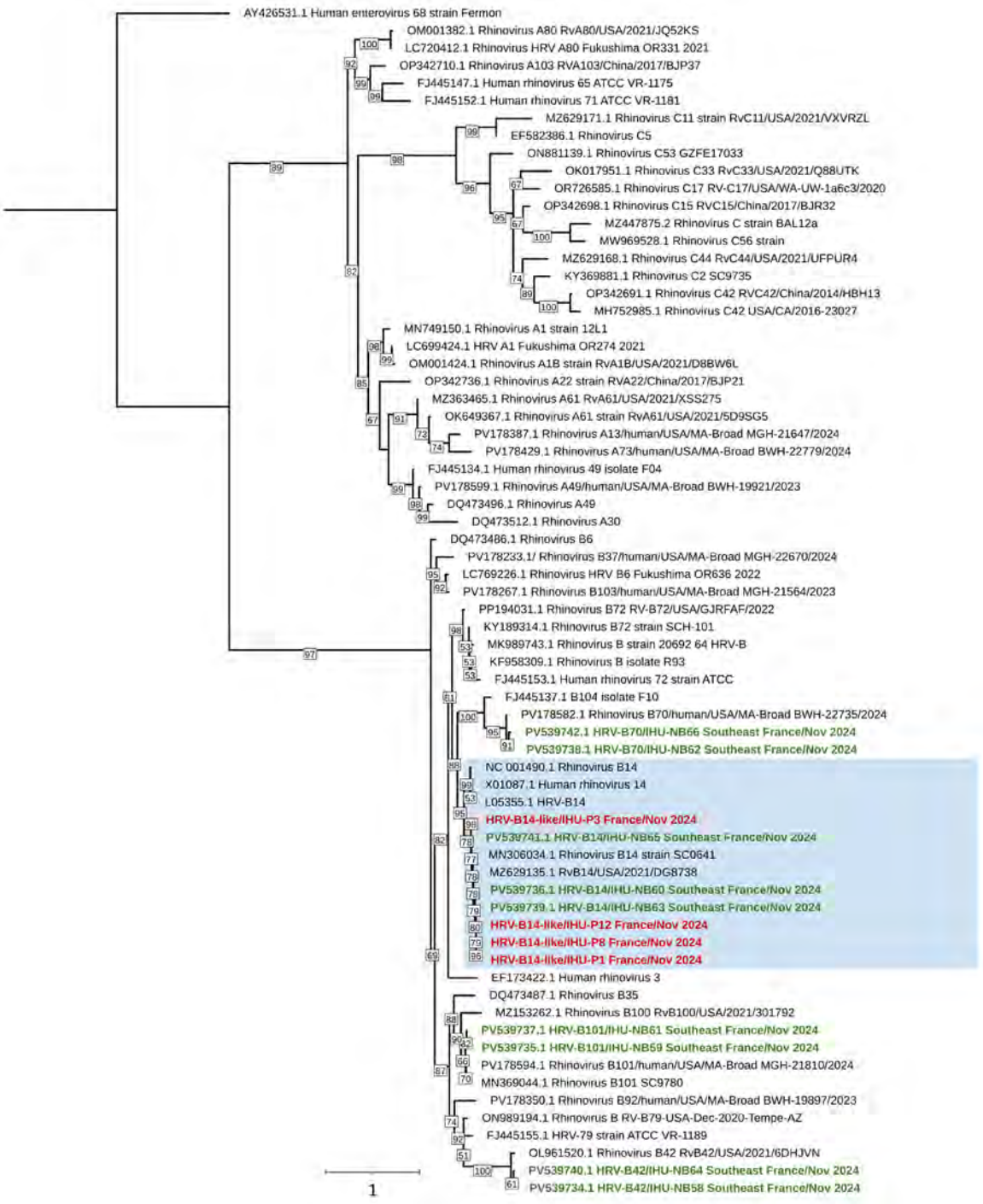

Figure 3. Phylogenetic tree of HRV-B sequences circulating in Marseille during severe respiratory illness and death associated with outbreak of HRV-B14 among older adults, France, 2024. Viral protein 1–encoding gene sequence alignment was performed by using MUSCLE (https://www.ebi.ac.uk/Tools/msa/muscle) with standard parameters for nucleotide sequences. Blue background indicates the HRV-B14 sequences; red font indicates sequences obtained from the cluster of cases among older adults; green font indicates sequences obtained from other HRV RNA–positive samples detected in our laboratory during the same timeframe as the outbreak. All others were downloaded from GenBank; accession numbers are indicated. The sequence obtained from patient P6 does not appear in this tree because it was a partial sequence and does not align with the genome region used in this analysis. The IQ-TREE software was used to build the tree with the general time-reversible model plus empirical base frequencies plus FreeRate model with 10 rate categories model identified as the most suitable by the best-fit model research module according to the Bayesian information criterion. A total of 10,000 ultra-fast bootstrap replicates were performed. Scale bar indicates nucleotide substitutions per site. HRV, human rhinovirus.

to obtain consensus sequences, one of 4,447 nt in 3 contigs for one sample, and the other of 1,019 nt for the other sample (Appendix). The negative control had no HRV reads.

We designed in-house PCR systems by using the Primer3Plus web application (https://www.primer3plus.com/index.html) to fill gaps in reconstructed HRV-B14 genomes (Appendix Table 3). Then, we used IQ-TREE (http://www.iqtree.org) to select the best model for each alignment and built maximum-likelihood phylogenetic trees. We visualized trees incorporating all complete HRV-B14 genomes by using iTOL version 7 (https://itol.embl.de).

Five days after we received the initial samples, we received additional samples from the LTCF outbreak; in total, multiplex qPCRs eventually detected HRV RNA in 13/19 nasopharyngeal swab samples from 10/13 patients. Eight samples tested positive with the BioFire assay and negative with the FTD assay, (Table; Appendix Table 2). An HRV-B14–specific qPCR we designed from partial genomes was positive for 5 patients (Appendix Table 3).

Pre-NGS viral nucleic acid enrichment using the Respiratory Viral Research Panel (Twist Bioscience, https://www.twistbioscience.com) enabled us to obtain 5 partial HRV-B14 genomes from 5 patients. Genomes were 913–6,644 nt in length and 13%–86% of the GenBank reference genome (accession no. NC_001490.1). In the phylogenetic tree, those 5 genomes clustered together with 100% bootstrap value near 5 other genomes available in public databases (Figure 2). However, 1 genome from patient P3 stood apart; its nucleotide similarity was 97.1%–98.1% with the 4 other genomes, whereas those 4 genomes had 99.9%–100.0% similarity to each other. Sequencing of the HRV virus capsid protein (VP) 1–encoding gene confirmed HRV-B14 for 4 of the initial 11 samples tested from the LTCF (Table).

We also tested 86 residue nasopharyngeal swab samples collected in southeastern France as part of routine diagnostic testing during the same timeframe as the cases from the LTC facility during late autumn 2024. Viral capsid VP1-encoding genotyping for all 86 nasopharyngeal swab samples identified 9 additional HRV-B sequences, 3 of which were HRV-B14 on the basis of BLAST (https://blast.ncbi.nlm.nih.gov) similarity and phylogeny (Figure 3).

The outbreak among LTCF residents resulted in 18 severe illnesses, from which 8 (44%) patients died. Of note, metagenomic methods enabled us to identify HRV-B14 within ≈30 hours of receiving samples; without those methods, the cause of the outbreak would have largely remained elusive.

Viral nucleic acid enrichment successfully lengthened the HRV-B14 genomes from the LTCF outbreak, 1 of which differed from the 4 others, indicating ≥2 closely related HRV-B14 strains were circulating during this outbreak. In addition, HRV-B14 was detected in 3% of HRV-positive samples received at our laboratory during the same period as the LTCF outbreak, indicating that HRV-B14 circulated in that geographic area in fall of 2024.

Previous metagenomics-based approaches have successfully identified various pathogens during outbreak investigations (*6*–*10*). For instance, in the United States, metagenomics used on 6 nasopharyngeal swab samples from 4 case-patients in a pulmonary ward and on 10 nasopharyngeal swab samples from 9 control outpatients enabled investigators to determine that case-patients' HRV sequences were not genetically related, dispelling concerns of single-source nosocomial transmission ≤24 hours of receiving samples (*7*). That case demonstrates the benefits of metagenomics in routine settings.

During the LTCF outbreak, *S. aureus* DNA was the only other pathogen detected by qPCR, and only in 1 sample. Notwithstanding that finding, co-infections might have been missed because specific qPCR, serologic, or culture assays were not used for all possible infectious agents; because viral or microbial loads were too low for detection; or because our laboratory was not involved in first-line diagnosis and the time between respiratory sample collection and testing at our laboratory was up to 10 days.

Conclusions

Severe and life-threatening HRV infections previously have been reported among older persons (*11*,*12*). Illness severity as assessed through rates of hospital admission, intensive care unit admission, and death in those studies were similar to those previously reported among immunocompromised adults infected with the 2009 influenza A(H1N1) pandemic virus (*11*,*12*) or to rates among hematopoietic cell transplant recipients with RSV or influenza virus infection (*13*,*14*). We speculate that HRV could lead to severe disease and death in fragile older persons, as seen with RSV (*1*), but data are scarce. Moreover, those prior assessments did not address whether severity differed between viral genotypes, and no specific data on HRV-B14 epidemiology, infectiousness, or clinical severity are available.

In summary, our findings indicate ≥1 HRV-B14 strain was circulating and caused severe illness and death among a population of older adults in southeastern France. Rapid identification (≈30 hours) of

the viral etiology in this case demonstrates that expanded use of real-time metagenomics for routine diagnostic testing in clinical virology laboratories, particularly targeting respiratory viruses other than vaccine-preventable influenza viruses and RSV, could enable early detection and management of such respiratory pathogens.

This study regards data that were registered on the Health Data Access Portal of Marseille Public and University hospitals (Assistance Publique-Hôpitaux de Marseille [AP-HM]) and was approved by the Ethics and Scientific Committee of AP-HM (approval nos. CSE_PADS25-3 and CSE_PADS25-49).

Human rhinovirus B14 sequences from this study were deposited into GenBank (accession nos. PV539734–42 and PV477051–8) (Appendix Tables 1, 2).

This work was supported by the French government under the Investments for the Future program managed by the National Agency for Research, Méditerranée-Infection 10-IAHU-03, and by the Contrat Plan Etat-Région and the European funding FEDER IHUPERF. Funding sources had no role in the design and conduct of the study; collection, management, analysis, and interpretation of the data; and preparation, review, or approval of the manuscript.

B.L.S. and P.C. are scientific advisors for BioSellal and Triber Global.

About the Author

Dr. Andreani is a virologist and junior investigator at IHU Méditerranée Infection of Aix-Marseille University and Marseille Public and University Hospitals. His research interests cover respiratory viruses and giant viruses.

References

1. Tseng HF, Sy LS, Ackerson B, Solano Z, Slezak J, Luo Y, et al. Severe morbidity and short- and mid- to long-term mortality in older adults hospitalized with respiratory syncytial virus infection. J Infect Dis. 2020;222:1298–310. https://doi.org/10.1093/infdis/jiaa361
2. Godefroy R, Giraud-Gatineau A, Jimeno MT, Edouard S, Meddeb L, Zandotti C, et al. Respiratory syncytial virus infection: its propensity for bacterial coinfection and related mortality in elderly adults. Open Forum Infect Dis. 2020;7:ofaa546. https://doi.org/10.1093/ofid/ofaa546
3. Giraud-Gatineau A, Colson P, Jimeno MT, Zandotti C, Ninove L, Boschi C, et al. Comparison of mortality associated with respiratory viral infections between December 2019 and March 2020 with that of the previous year in Southeastern France. Int J Infect Dis. 2020;96:154–6. https://doi.org/10.1016/j.ijid.2020.05.001
4. Bajema KL, Yan L, Li Y, Argraves S, Rajeevan N, Fox A, et al. Respiratory syncytial virus vaccine effectiveness among US veterans, September, 2023 to March, 2024: a target trial emulation study. Lancet Infect Dis. 2025;25:625–33. https://doi.org/10.1016/S1473-3099(24)00796-5
5. Wurtz N, Penant G, Jardot P, Duclos N, La Scola B. Culture of SARS-CoV-2 in a panel of laboratory cell lines, permissivity, and differences in growth profile. Eur J Clin Microbiol Infect Dis. 2021;40:477–84. https://doi.org/10.1007/s10096-020-04106-0
6. Slavov SN. Routine detection of viruses through metagenomics: where do we stand? Am J Trop Med Hyg. 2025;112:479–80. https://doi.org/10.4269/ajtmh.24-0652
7. Greninger AL, Waghmare A, Adler A, Qin X, Crowley JL, Englund JA, et al. Rule-out outbreak: 24-hour metagenomic next-generation sequencing for characterizing respiratory virus source for infection prevention. J Pediatric Infect Dis Soc. 2017;6:168–72. https://doi.org/10.1093/jpids/pix019
8. Greninger AL, Zerr DM, Qin X, Adler AL, Sampoleo R, Kuypers JM, et al. Rapid metagenomic next-generation sequencing during an investigation of hospital-acquired human parainfluenza virus 3 infections. J Clin Microbiol. 2016;55:177–82. https://doi.org/10.1128/JCM.01881-16
9. Javaid W, Ehni J, Gonzalez-Reiche AS, Carreño JM, Hirsch E, Tan J, et al. Real-time investigation of a large nosocomial influenza A outbreak informed by genomic epidemiology. Clin Infect Dis. 2021;73:e4375–83. https://doi.org/10.1093/cid/ciaa1781
10. Li P, Wang K, Qiu S, Lin Y, Xie J, Li J, et al. Rapid identification and metagenomics analysis of the adenovirus type 55 outbreak in Hubei using real-time and high-throughput sequencing platforms. Infect Genet Evol. 2021;93:104939. https://doi.org/10.1016/j.meegid.2021.104939
11. Nicholson KG, Kent J, Hammersley V, Cancio E. Risk factors for lower respiratory complications of rhinovirus infections in elderly people living in the community: prospective cohort study. BMJ. 1996;313:1119–23. https://doi.org/10.1136/bmj.313.7065.1119
12. Hung IFN, Zhang AJ, To KKW, Chan JFW, Zhu SHS, Zhang R, et al. Unexpectedly higher morbidity and mortality of hospitalized elderly patients associated with rhinovirus compared with influenza virus respiratory tract infection. Int J Mol Sci. 2017;18:259. https://doi.org/10.3390/ijms18020259
13. Kraft CS, Jacob JT, Sears MH, Burd EM, Caliendo AM, Lyon GM. Severity of human rhinovirus infection in immunocompromised adults is similar to that of 2009 H1N1 influenza. J Clin Microbiol. 2012;50:1061–3. https://doi.org/10.1128/JCM.06579-11
14. Seo S, Waghmare A, Scott EM, Xie H, Kuypers JM, Hackman RC, et al. Human rhinovirus detection in the lower respiratory tract of hematopoietic cell transplant recipients: association with mortality. Haematologica. 2017;102:1120–30. https://doi.org/10.3324/haematol.2016.153767

Address for correspondence: Philippe Colson and Bernard La Scola, IHU Méditerranée Infection, 19-21 Blvd Jean Moulin, 13005 Marseille, France; email: philippe.colson@ap-hm.fr and bernard.la-scola@univ-amu.fr

Clinical, Molecular, and Zoonotic Perspectives on Human Cases of *Cryptosporidium* sp. OTUi

Tine Graakjær Larsen, Edgar Baz-González, Marianne Lebbad, Marielle Babineau, Anson V. Koehler, Lene Nielsen, Christen Rune Stensvold

We report a case of *Cryptosporidium* sp. OTUi identified in a tourist from Denmark who recently traveled to Indonesia. Previous detections include a traveler from Australia returning from Bali, a bat from the Philippines, and a patient from Australia. On the basis of those findings, we believe zoonotic transmission is plausible.

Surveillance for human cryptosporidiosis cases has been conducted in Denmark since 2023. Clinical microbiology departments can submit original fecal material from positive cases to Statens Serum Institut (SSI; Copenhagen, Denmark) for confirmation and molecular characterization (*1*). We followed that established process for a case of *Cryptosporidium* sp. OTUi identified in a person who had recently traveled to Indonesia.

The Study

During travel to Bali, Indonesia, a woman from Denmark experienced gastrointestinal symptoms including vomiting and diarrhea. She sought medical care after her return home because symptoms persisted. Multiplex PCR (QIAstat-Dx Gastrointestinal Panel; QIAGEN, https://www.qiagen.com) performed on a fecal sample from the patient at a regional clinical microbiology department identified *Cryptosporidium* spp., Shiga toxin–producing *Escherichia coli*, and norovirus group I and group II.

The woman was interviewed for surveillance purposes and reported having experienced symptoms for ≈14 days. Vomiting developed early, followed by diarrhea. She spent 2 weeks in Bali, primarily in Ubud, with a short stay in Canggu. Exposures included swimming pools and seawater. She reported no cave visits and no direct animal contact, except possible contact with a dog. She observed bats, particularly in Canggu. Similar symptoms developed in 2 travel companions shortly after her illness onset, but their diagnostic status was unknown.

As part of routine *Cryptosporidium* typing at SSI, we performed nested PCR targeting the 60-kDa glycoprotein (*gp60*) gene by using a previously described protocol (*2*). The sequence obtained (GenBank accession no. PX525565; subtype A17) shared >99% identity with another isolate (accession no. KJ506837; subtype A15G1), a relatively short sequence deposited in GenBank as *Cryptosporidium* sp. OTUi subtype AVK-2014. The sequence originated from a woman from Australia who had diarrhea in 2014 after returning from Bali (*3*). Both sequences belong to the same unnamed subtype family, defined as a group of phylogenetically related *gp60* sequences. A third sequence (GenBank accession no. PX092402; subtype A12G1), identified in 2024 in a woman from Australia with unknown travel history, also belonged to the same subtype family (*4*). Each of the 3 sequences represents a distinct subtype, as evidenced by differences in the TCA and TCG configuration within the repetitive region.

Because of the limited length of available human *gp60* sequences for comparison, we constructed 2 phylogenetic trees of *Cryptosporidium* spp. *gp60* subtype families by using sequence alignments of different lengths (Figure 1, panels A, B). For the longer alignment (Figure 1, panel A), the ACA and TCA repeat region was removed, but it was kept in the analysis of the shorter fragment (Figure 1, panel B). Our analysis reveals that all 3 human-derived *Cryptosporidium* sp. OTUi sequences cluster together (Figure 1, panel

Author affiliations: Statens Serum Institut, Copenhagen, Denmark (T.G. Larsen, C.R. Stensvold); Universidad de La Laguna, San Cristóbal de La Laguna, Tenerife, Canary Islands, Spain (E. Baz-González); Sjöbjörnsvägen, Stockholm, Sweden (M. Lebbad); The University of Melbourne, Melbourne, Victoria, Australia (M. Babineau, A.V. Koehler); Copenhagen University Hospital, Herlev and Gentofte, Denmark (L. Nielsen).

DOI: https://doi.org/10.3201/eid3205.260128

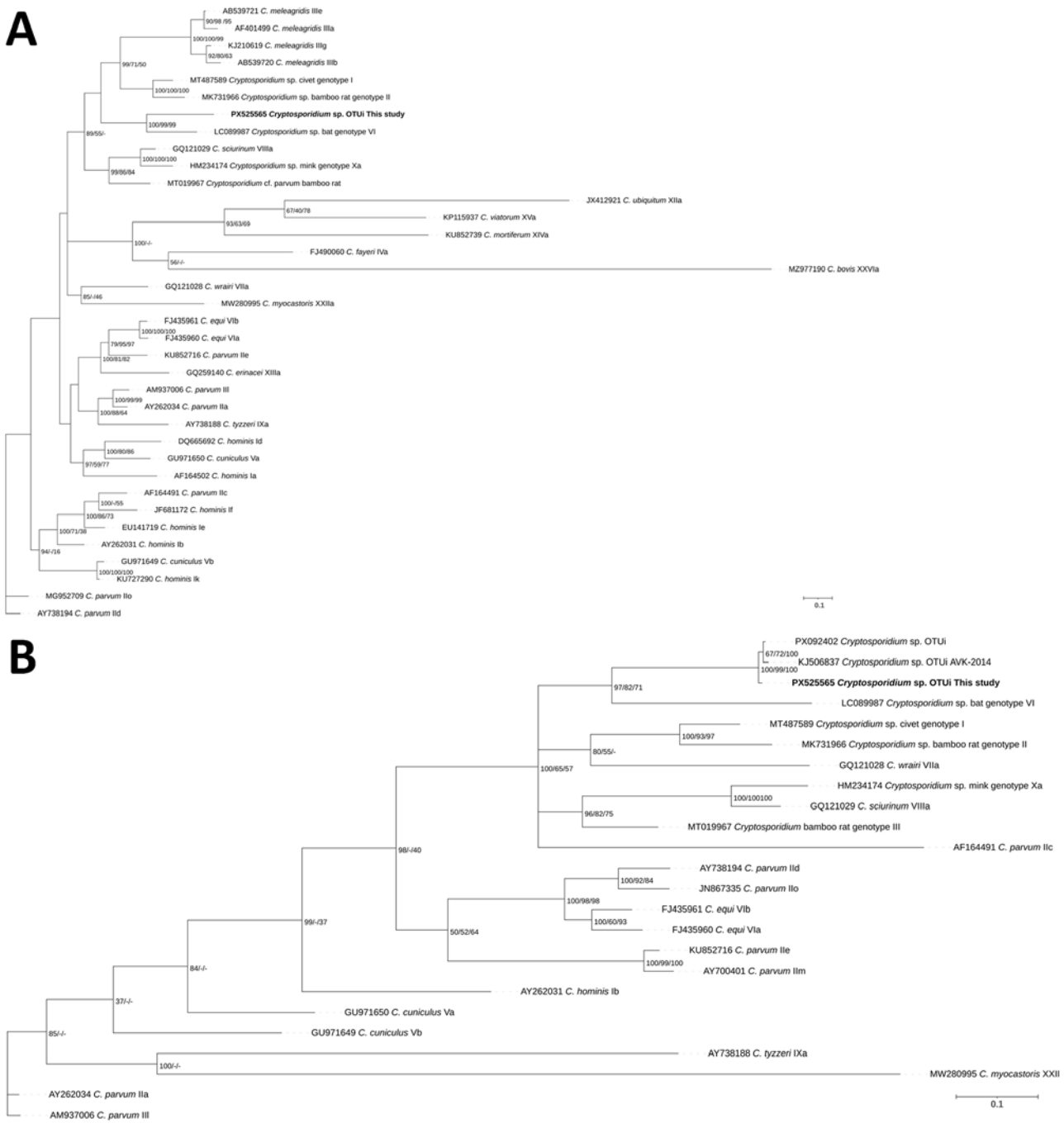

Figure 1. Phylogenetic trees inferred by using Bayesian analysis on the basis of partial nucleotide sequences of the *gp60* gene of *Cryptosporidium* sp. OTUi (GenBank accession no. PX525565) obtained from a woman in Denmark who had traveled to Indonesia (bold text) in a study of the clinical, molecular, and zoonotic perspectives on human cases of *Cryptosporidium* sp. OTUi. A) Analysis including reference sequences (n = 35) retrieved from GenBank. B) Because sequences from previous human cases in Australia (GenBank accession nos. KJ506837 and PX092402) were shorter, we used a reduced alignment, including relevant reference sequences (n = 23). For Bayesian analyses, substitution models were selected on the basis of the lowest Akaike information criterion score, using a general time reversible with invariable site plus discrete gamma model substitution. We performed Bayesian inference by using MrBayes v3.2.7 (*13*) with 5 million generations, 4 chains, and sampling every 1,000 generations. The first 25% of trees were discarded as burn-in. We assessed convergence was assessed by SD of split frequencies <0.01 and a potential scale reduction factor of 1.0. Posterior probabilities and bootstrap support values from maximum-likelihood and neighbor-joining analyses are shown to the right of the nodes. Scale bars indicate substitutions per site.

B), and that their closest *gp60* relatives belong to the *Cryptosporidium* spp. bat genotype VI subtype family. Because *gp60* is a highly polymorphic locus used for subtyping and is known to exhibit recombination in some species, the phylogenetic patterns inferred from this marker reflect subtype family relationships but might not reflect species-level relationships.

We performed amplification and sequencing of the small subunit rRNA (*ssu*) and actin genes according to established methods (*5*,*6*). The *ssu* sequence obtained from the case in Denmark (GenBank accession no. PX498108) shared ≥99% identity with OTUi AVK-2014 (accession no. KJ506854) (660/661 bp), the *ssu* sequence derived from the tourist from Australia returning from Bali in 2014; PHBat1 (accession no. LC844807) (674/675 bp), derived from bat feces collected in the Philippines in 2019 (*7*); and the 2024 sample obtained from the woman from Australia (accession no. PV981443) (679/680 bp). The actin sequence from the case in Denmark (GenBank accession no. PX525564) shared >99% similarity with the actin sequence from PHBat1 (accession no. LC844808) (952/954 bp). The phylogenetic tree inferred from Bayesian analyses of concatenated *ssu* and actin sequences (Figure 2) reveals clustering of the 3 OTUi sequences in their own well-supported branch, which is nested within a broader group of branches comprising multiple *Cryptosporidium* spp. and genotypes.

The simultaneous detection of Shiga toxin–producing *E. coli* and norovirus group I and group II is not readily explained by bats as a potential source, because neither pathogen is typically associated with bats (*8*,*9*). Norovirus likely accounted for the acute

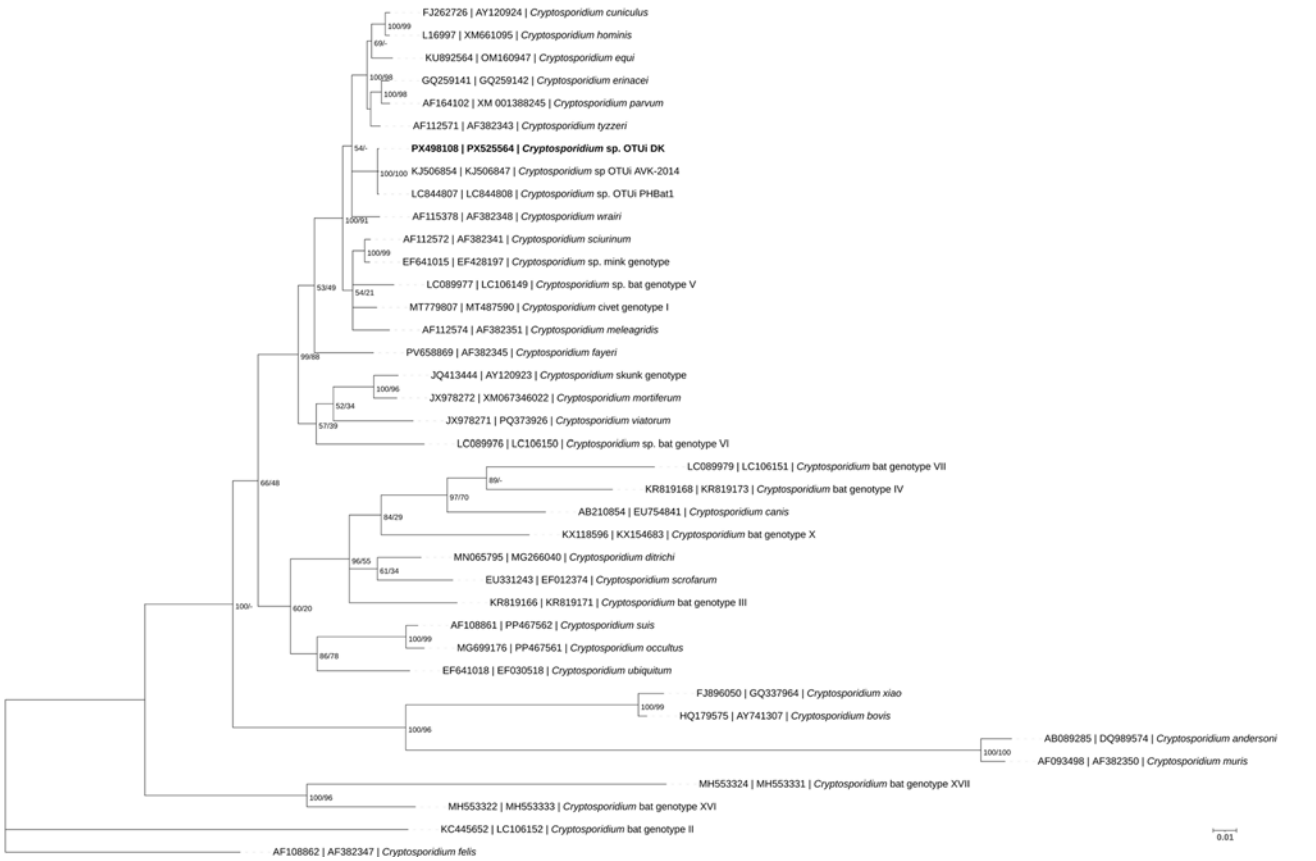

Figure 2. Phylogenetic tree inferred by partitioned Bayesian analysis on the basis of concatenated *ssu* and actin gene sequences of *Cryptosporidium* spp., including *Cryptosporidium* sp. OTUi identified from a woman in Denmark who had traveled to Indonesia (bold text) in a study of the clinical, molecular, and zoonotic perspectives on human cases of *Cryptosporidium*. GenBank accession numbers for *ssu* and actin sequences are provided. Alignments of *ssu* and actin were concatenated according to species identity and OTUi sample identity; only taxa with sequences available for both loci were included. For Bayesian analyses, substitution models were selected on the basis of the lowest Akaike information criterion score (general time reversible with invariable site plus discrete gamma model substitution for *ssu* and actin). Partitioned Bayesian inference was performed by using MrBayes v3.2.7 (*13*) with 10 million generations, 4 chains, and sampling every 1,000 generations; the first 25% of trees were discarded as burn-in. Convergence was confirmed by SD of split frequencies <0.01 and a potential scale reduction factor of 1.0. Posterior probabilities and bootstrap support values from maximum-likelihood analysis are shown to the right of the nodes. Scale bar indicates substitutions per site.

vomiting period, whereas the prolonged diarrhea is consistent with cryptosporidiosis. Because of the concurrent detection of 3 enteric pathogens and the temporal clustering of gastrointestinal illness (of unknown cause) among the patient's 2 travel companions, a more plausible explanation is shared exposure to food or water contaminated with fecal material from multiple human or animal sources, rather than transmission from a single reservoir. Contamination of food or water with bat feces is a plausible transmission pathway, particularly where bats roost near agricultural areas and water sources. Similar mechanisms have been proposed for Nipah virus transmission through contaminated food products (*10*,*11*). Ubud and Canggu represent semiurban environments, and human activity overlaps with wildlife habitats, potentially enabling exposure. Also, produce sold within those villages can have originated from more bat-friendly areas. Thus, contamination of water or food with bat feces seems a plausible source of this human *Cryptosporidium* sp. OTUi infection; however, alternative human or animal sources should also be considered.

Bats are typically infected with bat-specific *Cryptosporidium* spp. genotypes, of which >20 have been identified on the basis of *ssu* gene sequencing. The risk of zoonotic transmission from bats is generally considered low because most described bat genotypes are phylogenetically distinct from *Cryptosporidium* spp. commonly found in humans, and they have been detected exclusively in Chiroptera. In addition, only a few instances of human-pathogenic species (*C. parvum*, *C. hominis*, and *C. tyzzeri*) have been detected in bats, without evidence of active infection, suggesting that bats might serve only as mechanical carriers (*12*).

Only 1 *gp60* sequence related to bat genotypes is currently available in GenBank, specifically *Cryptosporidium* spp. bat genotype VI (accession no. LC089987). This scarcity of sequence data might be attributable to primer specificity, because the *gp60* gene exhibits extensive genetic polymorphism or because *gp60* is a single-copy gene, which can affect analytical sensitivity. The primers used in this study amplify a fragment of the *gp60* gene from *C. parvum*, *C. hominis*, and other phylogenetically related species, including *Cryptosporidium* spp. bat genotype VI and *Cryptosporidium* sp. OTUi, but might not amplify other bat genotypes.

The high sequence identity across loci among geographically and temporally distinct human and bat isolates suggests a shared epidemiologic origin. Phylogenetic proximity to *Cryptosporidium* spp. bat genotype VI on the basis of the *gp60* gene further supports a zoonotic link. The association of 2 human cases with travel to Bali suggests this *Cryptosporidium* spp. genotype might be endemic in Bali and potentially maintained by a zoonotic reservoir. The 2019 bat sample originated from a forest roundleaf bat in the Philippines, a nonmigratory species native to the Philippines but not to Bali (*7*). Nevertheless, related bat species inhabit Bali, and connections between bat populations might occur through limited migration or through other hosts, enabling spillover to humans. Subsequent shedding of *Cryptosporidium* sp. OTUi by infected humans could enable transmission through fecal contamination of food or water, amplifying the risk to others.

Conclusions

This investigation highlights the value of molecular surveillance and multilocus typing for detecting emerging *Cryptosporidium* genotypes and for elucidating potential infection sources. Clustering of *Cryptosporidium* sp. OTUi among travelers returning from Bali, combined with its phylogenetic relationship to a bat-associated genotype, supports regional endemicity and supports the hypothesis of bats being a reservoir for human cryptosporidiosis. Improved genomic characterization of bat-associated *Cryptosporidium* infection and enhanced environmental surveillance are needed to better understand transmission dynamics and assess the public health significance of this parasite.

This study was conducted as part of a task mandated to Statens Serum Institut under national legislation, and approval from ethics committees was not required. The Danish Data Protection Agency serves as the national supervisory authority for scientific research. As of May 25, 2018, when the European General Data Protection Regulation came into force, approval from the Data Protection Agency is no longer required for such studies. However, the Statens Serum Institut is required to maintain records of data processing activities. This study was covered by Statens Serum Institut records of processing activities (protocol no. 25/03248).

Sequences generated from the patient from Denmark are available in GenBank (accession nos. PX525565, PX498108, and PX525564).

About the Author

Dr. Larsen is a medical doctor currently working at Statens Serum Institut, the national public health institute of Denmark. Her interests are focused on surveillance and outbreak investigation, particularly of *Cryptosporidium*.

References

1. Larsen TG, Ethelberg S, Nielsen HL, Hartmeyer GN, Nielsen L, Zangenberg M, et al. From rare to recognized: enhanced detection uncovers *Cryptosporidium* endemicity and species diversity in Denmark. Emerg Microbes Infect. 2025; 14:2529893. https://doi.org/10.1080/22221751.2025.2529893
2. Alves M, Xiao L, Sulaiman I, Lal AA, Matos O, Antunes F. Subgenotype analysis of *Cryptosporidium* isolates from humans, cattle, and zoo ruminants in Portugal. J Clin Microbiol. 2003;41:2744–7. https://doi.org/10.1128/JCM.41.6.2744-2747.2003
3. Koehler AV, Whipp M, Hogg G, Haydon SR, Stevens MA, Jex AR, et al. First genetic analysis of *Cryptosporidium* from humans from Tasmania, and identification of a new genotype from a traveller to Bali. Electrophoresis. 2014;35:2600–7. https://doi.org/10.1002/elps.201400225
4. Babineau M, Koehler AV, Sait ML, Mercoulia K, Dougall S, McAllister J, et al. Large-scale molecular epidemiological survey of *Giardia* and *Cryptosporidium* in Victoria, Australia (2020–2024), reveals novel subtypes and outbreak-associated lineages. J Clin Microbiol. 2026;0:e01558-25. https://doi.org/10.1128/jcm.01558-25
5. Stensvold CR, Larsen TG, Grüttner J, Nielsen L, Engberg J, Lebbad M. Rodent-adapted *Cryptosporidium* infection in humans: seven new cases and review of the literature. One Health. 2024;18:100682. https://doi.org/10.1016/j.onehlt.2024.100682
6. Lebbad M, Winiecka-Krusnell J, Stensvold CR, Beser J. High diversity of *Cryptosporidium* species and subtypes identified in cryptosporidiosis acquired in Sweden and abroad. Pathogens. 2021;10:523. https://doi.org/10.3390/pathogens10050523
7. Xu L, Fukuda Y, Murakoshi F, Alviola P, Masangkay J, Recuenco FC, et al. Molecular characterization and zoonotic risk assessment of *Cryptosporidium* spp. in Philippine bats. Food Waterborne Parasitol. 2024;38:e00249. https://doi.org/10.1016/j.fawpar.2024.e00249
8. Yang L, Wang Q, Xu L, Tu C, Huang X, He B. Detection and characterization of a novel norovirus in bats, China. Virol Sin. 2018;33:100–3. https://doi.org/10.1007/s12250-018-0010-9
9. Nowak K, Fahr J, Weber N, Lübke-Becker A, Semmler T, Weiss S, et al. Highly diverse and antimicrobial susceptible *Escherichia coli* display a naïve bacterial population in fruit bats from the Republic of Congo. PLoS One. 2017; 12:e0178146. https://doi.org/10.1371/journal.pone.0178146
10. Luby SP, Rahman M, Hossain MJ, Blum LS, Husain MM, Gurley E, et al. Foodborne transmission of Nipah virus, Bangladesh. Emerg Infect Dis. 2006;12:1888–94. https://doi.org/10.3201/eid1212.060732
11. Khan MS, Hossain J, Gurley ES, Nahar N, Sultana R, Luby SP. Use of infrared camera to understand bats' access to date palm sap: implications for preventing Nipah virus transmission. EcoHealth. 2010;7:517–25. https://doi.org/10.1007/s10393-010-0366-2
12. Barbosa AD, Egan S, Feng Y, Xiao L, Ryan U. How significant are bats as potential carriers of zoonotic *Cryptosporidium* and *Giardia?* Curr Res Parasitol Vector Borne Dis. 2023;4:100155. https://doi.org/10.1016/j.crpvbd.2023.100155
13. Huelsenbeck JP, Ronquist F. MRBAYES: Bayesian inference of phylogenetic trees. Bioinformatics. 2001;17:754–5. https://doi.org/10.1093/bioinformatics/17.8.754

Address for correspondence: Christen Rune Stensvold, Statens Serum Institut, Artillerivej 5, DK-2300 Copenhagen S, Denmark; email: run@ssi.dk

Highly Pathogenic Avian Influenza A(H5N1) Clade 2.3.4.4b Virus and Mass Mortality in Eurasian Cranes, Germany, 2025

Anne Günther, Christof Herrmann, Julia Sehl-Ewert, Simon Piro, Ann Kathrin Ahrens, Sten Calvelage, Anne Pohlmann, Martin Beer, Timm Harder

In autumn 2025, highly pathogenic avian influenza A(H5N1) clade 2.3.4.4b virus, genotype EA-2024-DI.2.1, caused systemic infections leading to a mass mortality event among the western migrating subpopulation of Eurasian cranes (*Grus grus*) in Germany. Gregarious behavior at feeding and resting sites likely promoted rapid viral spread within the population.

Eurasian cranes (*Grus grus*) migrate along eastern, central, and western European flyways. Mass mortalities caused by goose/Guangdong (Gs/Gd)–like highly pathogenic avian influenza viruses (HPAIVs) of subtype H5 have shown susceptibility in *G. grus* cranes previously, on the eastern and central flyway in West Asia during the 2021–22 and 2024–25 HPAI seasons (*1*), and in Eastern Europe during 2023–24 (*2*,*3*). Cranes on the Western European flyway were spared from severe outbreak events, despite the ongoing HPAIV enzootic in Europe, until October 2025, when widespread deaths were detected in Germany, and thereafter in France and Spain.

Each year, >420,000 cranes migrate through Germany (*4*). Birds migrating from Scandinavia typically roost along the coast in Mecklenburg-Western Pomerania, whereas cranes from Finland, Poland, and the Baltic region prefer inland staging sites such as Lake Galenbeck, the Müritz region, Rhin-Havelluch, or the Berga/Kelbra reservoir (Figure 1). Birds that roost in the roosting region Diepholzer fen (Figure 1) in northwestern Germany continue on to wintering areas in France and Spain.

The first deceased cranes in Germany were found in early October 2025 at Lake Galenbeck and were confirmed HPAIV A(H5N1)–positive shortly afterward. As of March 2026, no increased mortality has been reported from regions north (Sweden) and east (Poland and the Baltic countries) of the index site. Six cranes associated with the initial outbreak underwent necropsy. Carcasses were well preserved and in good nutritional and body condition. Gross lesions were consistent with an acute systemic process and dominated by pancreatic necrosis, pulmonary edema, and occasional epicardial and proventricular hemorrhages (Appendix 1, https://wwwnc.cdc.gov/EID/article/32/5/26-0170-App1.pdf). We examined 3 birds histopathologically. Immunohistochemistry revealed the highest influenza A virus–specific antigen loads in the central nervous system (CNS) and pancreas; moderate loads in the heart, spleen, and kidneys; and low antigen loads in respiratory and intestinal tissues. Despite widespread viral antigen distribution, necrosis was present only in subsets of antigen-positive areas. The lesion pattern largely corresponds to previous reports in cranes, particularly severe pancreatic necrosis and CNS involvement (*3*). Because immunohistochemistry was not performed in the previous study, we cannot directly compare viral antigen loads. In our cases, widespread antigen detection with only limited inflammation and necrosis suggests a peracute and rapidly progressive disease course (Figure 2; Appendix 1). Reported neurologic signs in the field, including uncoordinated movements and lack of escape behavior, correlate with widespread CNS infection.

We confirmed HPAIV H5N1 infection by real-time quantitative reverse transcription PCR in

Author affiliations: Friedrich-Loeffler-Institut, Greifswald–Insel Riems, Germany (A. Günther, J. Sehl-Ewert, A.K. Ahrens, S. Calvelage, A. Pohlmann, M. Beer, T. Harder); Agency for Environment, Nature Conservation, and Geology Mecklenburg-Western Pomerania, Güstrow, Germany (C. Herrmann, S. Piro)

DOI: https://doi.org/10.3201/eid3205.260170

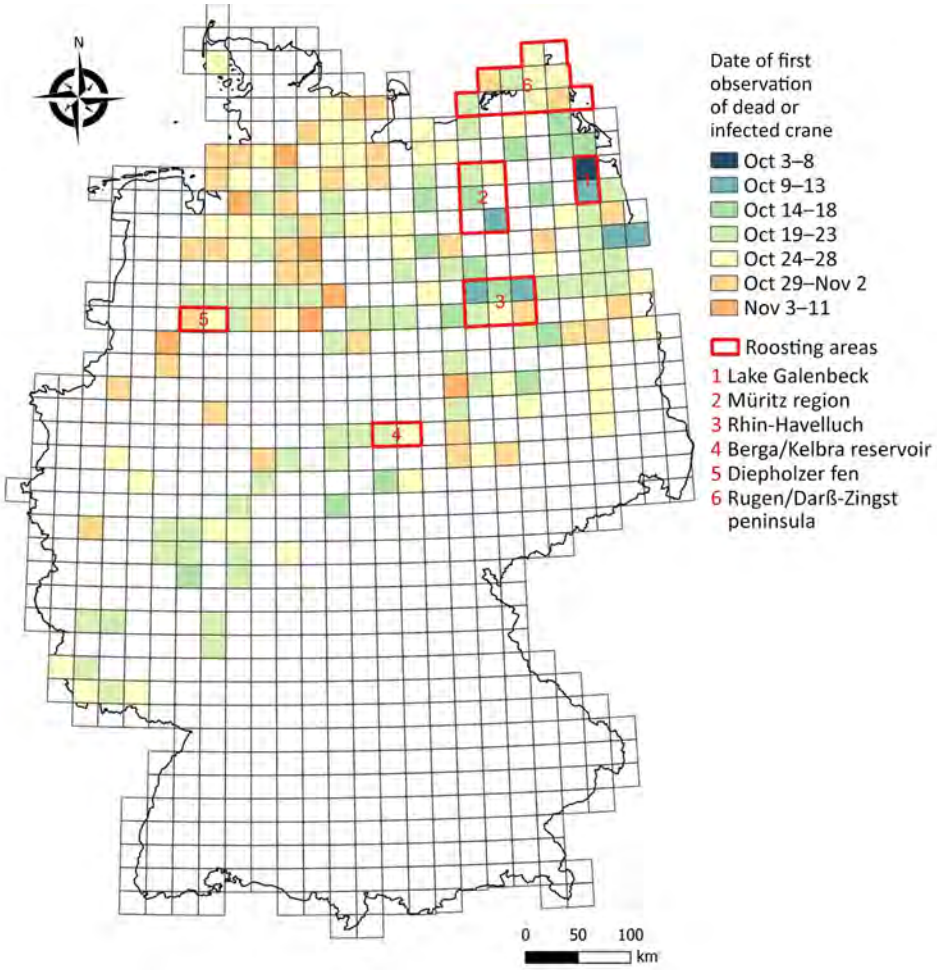

Figure 1. Locations of notifications for deceased or infected cranes in study of highly pathogenic avian influenza A(H5N1) clade 2.3.4.4b virus, Germany, 2025. Notifications are from the period October 3–November 11, 2025. Numbers indicate mentioned roosting areas.

oropharyngeal and cloacal swab samples and in lung and brain tissues, finding very high virus loads (Appendix 1). Genome sequencing of 9 cranes and 25 HPAIV H5N1–positive samples from wild birds, as well as 43 samples from domestic holdings, identified HPAIV H5N1 clade 2.3.4.4b of genotype EA-2024-DI.2.1 (Figure 3; Appendix 1). Since September 2025, DI.2.1-like viruses have been detected almost simultaneously at multiple sites across Europe (*5*), appearing to be a sublineage of the Gs/Gd-like HPAIV genotype EA-2024-DI.2, which dominated the European HPAIV epizootiology in 2024 and the first half of 2025 (*6*). Phylogenetic analyses indicated that all sequences derived from HPAIV H5–positive cranes fall into a monophyletic cluster of EA-2024-DI.2.1 (Figure 3). The cluster is interspersed with sequences from domestic poultry and other wild bird species from different families. That clustering pattern in the phylogenetic tree could indicate a closely linked and direct spread within crane flocks in Germany after a primary introduction. However, our early data do not enable us to reliably distinguish direct spread from the possibilities of a diffuse dissemination in wild or domestic birds, or both, with repeated spillover to crane populations, or dissemination from an unsampled host compartment with repeated spillover to the sampled species. The detection of mild or even asymptomatic cases (e.g., in dabbling ducks) and related sequence data will help to better discern dissemination patterns in avian wildlife.

Veterinary authorities and bird conservation organizations initiated carcass removal; efforts varied and were often hindered by the challenging wetland terrain. Removing carcasses has been deemed useful for reducing the incidence of infections in other gregarious species (*7*). Despite mitigation attempts, 18,164 deceased cranes were reported in Germany during October–December 2025, vastly outnumbering previously reported detections of HPAIV H5 clade 2.3.4.4b in cranes in Germany in 2020 (H5N8, n = 2) and 2023 (H5N1, n = 9).

By early November 2025, crane mortality slowed and finally almost stopped in Germany. As the cranes continued their migration, the virus spread to France

and Spain. At Lake du Der-Chantecoq in northeastern France, 4,000–5,000 dead cranes were recorded during October through mid-November; an estimated 15,000–20,000 cranes died across France. In Spain, the estimated range of fatalities was 1,000–1,500, including 900 around the Gallocanta lagoon. Altogether, the estimated mortality rate along the Western European flyway in autumn 2025 was ≈10% of the crane flyway population, >420,000 cranes (*4*). The nearly identical, phylogenetically very closely related sequences of HPAIV H5N1 from Eurasian cranes suggest that, once DI.2.1 entered the population, cranes became both severely affected hosts and efficient amplifiers, contributing to rapid intraspecies-specific spread along the flyway. Close contact at night roosts in shallow waters likely accelerated the transmission of the virus through contaminated surface water; even minimal environmental viral loads in surface water have been shown to be sufficient for infecting susceptible species (*8*).

The source species and location of the current genotype DI.2.1 of HPAIV H5N1 have not been elucidated. Additional sequence data from a broader European perspective will help to identify HPAIV H5N1 outbreaks in poultry farms as possible sources or sinks of the virus and to trace transmission chains. Although cranes dominated in the clinical manifestation of the current H5N1 epizootic, they may not necessarily be the main drivers in virus spread. The same virus variant was detected in Germany simultaneously in several anseriform species, representing other possible reservoir host groups, such as geese, wigeons, and mallards (Figure 3; Appendix 1). However, when compared with that of previous seasons, mortality in those species was low and sporadic; possible causes were partial population immunity or characteristics of the current H5N1 genotype. Although those species might have been clinically less vulnerable, they were not necessarily protected from virus infection

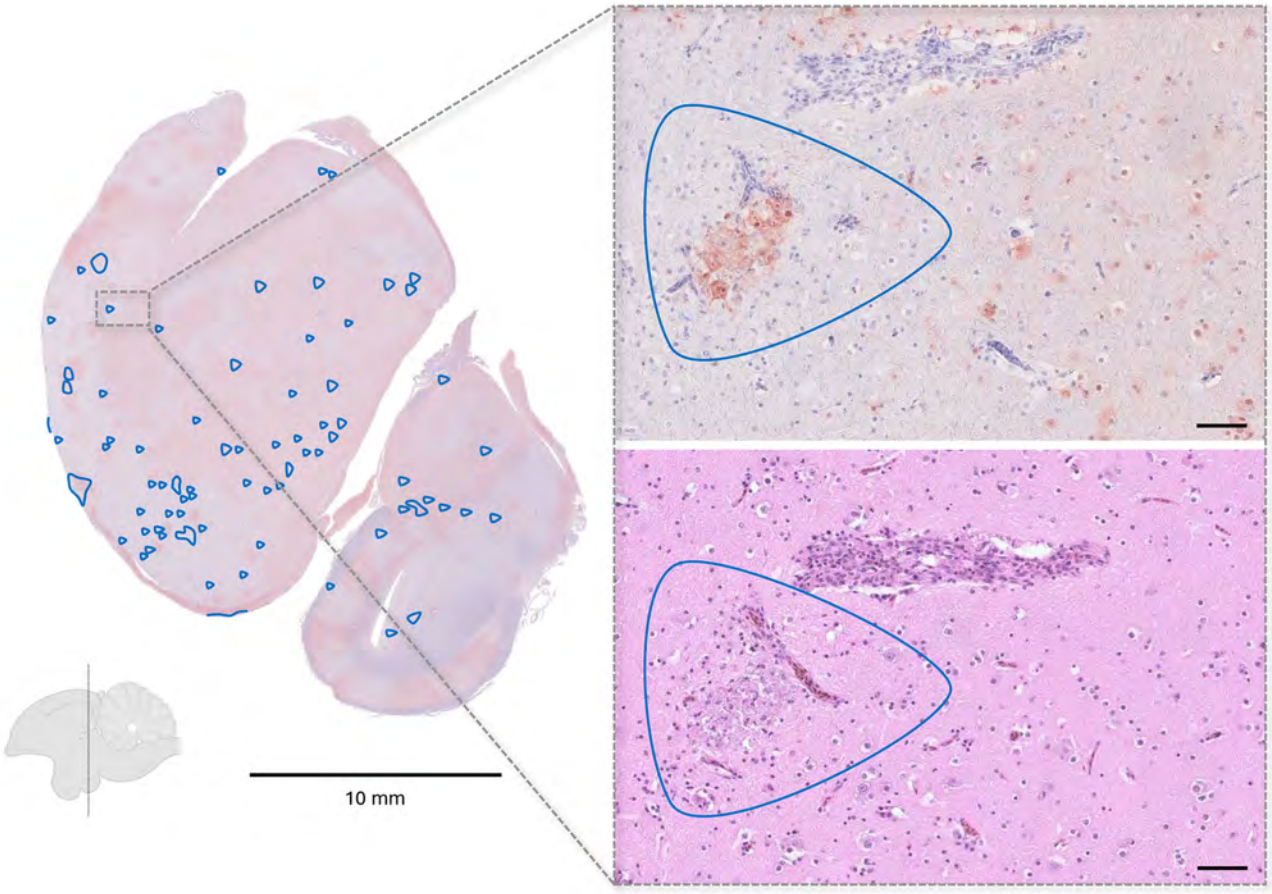

Figure 2. Representative histopathologic findings in influenza A(H5N1)–infected cranes from study of highly pathogenic avian influenza A(H5N1) clade 2.3.4.4b virus causing mass mortality in cranes, Germany, 2025. Immunohistochemistry of a coronal brain section at the level of the nidopallium demonstrating widespread viral antigen detection (brown staining) with only limited inflammatory and necrotic changes (blue outlines). Callout images at right show the corresponding region in consecutive sections, with abundant antigen-positive cells in immunohistochemistry (top) but only a small necrotic focus in the matching hematoxylin and eosin–stained section (bottom). Scale bars in callout images represent 50 μm.

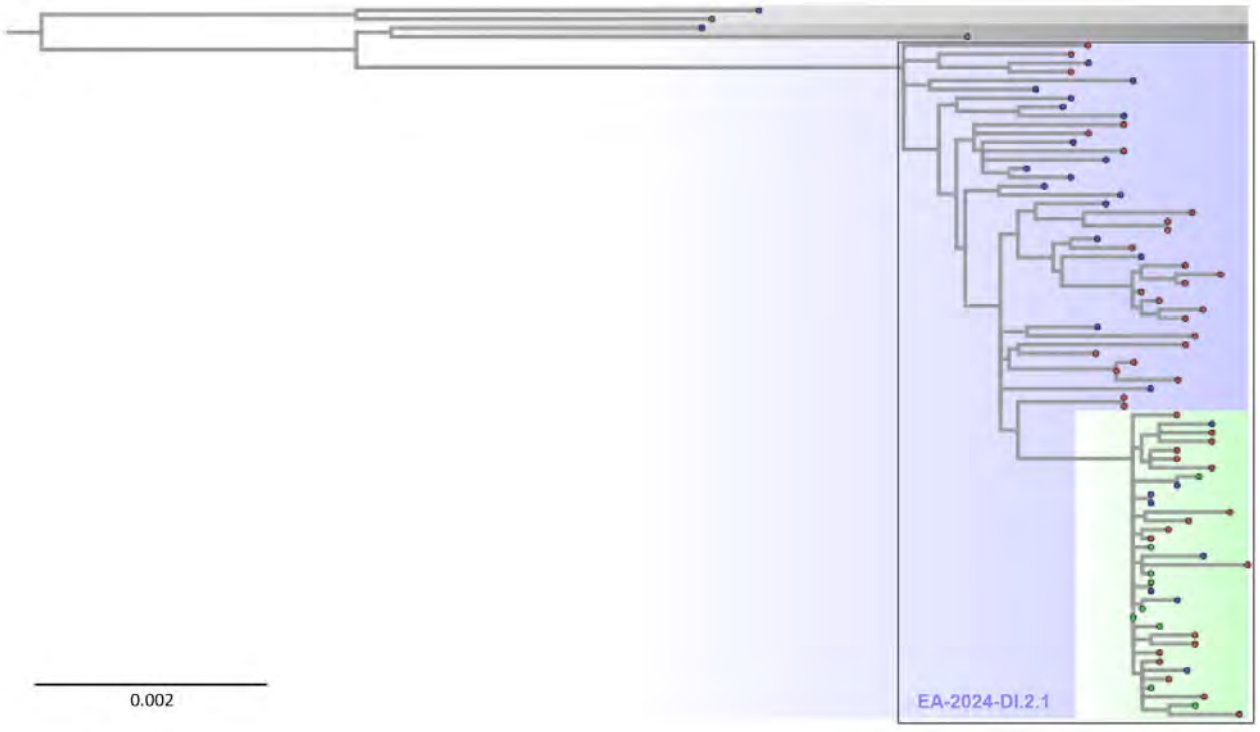

Figure 3. Maximum-likelihood tree based on whole-genome analyses from study of highly pathogenic avian influenza A(H5N1) clade 2.3.4.4b virus causing mass mortality in cranes, Germany, 2025. Tree depicts the H5N1 genotype EA-2024-DI.2.1 cluster (blue shading and text) comprising poultry (red tip) and wild bird cases (blue tip) from Germany. Recent example sequences for previous dominating genotypes DI.2 and DI.1 (gray) are included for comparison above the tree. Scale bar indicates substitutions per site. An expanded figure showing the tree in more detail is available online (https://wwwnc.cdc.gov/EID/article/32/5/26-0170-F3.htm). A list of virus sequences with relevant metadata is provided (Appendix 2, https://wwwnc.cdc.gov/EID/article/32/5/26-0170-App2.xlsx).

and excretion. In contrast, the crane population appeared to be fully susceptible, likely because of a lack of prior exposure to HPAIV H5 in Western Flyway populations; other unresolved intrinsic (e.g., cell receptor distributions, immune genetics) and extrinsic factors might have been involved. Unfortunately, no stored serum samples are available to confirm the assumption of a seronegative population. Furthermore, it remains unclear if HPAIV H5 circulation influenced cranes' migratory behavior, such as avoiding heavily affected roosting sites.

As of November 17, 2025, more than 18,000 dead cranes had been reported in Germany alone in this outbreak. The full effect of the HPAI-associated mass mortality on the population structure of the Western Flyway crane population must be studied. The event highlights critical knowledge gaps in our understanding the epidemiology of HPAIV H5 in wild birds; those gaps primarily result from inadequate active monitoring and the lack of serologic data needed to assess population immunity. In addition, the networks driving HPAIV H5 transmission and spread within and between wild bird and poultry populations remain poorly understood. The characteristics of the current EA-2024-DI.2.1 genotype require detailed investigation, particularly in wild Anseriformes birds.

This article was preprinted at https://www.biorxiv.org/content/10.64898/2025.12.08.692485v1.

Acknowledgments

We thank Diana Parlow and Marco Beerbohm for support in performing laboratory analyses and necropsies. We thank G. Nowald, Kranichschutz Deutschland gGmbH, and all members of the regional working groups of Kranichschutz Deutschland, NABU, for data on migration and mortality of Eurasian cranes. Further, numerous volunteers have reported fatalities, collected field data, and participated in the removal of carcasses; we express our gratitude for their engagement as well as to the DDA/Federation of German Avifaunists for providing the valuable data on dead and sick cranes from the online portal ornitho.de via its partner Kranichschutz Deutschland. We thank the Institute of Epidemiology for curating the avian influenza database in Germany and for granting us access to it.

The analyses presented in this study do not require ethical permits in terms of experimental animal trials. The investigations are based on material submitted in the context of animal disease surveillance in Germany.

This work was funded by the European Union (grant agreement no. 101084171; Kappa-Flu). Views and opinions expressed are however those of the author(s) only and do not necessarily reflect those of the European Union or REA. Neither the European Union nor the granting authority can be held responsible for them.

About the Author

Dr. Günther is a veterinarian and a postdoctoral researcher at the Friedrich-Loeffler-Institut, Greifswald–Insel Riems, Germany. Her primary research interests are avian viruses and other pathogens with potential influence on avian species conservation, wildlife, and public health concerns.

References

1. Nadler-Valency R, Lourie E, Sela-Klein D. Avian influenza (H5N1) outbreak report in wild birds—Hula Valley, Israel a comparison of two outbreaks (2021/22 and 2024). Isr J Vet Med. 2025;80.
2. European Food Safety Authority, European Centre for Disease Prevention and Control, European Union Reference Laboratory for Avian Influenza; Adlhoch C, Fusaro A, Gonzales JL, et al. Avian influenza overview September–December 2023. EFSA J. 2023;21:e8539. https://doi.org/10.2903/j.efsa.2023.8539
3. Djurdjevic B, Petrovic T, Gajdov V, Vidanovic D, Vucicevic I, Samojlovic M, Pajic M. Natural infection of common cranes (*Grus grus*) with highly pathogenic avian influenza H5N1 in Serbia. Front Vet Sci. 2024;11:1462546. https://doi.org/10.3389/fvets.2024.1462546
4. Nowald G. Cranes in Germany and Europe: review of 2024 with special consideration of the weather. In: Nowald G, Paschke K, Sorgatz C, Kettner A, editors. The year of the crane 2024/2025. Günz (Germany): NABU Erlebniszentrum Kranichwelten; 2025. p. 6–11.
5. European Food Safety Authority, European Union Reference Laboratory for Avian Influenza; Ducatez M, Fusaro A, Gonzales JL, Kuiken T, et al. Unprecedented high level of highly pathogenic avian influenza in wild birds in Europe during the 2025 autumn migration. EFSA J. 2025;23:9811. https://doi.org/10.2903/j.efsa.2025.9811
6. European Food Safety Authority, European Centre for Disease Prevention and Control, European Union Reference Laboratory for Avian Influenza; Alexakis L, Buczkowski H, et al. Avian influenza overview December 2024–March 2025. EFSA J. 2025;23:9352. https://doi.org/10.2903/j.efsa.2025.9352
7. Knief U, Bregnballe T, Alfarwi I, Ballmann MZ, Brenninkmeijer A, Bzoma S, et al. Highly pathogenic avian influenza causes mass mortality in Sandwich Tern *Thalasseus sandvicensis* breeding colonies across north-western Europe. Bird Conserv Int. 2024;34:e6. https://doi.org/10.1017/S0959270923000400
8. Ahrens AK, Selinka HC, Mettenleiter TC, Beer M, Harder TC. Exploring surface water as a transmission medium of avian influenza viruses—systematic infection studies in mallards. Emerg Microbes Infect. 2022;11:1250–61. https://doi.org/10.1080/22221751.2022.2065937

Address for correspondence: Timm Harder, Friedrich-Loeffler-Institut, Federal Research Institute for Animal Health, Südufer 10, 17493 Greifswald–Insel Riems, Germany; email: timm.harder@fli.de

Genomic Analysis of Sin Nombre Virus Sequences, Northwestern United States, 2023

Grant Rickard,[1] Ricardo Rivero,[1] A. Catherine Grady, Jennifer Horton, Cody J. Lauritsen, Stephen Fawcett, Samuel M. Goodfellow, Hanna N. Oltean, M. Pilar Fernandez, Stephanie N. Seifert

We report Sin Nombre virus (SNV) genome sequences in the northwestern United States, including SNV sequences recovered from montane voles. Analysis of samples collected from 189 individual rodents revealed high SNV prevalence in the region and evidence of virus reassortment or coinfection, highlighting ongoing virus diversification in rodents.

Sin Nombre virus (SNV; *Orthohantavirus sinnombreense*), is a member of the family Hantaviridae and the primary cause of hantavirus pulmonary syndrome in North America. First identified during a 1993 outbreak in the Four Corners region of the United States, SNV is linked to severe respiratory disease and high mortality rates (*1*). During 1993–2022, a total of 864 hantavirus pulmonary syndrome cases were reported in the United States, with a 36% case-fatality rate (*2*,*3*); 109 of those cases occurred in the northwestern states of Idaho, Oregon, and Washington.

SNV primarily is maintained by *Peromyscus* spp. deer mice, widespread rodents that are frequently associated with agricultural and peridomestic settings. Human infection usually results from inhalation of aerosolized virus particles from contaminated excreta (*4*,*5*), and zoonotic risk is influenced by ecologic factors (*6*). Although SNV commonly is detected in deer mice, several reported detections in sympatric rodent species, and broad geographic distributions suggest greater complexity in hantavirus maintenance (*7*–*9*).

Virus genomic surveillance can provide insights on virus evolution and spread (*10*), but <100 full SNV genomes have been published, none of which are from the northwestern United States (*3*). We report detection and genome sequences of SNV in the northwestern United States in montane voles and western deer mice.

The Study

During June–August 2023, we live-trapped rodents at farms and natural areas in the Palouse region of eastern Washington and western Idaho (Figure 1), a major agricultural hub dominated by wheat and canola fields. We conducted sampling over 3 consecutive nights, including repeated fecal sampling with mark-recapture and lethal collection on the third night. We collected and tested samples from 189 rodents across agricultural and natural landscapes in the Palouse. We identified species using morphologic criteria in consultation with regional experts. We deployed Sherman live traps at 8 farms and 2 forested sites in 2 grids (100 m × 30 m) at each location. All procedures followed American Veterinary Medical Association guidelines and were approved by the Washington State University Institutional Animal Care and Use Committee (Animal Study Approval Form no. 6927). We performed sampling under Idaho scientific collections permits 36112 and JOE1 and Washington state scientific collections permit SEIFERT 23–122.

We collected fecal samples on all trapping nights, in addition to serum, lung tissue, and bladder tissue on the third and final trapping night at each site. We report only data from the final capture for each individual rodent sampled. Across all sites, we collected samples from 2 creeping voles (*Microtus oregoni*),

Author affiliations: University of Washington School of Medicine, Seattle, Washington, USA (G. Rickard); Washington State University Paul G. Allen School for Global Health, Pullman, Washington, USA (G. Rickard, R. Rivero, A.C. Grady, J. Horton, C.J. Lauritsen, S. Fawcett, M.P. Fernandez, S.N. Seifert); Children's Hospital Los Angeles, Los Angeles, California, USA (S.M. Goodfellow); Washington State Department of Health Zoonotic and Vector-borne Disease Program, Tumwater, Washington, USA (H.N. Oltean)

DOI: https://doi.org/10.3201/eid3205.251476

[1]These first authors contributed equally to this article.

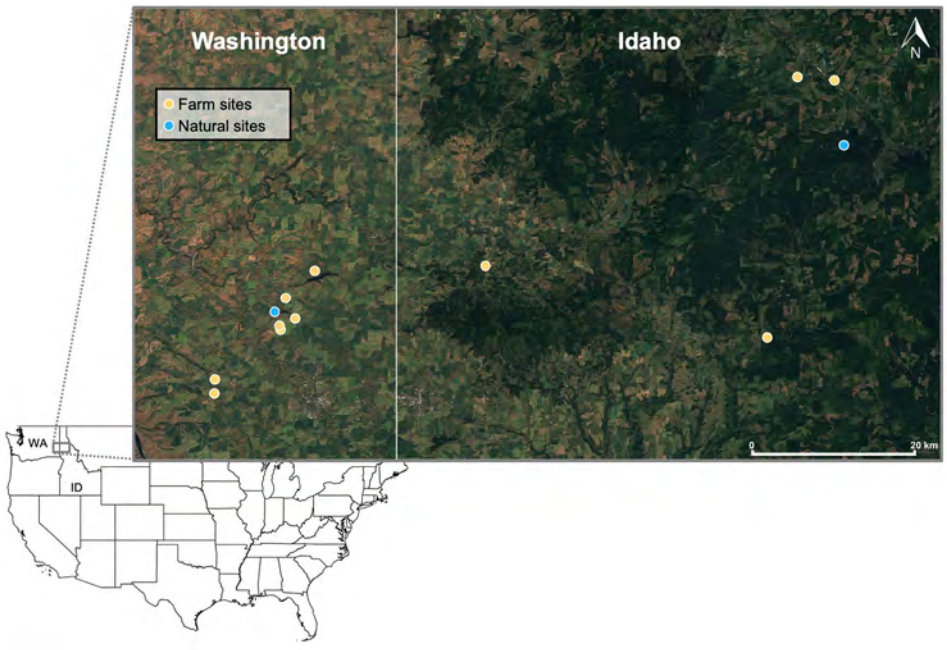

Figure 1. Locations of successful unique rodent sampling grids, by location type, in a study of Sin Nombre virus in rodent species sampled from farms and natural sites, Palouse region, eastern Washington and western Idaho, USA, 2023. Inset map indicates location of study area relative to rest of United States. Basemap generated in Sentinel-2 Cloudless (EOX IT Services, https://eox.at). State boundary based on US Census Bureau cartographic boundary files (https://www.census.gov/geographies/mapping-files/time-series/geo/carto-boundary-file.html).

Table. Serologic and quantitative reverse transcription PCR results for Sin Nombre virus in rodent species sampled from farm sites and natural sites, Palouse region, eastern Washington and western Idaho, USA, 2023*

Site and species	Age category/sex	Sample type, no. (%)			
		Blood	Lung	Bladder	Fecal
Farm site					
Western meadow vole (*Microtus drummondii*)	Adult/F	ND	0/1	0/1	0/1
	Adult/M	1/1	0/2	0/1	0/1
	Juvenile/M	0/1	ND	0/1	0/1
	Total	1/2 (50)	0/3	0/3	0/3
Montane vole (*Microtus montanus*)	Adult/F	0/2	0/2	0/2	0/4
	Adult/M	3/3	1/3	0/3	0/5
	Juvenile/F	0/1	0/1	0/1	0/4
	Juvenile/M	1/2	1/3	0/3	0/4
	Total	4/8 (50)	2/9 (22)	0/9	0/17
Creeping vole (*Microtus oregonii*)	Juvenile/F	ND	0/1	0/1	0/1
	Juvenile/M	0/1	0/1	0/1	0/1
	Total	0/1	0/2	0/2	0/2
House mouse (*Mus musculus*)	Adult/M	ND	ND	ND	0/1
	Juvenile/F	ND	ND	ND	0/1
	Total	ND	ND	ND	0/2
Yellow-pine chipmunk (*Neotamias amoenus*)	Adult/F	ND	ND	ND	0/1
Least chipmunk (*Neotamias minimus*)	Adult/F	0/1	0/1	0/1	0/2
	Adult/M	ND	ND	ND	0/1
	Juvenile/F	0/1	0/1	0/1	0/1
	Juvenile/M	1/2	0/1	0/2	0/3
	Total	1/4 (25)	0/3	0/4	0/7
Western deer mouse (*Peromyscus sonoriensis*)	Adult/F	5/25	1/27	0/27	0/35
	Adult/M	11/28	7/28	2/27	0/35
	Juvenile/F	6/15	0/16	0/16	0/24
	Juvenile/M	2/14	1/14	0/14	0/15
	Total	24/82 (29)	9/85 (11)	2/84 (2)	0/109
Natural site					
Montane vole (*Microtus montanus*)	Adult/F	ND	0/1	0/1	0/1
Least chipmunk (*Neotamias minimus*)	Adult/F	0/1	0/1	0/1	0/1
	Adult/M	0/1	0/1	0/1	0/1
	Total	0/2	0/2	0/2	0/2
Western deer mouse (*Peromyscus sonoriensis*)	Adult/F	2/8	0/10	0/10	0/12
	Adult/M	3/9	2/11	0/11	0/14
	Juvenile/F	0/7	0/7	0/7	0/8
	Juvenile/M	1/10	0/10	0/10	0/10
	Total	6/34 (18)	2/38 (5)	0/38	0/44

18 montane voles (*Microtus montanus*), 4 western meadow voles (*Microtus drummondii*), 2 house mice (*Mus musculus*), 153 western deer mice (*Peromyscus sonoriensis*), 1 yellow pine chipmunk (*Neotamias amoenus*), and 9 least chipmunks (*Neotamias minimus*).

We used SNV nucleocapsid protein (BEI Resources, https://www.beiresources.org) to assess seroreactivity in rodent serum samples. We immobilized the nucleocapsid protein on Maxisorp-plates (Thermo Fisher Scientific, https://www.thermofisher.com) and applied serum diluted 1:100. We detected nucleocapsid protein bound antibodies with horseradish peroxidase-conjugated goat anti-rat secondary antibody (AbCAM, https://www.abcam.com). We assessed seropositivity for each plate as the mean optical density of 4 naive serum controls ±3 SD.

We extracted total RNA from tissue samples and fecal samples by using the Zymo Quick-RNA MagBead kit (Zymo Research, https://www.zymoresearch.com), according to the manufacturer's protocol for

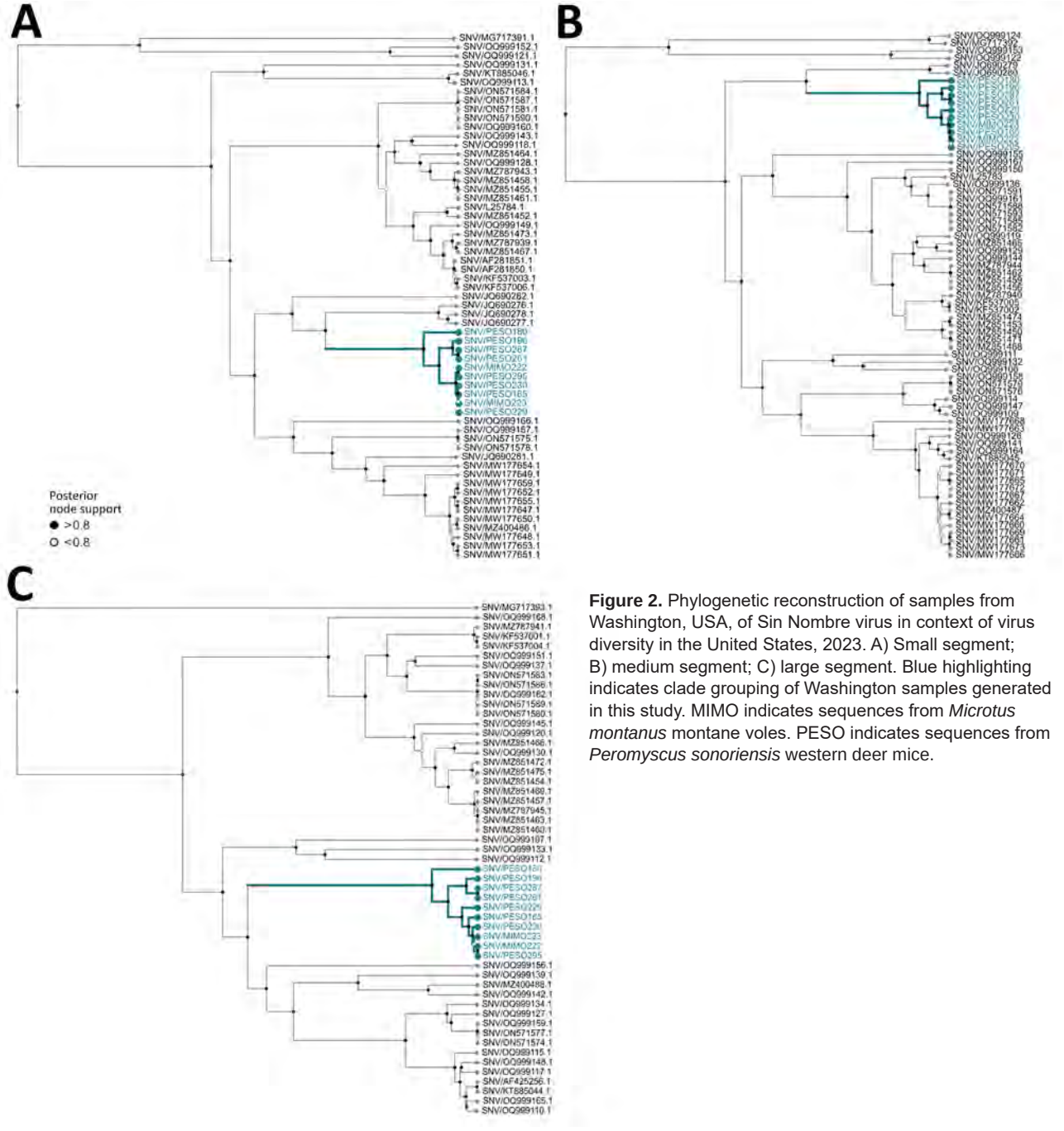

Figure 2. Phylogenetic reconstruction of samples from Washington, USA, of Sin Nombre virus in context of virus diversity in the United States, 2023. A) Small segment; B) medium segment; C) large segment. Blue highlighting indicates clade grouping of Washington samples generated in this study. MIMO indicates sequences from *Microtus montanus* montane voles. PESO indicates sequences from *Peromyscus sonoriensis* western deer mice.

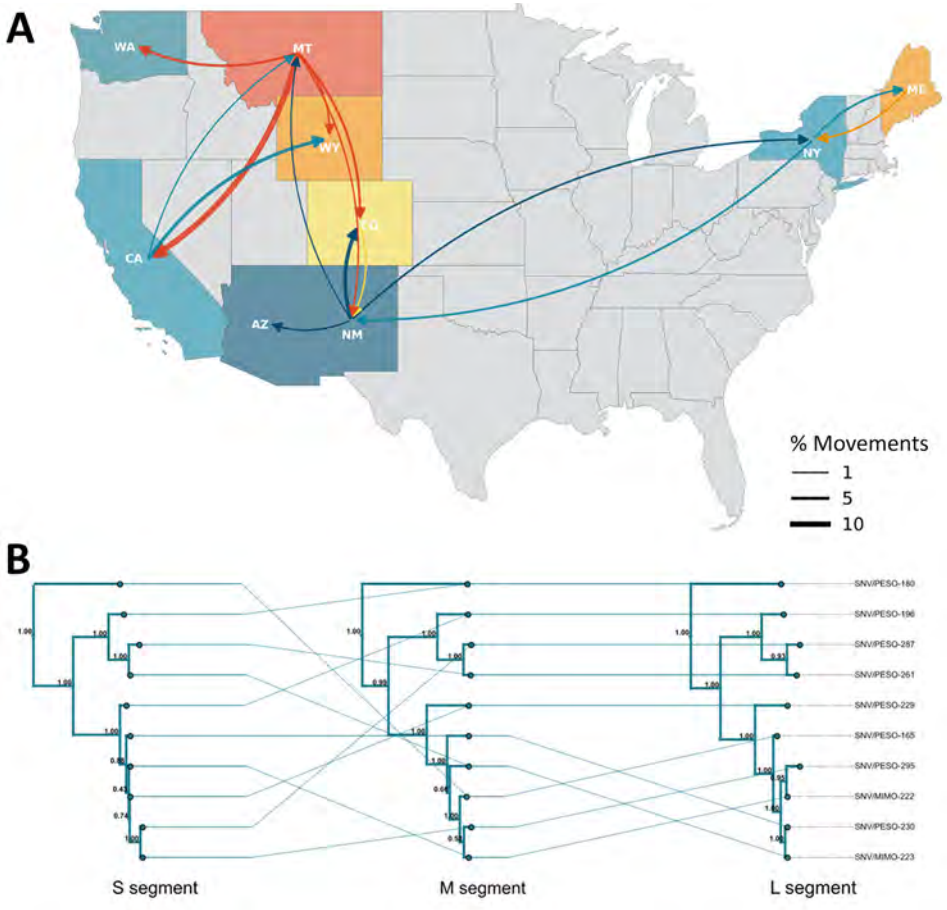

Figure 3. Evolutionary dynamics of Sin Nombre virus sequences, Washington, USA, 2023. A) Phylogeographic reconstruction of movements between discrete states using Markov jumps. Curve weight reflects Bayes factor support. B) Tanglegram showing topologic changes across segment trees. Connecting lines link variants. Major shifts indicate reassortment. Posterior node support shown at each node. L, large; M, medium; S, small.

each sample type. We detected presence of virus RNA by using quantitative reverse transcription PCR (qRT-PCR), as previously described (*11*), with an internal control targeting the *P. maniculatus* hypoxanthine-guanine phosphoribosyltransferase gene to monitor extraction and amplification performance with in-house–designed forward primer (5′-CAAAGCCTAAGAGGAGAGTTCA-3′), reverse primer (5′-GATGGCCGCAGAACTAGAA-3′), and probe (5HEX/AGGAGTCCC/ZEN/ATTGATGTTGCCAGT/3IABkFQ).

Western deer mice demonstrated high prevalence by serologic testing (26%) and qRT-PCR (9.8%) across all sites (Table). Among qRT-PCR–positive western deer mice, lung cycle threshold (Ct) values ranged from 18.1 to 34.1 (mean 25.3). Two adult male western deer mice had qRT-PCR–positive bladder samples with Ct values of 31.9 and 33.6; both rodents had low lung Ct values (18.1 and 21.5). Montane voles on farmlands showed the highest prevalence, having 50% seroprevalence and 22.2% qRT-PCR–positive lung tissue samples (Table) and Ct values of 29.5 and 26.5, which were within the range observed in western deer mice. We note recent findings in New Mexico showing similarly high prevalence for SNV in diverse rodent taxa, including recovery of infectious virus (*9*). Fewer lung samples were qRT-PCR–positive than seropositive rodents. We deposited surveillance data for this study in the Pathogen Harmonized Surveillance database (https://pharos.viralemergence.org/projects/?prj = prjdGTXI9IIBo).

We modeled SNV lung positivity detected by qRT-PCR as a binary outcome by using logistic regression with mean bias reduction in the R 4.1.3 brglm2 package (The R Project for Statistical Computing, https://www.r-project.org) for species with qRT-PCR–positive lung tissue samples. Predictors were land type (forest or farm), sex, age, and species (*M. montanus* montane voles or *P. sonoriensis* western deer mice). Male rodents had significantly higher odds of qRT-PCR positivity in lung tissue samples than did female rodents (odds ratio 9.42 [95% CI 1.76–50.5]), whereas land type, species, and age were not significant predictors. Elevated SNV prevalence in male deer mice aligns with known SNV ecology, although the precise mechanism is unknown (*12*).

We sequenced SNV by using a tiled amplicon scheme proposed by Goodfellow et al. (*13*) on the Oxford Nanopore platform (https://nanoporetech.com). We quality controlled reads, trimmed primers,

mapped reads, and extracted the consensus sequence by using an in-house assembly pipeline (https://github.com/viralemergence/SNVler). We recovered sequence data for all 3 SNV genome segments from 10 individual rodents, including 2 montane voles; segment completeness ranged from 24% to 100% and depth ranged from 6.8 to 476.1 times (GenBank accession nos. PX401008–37). To address persistent medium-segment dropouts, we designed flanking primers (MsegFor 5′-GCAGGTAGCTGATCTCAAG-3′ and MsegR 5′-CCAGTCCATGTAAGAGGTAC-3′) for amplification and sequencing, improving assemblies and guiding future refinement of the primer set for SNV in the northwestern United States.

We analyzed segment-wise alignments curated from GenBank in BEAST 1.10.5 (https://beast.community) (strict clock, exponential coalescent), using uniform tip sampling for incomplete collection dates (*14*). Estimated clock rates were 1.19×10^{-4}, 1.203×10^{-4}, and 1.223×10^{-4} substitutions/site/year; root-to-tip regression resulted in R^2 values of 0.197 (p value 4.16×10^{-04}) for the small segment, 0.067 (p-value 0.0282) for the medium segment, and 0.257 (p value 1.056×10^{-04}) for the large segment, suggesting a weak temporal signal. This pattern probably reflects confounding between sampling time and geographic structure, underscoring the need for broader spatial and temporal sequencing to resolve the SNV phylogeny. Palouse sequences formed a distinct clade closest to SNV genomes from Montana collected during 2008–2009 (*11*) (Figure 2).

Discrete phylogeography based on the small segment tree inferred introduction into Washington from Montana circa 1915 (95% highest posterior density 1873–1982), followed by local diversification (Figure 3, panel A). Bayesian stochastic search variable selection analysis (*15*) shows low support for Montana–Washington movement, suggesting unsampled intermediates and illustrating the need for improved genomic surveillance. Topologic discordance among viral segments (Figure 3, panel B) supports reassortment or coinfection with segment-specific differences in within-host abundance that could influence consensus recovery. Local variants from western deer mice and montane voles cluster with high support, suggesting cross-species transmission between rodents in the northwestern United States (Figure 3, panel A).

Conclusions

We report SNV genome sequences from the northwestern United States, addressing a longstanding regional data gap. Our findings indicate reassortment or co-infection among sympatric rodent hosts, underscoring the complexity of SNV evolution and maintenance. Developing targeted primers to overcome chronic regional dropout enabled recovery of key genomic regions and will guide efforts to recover SNV genomes in this understudied region. Clarifying how multiple hosts contribute to virus exchange will improve understanding of transmission dynamics and zoonotic risk.

Acknowledgments

We thank Steven Bradfute for helpful discussions and guidance on recovering full viral genome sequences and the many field technicians who supported collections in the summer of 2023.

This publication was made possible by the Centers for Disease Control and Prevention Center for Forecasting and Outbreak Analytics (cooperative agreement CDC-RFA-FT-23-0069). S.N.S., R.R., and J.H. received support from US National Science Foundation (grant no. NSF DBI 2515340).

About the Author

Mr. Rickard is a medical student at the University of Washington School of Medicine at the regional campus in Bozeman, Montana. His primary research interests include inclusive healthcare in rural communities. Mr. Rivero is a PhD candidate at Washington State University, Pullman, Washington. His primary research interests include the intersection of viral evolution and public health.

References

1. Nichol ST, Spiropoulou CF, Morzunov S, Rollin PE, Ksiazek TG, Feldmann H, et al. Genetic identification of a hantavirus associated with an outbreak of acute respiratory illness. Science. 1993;262:914–7. https://doi.org/10.1126/science.8235615
2. Schmaljohn C, Hjelle B. Hantaviruses: a global disease problem. Emerg Infect Dis. 1997;3:95–104. https://doi.org/10.3201/eid0302.970202
3. Whitmer SLM, Whitesell A, Mobley M, Talundzic E, Shedroff E, Cossaboom CM, et al. Human *Orthohantavirus* disease prevalence and genotype distribution in the U.S., 2008–2020: a retrospective observational study. Lancet Reg Health Am. 2024;37:100836. https://doi.org/10.1016/j.lana.2024.100836
4. Zeitz PS, Butler JC, Cheek JE, Samuel MC, Childs JE, Shands LA, et al. A case-control study of hantavirus pulmonary syndrome during an outbreak in the southwestern United States. J Infect Dis. 1995;171:864–70. https://doi.org/10.1093/infdis/171.4.864
5. Childs JE, Ksiazek TG, Spiropoulou CF, Krebs JW, Morzunov S, Maupin GO, et al. Serologic and genetic identification of *Peromyscus maniculatus* as the primary rodent reservoir for a new hantavirus in the southwestern United States. J Infect Dis. 1994;169:1271–80. https://doi.org/10.1093/infdis/169.6.1271

6. Glass GE, Cheek JE, Patz JA, Shields TM, Doyle TJ, Thoroughman DA, et al. Using remotely sensed data to identify areas at risk for hantavirus pulmonary syndrome. Emerg Infect Dis. 2000;6:238–47. https://doi.org/10.3201/eid0603.000303
7. Goodfellow SM, Nofchissey RA, Schwalm KC, Cook JA, Dunnum JL, Guo Y, et al. Tracing transmission of Sin Nombre virus and discovery of infection in multiple rodent species. J Virol. 2021;95:e0153421. https://doi.org/10.1128/JVI.01534-21
8. Goodfellow SM, Nofchissey RA, Arsnoe D, Ye C, Lee S, Park J, et al. Case of human orthohantavirus infection, Michigan, USA, 2021. Emerg Infect Dis. 2024;30:817–21. https://doi.org/10.3201/eid3004.231138
9. Goodfellow SM, Nofchissey RA, Ye C, Banther-McConnell JK, Suriyamongkol T, Cook JA, et al. A human pathogenic hantavirus circulates and is shed in taxonomically diverse rodent reservoirs. PLoS Pathog. 2025;21:e1012849. https://doi.org/10.1371/journal.ppat.1012849
10. Hadfield J, Megill C, Bell SM, Huddleston J, Potter B, Callender C, et al. Nextstrain: real-time tracking of pathogen evolution. Bioinformatics. 2018;34:4121–3. https://doi.org/10.1093/bioinformatics/bty407
11. Williamson BN, Meade-White K, Boardman K, Schulz JE, Telford CT, Figueroa Acosta DM, et al. Continuing orthohantavirus circulation in deer mice in western Montana. Viruses. 2021;13:6. https://doi.org/10.3390/v13061006
12. Warner BM, Stein DR, Griffin BD, Tierney K, Leung A, Sloan A, et al. Development and characterization of a Sin Nombre virus transmission model in *Peromyscus maniculatus*. Viruses. 2019;11:2. https://doi.org/10.3390/v11020183
13. Goodfellow SM, Nofchissey RA, Ye C, Dunnum JL, Cook JA, Bradfute SB. Use of a novel detection tool to survey orthohantaviruses in wild-caught rodent populations. Viruses. 2022;14:682. https://doi.org/10.3390/v14040682
14. Suchard MA, Lemey P, Baele G, Ayres DL, Drummond AJ, Rambaut A. Bayesian phylogenetic and phylodynamic data integration using BEAST 1.10. Virus Evol. 2018;4:vey016. https://doi.org/10.1093/ve/vey016
15. Lemey P, Rambaut A, Drummond AJ, Suchard MA. Bayesian phylogeography finds its roots. PLOS Comput Biol. 2009;5:e1000520. https://doi.org/10.1371/journal.pcbi.1000520

Address for correspondence: Stephanie N. Seifert, Washington State University, Allen Center, 240 SE Ott Rd, Pullman, WA 99164, USA; email: stephanie.seifert@wsu.edu

Serologic Surveillance of Highly Pathogenic Avian Influenza Virus Subtype H5 in Wildlife, Northeast Germany, 2023–2025

Anne Günther, Josefine Wassermann, Jonas Heck, Marin Bussi, Andrea Aebischer, Christoph Staubach, Hannes Bergmann, Fabian H. Leendertz, Martin Beer, Gereon Schares, Kerstin Wernike

We tested wild ruminants, boar, and carnivores in northeast Germany for highly pathogenic avian influenza subtype H5 antibodies. Wild ruminants were seronegative, but 3.5% of boar and 12.5%–21.9% of carnivores were seropositive, indicating frequent spillover. Because such events might accelerate mammalian (and ultimately human) adaptation, sustained monitoring remains essential.

The shift of seasonal epizootics toward a perpetual enzootic in Europe became a milestone in the epidemiology of highly pathogenic avian influenza viruses (HPAIV) (*1*). Rooted in a common ancestral virus of the goose/Guangdong influenza lineage in Southeast Asia, the evolving diversity of subtype H5 genotypes in Europe paved the way for the ongoing panzootic, globally threatening domestic and wild birds alike and resulting in numerous mammalian spillover infections worldwide. A broad and increasing spectrum of terrestrial, semiaquatic, and marine or aquatic mammalian species is affected (*2*). Despite the recent developments of mastitis in domestic cattle through ascending udder infections with HPAIV H5 (*3*), the more constant interface over the years was direct, often alimentary, exposure to HPAIV H5–positive prey or food (*4*).

Infections in predatory or scavenging species frequently caused neurologic signs, including severe encephalitis as cause of death (*5*). The concern about increasing chances for spillover events from birds to mammals proved to be justified already in the early stage of enzootic HPAIV H5 in Europe. However, those studies also suggested a certain level of asymptomatic infections and the possibility of surviving exposure (*6*).

We compared HPAIV H5 antibody prevalences between mammal groups in Germany that had frequent contact opportunities (carnivores) and conceivable or unlikely contact opportunities (omnivores and herbivores). We identify frequently affected host groups and factors that ultimately favor the risk for infection in carnivores.

The Study

During December 2023–February 2025, we collected samples from 644 hunted predator game (group I) and 343 hoofed game animals (groups II and III) in the context of an ongoing disease surveillance project in the federal state of Mecklenburg–Western Pomerania in northeast Germany. In particular, the offshore islands and the mainland coast form important avian migratory areas but also breeding habitats with a high overall species diversity and abundance of wild birds. Many of those species have been affected during various HPAI H5 epizootics and the recent enzootic (*7*).

Predator game consisted of 5 species of the taxonomic families Canidae, Procyonidae, and Mustelidae (Table). Cervidae, Bovidae, and Suidae form groups II and III with five different species in total (1 sampled individual animal remains unspecified). We screened nasal swab and, for group I, lung and brain samples (n = 980) by using quantitative reverse transcription PCR for influenza A virus (IAV) RNA (Appendix Table 1, https://wwwnc.cdc.gov/EID/article/32/5/25-1555-App1.pdf). All 980 samples tested negative.

Nucleoprotein (NP)–based ELISA indicated no seropositivity against IAV in wild ruminants, whereas 5.2% (95% CI 1.9%–11.0%) of the wild boar (*Sus scrofa*) and all carnivorous species, except the single tested European

Author affiliations: Friedrich-Loeffler-Institut, Greifswald–Insel Riems, Germany (A. Günther, J. Wassermann, J. Heck, A. Aebischer, C. Staubach, H. Bergmann, M. Beer, G. Schares, K. Wernike); Utrecht University, Utrecht, the Netherlands (M. Bussi); Helmholtz Institute for One Health, Greifswald, Germany (F.H. Leendertz); University of Greifswald, Greifswald (F.H. Leendertz)

DOI: https://doi.org/10.3201/eid3205.251555

pine marten (*Martes martes*), tested positive (Table) (Appendix). The subsequent ELISA for detection of H5-specific antibodies revealed 3.5% (95% CI 0.9%–8.7%) seropositive wild boar and 12.5% (95% CI 0.3%–52.7%) to 21.9% (95% CI 12.5%–34.0%) seropositive carnivorous species (Table; Appendix Table 1), thereby confirming most of the seropositivity caused by an IAV of subtype H5. The percentage of non–H5 IAV antibody-positive animals ranged from 4.7% (95% CI 0.9%–13.1%) in raccoons (*Procyon lotor*) and 4% (95% CI 2.4%–6.9%) in (red) foxes (*Vulpes vulpes*) to 1.7% (95% CI 0.2%–6.1%) in wild boar and 1.1% (95% CI 0.1%–3.9%) in raccoon dogs (*Nyctereutes procyonoides*). We also tested a subset of NP-antibody positive or negative samples through serum neutralization test to confirm the presence or absence of antibodies against subtype H5 (Appendix). We confirmed the ELISA findings in a representative subset of 8 IAV-positive but H5-negative carnivore samples and compared them with 4 H5-positive samples, whereas H5 seropositivity in wild boar samples remained below the detection limit of the serum neutralization test.

Wild ruminants represent mammalian species with rather unlikely contact possibilities to potentially infected wild birds and, as herbivores, no apparent interface in their diet. However, direct exposure cannot be ruled out, and low susceptibility might be another plausible explanation for our consistent seronegative findings. At the other end of the food chain, our serologic results suggest previous exposure of carnivores to subtype H5 viruses. Raccoons, foxes, and raccoon dogs represent the species with the highest proportion of seropositivity (Table). Despite similar host species tested, our results only partially confirm observations of previous studies, where mainly stone martens and foxes were found to be seropositive in about 1 third of the animals tested (*6*). That discrepancy indicates the relevance of factors other than host susceptibility and host occurrence.

Univariable regression analysis (Figure) revealed that foxes from the Island Rügen collected close to the bay coast, close to the Baltic Sea, or close to watercourses had an increased risk for H5-specific antibodies ($p<0.05$) (Appendix Table 2, 3). Seropositivity increased with age; 11.6% (10/86) of the juvenile and 23.5% (43/183) of the adult foxes were positive for H5-specific antibodies. A final multivariable model (Appendix Table 4) selected by stepwise forward–backward selection, which also included age, revealed that, with increasing distance to watercourses (e.g., flowing waters, water source areas, streams, ditches, rivers, and canals), the risk for foxes being positive for H5-specific antibodies decreased ($p<0.0001$); however, with increasing distance to shrubland (e.g., hedges, bushes, field crops, groups of trees, rows of trees, avenues, dominant single trees, and groups of shrubs), the risk increased ($p<0.005$). In contrast, high proportions of shrubland in a 2.5-km buffer zone around the sampling site of foxes represented a protective factor ($p<0.005$), supporting the assumption of less exposure to HPAIV through water-associated

Table. Overview of species sampled for serologic and molecular screening for highly pathogenic avian influenza subtype H5 antibodies, grouped according to feeding behavior, northeast Germany, December 2023–February 2025*

	Serologic screening					Molecular screening	
Group and species	Total no. animals tested	No. IAV antibody–positive	IAV antibody–positive, % (95% CI)	No. H5 antibody–positive	H5 antibody–positive, % (95% CI)	Total no. animals tested†	No. IAV RNA–positive
Carnivores (group I)	606‡	120	19.8 (16.7–23.2)	100§	16.5 (13.6–19.7)	644	0
(Red) fox (*Vulpes vulpes*)	354	73	20.6 (16.5–25.2)	58	16.4 (12.7–20.7)	376	0
Raccoon dog (*Nyctereutes procyonoides*)	179	29	16.2 (11.1–22.4)	27	15.1 (10.2–21.2)	194	0
Raccoon (*Procyon lotor*)	64	17	26.6 (16.3–39.1)	14	21.9 (12.5–34.0)	65	0
European badger (*Meles meles*)	8	1	12.5 (0.3–52.7)	1	12.5 (0.3–52.7)	8	0
European pine marten (*Martes martes*)	1	0	0 (0.0–97.5)	NT	NT	1	0
Omnivores, wild boar (*Sus scrofa*) (group II)	115	6	5.2 (1.9–11.0)	4	3.5 (0.9–8.7)	114	0
Herbivores (group III)	228	0	0 (0.0–1.6)	NT	NT	222	0
European fallow deer (*Dama dama*)	106	0	0 (0.0–3.4)	NT	NT	106	0
Roe deer (*Capreolus capreolus*)	91	0	0 (0.0–4.0)	NT	NT	91	0
Red deer (*Cervus elaphus*)	23	0	0 (0.0–14.8)	NT	NT	23	0
Mouflon (*Ovis gmelini musimon*)	7	0	0 (0.0–40.9)	NT	NT	1	0
Unknown	1	0	0 (0.0–97.5)	NT	NT	1	0

*Results refer to screenings on generic antibodies against IAV or specific for subtype H5 on the basis of 2 subsequent multispecies ELISA tests. Quantitative reverse transcription real-time PCR results shown for swab or organ tissue samples tested for influenza A virus RNA. IAV, influenza A virus; NT, not tested.
†Includes 1 omnivore and 6 herbivores with blood sample only and no swab or organ tissue sample for molecular analyses.
‡Includes 38 animals with swab or organ tissue sample only and no blood sample for serologic analyses.
§Includes 6 IAV antibody–positive samples not tested for H5 antibody because of limited sample volume.

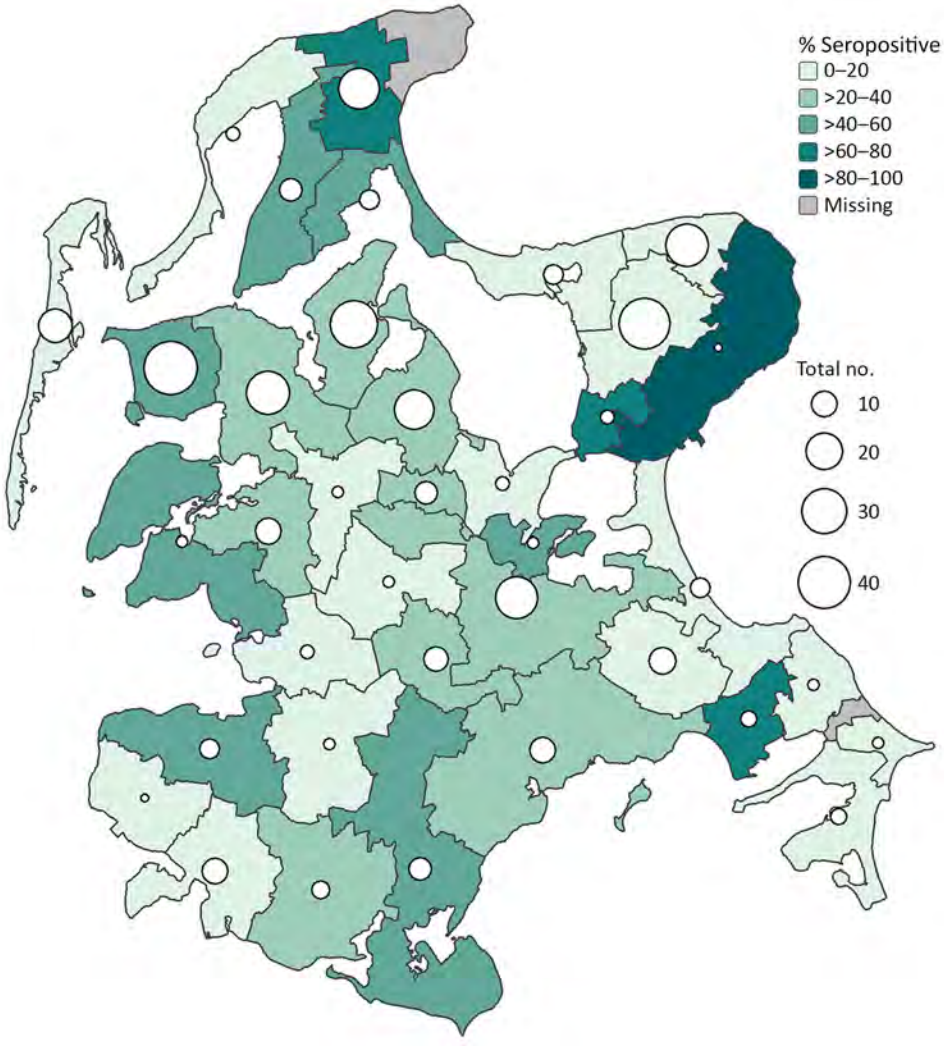

Figure. Percentage of highly pathogenic avian influenza subtype H5 seropositive juvenile and adult red foxes (*Vulpes vulpes*), by municipality, on the Island Rügen, northeast Germany, December 2023–February 2025. White circles represent total numbers of sampled and analyzed foxes per municipality.

hosts, including Anseriformes birds, for example, that are known to graze on open lands.

The possible existence of a similar correlation for omnivorous species might serve as explanation for the 3.5% (95% CI 0.9%–8.7%) seropositivity in wild boar. In addition to their scavenging or predatory behavior (*8*), wild boars have been described as nest robbers of waterfowl species in other wetland areas in Europe (*9*). All individual animals with H5-specific antibodies belonged to family groups roaming in water-associated zones (e.g., the Island Rügen and Fischland-Darß-Zingst) (Appendix Table 1), where a higher likelihood of interaction with waterfowl species can be expected.

After the previous HPAIV H5N8 epizootic during 2016–2017, a broad serologic investigation in wild boars was conducted in southern Germany (*10*). Low-level prevalence of H5N8 neutralizing antibodies (1.13%) were detected; a single positive case occurred close to a prior HPAI outbreak in waterfowl (*10*,*11*). In domestic pigs the overall susceptibility in experimental settings remained low despite a high infectious dose of a single clade 2.3.4.4b strain (*12*); however, studies using different genotypes indicate variability in susceptibility, particularly in the extent of seroconversion (*13*,*14*).

Although little is known about the persistence of AIV antibodies in wild mammals, serologic surveillance might provide a more complete picture of past exposure to potentially infected avian (reservoir) hosts than molecular testing alone. The discrepancy in NP- and H5-antibody detection leaves the possibility of other AIV subtypes undergoing initial seroconversion, so a combination of testing approaches seems advisable.

Conclusions

H5-specific antibodies in carnivores and wild Suidae species indicate ongoing spillover events, especially in wetland habitats potentially shared with main (reservoir) hosts (Anseriformes and Charadriiformes). The role of wild boars warrants further attention

because Suidae species are considered mixing vessels for swine-, human-, and avian-derived IAVs (*15*). Every such infection in mammalian species provides opportunities for virus adaptations, so continuous surveillance is recommended. Consequently, continuous surveillance also should be considered for pet animals in hotspot areas (e.g., free-ranging cats or hunting dogs) as further potential bridges for transmitting infections from wildlife to private households.

Acknowledgments

We thank all hunters contributing to this study, especially the hunters organized by the Jagdverband Rügen-Hiddensee; Bianka Hillmann, Julien Schäfer, Alrik-Markis Kunisch, Martina Abs, Kristin Trippler, and Diana Parlow for excellent technical assistance; and Ralf Redmer, Thomas Pieper, Marco Beerbohm, Sophia Ziegler, Timm Harder, and Ronja Piesche for the help during dissection and laboratory diagnostics. Many thanks to the federal state of Mecklenburg–Western Pomerania for providing data (Biotoptypen-und Nutzungstypenkartierung) and to the Bundesamt für Kartografie und Geodäsie for providing data (Digitale Basis-Landschaftsmodell).

The study is part of the One Health project Wildlife Disease Monitoring in Mecklenburg–Western Pomerania through an Integrated One Health Surveillance Response System funded by the Initialisierungs-und Vernetzungsfonds für Infektionsforschung managed by the Helmholtz Institute for One Health. Funded by the European Union under grant agreement (101084171) – (Kappa-Flu). Views and opinions expressed are however those of the author(s) only and do not necessarily reflect those of the European Union or REA. Neither the European Union nor the granting authority can be held responsible for them.

About the Author

Dr. Günther is a veterinarian and a postdoctoral researcher at the Friedrich-Loeffler-Institut, Greifswald–Insel Riems, Germany. Her primary research interests are avian viruses and other pathogens with potential influence on avian species conservation, wildlife, and public health concerns.

References

1. Pohlmann A, King J, Fusaro A, Zecchin B, Banyard AC, Brown IH, et al. Has epizootic become enzootic? Evidence for a fundamental change in the infection dynamics of highly pathogenic avian influenza in Europe, 2021. MBio. 2022;13:e0060922. https://doi.org/10.1128/mbio.00609-22
2. Plaza PI, Gamarra-Toledo V, Euguí JR, Lambertucci SA. Recent changes in patterns of mammal infection with highly pathogenic avian influenza A(H5N1) virus worldwide. Emerg Infect Dis. 2024;30:444–52. https://doi.org/10.3201/eid3003.231098
3. Butt SL, Nooruzzaman M, Covaleda LM, Diel DG. Hot topic: influenza A H5N1 virus exhibits a broad host range, including dairy cows. JDS Commun. 2024;5(Suppl 1):S13–9. https://doi.org/10.3168/jdsc.2024-0638
4. Alkie TN, Cox S, Embury-Hyatt C, Stevens B, Pople N, Pybus MJ, et al. Characterization of neurotropic HPAI H5N1 viruses with novel genome constellations and mammalian adaptive mutations in free-living mesocarnivores in Canada. Emerg Microbes Infect. 2023;12:2186608. https://doi.org/10.1080/22221751.2023.2186608
5. Bordes L, Vreman S, Heutink R, Roose M, Venema S, Pritz-Verschuren SBE, et al. Highly pathogenic avian influenza H5N1 virus infections in wild red foxes (*Vulpes vulpes*) show neurotropism and adaptive virus mutations. Microbiol Spectr. 2023;11:e0286722. https://doi.org/10.1128/spectrum.02867-22
6. Chestakova IV, van der Linden A, Martin BB, Caliendo V, Vuong O, Thewessen S, et al. High number of HPAI H5 virus infections and antibodies in wild carnivores in the Netherlands, 2020–2022. Emerg Microbes Infect. 2023;12:2270068. https://doi.org/10.1080/22221751.2023.2270068
7. Abrahantes JC, Aznar I, Catalin I, Kohnle L, Mulligan KF, Mur L, et al.; European Food Safety Authority (EFSA). Avian influenza annual report 2023. EFSA J. 2025;23:e9197.
8. Barrios-Garcia MN, Ballari SA. Impact of wild boar (*Sus scrofa*) in its introduced and native range: a review. Biol Invasions. 2012;14:2283–300. https://doi.org/10.1007/s10530-012-0229-6
9. Barasona JA, Carpio A, Boadella M, Gortazar C, Piñeiro X, Zumalacárregui C, et al. Expansion of native wild boar populations is a new threat for semi-arid wetland areas. Ecol Indic. 2021;125:125. https://doi.org/10.1016/j.ecolind.2021.107563
10. Schülein A, Ritzmann M, Christian J, Schneider K, Neubauer-Juric A. Exposure of wild boar to influenza A viruses in Bavaria: analysis of seroprevalences and antibody subtype specificity before and after the panzootic of highly pathogenic avian influenza viruses A (H5N8). Zoonoses Public Health. 2021;68:503–15. https://doi.org/10.1111/zph.12841
11. Globig A, Staubach C, Sauter-Louis C, Dietze K, Homeier-Bachmann T, Probst C, et al. Highly pathogenic avian influenza H5N8 clade 2.3.4.4b in Germany in 2016/2017. Front Vet Sci. 2018;4:240. https://doi.org/10.3389/fvets.2017.00240
12. Graaf A, Piesche R, Sehl-Ewert J, Grund C, Pohlmann A, Beer M, et al. Low susceptibility of pigs against experimental infection with HPAI virus H5N1 clade 2.3.4.4b. Emerg Infect Dis. 2023;29:1492–5. https://doi.org/10.3201/eid2907.230296
13. Kwon T, Trujillo JD, Carossino M, Lyoo EL, McDowell CD, Cool K, et al. Pigs are highly susceptible to but do not transmit mink-derived highly pathogenic avian influenza virus H5N1 clade 2.3.4.4b. Emerg Microbes Infect. 2024;13:2353292. https://doi.org/10.1080/22221751.2024.2353292
14. Kwon T, Trujillo JD, Carossino M, Machkovech HM, Cool K, Lyoo EL, et al. Pathogenicity and transmissibility of bovine-derived HPAI H5N1 B3.13 virus in pigs. Emerg Microbes Infect. 2025;14:2509742. https://doi.org/10.1080/22221751.2025.2509742
15. Abdelwhab EM, Mettenleiter TC. Zoonotic animal influenza virus and potential mixing vessel hosts. Viruses. 2023;15:980. https://doi.org/10.3390/v15040980

Address for correspondence: Martin Beer or Kerstin Wernike, Friedrich-Loeffler-Institut, Federal Research Institute for Animal Health, Südufer 10, 17493 Greifswald–Insel Riems, Germany; email: martin.beer@fli.de or kerstin.wernike@fli.de

Replication Efficiency of Contemporary Highly Pathogenic Avian Influenza A(H5N1) Virus Isolates in Human Nasal Epithelium Model

Meaghan Flagg,[1] Christopher J. Winski,[1] Bridget G. Brackney, Tessa R. Lutterman, Johan A. Ortiz-Morales,[2] Brandi N. Williamson, Emmie de Wit

Replication of influenza A virus in human nasal epithelium affects transmissibility and disease. We compared virus replication and immune responses in human nasal epithelium infected with seasonal and highly pathogenic avian influenza A(H5N1) viruses. Contemporary H5N1 viruses replicated better than the historical isolate; however, interferon response to B3.13 genotype viruses was dampened.

Since March 2024, a total of 70 human cases of highly pathogenic avian influenza (HPAI) A(H5N1) have been reported in the United States as a result of sporadic spillover events from poultry and dairy cattle (*1*). HPAI H5N1 clade 2.3.4.4b genotype B3.13 was responsible for many of the early cases (*2*). On January 31, 2025, HPAI H5N1 clade 2.3.4.4b genotype D1.1 was detected in dairy cattle (https://www.aphis.usda.gov/news/program-update/aphis-confirms-d11-genotype-dairy-cattle-nevada-0); D1.1 was later identified in humans (*1*). Those spillover events sparked global health concerns about the potential for large-scale spread of clade 2.3.4.4b HPAI H5N1 viruses and their risk to human and animal health.

Seasonal influenza A and HPAI H5N1 viruses both cause severe respiratory disease despite different tissue tropisms. Seasonal influenza A viruses primarily infect the upper respiratory tract (URT), whereas HPAI H5N1 viruses preferentially replicate in the lower respiratory tract (LRT). This contrast in tissue affinity is explained by differences in receptor specificity and has been implicated in transmission efficiency (*3*). Specifically, the URT predominantly expresses sialic acids linked to galactose by an α-2,6 linkage; the LRT expresses sialic acid linked to galactose via α-2,3. Despite the inefficient human-to-human transmission of HPAI H5N1 viruses, recent emergence and circulation of new genotypes in mammals emphasize the need to characterize these novel viruses in relevant respiratory tract models. Here, we compare the replication kinetics and host innate immune responses in human nasal epithelium of several seasonal influenza A virus isolates and historical and contemporary HPAI H5N1 virus isolates of 3 different genotypes.

The Study

The nasal epithelium is the primary site of entry for influenza A virus in humans. Structurally, nasal tissue is composed of goblet, ciliated, and basal cells that produce mucin and form tight junctions as host defense mechanisms (*4*). The ability to study the nasal epithelium in vitro has substantially improved with recent advances in airway model development. The Mattek EpiNasal (https://www.mattek.com) tissue model is derived from primary human nasal epithelial cells and accurately recapitulates the in vivo mucociliary phenotype. We used the model to study growth kinetics of 8 influenza A virus isolates (Table; Appendix Figure 1, https://wwwnc.cdc.gov/EID/article/32/5/26-0053-App1.pdf) and the host response to infection.

Author affiliation: National Institute of Allergy and Infectious Diseases, National Institutes of Health, Hamilton, Montana, USA

DOI: https://doi.org/10.3201/eid3205.260053

[1]These authors contributed equally to this article.
[2]Current affiliation: LSU Health, Shreveport, Louisiana, USA.

Table. Influenza A virus isolates used in study of replication efficiency of contemporary highly pathogenic avian influenza A(H5N1) virus isolates in human nasal epithelium model*

Isolate	Subtype	Clade	Genotype	Known mammalian adaptions	Symptoms, disease Severity	References	GISAID identifier
A/Brisbane/59/2007	H1N1	NA	NA	PB2 E627K	Unknown	(*5*)	EPI_ISL_356921
A/New York/470/2004	H3N2	NA	NA	PB2 E627K	Unknown	(*6*)	EPI_ISL_8959
A/Vietnam/1203/2004	H5N1	1	NA	PB2 E627K	Severe respiratory distress resulting in fatality	(*7*)	NCBI: txid284218
A/Texas/37/2024	H5N1	2.3.4.4b	B3.13	PB2 E627K	Mild respiratory symptoms and conjunctivitis	(*2*)	EPI_ISL_19027114
A/bovine/Ohio/B24-OSU-342/2024	H5N1	2.3.4.4b	B3.13	PB2 M631L	NA	(*8*)	EPI_ISL_19178076
A/mountain lion/MT/1/2024	H5N1	2.3.4.4b	B3.6	None	Mountain lion found dead	(*9*)	EPI_ISL_19083124
A/Wyoming/01/2025	H5N1	2.3.4.4b	D1.1	PB2 E627K	Severe respiratory disease requiring hospitalization	https://www.cdc.gov/bird-flu/spotlights/h5n1-response-02262025.html	EPI_ISL_19749443
A/Nevada/10/2025	H5N1	2.3.4.4b	D1.1	PB2 D701N	Conjunctivitis		EPI_ISL_19726293

*All virus isolates were sequenced and found to be identical to sequences deposited in GISAID (https://www.gisaid.org) or GenBank. NCBI, National Center for Biotechnology Information; NA, not available; PB, polymerase basic.

HPAI H5N1 isolate A/Texas/37/2024 (B3.13 genotype) replicated most efficiently in nasal tissue even when compared with seasonal isolates (Figure 1). Although we noted differences in replication kinetics between viruses of the same genotype, the B3.13 and D1.1 genotype isolates replicated more efficiently than the historical HPAI H5N1 isolate A/Vietnam/1203/2004. The B3.6 HPAI H5N1 isolate A/

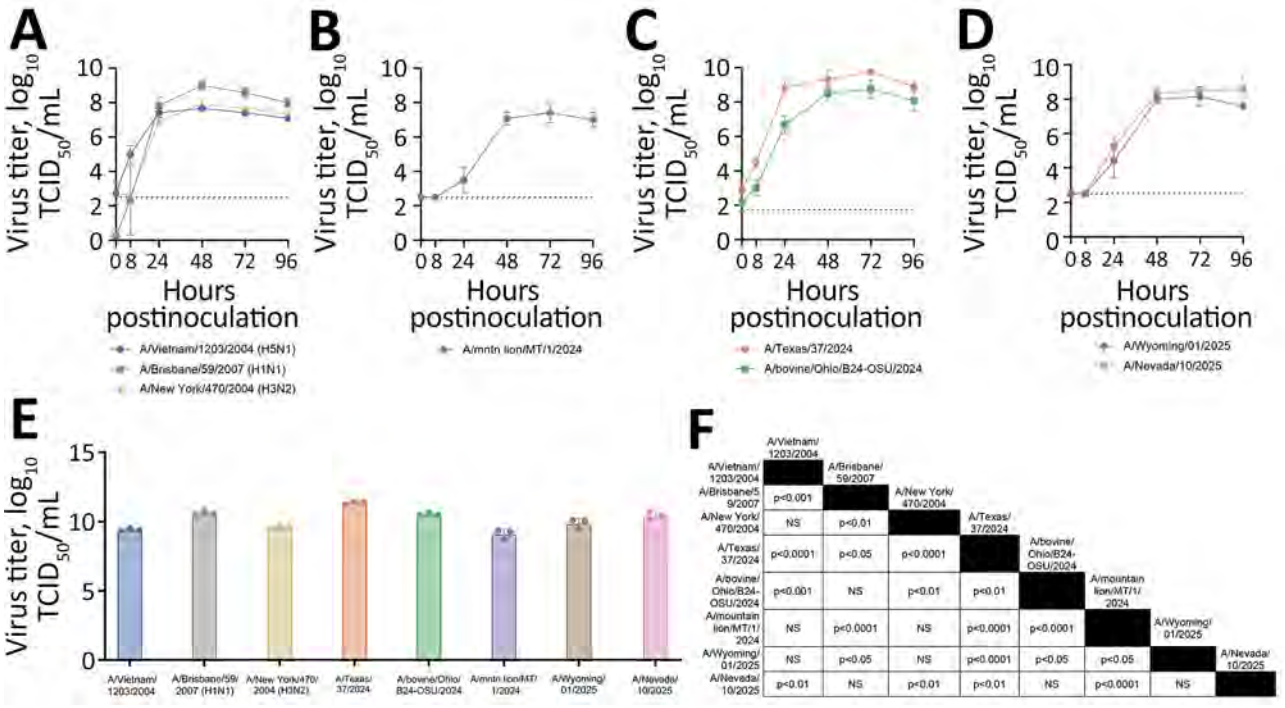

Figure 1. Replication of seasonal and highly pathogenic avian influenza (HPAI) A viruses in human nasal epithelium cultures in study of replication efficiency of contemporary HPAI H5N1 virus isolates in human nasal epithelium model. A–D) Virus replication in historical (A) and HPAI H5N1 genotype clade 2.3.4.4b B3.13 (B), B3.6 (C), and D1.1 (D) virus strains. We inoculated Mattek EpiNasal cultures (https://www.mattek.com) with a multiplicity of infection of 0.1 $TCID_{50}$ per cell. We harvested apical supernatant at 0, 8, 24, 48, 72, and 96 hours postinoculation and titered on MDCK cells. Data points and error bars represent the geometric mean ±SD of 3 biologic replicates from a single donor; dashed line indicates lower limit of detection. E) Area under the curve of data from 0–96 hours postinoculation as shown in panels A–D. Error bars indicate SD. F) Statistical analysis of data in panel E performed using 1-way analysis of variance with multiple comparisons (Tukey). NS, not significant; $TCID_{50}$, 50% tissue culture infectious dose.

mountain lion/MT/1/2024 replicated least efficiently (Figure 1). Presence of known mammalian adaptations of polymerase basic (PB) 2 E627K, PB2 D701N, and PB2 M631L was associated with more efficient virus replication (Table; Figure 1).

Next, we assessed the host innate immune response to infection by quantifying interferon-stimulated gene (ISG) 15, interferon-induced transmembrane protein 3, myxovirus resistance 1, and proinflammatory cytokines interleukin 6 (IL-6), tumor necrosis factor α, and interleukin 1β (IL-1β), as previously described (*10*). B3.13 genotype viruses induced lower ISG responses than did D1.1 and historical HPAI H5N1 viruses, as well as seasonal influenza A viruses (Figure 2). Of note,

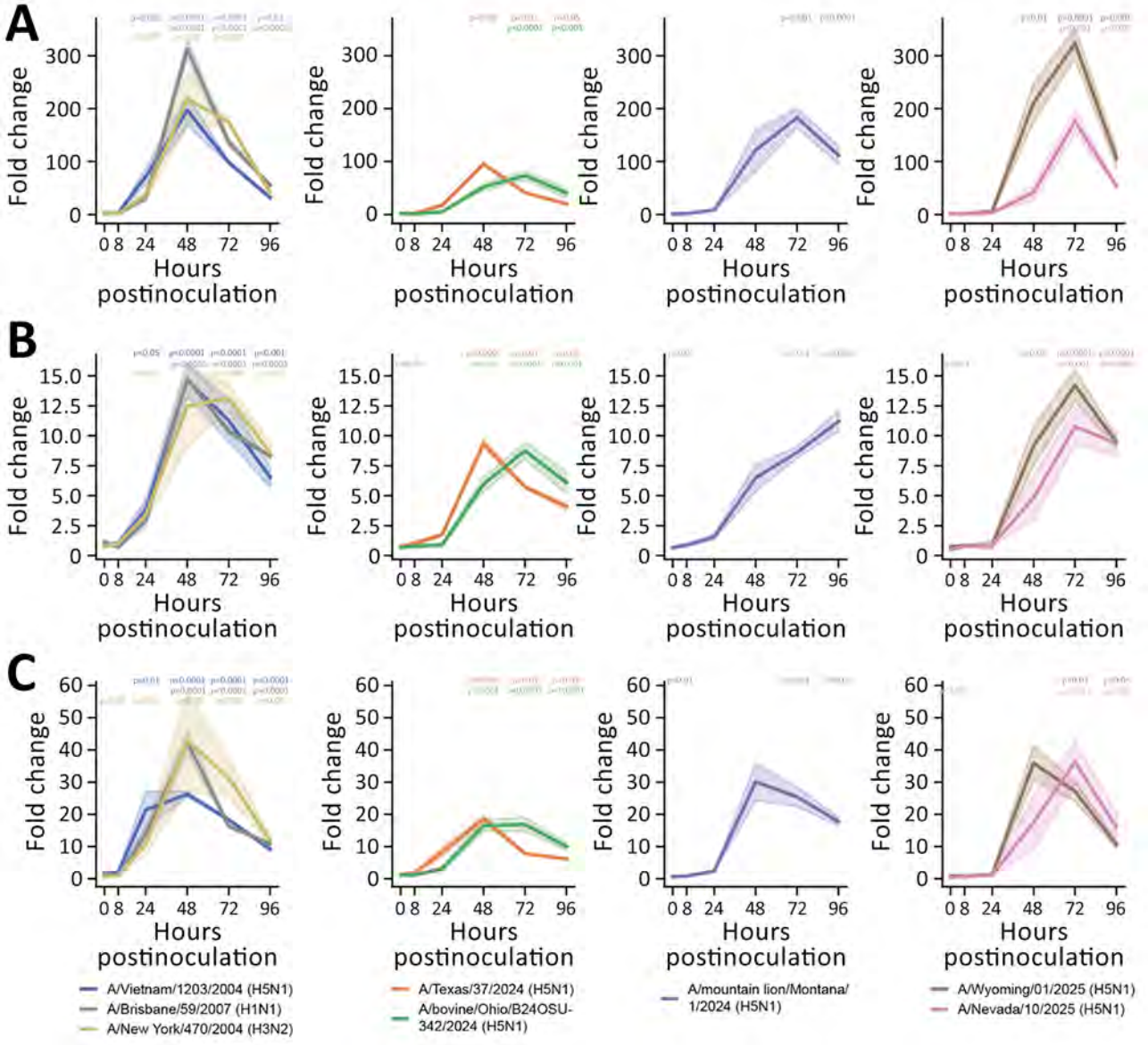

Figure 2. Induction of interferon-stimulated genes in human nasal epithelium infected with seasonal influenza A and highly pathogenic avian influenza (HPAI) A(H5N1) viruses in study of replication efficiency of contemporary HPAI H5N1 virus isolates in human nasal epithelium model. We inoculated Mattek EpiNasal cultures (https://www.mattek.com) with a multiplicity of infection of 0.1 50% tissue culture infectious dose per cell and extracted RNA from cells at 0, 8, 24, 48, 72, and 96 hours postinoculation. We ran quantitative reverse transcription PCR using primers (Integrated DNA Technologies, https://www.idtdna.com) to detect interferon-stimulated gene 15 (A), interferon-induced transmembrane protein 3 (B), and myxovirus resistance 1 (C) for historical and clade 2.3.4.4b highly pathogenic avian HPAI H5N1 genotype B3.13, B3.6, and D1.1 virus strains. Lines indicate median; shading indicates 95% CI. We normalized data to internal controls (ACTB and GAPDH) and calculated fold change relative to timepoint-matched mock-infected controls. Fold change is reported for 3 biologic replicates. We performed statistical analysis using 2-way analysis of variance with Dunnett posttest.

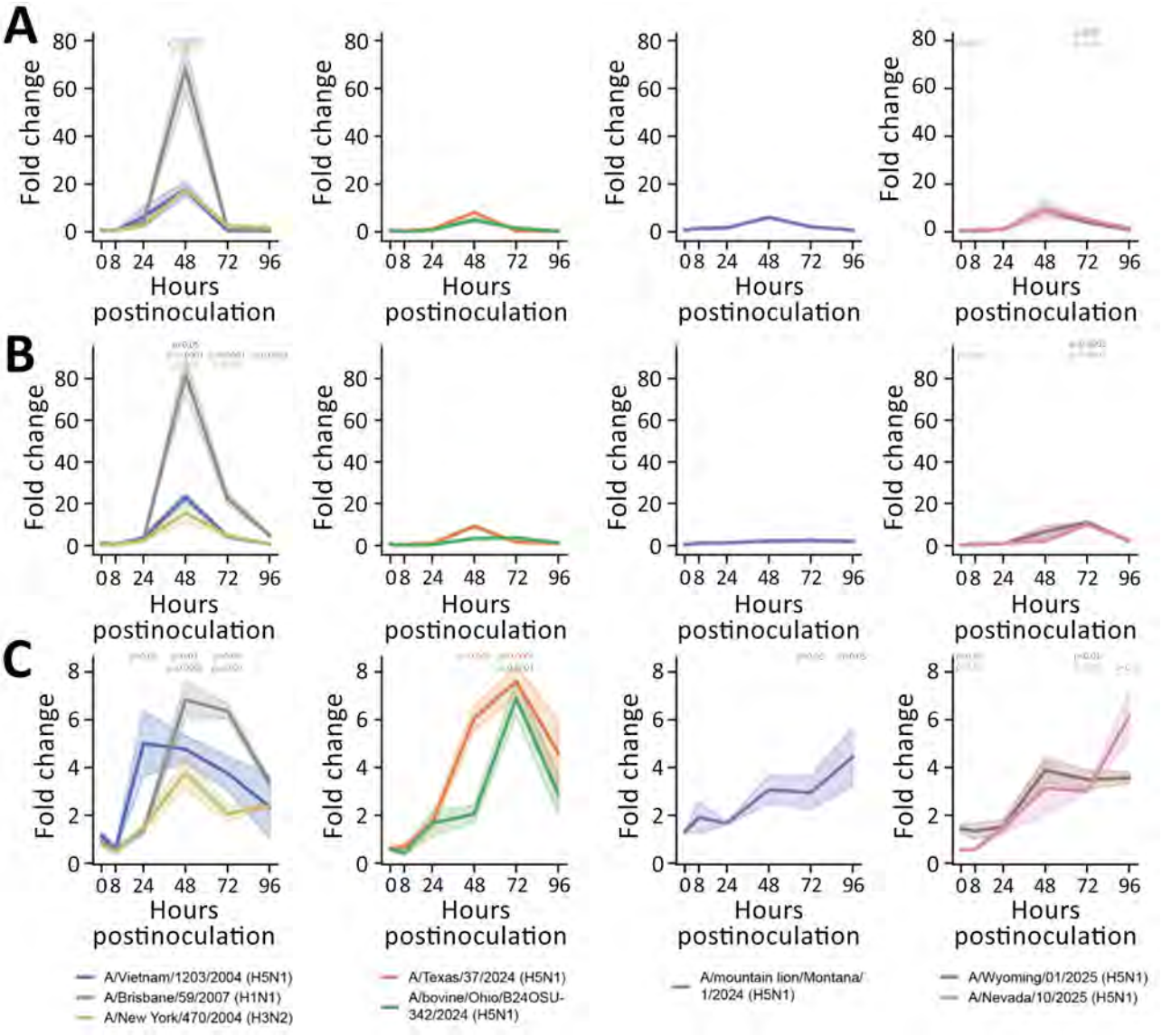

Figure 3. Induction of proinflammatory cytokines in human nasal epithelium infected with seasonal influenza A and highly pathogenic avian influenza (HPAI) A(H5N1) viruses in study of replication efficiency of contemporary HPAI H5N1 virus isolates in human nasal epithelium model. We inoculated Mattek EpiNasal cultures (https://www.mattek.com) with a multiplicity of infection of 0.1 50% tissue culture infectious dose per cell. RNA was extracted from cells at 0, 8, 24, 48, 72, and 96 hours postinoculation. We ran quantitative reverse transcription PCR using primers (Integrated DNA Technologies, https://www.idtdna.com) to detect interleukin 6 (A), tumor necrosis factor α (B), and interleukin 1β (C) for historical and clade 2.3.4.4b HPAI H5N1 genotype B3.13, B3.6, and D1.1 strains. Lines indicate medians; shading indicates 95% CIs. We normalized data to internal controls (ACTB and GAPDH) and calculated fold change relative to timepoint-matched mock-infected controls. Fold change is reported for 3 biologic replicates. We performed statistical analysis using 2-way analysis of variance with Dunnett posttest.

dampened ISG response occurred despite high levels of virus replication (Figure 1). In contrast, the HPAI H5N1 A/mountain lion/MT/1/2024 isolate replicated to the lowest titers yet resulted in induction of ISGs similar to A/Vietnam/1203/2004 (Figure 2). ISGs peaked earlier and higher in human nasal epithelium inoculated with D1.1 A/Wyoming/01/2025 isolated from a severe case than for D1.1 A/Nevada/10/2025 isolated from a mild case (Table; Figure 2). We observed a different pattern for induction of proinflammatory cytokines. Only infection with the seasonal influenza A viruses and A/Vietnam/1203/2004 resulted in increased expression of all 3 proinflammatory cytokines. All other isolates only induced notable IL-1β expression, but not IL-6 or tumor necrosis factor α (Figure 3).

HPAI H5N1 virus replication can be affected by the physiologic temperature of the human nasal mucosa, for which the reference is 33°C (*11*,*12*). To

address the potential effect of temperature on virus replication, we quantified virus replication kinetics at 37°C and 33°C in MDCK cells. At 8 hours postinoculation, the titers of HPAI H5N1 virus isolates were lower at 33°C than at 37°C (Appendix Figure 2). However, all viruses reached the same maximum titer at 33°C and 37°C. In addition, the relative difference observed between viruses at 37°C were similar at 33°C, suggesting that adjusting the temperature in the nasal epithelial cultures to 33°C would not have substantially altered our results.

The sporadic infections of mammals with HPAI H5N1 viruses coupled with the emergence of new genotypes raises questions regarding the pandemic potential of such viruses. Our use of a human nasal epithelium model to compare virus replication kinetics of and host immune responses to seasonal influenza A viruses and HPAI H5N1 clade 2.3.4.4b viruses from different genotypes showed that HPAI H5N1 B3.6 isolate A/mountain lion/MT/1/2024 was the least efficient at replicating in the nasal epithelium. Of note, the HPAI H5N1 A/bovine/Ohio/B24-OSU-342/2024 isolate lacks the canonical PB2 E627K substitution but has the PB2 M631L substitution, which was recently shown to increase polymerase activity in mammalian cell culture and increase virulence in a mouse model (*8*).

Previously, we compared replication kinetics of contemporary versus historical HPAI H5N1 viruses in a human alveolar organoid LRT model (*10*). In the LRT, the historical HPAI H5N1 virus replicated more efficiently than the contemporary HPAI H5N1 isolates, in contrast to our observations in the URT in this study. That finding suggests that the contemporary HPAI H5N1 viruses are better adapted to replicate in the human nasal epithelium.

Our study provides novel insights regarding the biological differences among influenza A viruses in the human nasal epithelium. Specifically, we observed a correlation between mammalian adaptation and replication efficiency in the human URT. Recently published work comparing B3.13 and D1.1 isolates in human nasal epithelium observed that the D1.1 isolate replicated better than the B3.13 isolate (*13*). That study used only 1 virus per genotype, and the B3.13 isolate was not a human isolate and lacked the PB2 E627K mammalian adaptation, which likely explains the reduced virus replication. Nonetheless, despite several studies highlighting the efficient replication of contemporary HPAI H5N1 viruses in the nasal epithelium, we see no evidence of human-to-human transmission. Existing immunity could partially explain that finding. A study using ferret models found that prior exposure to seasonal influenza A(H1N1) virus significantly reduced nasal shedding of contemporary H5N1 virus and prevented infection with H5N1 in a contact transmission setting (*14*). Thus, seasonal influenza A viruses have the potential to prime the immune system and prevent infection and transmission of contemporary HPAI H5N1 viruses. Influenza A(H1N1)pdm09–like viruses are still circulating in humans, and serosurveillance of exposed dairy farm workers revealed high (66%) prevalence of pdm09 neutralizing H1N1 antibodies (*15*). Therefore, existing immunity to influenza A(H1N1)pdm09–like viruses might protect against contemporary H5N1 infection and onward transmission despite high capacity for virus replication in human nasal epithelium.

Conclusions

Our results reveal that contemporary HPAI H5N1 isolates with known mammalian adaptations replicate more efficiently than historical HPAI H5N1 virus used. Despite high levels of virus replication, ISG induction was limited in response to B3.13 genotype virus infection. Additional studies are needed to further understand how virus replication efficiency and innate immune responses affect mammalian transmission efficiency. Existing immunity to other influenza A viruses might protect against contemporary H5N1 infection and onward transmission.

This research was supported by the Intramural Research Program of the National Institutes of Health (NIH). The contributions of the NIH authors are considered works of the United States Government. The findings and conclusions presented in this paper are those of the authors and do not necessarily reflect the views of the NIH or the US Department of Health and Human Services.

Data included in this manuscript are available in Figshare at https://doi.org/10.6084/m9.figshare.31049938.

About the Author

Dr. Flagg is a postdoctoral fellow in the Molecular Pathogenesis Section of the Laboratory of Virology, Rocky Mountain Laboratories, National Institute of Allergy and Infectious Diseases, National Institutes of Health. Her primary interests are epithelial stem cell biology and repair during virus infection.

References

1. Rolfes MA, Kniss K, Kirby MK, Garg S, Reinhart K, Davis CT, et al. Human infections with highly pathogenic avian influenza A(H5N1) viruses in the United States from March 2024 to May 2025. Nat Med. 2025;31:3889–98. https://doi.org/10.1038/s41591-025-03905-2

2. Uyeki TM, Milton S, Abdul Hamid C, Reinoso Webb C, Presley SM, Shetty V, et al. Highly pathogenic avian influenza A(H5N1) virus infection in a dairy farm worker. N Engl J Med. 2024;390:2028–9. https://doi.org/10.1056/NEJMc2405371
3. van Riel D, den Bakker MA, Leijten LM, Chutinimitkul S, Munster VJ, de Wit E, et al. Seasonal and pandemic human influenza viruses attach better to human upper respiratory tract epithelium than avian influenza viruses. Am J Pathol. 2010;176:1614–8. https://doi.org/10.2353/ajpath.2010.090949
4. Deprez M, Zaragosi LE, Truchi M, Becavin C, Ruiz García S, Arguel MJ, et al. A single-cell atlas of the human healthy airways. Am J Respir Crit Care Med. 2020;202:1636–45. https://doi.org/10.1164/rccm.201911-2199OC
5. WHO Collaborating Centre for Reference and Research on Influenza. Characteristics of human influenza AH1N1, AH3N2, and B viruses isolated September 2007 to February 2008. London: The Centre; 2008.
6. Memoli MJ, Jagger BW, Dugan VG, Qi L, Jackson JP, Taubenberger JK. Recent human influenza A/H3N2 virus evolution driven by novel selection factors in addition to antigenic drift. J Infect Dis. 2009;200:1232–41. https://doi.org/10.1086/605893
7. Maines TR, Lu XH, Erb SM, Edwards L, Guarner J, Greer PW, et al. Avian influenza (H5N1) viruses isolated from humans in Asia in 2004 exhibit increased virulence in mammals. J Virol. 2005;79:11788–800. https://doi.org/10.1128/JVI.79.18.11788-11800.2005
8. Zhang L, Lai Y, Cui Y, Yang Q, Shao Y, Ding S, et al. Emergence of mammalian-adaptive PB2 mutations enhances polymerase activity and pathogenicity of cattle-derived H5N1 influenza A virus. Nat Commun. 2025;17:1011. https://doi.org/10.1038/s41467-025-67753-x
9. Kaiser F, Morris DH, Wickenhagen A, Mukesh R, Gallogly S, Yinda KC, et al. Inactivation of avian influenza A(H5N1) virus in raw milk at 63°C and 72°C. N Engl J Med. 2024;391:90–2. https://doi.org/10.1056/NEJMc2405488
10. Flagg M, Williamson BN, Ortiz-Morales JA, Lutterman TR, de Wit E. Comparison of contemporary and historic highly pathogenic avian influenza A(H5N1) virus replication in human lung organoids. Emerg Infect Dis. 2025;31:318–22. https://doi.org/10.3201/eid3102.241147
11. Tan KS, Liu J, Andiappan AK, Lew ZZR, He TT, Ong HH, et al. Unique immune and other responses of human nasal epithelial cells infected with H5N1 avian influenza virus compared to seasonal human influenza A and B viruses. Emerg Microbes Infect. 2025;14:2484330. https://doi.org/10.1080/22221751.2025.2484330
12. Zeng H, Goldsmith CS, Kumar A, Belser JA, Sun X, Pappas C, et al. Tropism and infectivity of a seasonal A(H1N1) and a highly pathogenic avian A(H5N1) influenza virus in primary differentiated ferret nasal epithelial cell cultures. J Virol. 2019;93:e00080-19. https://doi.org/10.1128/JVI.00080-19
13. Zhang X, Lam SJ, Chen LL, Fong CH, Chan WM, Ip JD, et al. Avian influenza virus A(H5N1) genotype D1.1 is better adapted to human nasal and airway organoids than genotype B3.13. J Infect Dis. 2026;233:e662–6. https://doi.org/10.1093/infdis/jiaf598
14. Restori KH, Weaver V, Patel DR, Merrbach GA, Septer KM, Field CJ, et al. Preexisting immunity to the 2009 pandemic H1N1 virus reduces susceptibility to H5N1 infection and disease in ferrets. Sci Transl Med. 2025;17:eadw4856. https://doi.org/10.1126/scitranslmed.adw4856
15. Mellis AM, Coyle J, Marshall KE, Frutos AM, Singleton J, Drehoff C, et al. Serologic evidence of recent infection with highly pathogenic avian influenza A(H5) virus among dairy workers—Michigan and Colorado, June–August 2024. MMWR Morb Mortal Wkly Rep. 2024;73:1004–9. https://doi.org/10.15585/mmwr.mm7344a3

Address for correspondence: Emmie de Wit, National Institute of Allergy and Infectious Diseases, National Institutes of Health, 903 S 4th St, Hamilton, MT 59840, USA; email: emmie.dewit@nih.gov

Tropism and Replication Competence of Cattle Influenza A(H5N1) Genotype B3.13 Virus in Human Bronchus and Lung Tissue

Kenrie P.Y. Hui, John C.W. Ho, Ka-Chun Ng, Richard J. Webby, Malik Peiris, John M. Nicholls, Michael C.W. Chan

In 2024, influenza A(H5N1) genotype B3.13 viruses emerged from cattle and caused mild spillover infections in humans. Using human bronchus and lung tissue, we evaluated tropism, replication, and pathogenesis of 2 cattle influenza isolates. Those viruses showed moderate replication competence and induced robust proinflammatory responses, suggesting potential risk for human health.

Highly pathogenic avian influenza (HPAI) H5N1 viruses remain a major global health concern, particularly because of sporadic spillover into mammals (*1*). HPAI A(H5N1) clade 2.3.4.4b viruses entered the United States through a trans-Atlantic introduction in late 2021, after which extensive reassortment among migratory birds produced the B3.13 and D1.1 genotypes. Those variants have spread widely, driving outbreaks in livestock and causing occasional human infections (*2*,*3*). Beginning in 2024, H5N1 clade 2.3.4.4b viruses were detected in dairy cattle across multiple US states, and those infections were linked to mild zoonotic cases in humans (*4*,*5*). To assess the health risks of emerging cattle-origin influenza viruses, we examined tropism, replication, receptor use, and innate immune responses of cattle H5N1 viruses in human respiratory tract explants.

The Study

We investigated newly emerged cattle influenza A(H5N1) genotype B3.13 virus strains A/dairy_cow/Ohio/B24OSU-439/2024 (H5N1/439) and A/dairy_cow/Texas/98638/2024 (H5N1/98638) in human bronchial and lung tissue cultures (Appendix, https://wwwnc.cdc.gov/EID/article/32/5/25-1926-App1.pdf). In brief, we obtained nonmalignant tissue cultures from patients who underwent elective surgery and consented to tissue use (Appendix). We used the RNeasy Micro Kit (QIAGEN, https://www.qiagen.com) to extract total RNA, according to manufacturer instructions, then reverse transcribed extracted RNA by using the PrimeScript RT Reagent Kit (TaKaRa Bio, Inc., http://www.takara-bio.com). We fixed the explant tissues for immunohistochemical staining of influenza viral proteins.

We compared explant cultures with 3 historical human isolates: H5N1/483, H5N6/39715, and H1N1pdm/415742 (Appendix Tables 1, 2). The historical virus strains showed different tropisms and area under the curve (AUC) levels to the explant tissue cultures at 24–48 hours postinfection (hpi). In bronchus tissues, H1N1pdm/415742 replication was highest, followed by H5N6/39715 (Figure 1, panels A, B). The H5N1/439 and H5N1/98638 cattle isolates showed substantially lower replication competence at 48 hpi than H1N1pdm/415742 and H5N6/39715 but much higher competence than the H5N1/483 avian isolate, which replicated poorly in the human bronchial tissues. In human lung tissues, H5N6/39715 replicated to the highest viral titers and AUC values at 24 hpi, followed by H5N1/483 (Figure 1, panels C, D). Both cattle isolates replicated to similar levels as H1N1pdm/415742, but isolate H5N1/439 had a slightly higher replication trend than H5N1/98638. The cattle-origin viruses replicated to lower titers than HPAI H5N1 but similar to H1N1pdm/415742 in human lung tissues, which aligns with other reports in human lung organoids (*6*). However, cattle-origin H5N1 genotype B3.13

Author affiliations: Centre for Immunology & Infection, Hong Kong, China (K.P.Y. Hui, J.C.W. Ho, M. Peiris, M.C.W. Chan); School of Public Health, Li Ka Shing Faculty of Medicine, University of Hong Kong, Hong Kong (K.P.Y. Hui, K.-C. Ng, M. Peiris, M.C.W. Chan); St. Jude Children's Research Hospital, Memphis, Tennessee, USA (R.J. Webby); School of Clinical Medicine, Li Ka Shing Faculty of Medicine, University of Hong Kong, Hong Kong (J.M. Nicholls)

DOI: https://doi.org/10.3201/eid3205.251926

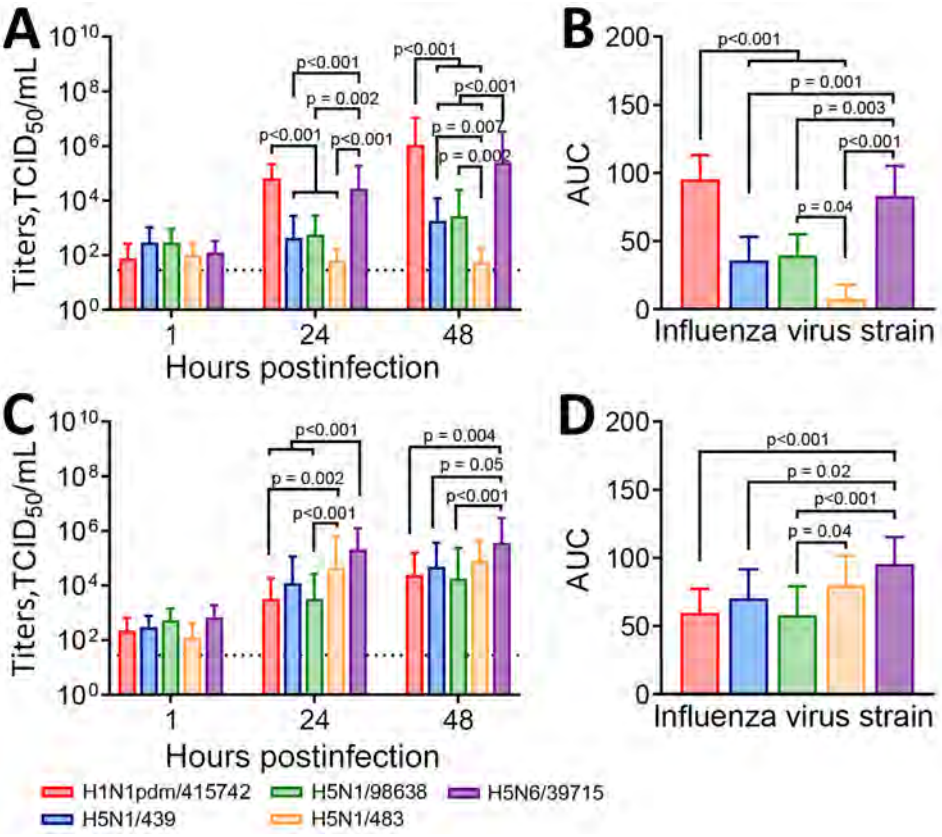

Figure 1. Viral replication kinetics in a study of ex vivo tropism and replication competence of cattle influenza A(H5N1) genotype B3.13 virus in human bronchus and lung tissue. A, B) Mean virus titers for bronchus tissues; C, D) mean virus titers for lung tissues. A, C) Culture supernatants of the infected human respiratory tissue explants were harvested at 1, 24, and 48 hours postinfection and viral titers determined by $TCID_{50}$ assays; dashed line indicates assay detection limit. Statistical significance was calculated by using 2-way analysis of variance with Tukey post-hoc test. Error bars indicate SD. B, D) AUC values calculated from influenza virus titers 24–48 hours postinfection are shown. Statistical significance was calculated by using 1-way analysis of variance with Tukey post-hoc test. Error bars indicate SD. AUC, area under the curve; $TCID_{50}$, 50% tissue culture infectious dose.

virus has lower replication than genotype D1.1 in human nasal and airway organoids (*7*). Replication competence in human respiratory tissues might be contributed by the 631L of polymerase basic protein 2 (Appendix Table 2), which promotes polymerase activity in human cells (*8*). In addition, the cattle-origin H5N1 viruses replicated to higher titers than avian H5N1 viruses in bronchial tissues, implying that the cattle-origin H5N1 viruses might be more transmissible than HPAI H5N1 viruses.

Immunohistochemical staining revealed the tissue and cellular tropism of cattle-origin H5N1 viruses. We found nucleoprotein (NP)–positive cells from H1N1pdm/415742 virus and to a lesser extent H5N6/39715 in the bronchial epithelium, infecting ciliated and nonciliated epithelial cells (Figure 2, panel A). In comparison, we noted moderate levels of NP-positive cells from cattle H5N1/439 and H5N1/98638 viruses in ciliated and nonciliated epithelial cells but identified no NP-positive cells from avian-origin H5N1/483 in the bronchial sections. In the lung sections, H5N1/483 and H5N6/39715 demonstrated the most extensive infections, followed by H5N1/439, H5N1/98638, and H1N1pdm/415742 (Figure 2, panel B). Together with the viral replication data, those results imply that cattle-origin H5N1/439 and H5N1/98638 viruses possess moderate replication capacity in upper and lower airways and are better adapted to human hosts than avian H5N1/483.

To test virus agglutination, we conducted selective desialylation on turkey red blood cells (TRBCs). For controls, we used H1N1pdm/415742, known for binding to α(2–6)-linked sialic acid (SA), and H5N1/483, known for binding to α(2,3)-linked SA. Treating TRBCs with Sialidase S (Agilent, https://www.agilent.com), which preferentially cleaves the α(2,3)-linked SA, prevented hemagglutination of avian H5N1/483 but did not affect H1N1pdm/415742, H5N1/439, or H5N1/98638 isolates (Table). Conversely, treating with Sialidase C (Agilent), which cleaves α(2,3) and α(2–6) linkages, and Sialidase A (Agilent), which cleaves α(2,3), α(2–6), α(2–8), and α(2–9) linkages, prevented hemagglutination of all the influenza strains. Those results suggest that the cattle-origin H5N1/439 and H5N1/98638 isolates resemble H1N1pdm/415742 and acquired at least partial affinity to α(2–6)-linked SA, which differs from the avian H5N1/483 virus, indicating that the 2 emergent cattle viruses could have a higher host adaption to humans.

A/Texas/37/2024 and other bovine-origin H5N1 isolates have shown dual binding affinity to α(2,3)-

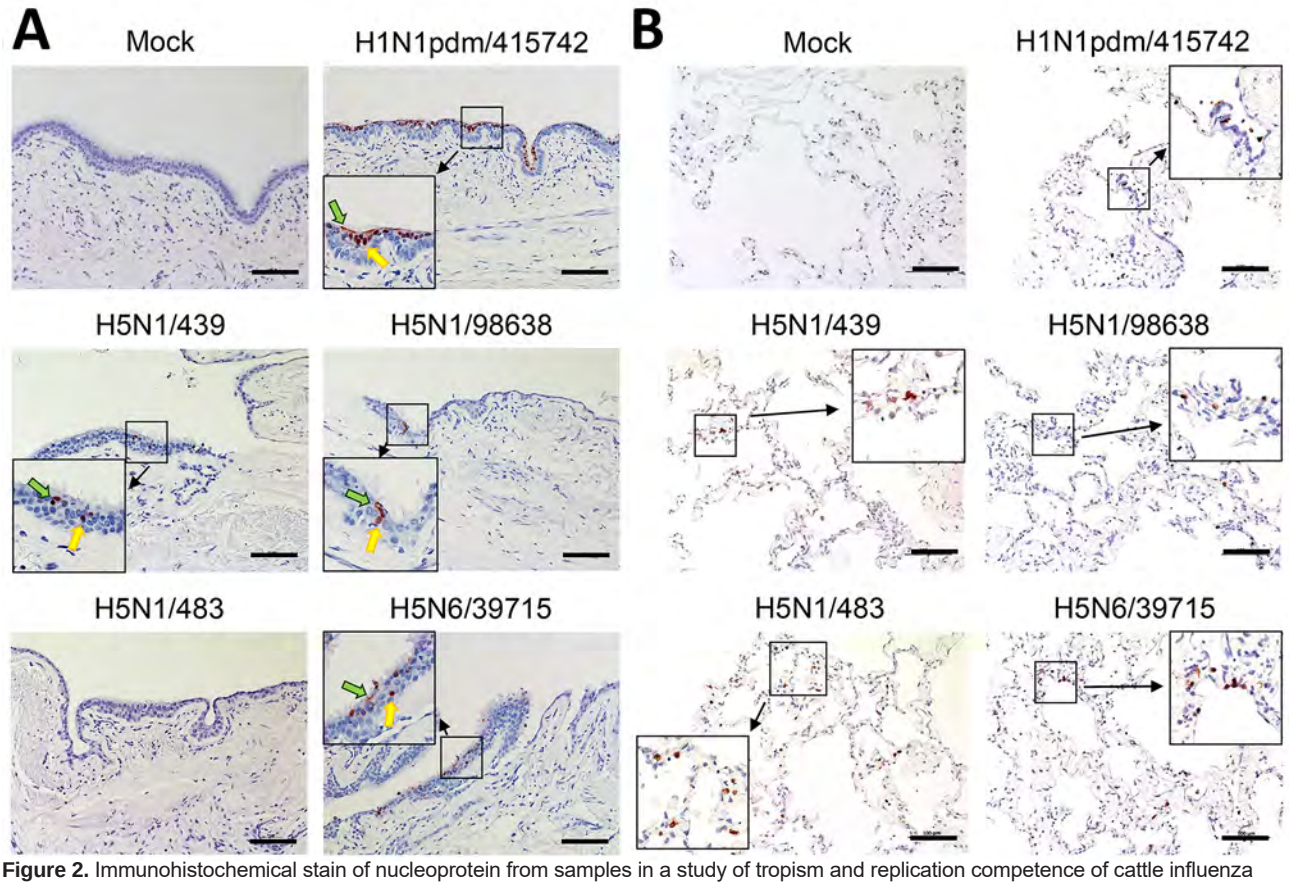

Figure 2. Immunohistochemical stain of nucleoprotein from samples in a study of tropism and replication competence of cattle influenza A(H5N1) genotype B3.13 virus in human bronchus and lung tissue. Formalin-fixed, paraffin-embedded sections of human bronchus (A) and lung (B) tissue explants at 48 hours postinfection are shown. Cells positive for influenza A nucleoprotein are indicated by red-brown color. Green arrows indicate ciliated cells; yellow arrows indicate nonciliated cells. Images are representatives of 3 separate donors. Cattle influenza A(H5N1) genotype B3.13 virus strains A/dairy_cow/Ohio/B24OSU-439/2024 (H5N1/439) and A/dairy_cow/Texas/98638/2024 (H5N1/98638) are compared with historical human isolates of highly pathogenic avian influenza strains H5N1/483, H5N6/39715, and H1N1pdm/415742 (Appendix Tables 1, 2, https://wwwnc.cdc.gov/EID/article/32/5/25-1926-App1.pdf). Scale bars indicate 100 μm.

and α(2–6)-linked SA (*7*–*10*). However, multiple studies reported contradictory findings on the α(2–6)-linked receptor-binding specificity for different bovine-origin H5N1 isolates (*11*–*13*). One study (*13*) reported that A/bovine/Ohio/B24OSU-432/2024, which has a hemagglutinin amino acid sequence identical to that of virus examined elsewhere (*10*), preferentially binds to avian-type α(2,3) sialoside receptors. Genotypic differences cannot explain the binding affinity discrepancies (Appendix Tables 3, 4), but they might be explained by technical differences in the assays and origins of virus propagation in mammalian cells or embryonated eggs, which affect glycosylation of progeny viruses and hence receptor-binding specificity. Moreover, the binding affinity of H5N1/439 and H5N1/98638 aligned with their high-

Table. Effects of desialylation on virus hemagglutination in a study of ex vivo tropism and replication competence of cattle influenza A(H5N1) genotype B3.13 virus in human bronchus and lung tissue*

	Desialylation treatments			
Influenza virus strain	Untreated	Sialidase S	Sialidase C	Sialidase A
A(H1N1)pdm09				
A/Hong Kong/415742/2009	16	16	0	0
Human A(H5N1)				
A/Hong Kong/483/1997	8	0	0	0
Cattle A(H5N1)				
A/dairy_cow/Ohio/B24OSU-439/2024	8	8	0	0
A/dairy_cow/Texas/98638/2024	8	8	0	0

*Studies performed in 0.5% turkey red blood cells. The reciprocal of hemagglutination titers is noted. Experiments were performed in triplicate and led to identical results. Substrate specificity of sialidases (all Agilent, https://agilent.com) are as follows: α(2,3)-linked sialic acid for sialidase S; α(2,3)- and α(2–6)-linked sialic acids for sialidase C; and α(2,3)-linked, α(2–6)-linked, α(2–8)-linked, and α(2–9)-linked sialic acids for sialidase A.

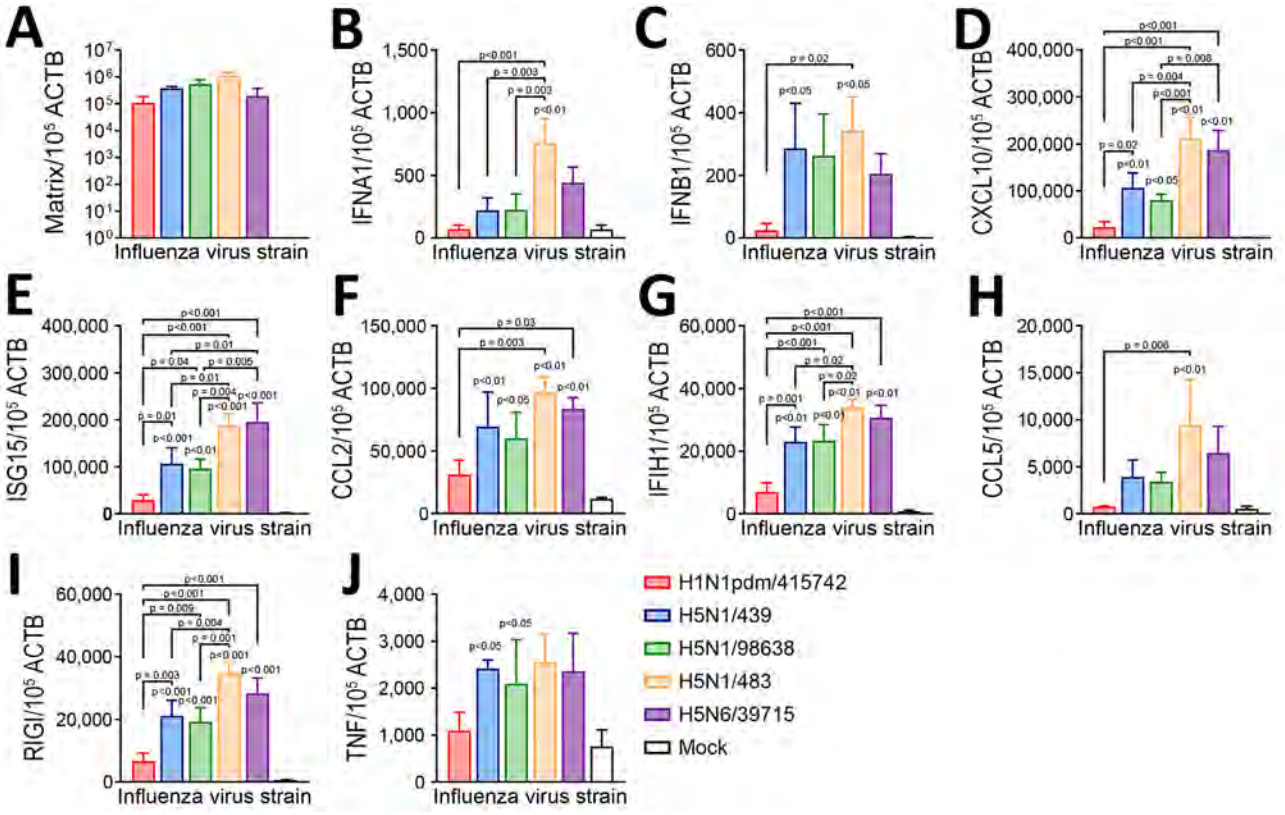

Figure 3. Cytokine and chemokine mRNA expressions in a study of tropism and replication competence of cattle influenza A(H5N1) genotype B3.13 virus in human lung tissue. A) Matrix gene; B) IFNA1; C) IFNB1; D) CXCL10; E) ISG15; F) CCL2; G) IFIH1; H) CCL5; I) RIGI; J) TNF. Expressions measured at 48 hours postinfection. Data were pooled from ≥3 independent experiments. Bars indicate mean, whiskers indicate SD. Statistical significance was calculated by using 1-way analysis of variance with Tukeys posthoc test. Statistical significance is in comparison with mock. ACTB, beta-actin; CCL, C-C motif chemokine ligand; CXCL, C-X-C motif chemokine ligand; IFIH, interferon induced with helicase C domain; IFNA, interferon alpha; IFNB, interferon beta; ISG, interferon-stimulated gene; RIGI, retinoic acid–inducible gene; TNF, tumor necrosis factor.

er replication competences in bronchial tissues than the avian-origin H5N1/483 virus, which predominantly expresses an α(2–6)-linked SA. Those findings suggest that the 2 cattle-origin H5N1 viruses have a higher potential for human-to-human transmission than avian-origin H5N1.

Because illness severity of H5N1 infection is associated with induction of proinflammatory cytokines (*14*), we compared innate immune responses among the 5 viruses in human lung tissue. HPAI H5N1/483 infection induced substantially higher mRNA expressions of interferon alpha 1 (IFNA1), C-X-C motif chemokine ligand 10 (CXCL10), interferon-stimulated gene 15 (ISG15), interferon induced with helicase C domain 1 (IFIH1), and retinoic acid–inducible gene I (RIGI) than cattle-origin H5N1/439 and H5N1/98638. However, we observed a trend of elevated C-C motif chemokine ligand 2 (CCL2) and ligand 5 (CCL5) expression (Figure 3). H5N6/39715 infection induced substantially higher levels of ISG15, CCL2, CXCL10, IFIH1, and RIGI than H1N1pdm/415742, but H5N6/39715 had higher CXCL10 induction than H5N1/98638 and elevated ISG15 compared with H5N1/98638 and H5N1/439.

The 2 cattle-origin H5N1 isolates induced similar immune responses and substantially higher levels of IFNB1, ISG15, tumor necrosis factor, CCL2, CXCL10, IFIH1, and RIGI over the mock-infected tissues (Figure 3). Proinflammatory gene induction by H5N1/439 and H5N1/98638 viruses had higher trends than proinflammatory induction by H1N1pdm/415742, and substantial differences in ISG15, CXCL10, IFIH1, and RIGI. Prior animal studies demonstrated that H5N1/439 and H5N1/98638 and a human isolate were lethal to mice and ferrets (*8*,*11*). However, we detected lower immune response induction and fewer proinflammatory cytokines in human lung tissues, consistent with other studies (*6*), suggesting that those factors might contribute to reduced pathogenicity of cattle-origin H5N1 compared with avian H5N1.

Conclusions

Viral titers and influenza NP-positive cells demonstrated that cattle-origin H5N1/439 and H5N1/98638 strains are better adapted to human upper airway tissues than avian H5N1/483 and have similar replication abilities as H1N1pdm/415742 in human lung explants. The ability to bind α(2–6)-linked SA further indicates a shift of receptor affinities that are more compatible with upper respiratory tissues. Innate immune responses of H5N1/439 and H5N1/98638 viruses in human lung tissue fell between those triggered by H1N1pdm/415742 and H5N1/483 viruses, indicating that cattle H5N1 viruses could pose a human health risk. Defining how these strains infect human tissues and shape immune responses is critical for anticipating outbreaks and reducing zoonotic transmission risks. Because influenza viruses continually evolve across diverse avian and mammalian hosts, sustained research and surveillance remain essential to prevent human infections.

Ethics approval of the use of human tissues was granted by the institutional review board of University of Hong Kong (approval no. UW 20–862).

Acknowledgments

We thank Michael Kuan Yew Hsin and Lucius Kwok Fai Lee for providing human tissues. We also thank Rachel H.H. Ching and Kevin Fung for their technical support.

This work was supported by grants from the InnoHK initiative of the Innovation and Technology Commission of the Hong Kong Special Administrative Region Government and Theme-Based Research Scheme under the University Grants Committee of Hong Kong Special Administrative Region (project no. T11-712/19-N).

About the Author

Dr. Hui is an assistant professor in the School of Public Health at the University of Hong Kong, China. Her research interests include risk assessment, understanding the pathogenesis of emerging respiratory viruses, and the development of therapeutic options for severe influenza diseases and coronavirus infections.

References

1. Peacock TP, Moncla L, Dudas G, VanInsberghe D, Sukhova K, Lloyd-Smith JO, et al. The global H5N1 influenza panzootic in mammals. Nature. 2025;637:304–13. https://doi.org/10.1038/s41586-024-08054-z
2. Mostafa A, Nogales A, Martinez-Sobrido L. Highly pathogenic avian influenza H5N1 in the United States: recent incursions and spillover to cattle. Npj Viruses. 2025;3:54. https://doi.org/10.1038/s44298-025-00138-5
3. Nguyen TQ, Hutter CR, Markin A, Thomas M, Lantz K, Killian ML, et al. Emergence and interstate spread of highly pathogenic avian influenza A(H5N1) in dairy cattle in the United States. Science. 2025;388:eadq0900. https://doi.org/10.1126/science.adq0900
4. Garg S, Reinhart K, Couture A, Kniss K, Davis CT, Kirby MK, et al. Highly pathogenic avian influenza A(H5N1) virus infections in humans. N Engl J Med. 2025;392:843–54. https://doi.org/10.1056/NEJMoa2414610
5. Uyeki TM, Milton S, Abdul Hamid C, Reinoso Webb C, Presley SM, Shetty V, et al. Highly pathogenic avian influenza A(H5N1) virus infection in a dairy farm worker. N Engl J Med. 2024;390:2028–9. https://doi.org/10.1056/NEJMc2405371
6. Flagg M, Williamson BN, Ortiz-Morales JA, Lutterman TR, de Wit E. Comparison of contemporary and historic highly pathogenic avian influenza A(H5N1) virus replication in human lung organoids. Emerg Infect Dis. 2025;31:318–22. https://doi.org/10.3201/eid3102.241147
7. Zhang X, Lam SJ, Chen LL, Fong CH, Chan WM, Ip JD, et al. Avian influenza virus A(H5N1) genotype D1.1 is better adapted to human nasal and airway organoids than genotype B3.13. J Infect Dis. 2026;233:e662–6. https://doi.org/10.1093/infdis/jiaf598
8. Gu C, Maemura T, Guan L, Eisfeld AJ, Biswas A, Kiso M, et al. A human isolate of bovine H5N1 is transmissible and lethal in animal models. Nature. 2024;636:711–8. https://doi.org/10.1038/s41586-024-08254-7
9. Song H, Hao T, Han P, Wang H, Zhang X, Li X, et al. Receptor binding, structure, and tissue tropism of cattle-infecting H5N1 avian influenza virus hemagglutinin. Cell. 2025;188:919–929.e9. https://doi.org/10.1016/j.cell.2025.01.019
10. Eisfeld AJ, Biswas A, Guan L, Gu C, Maemura T, Trifkovic S, et al. Pathogenicity and transmissibility of bovine H5N1 influenza virus. Nature. 2024;633:426–32. https://doi.org/10.1038/s41586-024-07766-6
11. Fabrizio TP, Kandeil A, Harrington WN, Jones JC, Jeevan T, Andreev K, et al. Genotype B3.13 influenza A(H5N1) viruses isolated from dairy cattle demonstrate high virulence in laboratory models, but retain avian virus-like properties. Nat Commun. 2025;16:6771. https://doi.org/10.1038/s41467-025-61757-3
12. Santos JJS, Wang S, McBride R, Adams L, Harvey R, Zhao Y, et al. Bovine H5N1 binds poorly to human-type sialic acid receptors. Nature. 2025;640:E18–20. https://doi.org/10.1038/s41586-025-08821-6
13. Chopra P, Ray SD, Page CK, Shepard JD, Kandeil A, Jeevan T, et al. Receptor-binding specificity of a bovine influenza A virus. Nature. 2025;640:E21–7. https://doi.org/10.1038/s41586-025-08822-5
14. Cheung CY, Poon LL, Lau AS, Luk W, Lau YL, Shortridge KF, et al. Induction of proinflammatory cytokines in human macrophages by influenza A (H5N1) viruses: a mechanism for the unusual severity of human disease? Lancet. 2002;360:1831–7. https://doi.org/10.1016/S0140-6736(02)11772-7

Address for correspondence: Michael C.W. Chan, School of Public Health, Li Ka Shing Faculty of Medicine, University of Hong Kong, 6/F William MW Mong Block, 21 Sasson Rd, Pokfulam, Hong Kong, China; email: mchan@hku.hk

Who is this person and what did he accomplish?

Here is a clue: He first described *Aegyptianella pullorum*, a new genus of piroplasm infecting birds, in 1929.

Who is he?

A. Camillo Golgi
B. Giuseppe Sanarelli
C. Matteo Carpano
D. Adelchi Negri
E. Aldo Castellani

Decide first, then see next page for the answer.

Matteo Carpano, Foundational Veterinary Scientist

Donato Antonio Raele, Nicola Cavaliere

This is a photograph of Matteo Carpano (November 23, 1874–October 31, 1952). Born in Manfredonia, Italy, Matteo Carpano emerged as one of Italy's most influential veterinary scientists, bridging early 20th Century microbiology with principles that today align closely with the One Health paradigm, a holistic approach that recognizes the interdependence of human, animal, and environmental health.

After graduating with top honors in veterinary medicine from the University of Naples, where he received the prestigious Gasparini Prize, Carpano ranked first in the national competition for permanent military veterinary officers. His military career, which culminated in the highest rank of the Corps, was defined not by administrative duties but by an unwavering dedication to laboratory research, teaching, and scientific innovation.

During 1911–1928, Carpano served as director of the Military Veterinary Bacteriology Laboratory in Rome, transforming it into one of the most advanced centers of veterinary microbiology in Europe. His research spanned bacteriology, parasitology, tropical pathology, and emerging infectious diseases, fields in which he consistently demonstrated both scientific rigor and remarkable intuition. The main hall of the laboratory now bears his name as a testament to his enduring impact.

Carpano's early fieldwork took him far beyond Italy. In 1903, he helped establish the Serum-Vaccinogen Institute in Eritrea to combat rinderpest virus. Despite contracting malaria and amoebic dysentery, he continued his investigations, even observing pathogen evolution on his own body. That extreme example of scientific dedication earned him the admiration of Governor Ferdinando Martini. Later, in Cyrenaica, Libya, he identified a bovine infection as a form of coast fever, correctly attributing it to *Theileria annulata*; that discovery contributed to improved diagnostic and control strategies in North Africa (*1*).

Figure. Matteo Carpano, 1930. Source: Historical archives of the city of Manfredonia, Italy.

His most productive international period unfolded in Egypt during 1928–1938, where he served as bacteriologist and chief pathologist for the government of Egypt after winning an international competition. In Cairo, he described anthrax infection in birds (*2*,*3*), identified a new *Corynebacterium* species affecting camels (*4*), and documented new species of ciliated protozoa in horses (*Bertolinella intestinalis*), expanding scientific understanding of pathogens in arid ecosystems (*5*). During those years, he also made

Author affiliation: Istituto Zooprofilattico Sperimentale della Puglia e della Basilicata, Foggia, Italy

DOI: https://doi.org/10.3201/eid3205.260029

the discovery that would forever link his name to parasitology: *Aegyptianella pullorum*, a new genus of piroplasm infecting birds. That finding remains one of the cornerstones of early protozoan taxonomy (*6*).

His contribution to entomology and vectorborne diseases was also substantial, especially in the study of leishmaniasis (*7*). and piroplasmosis (*8*,*9*). Although phlebotomine sand flies (*Sergentomyia antennata*) was originally described in 1912 (*10*), Carpano's 1930 work remains fundamental to the scientific literature because it provided the first detailed morphologic descriptions and illustrations of *S. antennata* sand fly populations in Egypt, which helped to establish local variants and their ecology (*7*). Italy's presence in Eritrea and later in Egypt reflected broader national ambitions for prestige and influence; its professionals were often showcased as embodiments of Italian scientific expertise abroad. Within that context, Carpano was presented internationally as a distinguished technical authority, yet his work remained strictly nonpolitical and was consistently well received by both local communities and governmental authorities.

His career was not without hardship. During his early years in Eritrea, Carpano suffered a devastating personal loss. His wife, Angelina, died in Asmara during an epidemic of typhus, at a time when he himself was deeply engaged in studying infectious diseases affecting both humans and animals in the African colonies. Professional tragedy struck decades later; much of Carpano's extensive archive of work in Africa and the Mediterranean region was destroyed during the 1941 British occupation of Eritrea and subsequent institutional neglect in Italy. Shifting veterinary research priorities led to the loss of his pioneering protozoologic work, which was unjustly dismissed as obsolete. Yet his scientific output remained extraordinary; reports were translated into multiple languages and featured in leading international journals. He contributed extensively to the *Journal of Parasitology* and to the *Treccani Italian Encyclopedia*, further cementing his role as a foundational figure in veterinary science.

Carpano's influence extended far beyond his own discoveries. Working across rural and periurban regions of southern Italy, he was among the first to recognize that zoonotic infections were shaped by environmental pressures, livestock management, and the movement of companion animals. His investigations into vectorborne pathogens revealed ecologic interactions between arthropod vectors and Mediterranean animal populations that had previously gone unnoticed. Although he did not use the term, his work anticipated the modern One Health framework, demonstrating how animal, human, and environmental health are inseparably linked. Those insights profoundly shaped veterinary public health in Italy and Europe. Carpano advocated for coordinated surveillance systems, improved diagnostic laboratories, and interdisciplinary training programs. As an adviser to the Ministry of Health, he helped develop national guidelines for vectorborne disease monitoring and strengthened collaborations between veterinary institutes and public health agencies. Many of those structures, especially the Istituti Zooprofilattici Sperimentali, still operate according to principles he championed.

His commitment to education was equally transformative. Carpano founded regional training centers for veterinarians in Puglia and Basilicata regions and mentored a generation of scientists who would become leaders in epidemiology, entomology, and infectious disease research. His emphasis on field observation, ecologic reasoning, and cross-species disease modeling encouraged young researchers to view zoonoses not as isolated outbreaks but as dynamic processes shaped by climate, human behavior, and animal health. Several of his students later credited him as the defining influence of their scientific careers.

Carpano's legacy continued to evolve long after his death in Rome. He acknowledged critiques that early surveillance programs focused too heavily on livestock while underestimating wildlife ecology or socioeconomic vulnerability. For him, veterinary public health was a discipline that had to evolve continuously, integrating new knowledge and ethics considerations.

Today, research inspired by Carpano continues to advance understanding of vectorborne diseases in Mediterranean environments, including canine leishmaniasis, tickborne rickettsioses, and emerging arboviruses. His work has contributed to improved diagnostic tools, risk-mapping systems, and community-based prevention strategies, strengthening Italy's capacity to respond to zoonotic threats.

Matteo Carpano's life illustrates how veterinary science can shape public health, scientific discovery, and community resilience. His pioneering work, from early bacteriological studies in Africa to modern One Health approaches, demonstrates that understanding zoonotic diseases requires an integrated vision of animals, humans, and the environment. As global health challenges grow increasingly complex, future generations might well regard Carpano not only as a distinguished Italian veterinarian but also as one of the architects of modern interdisciplinary disease prevention.

To honor his memory, the city of Manfredonia named a street after him and erected a bronze bust in the Villa Comunale, sculpted by Luigi Schingo. Yet his most enduring monument remains the scientific legacy that continues to guide veterinary and public health research today.

About the Author

Dr. Raele is a veterinary manager at the Istituto Zooprofilattico Sperimentale della Puglia e della Basilicata. His research focuses on viral diseases, vectors, and zoonosis.

References

1. Carpano M. Localizations of *Trypanosoma theileri* in the internal organs of cattle. Its life cycle [in French]. Ann Parasitol Hum Comp. 1932;10:305–22. https://doi.org/10.1051/parasite/1932104305
2. Carpano M. Anthrax infection in birds. Minist Agric Tech Bull. 1935;153:1–18.
3. Carpano M. Infection of birds with *Bacillus anthracis*. Boll Soc Intern Microbiol Sez Ital. 1935;3:7–9.
4. Carpano M. On a new *Corynebacterium* in the lymphatic lesions of the camel (*Corynebacterium dermonecroticum* n. sp. [in Italian]. Ann Ig. 1934;44:1–15.
5. Carpano M. On a new infusorian of the digestive apparatus of equines *Bertolinella intestinalis* n. g., n. sp. [in Italian]. Riv Parassitol. 1941;5:45–52.
6. Carpano M. Piroplasmosis in Egyptian fowls (*Egyptianella pullorum*). Bull Minist Agric Egypt. 1929;1:1–7.
7. Carpano M. On the different species of sandflies of Egypt [in Italian]. Ann Ig. 1930;40:647–59.
8. Carpano M. On the piroplasmids of chelonians and on a new species found in *Nuttallia guglielmi* turtles [in Italian]. Riv Parassitol. 1939;3:267–76.
9. Carpano M. On the piroplasmosis of carnivores and on a new piroplasm of feline *Babesiella felis* in the puma (*Felis concolor*) [in French]. Bull Minist Agric Cairo. 1934;137:1–5.
10. Newstead R. Notes on Phlebotomus, with descriptions of new species—Part I. Bull Entomol Res. 1912;3:361–7.

Address for correspondence: Donato Raele, Istituto Zooprofilattico Sperimentale della Puglia e della Basilicata, Via Manfredonia 20, Foggia 71100, Italy; email: donatoantonio.raele@izspb.it

etymologia revisited

Tularemia

[t-lə-rē-mē-ə]

An infectious, plaguelike, zoonotic disease caused by the bacillus *Francisella tularensis*. The agent was named after Tulare County, California, where the agent was first isolated in 1910, and Edward Francis, an Officer of the US Public Health Service, who investigated the disease. Dr. Francis first contracted deer fly fever from a patient he visited in Utah in the early 1900s. He kept a careful record of his 3-month illness and later discovered that a single attack confers permanent immunity. He was exposed to the bacterium for 16 years and even deliberately reinfected himself 4 times.

Tularemia occurs throughout North America, many parts of Europe, the former Soviet Union, the People's Republic of China, and Japan, primarily in rabbits, rodents, and humans. The disease is transmitted by the bites of deerflies, fleas, and ticks; by contact with contaminated animals; and by ingestion of contaminated food or water.

Reference

Dorland's illustrated medical dictionary, 31st edition. Philadelphia: Saunders; 2007; Benenson AS, editor. Control of communicable diseases manual. Washington: American Public Health Association; 1995; https://www.whonamedit.com

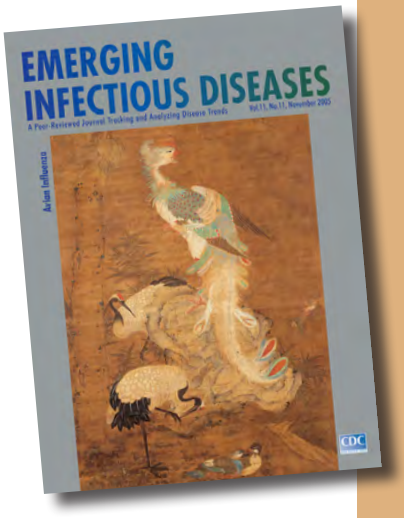

Originally published in November 2007

https://wwwnc.cdc.gov/eid/article/13/11/e1-1311_article

Serial Interval and Intervention Efficiency in Pertussis Outbreak, South Korea, 2024

Andrei R. Akhmetzhanov, Bianca de Padua, Jonathan Dushoff

Author affiliations: College of Public Health, National Taiwan University, Taipei, Taiwan (A.R. Akhmetzhanov, B. de Padua); McMaster University, Hamilton, Ontario, Canada (J. Dushoff)

DOI: https://doi.org/10.3201/eid3205.251304

We estimated an unmitigated mean serial interval during a school-based pertussis outbreak in South Korea at 14.7 (95% credible interval 9.0–27.4) days, comparable with previous estimates. Public health interventions reduced the effective reproduction number by 65% (95% credible interval 26%–88%), which likely brought it to <1 and contributed to curbing the outbreak.

Pertussis cases have increased worldwide recently, driven by waning vaccine immunity, disruptions to vaccination programs, and a reduction in transmission during the COVID-19 pandemic (*1*,*2*). In addition, there is an increase in reports of *B. pertussis* strains resistant to macrolide antimicrobial drugs, a first-line treatment, in the Western Pacific region since 2008, and specifically in Japan during 2024–2025 (*3*). As of mid-2025, Japan reported a 10-fold increase in pertussis cases compared with 2024, and South Korea reported a >20-fold increase.

The natural history of pertussis infections remains unclear, and more accurate estimates of epidemiologic time intervals are urgently needed, especially the serial interval (SI), which is the time interval between symptom onset in those spreading the infection and those being infected. In a recent investigation of a school-based pertussis outbreak in South Korea in 2024 (*4*), the mean SI was estimated to be 9.5 days, which closely aligned with another recent report (5) but greatly differed from a previous estimate of 20.5 days from the Netherlands (*6*). Although differences in case definitions could contribute to this discrepancy, the estimated observed SI was affected by public health interventions such as case isolation. It is necessary to estimate a counterfactual unmitigated SI for the future planning of outbreak response, because it more accurately reflects the natural history of the pathogen.

To estimate the unmitigated SI, we extracted the data from the previously published report (*4*) and built a latent transmission model to account for the effect of intervention (Appendix, http://wwwnc.cdc.gov/EID/article/32/5/25-1304-App1.pdf). Data were publicly available in the original publication, and no specific permission was required. During the outbreak, March–June 2024, the major intervention on April 17, 2024, followed a test-trace-isolate approach with screening of all suspected cases (*4*). The isolation of confirmed cases and prophylactic measures provided to close contacts have a dual effect on the transmission dynamics; they shorten the SI and reduces the reproduction number by lowering the contact rate (*7*).

We then fitted the transmission-pair data with a model that incorporated 2 consequences of intervention: a shortening of the SI distribution for transmissions in the postintervention period compared with the preintervention period, and a reduction in the mean number of secondary cases generated by a primary case in the postintervention period. The effect of the intervention was quantified by a transmission-reduction parameter, ε, which ranged from 0 (no effect of isolation) to 1 (no transmission after isolation). Following the parameters of the original study (*4*), we modeled the number of secondary cases with a negative binomial distribution. We assumed the overdispersion parameter was the same in both periods. We termed the resulting SI distribution (corresponding to preintervention dynamics) the unmitigated SI. We estimated the observed SI distribution for comparison when no effect of intervention was incorporated.

Statistical inference yielded a mean unmitigated SI of 14.7 days (95% credible interval [CrI] 9.0–27.4 days), a broader distribution than the observed SI (mean 10.4 days; 95% CrI 7.6–14.6 days) (Figure 1). The medians of both SIs were <10 days (9.9 days and 7.9 days); however, the unmitigated distribution had a much longer tail (95th percentile, 42.8 days). The unmitigated distribution we found is similar to that estimated in a study from the Netherlands (*6*), with the probability mass slightly shifted toward shorter time intervals. The Netherlands study recruited families of infants <6 months of age hospitalized with pertussis, potentially inducing selection bias toward more severe cases, which could explain the shift toward shorter intervals in our estimate.

We estimated a preintervention reproduction number of 1.4 (95% CrI 0.65–2.6) and an intervention efficiency of 65% (95% CrI 26%–88%), which represents the relative reduction in per case transmissibility after the intervention. The postintervention reproduction number was <1, at 0.45 (95% CrI 0.15–1.01). We illustrated the temporal variation in forward-

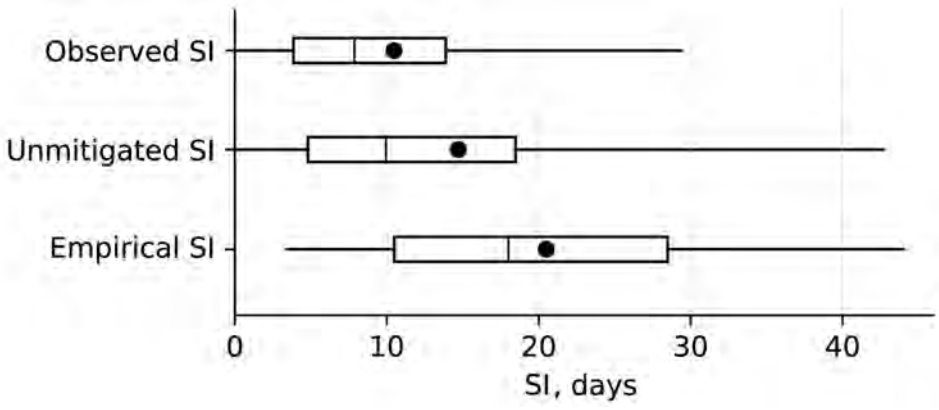

Figure 1. Comparison of estimated SI distributions from a school-based pertussis outbreak in South Korea, 2024. Observed SI from the original study on which we based our study (*4*) is shown compared to the unmitigated SI inferred after accounting for public health interventions and empirical SI from a household survey conducted in the Netherlands (*6*). Each boxplot displays the interquartile range (box tops and bottoms), 95% credible interval (whiskers), median (vertical line), and mean (solid circle). SI, serial interval.

looking reproduction number and mean generation time (mean SI) (*8*) (Figure 2).

Our findings suggest that isolation likely contributed to curbing the pertussis outbreak. The previous study mentioned that the delay between symptom onset and confirmation leading to case-isolation was ≈6 days on average and 25% of cases were confirmed after 20 days (*4*). Those results imply the isolation of cases was not immediate and that larger values of intervention efficiency could be achieved with shorter delays. Nevertheless, the effect of isolation cannot be disentangled from other supplementary interventions such as active case finding and targeted prevention for close contacts of case-patients. Because of the long unmitigated SI, a response relying solely on symptom-based isolation might be insufficient,

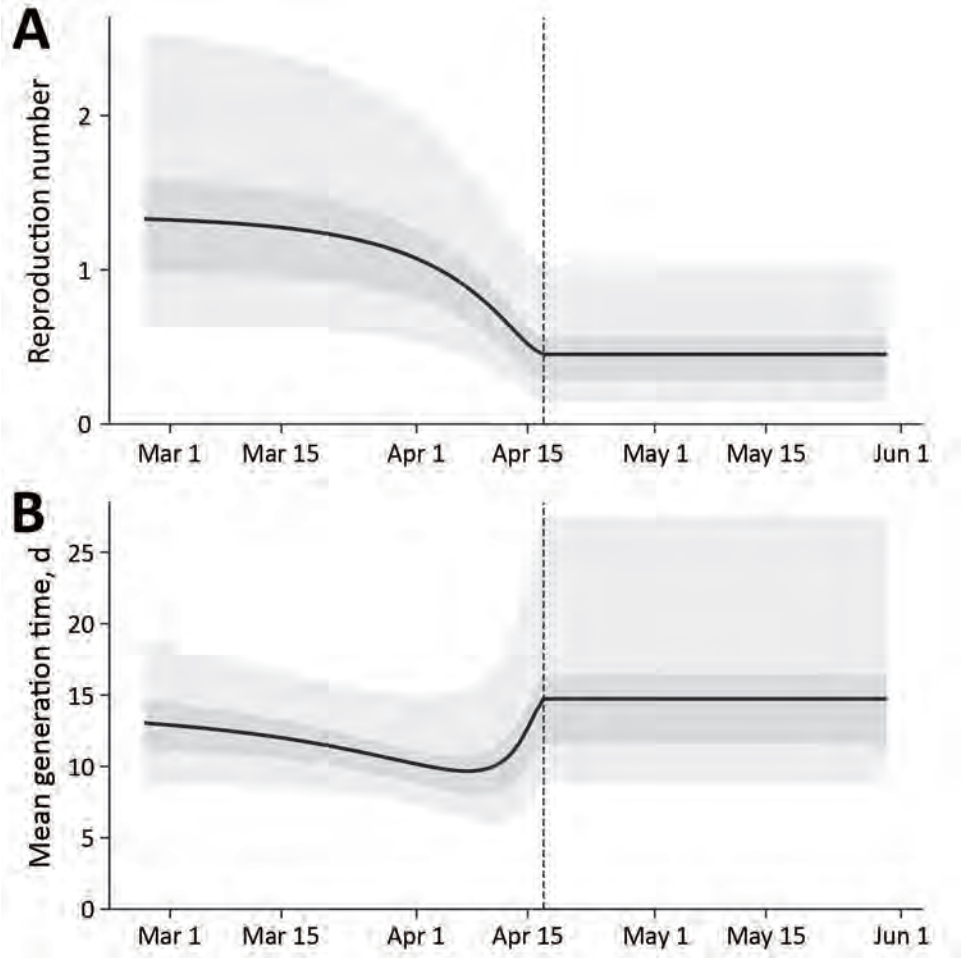

Figure 2. Temporal variation in the forward-looking reproduction number and the mean generation time across the outbreak period of a school-based pertussis outbreak in South Korea in 2024. A) Graph of the forward-looking reproduction number, defined as the average number of secondary infections generated by a case infected on a given date, accounting for interventions throughout their infectious period. B) Graph of the mean generation time, defined as the average interval between the infection of a primary case and the infections they cause. Vertical dashed line indicates the start of the main intervention (2024 Apr 17). Solid lines represent posterior means; light and dark shaded areas indicate 95% and 50% (interquartile) credible intervals.

which implies that rapid contact-tracing and preemptive testing are likely required to efficiently control future outbreaks.

This study was supported by a grant from the National Science and Technology Council, Taiwan (grant no. NSTC 113-2314-B-002-181-MY3).

About the Author

Dr. Akhmetzhanov is an associate professor at the College of Public Health, National Taiwan University, Taiwan. His research interests include epidemiology and prevention of infectious disease outbreaks.

References

1. Dyer O. Whooping cough: cases soar in US. BMJ. 2025;389:r704. https://doi.org/10.1136/bmj.r704
2. Wang S, Zhang S, Liu J. Resurgence of pertussis: epidemiological trends, contributing factors, challenges, and recommendations for vaccination and surveillance. Hum Vaccin Immunother. 2025;21:2513729. https://doi.org/10.1080/21645515.2025.2513729
3. Japan Institute for Health Security, National Institute of Infectious Diseases. Risk assessment: pertussis outbreak situation in Japan. 2025 [cited 2025 Jul 30]. https://id-info.jihs.go.jp/diseases/ha/pertussis/020/250422_JIHS_Pertussis_en.pdf
4. Cho UJ, Cho S, Lee H, Kang SK, Kim BI, Nam Y, et al. Transmission dynamics and parameters for pertussis during school-based outbreak, South Korea, 2024. Emerg Infect Dis. 2025;31:1330–6. https://doi.org/10.3201/eid3107.241643
5. Su Y, Dai R, Luo F, Zheng S, Hua C, He H, et al. Household transmission patterns and serial interval of pertussis in China. J Infect. 2024;89:106322. https://doi.org/10.1016/j.jinf.2024.106322
6. Te Beest DE, Henderson D, van der Maas NA, de Greeff SC, Wallinga J, Mooi FR, et al. Estimation of the serial interval of pertussis in Dutch households. Epidemics. 2014;7:1–6. https://doi.org/10.1016/j.epidem.2014.02.001
7. Chan YH, Nishiura H. Estimating the protective effect of case isolation with transmission tree reconstruction during the Ebola outbreak in Nigeria, 2014. J R Soc Interface. 2020;17:20200498. https://doi.org/10.1098/rsif.2020.0498
8. Park SW, Sun K, Champredon D, Li M, Bolker BM, Earn DJD, et al. Forward-looking serial intervals correctly link epidemic growth to reproduction numbers. Proc Natl Acad Sci U S A. 2021;118:e2011548118. https://doi.org/10.1073/pnas.2011548118

Address for correspondence: Andrei R. Akhmetzhanov, National Taiwan University; No. 17 Xuzhou Rd, Zhongzheng District, Taipei 10055, Taiwan; email: akhmetzhanov@ntu.edu.tw

Herpes Simplex Virus 1 in Trigeminal Ganglia of Trafficked Neotropical Primates, Peru, 2024

Fernando Vilchez-Delgado, Lin Zhou, Shannon O'Connor, Renato Colan, Leticia Escobar-Mendoza, A. Patricia Mendoza, Bruno M. Ghersi, Roy Andrade, Michael Talledo-Albújar, Marieke H. Rosenbaum

Author affiliations: Cummings School of Veterinary Medicine, North Grafton, Massachusetts, USA (F. Vilchez-Delgado, L. Zhou, S. O'Connor, B.M. Ghersi, M.H. Rosenbaum); Universidad Peruana Cayetano Heredia, San Martin de Porres, Lima, Peru (F. Vilchez-Delgado, L. Escobar-Mendoza, R. Andrade, M. Talledo-Albujar); National Forest and Wildlife Service, Lima (R. Colan); Washington University–St. Louis, St. Louis, Missouri, USA (A.P. Mendoza)

DOI: http://doi.org/10.3201/eid3205.251408

We detected herpes simplex virus 1 in the trigeminal ganglia of trafficked Neotropical primates (1 *Aotus azarai*; 3 *Sapajus macrocephalus*) in Peru. Tests also revealed *Saimiriine alphaherpesvirus* 1 in the trigeminal ganglia of 2 *Saimiri* sp. monkeys. Our findings suggest latency and raise concerns about diagnostic standards, viral reactivation, and spillover risks.

Illegal trafficking operations have lead to the extraction of thousands of Neotropical primates (NP) from the Peruvian Amazon, exposing them to humans and other domestic and wild species, creating opportunities for bidirectional zoonotic disease transmission and spillover (*1*). Among humans, herpes simplex virus 1 (HSV-1) infects around 67% of adults globally (*2*) and establishes lifelong latency in the trigeminal ganglia (TG) (*3*). HSV-1 infections in NP can cause mild or severe disease, sometimes leading to ulcerative lesions and neurologic impairment (*4*). Questions remain, however, regarding the ability of HSV-1 to establish latency in NP after natural infection.

During latency in humans, HSV-1 lytic gene expression is suppressed, but the latency-associated transcripts and associated microRNAs remain transcriptionally active (*5*). As a result, production of infectious viral particles ceases (*6*), and diagnostic approaches based on PCR testing of peripheral tissues, blood, or oral swab samples fail to detect latently infected persons. Trafficked NP with undetected HSV-1 infections might be placed into

Table. Herpesvirus detection in various organs and sample sites from trafficked Neotropical primates with *Alphaherpesvirus*-positive trigeminal ganglia, Peru, 2024

		Sample type						
Animal ID	Species	Trigeminal ganglia	Oral swab	Heart	Liver	Spleen	Kidney	Salivary glands
NE-004-24	*Sapajus*	HSV-1	SapLCV1	SapLCV1	NR	NR	NR	SapCMV1
NE-015-24	*Sapajus*	HSV-1	NR	NR	NR	NR	NR	NR
NE-020-24	*Aotus*	HSV-1	NR	NR	NR	HSV-1	HSV-1	NR
NE-033-24	*Sapajus*	HSV-1	NR	NR	NR	HSV-1	NR	NR
NE-011-24	*Saimiri*	SaHV-1	SsciLCV2	SsciLCV2	NR	NR	NR	SsciCMV1
NE-021-24	*Saimiri*	SaHV-1	SbolCMV1	SsciLCV2	NR	SsciLCV2	NR	SbolCMV1

*ID, identification; HSV-1, human simplexvirus 1; NR, negative results; SaHV-1, *Saimiriine* herpesvirus 1; SapCMV1, *Sapajus apella* cytomegalovirus 1; SapLCV1, *Sapajus apella* lymphocryptovirus 1; SbolCMV1, *Saimiri boliviensis* cytomegalovirus 1; SsciCMV1, *Saimiri sciureus* cytomegalovirus 1; SsciLCV2, *Saimiri sciureus* lymphocryptovirus 2.

rehabilitation centers and possibly released into wild populations, posing a threat to primate health and conservation (*7*,*8*).

To assess whether HSV-1 establishes latency in NP, we investigated the presence of viral DNA in the TG (and its absence in other tissues) in 37 trafficked NP carcasses representing 7 species (Appendix Table 1, https://wwwnc.cdc.gov/EID/article/32/5/25-1408-App1.pdf) in Peru. On gross examination, we observed no lesions suggestive of active HSV-1 infection, such as oral mucosal ulcers, and we classified all animals as asymptomatic on the basis of macroscopic findings alone.

We aseptically collected oral swab samples as well as TG, heart, liver, spleen, kidney, and salivary gland samples and preserved all samples in RNAlater (Thermo Fisher Scientific, https://www.thermofisher.com). When fresh carcasses were available, we preserved TG in 10% formalin for histologic confirmation (Appendix Figures 1, 2). In extracting DNA, we used a nested panherpesvirus PCR, targeting a 215–315 bp region of the DNA polymerase gene, as previously described (*9*) (Appendix). TG samples were positive for herpesvirus DNA (Appendix Table 2) in 13 (35%) NP. Sequencing results revealed *Alphaherpesvirinae* DNA from 6 of the samples and *Gammaherpesvirinae* DNA from the other 7 samples.

We identified HSV-1 in the TG of 4 (11%) NP sampled: 1 *Aotus azarai* monkey and 3 *Sapajus macrocephalus* monkey. We noted no HSV-1 in any of the 35 oral swab samples we analyzed, including those from TG-positive primates. In 2 of the 4 NP with HSV-1–positive TG, testing also revealed HSV-1 in the spleen, kidney, or both (Table). We observed *Saimiriine herpesvirus* 1, another alphaherpesvirus species, in the TG of 2 *Saimiri* monkeys.

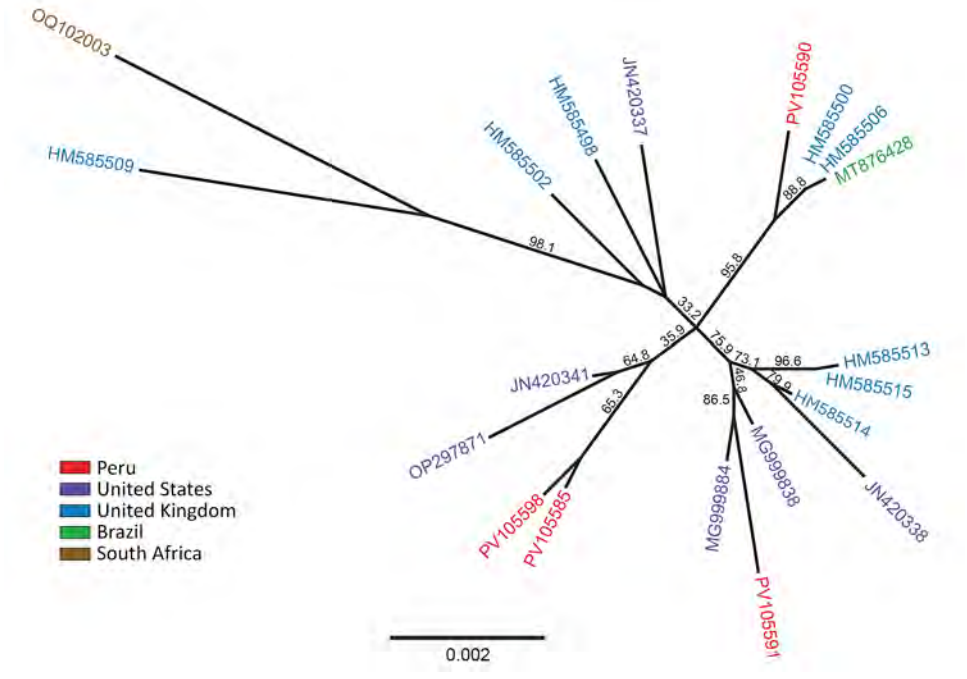

Figure. Maximum-likelihood phylogeny of herpes simplex virus 1 (HSV-1) created for study of HSV-1 in trigeminal ganglia of trafficked neotropical primates, Peru, 2024. Tree constructed from ≈4 kb of the UL30 DNA polymerase gene, applying the general time reversible substitution model with 1,000 bootstrap replicates. Red text indicates full-length HSV-1 DNA polymerase gene sequences detected in trigeminal ganglia of 4 primates from Peru. For comparison, we selected 16 additional reference sequences from GenBank (accession numbers provided) to represent diverse geographic regions worldwide. Phylogenetic analysis suggests a genetically diverse origin of HSV-1 infections in the primates evaluated, likely derived from genetically distinct introductions (spillovers). Sequences deposited in GenBank (accession nos. PV105585 [primate NE-004-24], PV105590 [primate NE-015-24], PV105591 [primate NE-020-24], and PV105598 [primate NE-033-24]).

Phylogenetic analysis of the full HSV-1 DNA polymerase gene (≈4 kb) revealed that 2 sequences (from primates NE-004-24 and NE-033-24) share a recent common ancestor. The remaining sequences are distributed across different branches of the phylogenetic tree, suggesting the infections originated from genetically distinct introductions (spillovers) rather than from a localized outbreak (Figure).

Multiorgan analysis revealed co-infections with 3 distinct herpesviruses, representing all herpesvirus subfamilies (*Alphaherpesvirinae*, *Betaherpesvirinae*, and *Gammaherpesvirinae*), in 3 TG-positive NP (Table). We noted cytomegaloviruses in the salivary glands of 3 of the TG-positive NP, as well as lymphocryptoviruses in the heart tissue, spleen, or both of those same 3 primates. We did not assess the herpesvirus status of organs from TG-negative NP.

Our findings suggest that, as in the case of human infections, HSV-1 may naturally establish latency in the TG of some NP. The detection of HSV-1 DNA in the spleen and kidney does not rule out latency, because latency also has been documented in nonneuronal cells, including neutrophils and B and T lymphocytes (*10*). Confirming true latency in NP would require herpesvirus reactivation studies and RNA sequencing from positive TG.

None of the NP with HSV-1–positive TG showed macroscopic lesions compatible with HSV-1 disease, and we detected no viral DNA in oral swabs. Those findings highlight a critical diagnostic challenge in detecting latent HSV-1 infections in live NP. Oral swab samples can be collected from living primates with minimal distress, but TG can only be obtained postmortem, precluding their use in health evaluations before releasing animals into the wild. Whether latently infected NP can undergo viral reactivation under natural stress conditions and transmit HSV-1 to humans or naive NP remains unknown.

In conclusion, we detected HSV-1 and *Saimiriine herpesvirus* 1 in the TG of NP, consistent with latency. Our findings underscore the relevance of TG as a target tissue for future research and broaden our understanding of the diversity and latency of alphaherpesviruses in NP. Our study also highlights the need for less invasive methods, such as specific antibody profiles or T-cell–specific biomarkers of latency, to identify latent herpesvirus infections in live NP. Identifying such infections can help mitigate potential spillover to other primates, including humans.

Acknowledgments

Thank you to Letícia Neves Ribeiro, Jaide Sierra Aroni, Diego Hurtado de Mendoza, Jhonathan Bazalar, Verónika Merino, volunteers, and members of the Unidad de Epidemiología Molecular IMTAvH-UPCH, Gobierno Regional de Madre de Dios, and the School of Veterinary Medicine and Animal Heath at Universidad Peruana Cayetano Heredia for offering their support and guidance.

This study was supported by funding from the Cummings School of Veterinary Medicine Roome International Fellowship and the Susan Westmorland Primate Conservation Fund. Funds were also provided by the American Association of Zoo Veterinarians' Wild Animal Health Fund (proposal 2024 no. 54) and by Morris Animal Foundation (grant ID no. D25ZO-424).

About the Author

Dr. Vilchez-Delgado is a doctor of veterinary medicine and 4th-year PhD student at the Cummings School of Veterinary Medicine, Tufts University, North Grafton, Massachusetts. His research focuses on the molecular diversity and cross-species transmission dynamics of herpesviruses in Neotropical primates rescued from the illegal wildlife trade in Peru.

References

1. Shanee N, Mendoza AP, Shanee S. Diagnostic overview of the illegal trade in primates and law enforcement in Peru. Am J Primatol. 2017;79:e22516. https://doi.org/10.1002/ajp.22516
2. Looker KJ, Magaret AS, May MT, Turner KME, Vickerman P, Gottlieb SL, et al. Global and regional estimates of prevalent and incident herpes simplex virus type 1 infections in 2012. PLoS One. 2015;10:e0140765. https://doi.org/10.1371/journal.pone.0140765
3. Theil D, Derfuss T, Paripovic I, Herberger S, Meinl E, Schueler O, et al. Latent herpesvirus infection in human trigeminal ganglia causes chronic immune response. Am J Pathol. 2003;163:2179–84. https://doi.org/10.1016/S0002-9440(10)63575-4
4. Gozalo AS, Montoya EJ, Weller RE. Dyscoria associated with herpesvirus infection in owl monkeys (*Aotus nancymae*). J Am Assoc Lab Anim Sci. 2008;47:68–71.
5. Roizman B, Zhou G, Du T. Checkpoints in productive and latent infections with herpes simplex virus 1: conceptualization of the issues. J Neurovirol. 2011;17:512–7. https://doi.org/10.1007/s13365-011-0058-x
6. Fan S, Cai H, Xu X, Feng M, Wang L, Liao Y, et al. The characteristics of herpes simplex virus type 1 infection in rhesus macaques and the associated pathological features. Viruses. 2017;9:26. https://doi.org/10.3390/v9020026
7. Mendoza AP, Vilchez Delgado F. Infectious diseases and primate trafficking in Peruvian wet markets. In: Miller M, Lamberski N, Calle P, editors. Fowler's zoo and wild animal medicine current therapy. New York, NY: Elsevier; 2023. https://doi.org/10.1016/B978-0-323-82852-9.00016-2
8. Mitman S, Rosenbaum M, Bello R, Knapp C, Nutter F, Mendoza P. Challenges to IUCN guideline implementation in the rehabilitation and release of trafficked primates in Peru. Primate Conserv. 2021;35:87–102. PMID: 35250169

9. VanDevanter DR, Warrener P, Bennett L, Schultz ER, Coulter S, Garber RL, et al. Detection and analysis of diverse herpesviral species by consensus primer PCR. J Clin Microbiol. 1996;34:1666–71. https://doi.org/10.1128/jcm.34.7.1666-1671.1996
10. Wang S, Song X, Rajewski A, Santiskulvong C, Ghiasi H. Stacking the odds: Multiple sites for HSV-1 latency. Sci Adv. 2023;9:eadf4904. https://doi.org/10.1126/sciadv.adf4904

Address for correspondence: Fernando Vilchez-Delgado, Cummings School of Veterinary Medicine, Tufts University, 200 Westboro Rd, North Grafton, MA 01527, USA; email: fernando_javier.vilchez_delgado@tufts.edu

Probable *Bartonella clarridgeiae* Prosthetic Valve Endocarditis and Aortic Root Abscess, Australia, 2020

Mark Cribb, Sarah Coghill

Author affiliation: Lismore Base Hospital, Northern New South Wales Health District, Lismore, New South Wales, Australia

DOI: https://doi.org/10.3201/eid3205.251558

We describe a case of endocarditis and aortic root abscess caused by *Bartonella clarridgeiae* bacteria in a patient in Australia. The patient initially sought care for leg pain and was found to have bilateral tibioperoneal trunk mycotic aneurysms. 16S rRNA PCR on excised aneurysm tissue identified the cause as *B. clarridgeiae*.

Bartonella species are gram-negative, fastidious, facultative intracellular bacteria (*1*). They are a cause of blood culture–negative endocarditis, infective endocarditis with negative blood cultures resulting from antibiotic exposure or fastidious pathogens (*2*). *B. clarridgeiae* is an emerging pathogen in the genus, first identified in 1995 and attributed as a human pathogen in 1997 (*3*,*4*). Tibioperoneal trunk (TPT) aneurysms are a rare clinical phenomenon; causes include trauma, vasculitis, and infective endocarditis or mycotic aneurysm (*5*). We describe a case of bilateral TPT aneurysms, prosthetic valve infective endocarditis, and aortic root abscess in a patient in Australia in 2020 that was caused by *B. clarridgeiae*, identified on 16S ribosomal RNA of aneurysm tissue samples.

A man in his 80s sought care at a local emergency department for pain in his left calf for 1 month. He had aortic stenosis requiring a transcatheter aortic valve implantation 2 years earlier. He had sought care several times over the previous 8 months with calf pain, chest pain, and lethargy. On examination, he was noted to have a swollen and tender left calf, a pansystolic murmur, 2 splinter hemorrhages, and a temperature of 37.9°C. He initially received intravenous cefazolin for possible cellulitis, later changed to amoxicillin/clavulanate.

Computed tomography (CT) angiogram demonstrated a hematoma in the left calf associated with a TPT pseudoaneurysm and a right TPT thrombus. The left TPT aneurysm was surgically repaired. Transesophageal echocardiography (TOE) showed no valvular incompetence or vegetations.

CT positron emission tomography scan demonstrated focal intense fluorodeoxyglucose activity at the transcatheter aortic valve implantation (SUVmax = 5.9) (Figure, panel A), postsurgical changes involving the left lower leg (Figure, panel B), and focal moderate activity at the right tibioperoneal trunk, indicating another mycotic aneurysm. We reviewed TOE findings again and identified an echolucent space at the sinus of Valsalva, consistent with an aortic root abscess. Therapy was switched to intravenous ceftriaxone and vancomycin. The patient was deemed not to be a cardiac surgery candidate.

Four sets of blood cultures were negative for bacteremia. Operative tissue culture tested negative for bacterial growth using standard media; we sent the tissue samples for 16S rRNA PCR. We conducted serologic testing for *Brucella* spp., *Coxiella burnettii*, syphilis, and HIV. We tested for *Bartonella* spp. using FOCUS Diagnostics Indirect Immunofluorescence Assay IgG kit for *B. henslae* and *B. quintana* IgG (http://focusdiagnostics.in). 16S rRNA PCR detected *B. clarridgeiae* DNA in operative tissue samples. Serology results for *B. henslae* bacteria were strongly positive (IgG ≥1:2,048 [<128]); all other serology results, including *B. quintana* testing, were negative. We performed PCR testing of blood with primers and probe targeting a conserved portion of the citrate synthase gene; results for *Bartonella* spp. DNA were negative.

We switched treatment to intravenous gentamicin with oral doxycycline (100 mg 2×/d). The patient experienced ongoing fevers and elevated C-reactive protein levels. Because of concern for treatment failure, we added oral ciprofloxacin for 6 weeks; repeated TOE showed stable changes. After 6 weeks, the patient continued oral doxycycline (100 mg 2×/d) for suppression; he remained well at a 2-year follow-up visit.

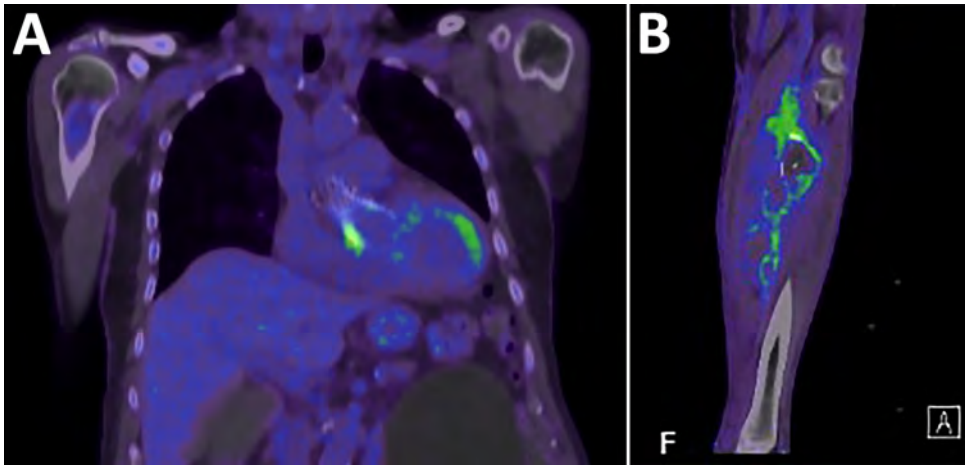

Figure. Positron emission tomography/computed tomography images from study of patient with *Bartonella clarridgeiae* prosthetic-valve endocarditis and aortic root abscess, Australia, 2020. A) Fluorodeoxyglucose activity at ventricular end of the transcatheter aortic valve implantation; B) repaired tibioperoneal trunk aneurysm in patient's left leg.

Early reports for bartonellosis associated *B. clarridgeiae* with cat-scratch disease (*6*). Cats are a reservoir for *B. clarridgeiae* and *B. henslae* (*4*,*7*); the patient we report kept multiple cats at home, although he recalled no preceding cat bite or scratch. A case of endocarditis and aortic root abscess caused by *B. clarridgeiae* diagnosed in 2019 was treated successfully with ceftriaxone, doxycycline, and heart valve replacement (*7*).

Serology has traditionally been a method for diagnosing bartonellosis; however, cross-reactivity can occur (*8*), as in this case. Molecular diagnostics are a valuable tool in accurate diagnosis of *Bartonella* endocarditis; emergence of pathogens such as *B. clarridgeiae* may be related to their increasing use (*1*,*8*). A limitation of our report is that the average nucleotide identity percentage is unavailable to confirm distinction between *Bartonella* species.

At the time of this case in 2020, the recommended treatment for *Bartonella* endocarditis was gentamicin for 2 weeks with doxycycline for 6 weeks (*3*). Because *Bartonella* endocarditis has been associated with infection-related glomerulonephritis (*9*), newer recommendations suggest doxycycline or azithromycin for 12 weeks and rifampin for 6 weeks (*2*). Other suggested therapies for *Bartonella* infections have included trimethoprim/sulfamethoxazole and ciprofloxacin (*3*). Because of concerns for treatment failure in our patient, we added ciprofloxacin empirically, without strong evidence available to guide treatment.

Delay in diagnosis of endocarditis is an unfortunate theme in mycotic aneurysm with low-medium virulence organisms (*10*). Our patient had a protracted manifestation over months, with nonspecific symptoms before diagnosis. This case reinforces the need for suspicion of endocarditis in patients seeking care for TPT aneurysms and highlights the pathogenicity of *B. clarridgeiae* bacteria in this context. Suspicion of and investigation for causes of blood culture–negative endocarditis including *Bartonella* spp. is therefore warranted in patients with TPT aneurysms, should initial microbiologic investigations be negative. Molecular diagnostics including 16S rRNA PCR can aid diagnosis.

About the Author

Dr. Cribb is a resident doctor at Lismore Base Hospital in New South Wales, Australia. His primary interests are in infectious diseases and medical microbiology.

References

1. McCormick DW, Rassoulian-Barrett SL, Hoogestraat DR, Salipante SJ, SenGupta D, Dietrich EA, et al. *Bartonella* spp. infections identified by molecular methods, United States. Emerg Infect Dis. 2023;29:467–76. https://doi.org/10.3201/eid2903.221223
2. DeSimone DC, Garrigos ZE, Marx GE, Tattevin P, Hasse B, McCormick DW, et al.; American Heart Association Council on Lifelong Congenital Heart Disease and Heart Health in the Young; Council on Clinical Cardiology; and Council on Quality of Care and Outcomes Research. Blood culture–negative endocarditis: a scientific statement from the American Heart Association. J Am Heart Assoc. 2025; 14:e040218. https://doi.org/10.1161/JAHA.124.040218
3. Rolain JM, Brouqui P, Koehler JE, Maguina C, Dolan MJ, Raoult D. Recommendations for treatment of human infections caused by *Bartonella* species. Antimicrob Agents Chemother. 2004;48:1921–33. https://doi.org/10.1128/AAC.48.6.1921-1933.2004
4. Kordick DL, Hilyard EJ, Hadfield TL, Wilson KH, Steigerwalt AG, Brenner DJ, et al. *Bartonella clarridgeiae*, a newly recognized zoonotic pathogen causing inoculation papules, fever, and lymphadenopathy (cat scratch disease). J Clin Microbiol. 1997;35:1813–8. https://doi.org/10.1128/jcm.35.7.1813-1818.1997
5. Akers DL Jr, Fowl RJ, Kempczinski RF. Mycotic aneurysm of the tibioperoneal trunk: case report and review of the literature. J Vasc Surg. 1992;16:71–4. https://doi.org/10.1016/0741-5214(92)90420-D

6. Logan JMJ, Hall JL, Chalker VJ, O'Connell B, Birtles RJ. *Bartonella clarridgeiae* infection in a patient with aortic root abscess and endocarditis. Access Microbiol. 2019;1:e000064. https://doi.org/10.1099/acmi.0.000064
7. Margileth AM, Baehren DF. Chest-wall abscess due to cat-scratch disease (CSD) in an adult with antibodies to *Bartonella clarridgeiae*: case report and review of the thoracopulmonary manifestations of CSD. Clin Infect Dis. 1998;27:353–7. https://doi.org/10.1086/514671
8. Pinheiro Santos J, Sousa R, Santos A, Laranjeira Santos Á., Fragata J. Infective endocarditis due to *Bartonella quintana* in a patient with biological aortic prosthesis. Port J Card Thorac Vasc Surg. 2021;26:59–61. https://doi.org/10.48729/pjctvs.154
9. Shrestha NK, Kanyo EC, Nakhoul GN, Herlitz LC, Gordon SM. Association between causative pathogen and occurrence of infection-related glomerulonephritis in infective endocarditis. Clin Infect Dis. 2024;78:1551–3. https://doi.org/10.1093/cid/ciae213
10. González I, Sarriá C, López J, Vilacosta I, San Román A, Olmos C, et al. Symptomatic peripheral mycotic aneurysms due to infective endocarditis: a contemporary profile. Medicine (Baltimore). 2014;93:42–52. https://doi.org/10.1097/MD.0000000000000014

Address for correspondence: Mark Cribb, c/o Lismore Base Hospital, 60 Uralba St, Lismore, NSW 2480, Australia; email: markcribba@gmail.com

Borrelia turicatae in Ticks from Animals in a Public Park, Aguascalientes, Mexico

Edwin Vázquez-Guerrero,[1] Gustavo Paniagua-Campos,[1] Alexander R. Kneubehl, Paulina Estrada-de los Santos, Job E. Lopez, J. Antonio Ibarra

Author affiliations: Instituto Politécnico Nacional, Mexico City, Mexico (E. Vázquez-Guerrero, G. Paniagua-Campos, P. Estrada-de los Santos, J.A. Ibarra); Baylor College of Medicine, Houston, Texas, USA (A.R. Kneubehl, J.E. Lopez)

DOI: https://doi.org/10.3201/eid3205.251925

We obtained 5 isolates of *Borrelia turicatae* from ticks captured in a public park in Aguascalientes, Mexico. A serologic survey in resident fauna showed antibodies against *B. turicatae*. Relapsing fever borrelias are present in *Ornithodoros turicata* ticks and circulate in a zoonotic cycle, posing a risk for human infection.

[1]These authors contributed equally to this article.

Ornithodoros turicata ticks were originally described in Mexico by Alfredo Dugès at the end of the 19th Century. In 1936, it was implicated as the vector of tick-borne relapsing fever (TBRF) when febrile patients were first described in the city of Aguascalientes, in central Mexico (*1*). *Borrelia turicatae* is the species of TBRF spirochete transmitted by *O. turicata*, an argasid tick has been found in multiple regions of the United States and Mexico (*2*,*3*). We isolated *B. turicatae* from *O. turicata* ticks captured in the northern state of Sinaloa and used the diagnostic recombinant glycerophosphodiester phosphodiesterase (rGlpQ) antigen to detect circulating antibodies in clinical patients (*4*,*5*). Those findings indicated that *B. turicatae* and its vector are endemic in regions of Mexico, with spillover into human populations. However, TBRF in Mexico and in many other regions worldwide is a neglected disease that is often misdiagnosed because its symptoms are frequently confused with those of other diseases, such as malaria and brucellosis (*4*).

We obtained 5 isolates of *B. turicatae* from *O. turicata* ticks collected at La Pona Park in Aguascalientes, Mexico, in January and April 2023 (Figure 1). We examined tick specimens morphologically and molecularly by taxonomically analyzing a fragment of the mitochondrial genome, as described (*6*). Using a mouse model (either C57BL/6 or DBA/2J) (*5*), we evaluated the ticks by feeding them on the animals and assessing murine infection. We performed bacterial isolation as previously described by culturing blood samples from mice with spirochetemia in liquid, modified, and supplemented Barbour-Stoenner-Kelly II media supplemented with 10 μg/mL rifampin, 4 μg/mL phosphomycin, and 0.5 μg/mL amphotericin B (*5*). We amplified the 16S rRNA genes from each isolate by PCR, then sequenced and taxonomically analyzed them to confirm that all 5 isolates were *B. turicatae*; we named the isolates AGU1–AGU5. Of the 5 isolates, we sequenced genomic DNA from isolates AGU1–4 using NovaSeq X (Illumina, https://www.illumina.com); we used MinION for AGU1–3 and PromethION P2 Solo for AGU4 (Oxford Nanopore Technologies, https://nanoporetech.com). We base-called nanopore sequencing data using Dorado version 7.4.12 with the version 4.3.0 (https://github.com/nanoporetech/dorado) super-accurate base-calling model. We generated Illumina data using the Illumina DNA library prep kit 2 × 150 bp. We assembled chromosome-resolved and plasmid-resolved genome assemblies from Oxford Nanopore and Illumina data as previously described (*7*), with some modifications. We inferred a maximum-likelihood species tree as previously described; the

tree demonstrated that AGU1–AGU4 clustered with *B. turicatae* 91E135, BTE5EL, and BTCAM1 strains (Appendix Figure, https://wwwnc.cdc.gov/EID/article/32/5/25-1925-App1.pdf). Both 91E135 and BTE5EL originated in Texas, USA, whereas BTCAM1 originated in Sinaloa, Mexico. AGU1–AGU5 are the southernmost *B. turicatae* isolates identified as of April 2026.

As part of our investigation, we captured wild fauna in La Pona public park to determine whether local animals were exposed to *Borrelia* spp. We collected blood samples in accordance with animal welfare guidelines (*8*). We captured 5 opossums (*Didelphis virginiana*), 1 deer mouse (*Peromyscus* sp.), and 1 feral cat (*Felis silvestris catus*) and tested serum samples by immunoblotting to detect antibodies against *B. turicatae* protein lysates, rGlpQ, and rBipA, as described previously (*4*,*5*). Results showed that the opossum and cat serum samples were reactive with *B. turicatae* protein lysates rGlpQ, and rBipA (Figure 2). None of the opossum samples were negative for the immunoblotting test, which might be a limitation of our study; however, opossum and cat serum samples from other states tested negative. Our results

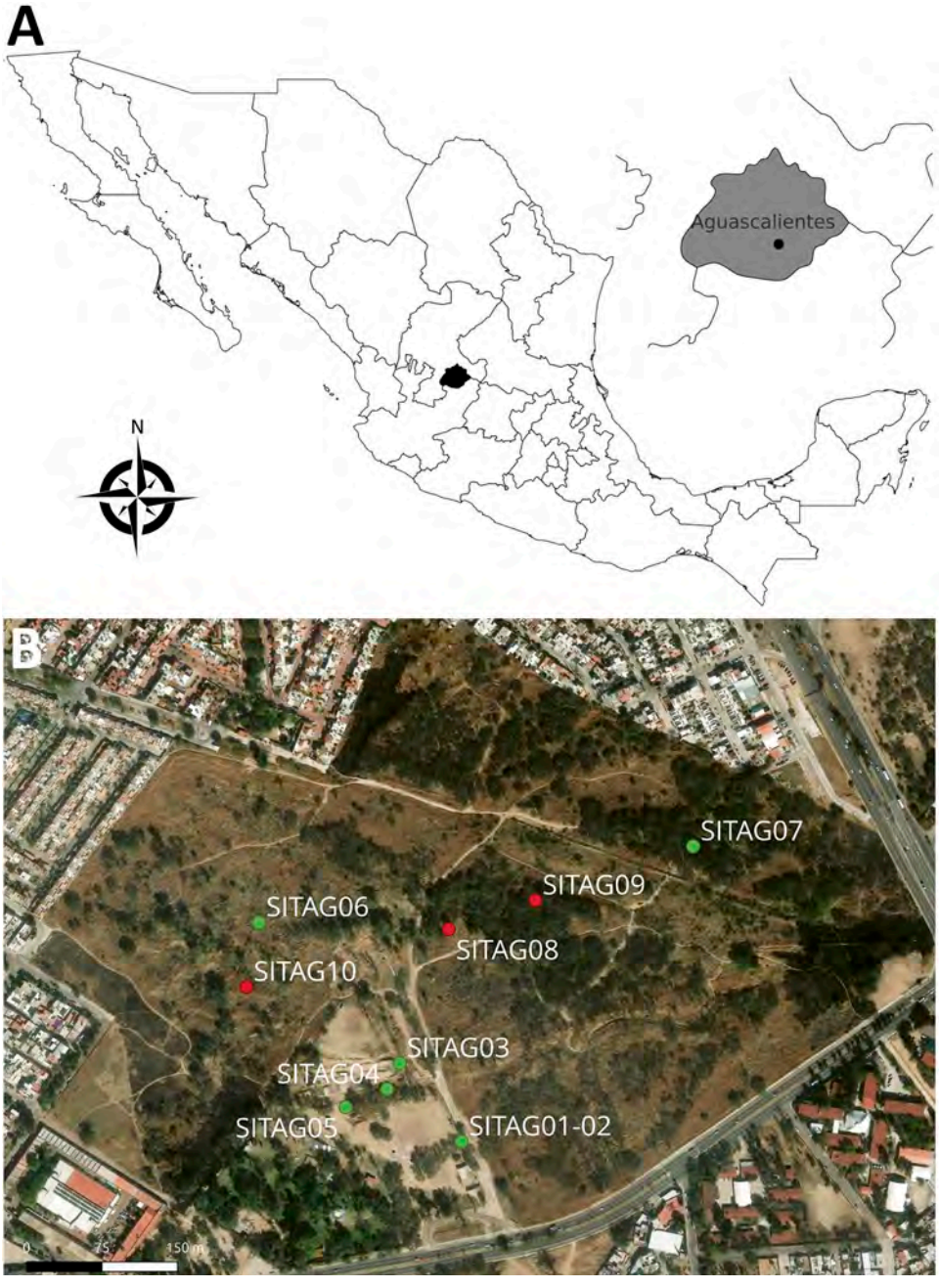

Figure 1. Locations of collection sites in study of *Borrelia turicatae* in ticks from animals in a public park, Aguascalientes, Mexico. A) Location of the state of Aguascalientes (black shading) in Mexico; inset at right shows the approximate location of the city of Aguascalientes (black dot). Map created using QGIS version 3.34 (https://qgis.org). B) Terrain map of La Pona Park in Aguascalientes. Green dots indicate collection sites where ticks were captured (SITAG01–07, 21°53′10.6" N 102°15′59.6" W; 21°53′13.4" N 102°16′01.7" W; 21°53′12.5" N 102°16′02.1" W; 21°53′18.2" N 102°16′06.6" W; 21°53′20.9" N 102°15′51.5" W; 21°53′11.1" N 102°16′03.1" W). Red dots indicate the 3 collection sites for resident fauna (SITAG08, 21°53′18" N, 102°16′00" W; SITAG09, 21°53′19" N, 102°15′57" W; SITAG10, 21°53′16" N, 102° 16′ 07" W). Map created using the ArcGIS imagery basemap (https://services.arcgisonline.com/ArcGIS/rest/services/World_Imagery/MapServer).

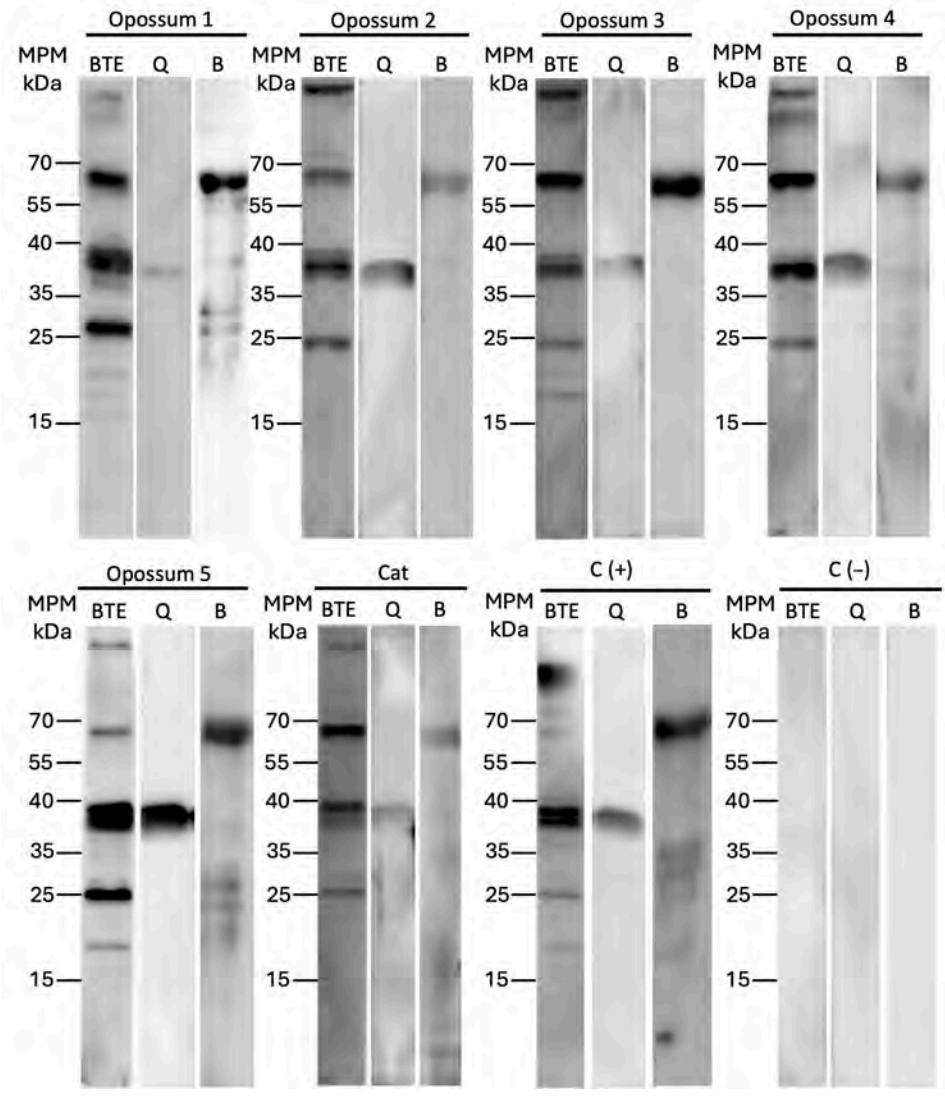

Figure 2. Immunoblot results assessing antibody responses in study of *Borrelia turicatae* in ticks from animals in a public park, Aguascalientes, Mexico. Images show responses in opossums and a feral cat captured in La Pona Park, along with mouse controls. C (+) is an immunoblot using a serum sample from a positive control mouse infected with *B. turicatae*. C (–) is from a negative control (serum from a nonexposed mouse). We used recombinant horseradish peroxidase protein A/G (Thermo Fisher Scientific, https://www.thermofisher.com) as the secondary ligand for the detection of both opossum and cat antibodies. BTE, *B. turicatae* protein extracts; Q, recombinant GlpQ; B, *B. turicatae* recombinant BipA.

suggest that *B. turicatae* circulates in a tick–opossum–feral cat infectious cycle.

Our findings support efforts to understand the mechanisms maintaining *B. turicatae* in nature, the distribution of infected *O. turicata* ticks, and the public health impact. Although we identified endemic foci of infected ticks, we did not determine the prevalence of *B. turicatae* in these populations. Understanding prevalence is relevant to public health because *B. turicatae* can be vertically transmitted from female ticks to their offspring at rates as high as 40% (*9*). Public parks and human dwellings have been shown to be a source for infected soft ticks in the southern United States and likely in human infections (*10*), but that relationship has been scarcely studied in Mexico. Given that unhoused and underserved persons reside in La Pona public park, they are at risk for exposure to *O. turicata* ticks and infection with *B. turicatae*. Our future work will focus on defining the tick–vertebrate infectious cycle of *B. turicatae* and assessing its effect on human populations living in or around La Pona Park. Clinicians should be aware of this potential zoonotic risk to humans in the area.

Acknowledgments

We thank the authorities of the Aguascalientes city municipality for permission to collect ticks and capture animals in La Pona. We also thank our research groups at Laboratorio de Genética Microbiana and Baylor University.

The animal protocol followed in this study was approved by our Research Ethics Committee at ENCB Instituto Politécnico Nacional (no. ZOO-001-2022e1). Capture of wild fauna was approved by Secretaría de Medio Ambiente y Recursos Naturales, Government of Mexico (no. SGPA/DGVS/0564/21).

Borrelia turicatae sequencing data and genome assemblies were submitted to GenBank associated with BioProject PRJNA1338334.

Secretaría de Investigación y Posgrado IPN provided financial support for this study (project nos. 20250266, 20253924, and 20260917).

About the Author

Dr. Vázquez-Guerrero is a physician, pediatrician, and infectious disease specialist in Mexico. His areas of interest include vectorborne infectious diseases and microbiology.

References

1. Dugès A. *Turicata* of Guanajuato. Artículo en el periódico "El Repertorio" de Guanajuato. 1876;Sect. 11–12.
2. Donaldson TG, Pèrez de León AA, Li AY, Castro-Arellano I, Wozniak E, Boyle WK, et al. Assessment of the geographic distribution of *Ornithodoros turicata* (Argasidae): climate variation and host diversity. PLoS Negl Trop Dis. 2016; 10:e0004383. https://doi.org/10.1371/journal.pntd.0004383
3. Guzmán-Cornejo C, Herrera-Mares A, Robbins RG, Rebollo-Hernández A. The soft ticks (Parasitiformes: Ixodida: *Argasidae*) of Mexico: species, hosts, and geographical distribution. Zootaxa. 2019;4623:485–525. https://doi.org/10.11646/zootaxa.4623.3.3
4. Vázquez-Guerrero E, Gordillo-Pérez G, Ríos-Sarabia N, Lopez JE, Ibarra JA. Case report: exposure to relapsing fever group borreliae in patients with undifferentiated febrile illness in Mexico. Am J Trop Med Hyg. 2023; 108:510–2. https://doi.org/10.4269/ajtmh.22-0386
5. Vázquez-Guerrero E, Kneubehl AR, Pellegrini-Hernández P, González-Quiroz JL, Domínguez-López ML, Krishnavajhala A, et al. *Borrelia turicatae* from ticks in peridomestic setting, Camayeca, Mexico. Emerg Infect Dis. 2024;30:380–3. https://doi.org/10.3201/eid3002.231053
6. Vázquez-Guerrero E, González-Quiroz JL, Domínguez-López ML, Kneubehl AR, Krishnavajhala A, Curtis MW, et al. New records of *Ornithodoros turicata* (Ixodida: Argasidae) in rural and urban sites in the Mexican states of Aguascalientes and Zacatecas indicate the potential for tick-borne relapsing fever. Exp Appl Acarol. 2023;91:99–110. https://doi.org/10.1007/s10493-023-00830-2
7. Kneubehl AR, Krishnavajhala A, Leal SM, Replogle AJ, Kingry LC, Bermúdez SE, et al. Comparative genomics of the Western Hemisphere soft tick-borne relapsing fever borreliae highlights extensive plasmid diversity. BMC Genomics. 2022;23:410. https://doi.org/10.1186/s12864-022-08523-7.
8. Sikes RS; Animal Care and Use Committee of the American Society of Mammalogists. 2016 guidelines of the American Society of Mammalogists for the use of wild mammals in research and education. J Mammal. 2016;97:663–88. https://doi.org/10.1093/jmammal/gyw078
9. Filatov S, Krishnavajhala A, Lopez JE. Autogenous reproduction by *Ornithodoros turicata* (Ixodida: Argasidae) females and vertical transmission of the tick-borne pathogen *Borrelia turicatae* (Spirochaetales: *Borreliaceae*). Appl Environ Microbiol. 2023;89:e0103223. https://doi.org/10.1128/aem.01032-23
10. Bissett JD, Ledet S, Krishnavajhala A, Armstrong BA, Klioueva A, Sexton C, et al. Detection of tickborne relapsing fever spirochete, Austin, Texas, USA. Emerg Infect Dis. 2018;24:2003–9. https://doi.org/10.3201/eid2411.172033

Address for correspondence: J. Antonio Ibarra, Instituto Politecnico Nacional, Microbiología Prol. Carpio y Plan de Ayala SN Col. Santo Tomas, Ciudad de México, 11340, Mexico; jibarrag@ipn.mx

Genomic Surveillance of Lassa Virus through In-Country Sequencing, Guinea

Jacob Camara,[1] Giuditta Annibaldis,[1] Joon Klaps,[1] Kékoura Ifono,[1] Fara Raymond Koundouno, Youssouf Sidibé, Sarah Ryter, Moussa Conde, Saa Lucien Millimono, Mette Hinrichs, Julia Hinzmann, Nils Peter Petersen, Mia Le, Annick Renevey, Ehizojie Ehiremen Emua, Philippe Lemey, Simon Dellicour, Stephan Günther, N'Faly Magassouba,[2] Sophie Duraffour,[2] Liana Eleni Kafetzopoulou,[2] Sanaba Boumbaly[2]

Author affiliations: Center for Virology Research—Laboratory for Viral Hemorrhagic Fevers in Guinea, Conakry, Guinea (J. Camara, M. Conde, N. Magassouba, S. Boumbaly); Bernhard Nocht Institute for Tropical Medicine, Hamburg, Germany (G. Annibaldis, S. Ryter, M. Hinrichs, J. Hinzmann, N.P. Petersen, M. Le, A. Renevey, S. Günther, S. Duraffour); German Center for Infection Research, partner site Hamburg–Lübeck–Borstel–Riems, Hamburg (G. Annibaldis, S. Ryter, M. Hinrichs, J. Hinzmann, N.P. Petersen, M. Le, A. Renevey, S. Günther, S. Duraffour); Rega Institute, KU Leuven, Leuven, Belgium (J. Klaps, P. Lemey, S. Dellicour, L.E. Kafetzopoulou); Laboratory for Viral Hemorrhagic Fevers of Guéckédou, Prefectural Health Department of Guéckédou, Guéckédou, Guinea (K. Ifono, F.R. Koundouno, S.L. Millimono); Laboratory for Viral Hemorrhagic Fevers at Regional Hospital of N'Zérékoré, Regional Hospital of N'Zérékoré, N'Zérékoré, Guinea (Y. Sidibé); University of Hamburg, Hamburg (M. Le); Irrua Specialist Teaching Hospital,

[1]These first authors contributed equally to this article.
[2]These senior authors contributed equally to this article.

Irrua, Nigeria (E.E. Emua); Spatial Epidemiology Lab, Université Libre de Bruxelles, Brussels, Belgium (S. Dellicour); Interuniversity Institute of Bioinformatics in Brussels, Université Libre de Bruxelles, Vrije Universiteit Brussel, Brussels (S. Dellicour); Leiden University Medical Center, Leiden, the Netherlands (L.E. Kafetzopoulou)

DOI: https://doi.org/10.3201/eid3205.260386

Strengthened in-country sequencing generated 28 Lassa virus genomes from human clinical cases in Guinea, expanding knowledge of Lassa fever in the country. Phylogeographic analysis revealed cross-border exchange between Liberia and the N'Zérékoré region and a Sierra Leone introduction into Guéckédou. Enhanced genomic surveillance is crucial to guide public health.

Lassa fever (LF) is a life-threatening viral hemorrhagic disease endemic to West Africa; early clinical symptoms are indistinguishable from other febrile illnesses, complicating diagnosis and surveillance (*1*). The causative agent, Lassa virus (LASV), is a *Mammarenavirus* (*Arenaviridae* family) with a bisegmented (small [S] and large [L] segments) ambisense RNA genome that exhibits distinct phylogenetic structure across its endemic regions. Lineages I–III and VI circulate in Nigeria, lineage IV predominates in the Mano River Union countries (Guinea, Sierra Leone, and Liberia), and additional distinct lineages circulate in Mali/Côte d'Ivoire (lineage V) and Togo (lineage VII). Although LF cases are only sporadically reported in Guinea, serologic evidence from the southeastern (forested) and central regions indicates broad population exposure (*2*,*3*). Sequencing efforts thus far have generated partial LASV genomes from rodent reservoirs in Upper Guinea (*4*), whereas genomes from human infections remain limited (*5*,*6*). Sparse genomic data limit our understanding of geogenomic variation, outbreak dynamics, and clinical correlations, highlighting the need for enhanced genomic surveillance to inform diagnostics, epidemiology, and patient management.

To expand viral surveillance and diagnostic capabilities locally in Guinea, genomic capacity strengthening was initiated in 2021 at the Centre de recherche en Virologie–Laboratoire des Fièvres Hémorragiques Virales de Guinée (CRV-LFHVG; Conakry, Guinea). Sequencing infrastructure was initially established in response to the COVID-19 pandemic using targeted Nanopore sequencing (Oxford Nanopore Technologies, https://nanoporetech.com) (*7*). In 2022–2023, laboratory capacity was expanded to include metagenomic sequencing (*8*,*9*), integrated within the diagnostic network of 3 surveillance laboratories for viral hemorrhagic fevers across Guinea: CRV-LFHVG, the national reference laboratory in Conakry, and 2 satellite laboratories in the forest region, in Guéckédou (Laboratoire des Fièvres Hémorragiques Virales de Guéckédou; LFHV-GKD) and N'Zérékoré (Laboratoire des Fièvres Hémorragiques Virales de Hôpital Régional de N'Zérékoré; LFHV-HRNZE). During 2020–2024, this laboratory network confirmed a total of 36 LF cases (F.R. Koundouno et al., unpub. data, https://www.medrxiv.org/content/10.64898/2026.02.24.26346968v1), including a nosocomial outbreak in Conakry in 2022 (*10*). In-country metagenomic nanopore sequencing was performed at CRV-LFHVG to investigate the viral diversity of the confirmed LF cases. A total of 28 LF cases were successfully sequenced, all of which yielded sufficient genomic coverage for downstream phylogenetic analysis (Appendix Table, https://wwwnc.cdc.gov/EID/article/32/5/26-0386-App1.pdf). Most sequencing yielded near-complete genomes for both segments (Appendix Table), and all sequences were phylogenetically classified as lineage IV.

Phylogenetic analysis revealed that many of the newly sequenced genomes from Guinea are substantially divergent from previously characterized cases; branch lengths suggest years to decades of virus circulation in the natural reservoir before sampling in human cases (Figures 1, 2). Bayesian phylogeographic reconstruction estimated substitution mean rates of 8.5×10^{-4} (S segment) and 8.2×10^{-4} (L segment) substitutions/site/year, placing the root of lineage IV in the 17th–18th Centuries, likely originating in southeastern (forested) Guinea (Figures 1, 2).

Spatial viral diversity in Guinea is organized into 3 predominant geographic clusters, mainly associated with the areas of Guéckédou, N'Zérékoré, and Faranah. That factor should be interpreted cautiously, because Guéckédou and N'Zérékoré both have surveillance laboratories, and sequences from the Faranah region originate from rodent reservoirs sampled during previous studies. Consequently, the inferred geographic clustering might be driven, at least in part, by uneven sampling. Two cocirculating sublineages of LASV were identified in the N'Zérékoré region: an older IVb lineage, which has been long-established locally (M00539, M00541, G0405, G0870, G0934); and the IVa lineage, which traces back to multiple independent introductions (M00363, M00542, M00364, G0274) from Ganta, northeastern Liberia, with common ancestors dating to the 1950s–1980s (Figure 1, panel D; Figure 2). In Guéckédou, we detected an imported LASV case originating from the Kenema area of Sierra Leone (G0959) (Figure 1, panel C; Figure 2),

illustrating that sporadic introductions from neighboring LASV-endemic regions to Guinea can occur and contribute to Guinean LASV diversity.

We included 4 LF cases from Conakry, in the western part of Guinea, all of which were associated to a previously reported nosocomial transmission chain linked to a travel case from a LASV-endemic area (*10*) (Appendix). The LASV sequences (G0780, G0795, G0796, G0797) show minimal between-sequence variation (L segment, 0–4 mutations; S segment, 0–1 mutations), consistent with a single transmission event. We identified all 4 genomes as a reassortant LASV variant with their 2 segments clustering significantly differently (Appendix). Their L segments clustered with sequences previously identified in Faranah (lineage IVb in Figure 2, panel A), and their S segments clustered with sequences previously identified in Guéckédou (lineage IVb in Figure 2, panel B).

This study increases the available LASV sequences derived from human clinical cases and provides new genomic insights into LASV circulation in Guinea. Our findings were made possible through strengthened laboratory diagnostics in LF-endemic areas (Guéckédou and N'Zérékoré) and the establish-

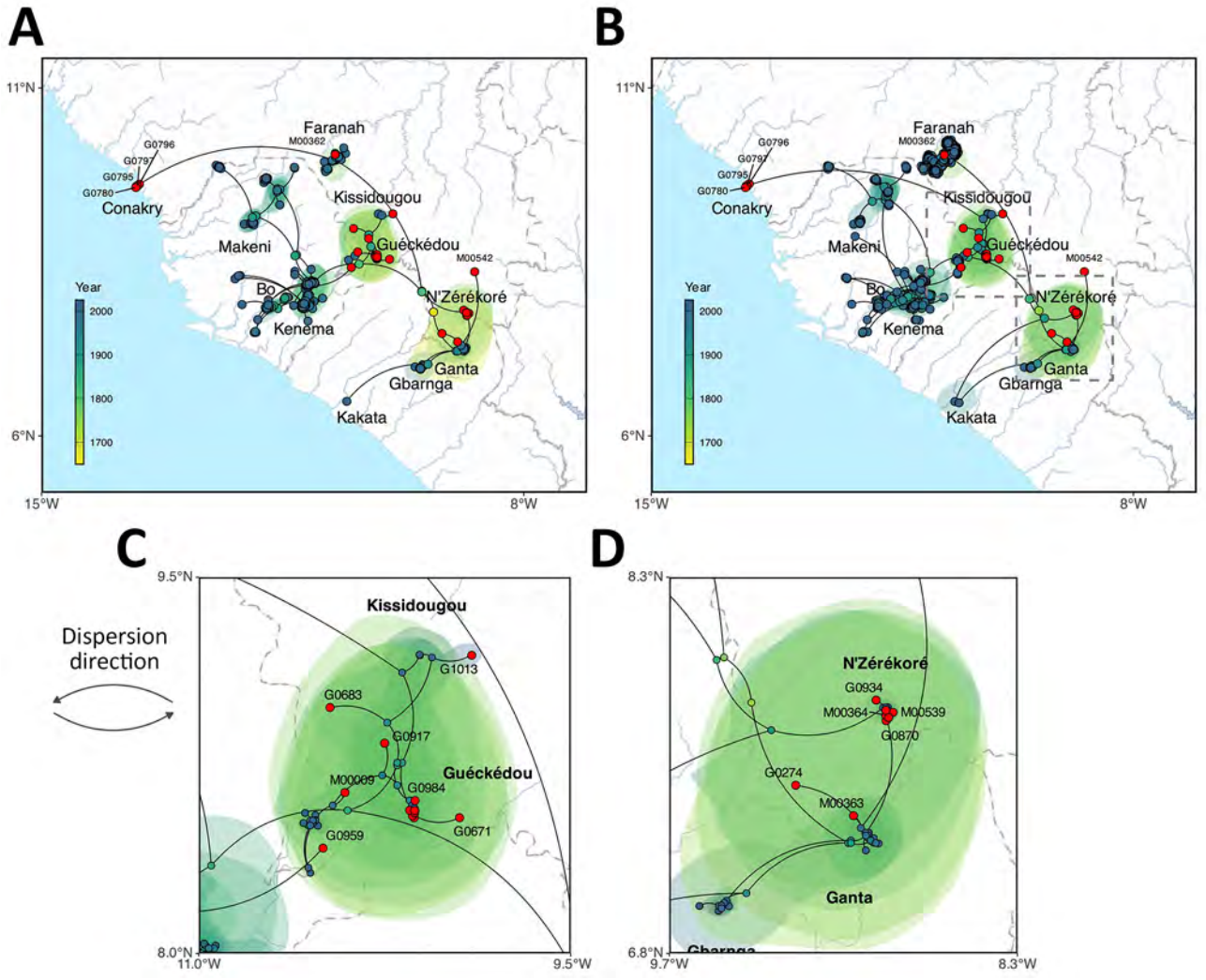

Figure 1. Phylogeographic reconstruction of the dispersal history of Lassa virus lineage IV from study of genomic surveillance of Lassa virus through in-country sequencing, Guinea. A, B) Results of the continuous phylogeographic inference based on large (A) and small (B) segment sequences. For each analysis, the corresponding maximum clade credibility tree is mapped with internal and tip nodes colored according to their estimated time of occurrence and sampling date. Tip nodes corresponding to newly sequenced cases from this study are highlighted in red. Shaded polygons represent the 80% highest posterior density regions, reflecting uncertainty in internal node location inference. The estimated root of lineage IV, dating to the 17th–18th Centuries, is indicated by dashed squares in the southeastern (forested) region of Guinea. C, D) Maps highlighting specific transmission dynamics in Guéckédou (C) and N'Zérékoré (D), illustrating the dense local clustering and the cross-border introductions from Liberia (Ganta) into the N'Zérékoré region.

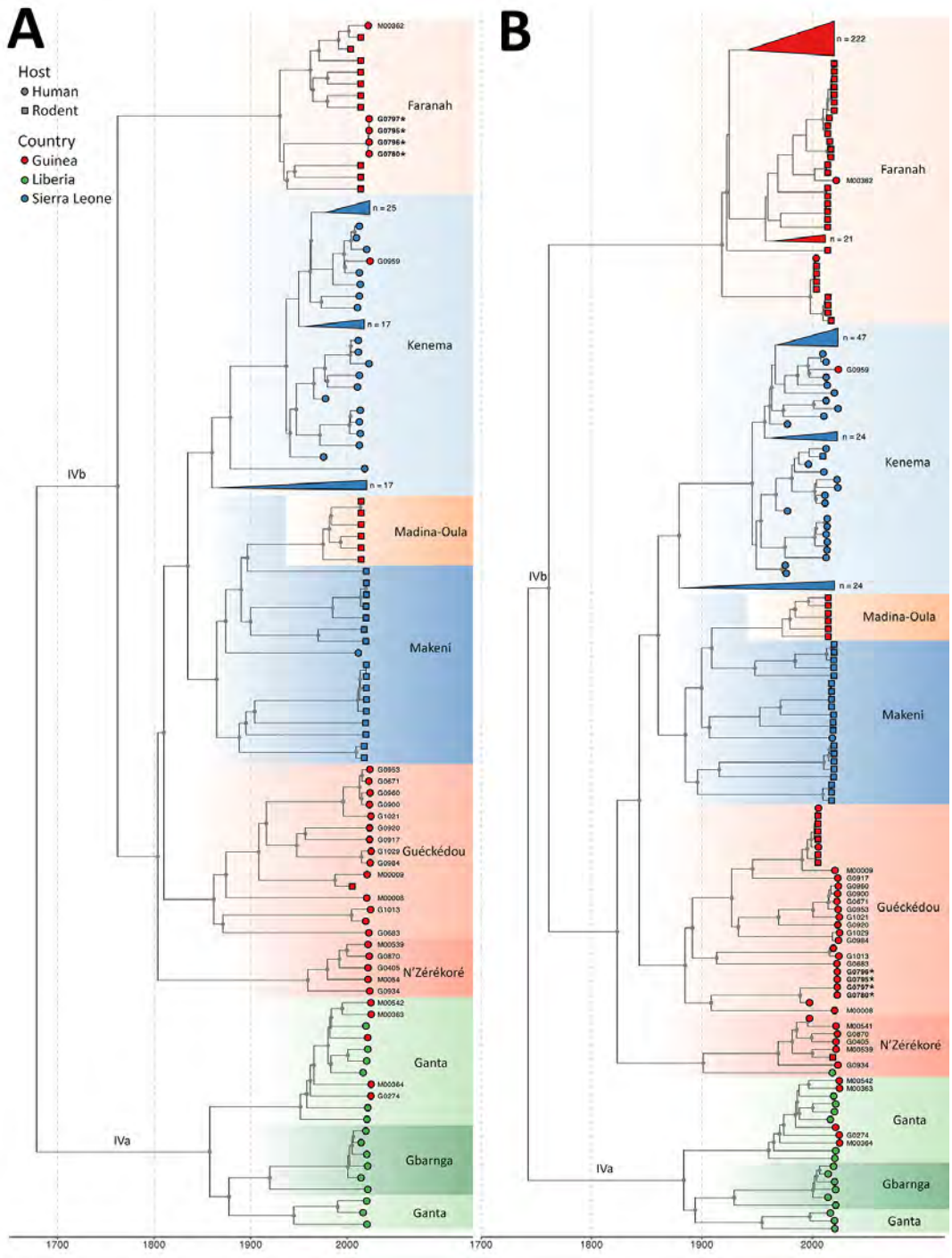

Figure 2. Temporal evolution of the large and small segments of Lassa virus from study of genomic surveillance of Lassa virus through in-country sequencing, Guinea. Time-scaled maximum clade credibility trees are shown for the large (A) and small (B) segments. Tips are colored by country of origin. Sublineages are annotated and colored by their predominant geographic location (e.g., Kenema, Faranah, Ganta). Clades that fall outside the sequence diversity of interest (i.e., clades that have no association with the sequences reported in this article) are collapsed and annotated with the total number of sequences they include. Gray dots indicate internal nodes with a clade credibility of >80%. Sequences reported in this manuscript have their sample identification codes indicated next to their respective tip. We detected 2 cocirculating sublineages of Lassa virus in N'Zérékoré: a locally established IVb lineage (M00539, M00541, G0405, G0870, G0934), and the IVa lineage linked to the region of Ganta in Liberia (M00363, M00542, M00364, G0274). The sample from Guéckédou (G0959) grouped within the Kenema, Sierra Leone, Lassa virus cluster, reflecting its travel-linked origin. Strains that form the nosocomial transmission chain with reassorted genomes have been highlighted in bold and are indicated with a star.

ment of new sequencing capacity for viral hemorrhagic fevers at CRV-LFHVG, Conakry. Ongoing genomic surveillance remains crucial for guiding public health interventions, as well as for the development of appropriate medical countermeasures.

This article was preprinted at https://www.medrxiv.org/content/10.64898/2026.03.04.26347418v1.

Acknowledgments

We thank the Agence Nationale de Sécurité Sanitaire, the Ministry of Health of the Republic of Guinea, the "Délégations Régionale et Préfectorale de la Santé," and the healthcare workers involved in the response.

This descriptive research, using anonymized diagnostic surveillance data, has been approved by the National Ethics Committee of Guinea (CNERS) under the number 009/CNERS/25. This work is part of the Nagoya permit number 006/2023/PN.

The work was supported by the German Federal Ministry of Health through support of the World Health Organization Collaborating Centre for Arboviruses and Hemorrhagic Fever Viruses at the Bernhard-Nocht-Institute for Tropical Medicine (agreement ZMV I1-2517WHO005), the Global Health Protection Program (GHPP, agreements ZMV I1-2517GHP-704, ZMVI1-2519GHP704, and ZMI1-2521GHP921 until end of 2022 and, from 2023, agreements ZMI5-2523GHP006 and ZMI5-2523GHP008), the COVID-19 surge fund (BMG ZMVI1-2520COR001), the Research and Innovation Programme of the European Union under H2020 grant agreement n°871029-EVA-GLOBAL, and the Research Foundation–Flanders (Fonds voor Wetenschappelijk Onderzoek–Vlaanderen, G005323N and G051322N, 1SH2V24N, 12X9222N). The BNITM is a member of the German Center for Infection Research (DZIF, partner site Hamburg–Lübeck–Borstel–Riems, Hamburg, Germany), and all works performed in this study have been supported by DZIF. The funders had no role in the design of the study; in the collection, analyses, or interpretation of data; in the writing of the manuscript, or in the decision to publish the results.

G.A., F.R.K., Y.S., S.G., N.F.M., S.Du., L.E.K., and S.B. conceived and designed the study. J.C., G.A., K.I., F.R.K., Y.S., S.R., M.C., S.L.M., M.H., and J.H. collected data or performed laboratory diagnostics. J.C., G.A., K.I., S.R., M.C., S.L.M., M.H., J.H., N.P.P., M.L., and A.R. performed sequencing or sequence validation. J.C., G.A., J.K., K.I., S.R., M.C., S.L.M., and S.De. conducted formal phylogenetic analysis. J.K. and S.De. performed phylogeography analysis. J.C., G.A., J.K., K.I., F.R.K., Y.S., S.R., M.H., J.H., A.R., E.E.E., P.L., S.G., N.F.M., S.Du., L.E.K., and S.B. implemented the project. P.L., S.G., N.F.M., S.Du., and S.B. acquired funding. J.C., G.A., J.K., K.I., S.G., N.F.M., S.Du., L.E.K., and S.B. wrote the manuscript. All authors edited the manuscript. All authors read and approved the contents of the manuscript.

During the preparation of this work the authors used ChatGPT/free version to edit some sentences. After using this tool/service, the authors reviewed and edited the content as needed and take full responsibility for the content of the publication.

About the Authors

Mr. Camara leads the sequencing team at Centre de recherche en Virologie–Laboratoire des Fièvres Hémorragiques Virales de Guinée (CRV-LFHVG) in Conakry, Guinea, where he oversees genomic sequencing activities and data generation. Dr. Annibaldis is based at the Bernhard Nocht Institute for Tropical Medicine in Hamburg, Germany, where she coordinates strengthening projects for viral hemorrhagic fevers surveillance. Her work focuses on sequencing capacity and laboratory system strengthening in Guinea and Nigeria.

References

1. Garry RF. Lassa fever—the road ahead. Nat Rev Microbiol. 2023;21:87–96. https://doi.org/10.1038/s41579-022-00789-8
2. Kernéis S, Koivogui L, Magassouba N, Koulemou K, Lewis R, Aplogan A, et al. Prevalence and risk factors of Lassa seropositivity in inhabitants of the forest region of Guinea: a cross-sectional study. PLoS Negl Trop Dis. 2009;3:e548. https://doi.org/10.1371/journal.pntd.0000548
3. Mariën J, Nuismer SL, Magassouba N, Soropogui B, Günther S, Becker-Ziaja B, et al. Serosurveillance identifies an endemic hotspot of Lassa fever in Faranah, Upper Guinea. J Infect Dis. 2025;232:e830–8. https://doi.org/10.1093/infdis/jiaf308
4. Fichet-Calvet E, Ölschläger S, Strecker T, Koivogui L, Becker-Ziaja B, Camara AB, et al. Spatial and temporal evolution of Lassa virus in the natural host population in Upper Guinea. Sci Rep. 2016;6:21977. https://doi.org/10.1038/srep21977
5. Magassouba N, Koivogui E, Conde S, Kone M, Koropogui M, Soropogui B, et al. A sporadic and lethal Lassa fever case in Forest Guinea, 2019. Viruses. 2020;12:1062. https://doi.org/10.3390/v12101062
6. Wiley MR, Fakoli L, Letizia AG, Welch SR, Ladner JT, Prieto K, et al. Lassa virus circulating in Liberia: a retrospective genomic characterisation. Lancet Infect Dis. 2019;19:1371–8. https://doi.org/10.1016/S1473-3099(19)30486-4
7. Magassouba N, Gustani-Buss E, Ifono K, Nelson EV, Camara J, Annibaldis G, et al. Two years of SARS-CoV-2 genomic surveillance capacity development in Guinea. Sci Rep. 2026;16:11225. https://doi.org/10.1038/s41598-026-46736-y
8. Camara J, Sidibé Y, Annibaldis G, Soropogui B, Ryter S, Condé M, et al. Dengue diagnosis in Guinea in two returning travelers from Côte d'Ivoire: a case report. IJID Reg. 2025;17:100777. https://doi.org/10.1016/j.ijregi.2025.100777

9. Koundouno FR, Kafetzopoulou LE, Faye M, Renevey A, Soropogui B, Ifono K, et al. Detection of Marburg virus disease in Guinea. N Engl J Med. 2022;386:2528–30. https://doi.org/10.1056/NEJMc2120183
10. Annibaldis G, Soropogui B, Ifono K, Camara J, Kaba ML, Berete F, et al. Nosocomial outbreak of Lassa fever in Conakry, Guinea, 2022. J Infect Dis. 2026 Apr 23 [Epub ahead of print]. https://doi.org/10.1093/infdis/jiag229

Address for correspondence: Giuditta Annibaldis, Bernhard Nocht Institute for Tropical Medicine (BNITM), Bernhard Nocht Straße 74, 20359, Hamburg, Germany; email: giuditta.annibaldis@bnitm.de

Highly Pathogenic Avian Influenza A(H5N1) Virus RNA in Bovine Semen, California, USA, 2024

Ailam Lim,[1] Keith Poulsen,[1] Leonardo C. Caserta, Lizheng Guan, Eryn Opgenorth, Maxwell P. Beal, Amie J. Eisfeld, Yoshihiro Kawaoka, Diego G. Diel

Author affiliations: University of Wisconsin–Madison Wisconsin Veterinary Diagnostic Laboratory, Madison, Wisconsin, USA (A. Lim, K. Poulsen, E. Opgenorth); University of Wisconsin–Madison, Madison (A. Lim, K. Poulsen, L. Guan, A.J. Eisfeld, Y. Kawaoka); Cornell University Animal Health Diagnostic Center, College of Veterinary Medicine, Ithaca, New York, USA (L.C. Caserta, D.G. Diel); Mill Creek Veterinary Services, Visalia, California, USA (M.P. Beal); Dakota Dairy Health, Brookings, South Dakota, USA (M.P. Beal); University of Tokyo Institute of Medical Science, Tokyo, Japan (Y. Kawaoka); University of Tokyo Pandemic Preparedness, Infection and Advanced Research Center, Tokyo (Y. Kawaoka); Japan Institute for Health Security, National Institute of Global Health and Medicine, Tokyo (Y. Kawaoka)

DOI: https://doi.org/10.3201/eid3205.251639

Since March 2024, highly pathogenic avian influenza (HPAI) A(H5N1) virus has infected dairy cattle in the United States, prompting concern about novel transmission routes. During an outbreak in California, HPAI H5N1 RNA was detected in an asymptomatic bull's semen. Although infectious virus was not isolated, semen-associated transmission risks and biosecurity practices remain a concern.

[1]These authors contributed equally to this article.

Since March 2024, detection of clade 2.3.4.4b highly pathogenic avian influenza (HPAI) A(H5N1) in US dairy cattle has raised concerns about the virus's ability for cross-species transmission, adaptation to mammals, and novel transmission routes, including milk (*1*,*2*). Multiple pathogenic viruses are transmitted in bovine semen, and detection of HPAI in turkey semen has prompted questions about the potential role of HPAI transmission in bovine semen (*3*,*4*). Shedding of HPAI H5N1 in bovine semen could result in silent viral spread within herds and across geographic regions through artificial insemination. Although clinical HPAI disease has been reported in female calves and pregnant animals, reports of diseased bulls in dairy farms or beef cattle are lacking. Many questions about the pathophysiology of HPAI H5N1 in US dairy herds remain unanswered, but movement of lactating cows is a recognized risk factor for interstate disease spread. In this diagnostic study, we sought evidence of HPAI H5N1 shed through semen in natural breeding bulls on an HPAI H5N1–affected dairy farm in California.

The HPAI H5N1 genotype B3.13 outbreak in California began in August 2024 and likely resulted from the interstate movement of infected cows, which led to the rapid spread of the virus within the state. In October 2024, infection in a 4,500-head Holstein dairy was detected by reverse transcription PCR (RT-PCR) for H5N1 RNA in bulk tank milk samples. Clinical signs in lactating dairy cows consisted of decreased milk production, mastitis, lethargy, dehydration, anorexia, and pyrexia (>104.0°F). The herd experienced a 60% illness rate over 3 weeks. About 4 weeks after detection, the herd veterinarian collected diagnostic samples from 3 individual 3-year-old Holstein bulls; samples consisted of deep nasal swabs, preputial scrapings, preejaculate seminal fluid, semen, and serum samples. Those samples were sent to the Wisconsin Veterinary Diagnostic Laboratory (Madison, WI, USA) for testing. Subjectively, the semen appeared to have low sperm concentration and volume, although total sperm count was not measured. The poor semen quality was likely because of timing and suboptimal sampling conditions; the bulls had been comingled with cows the same day for breeding.

Initially, we examined the samples for influenza A virus (IAV) using various methods (Table; Appendix, https://wwwnc.cdc.gov/EID/article/32/5/25-1639-App1.pdf). Deep nasal swabs, preputial scrapes, preejaculate seminal fluids, and semen samples were tested using multiple IAV Matrix RT-PCRs (*5*,*6*). IAV RNA was detected at a low level in semen from bull 1 by 3 different PCR assays, but bull 2 and bull 3 tested

Table. Influenza A virus testing results for samples collected from 3 bulls in HPAI H5N1–infected farm in study of HPAI H5N1 virus RNA in bovine semen, California, USA, 2024*

Bull no.	Specimen type	IAV ELISA result (sample/positive control ratio)	IAV RT-PCR result (Ct)†	H5 RT-PCR result (Ct)†	Clade 2.3.4.4b RT-PCR result (Ct)†	Virus isolation
Bull 1	Serum	Negative (0.620)	NP	NP	NP	Negative
	Deep nasal swabs	NP	Negative	NP	NP	Negative
	Preputial scrape	NP	Negative	NP	NP	Negative
	Preejaculate	NP	Negative	NP	NP	Negative
	Semen	NP	Detected:‡ detected (38.2/39.5);§ negative/detected (39.1);¶ detected (37.9/38.9)#	Negative	Detected (39.6)	Negative
Bull 2	Serum	Negative (1.000)	NP	NP	NP	NP
	Deep nasal swabs	NP	Negative	NP	NP	NP
	Preputial scrape	NP	Negative	NP	NP	NP
	Preejaculate	NP	Negative	NP	NP	NP
	Semen	NP	Negative	NP	NP	NP
Bull 3	Serum	Negative (0.880)	NP	NP	NP	NP
	Deep nasal swabs	NP	Negative	NP	NP	NP
	Preputial scrape	NP	Negative	NP	NP	NP
	Preejaculate and semen	NP	Negative	NP	NP	NP

*Ct, cycle threshold; HPAI, highly pathogenic avian influenza; IAV, influenza A virus; NP, not performed; RT-PCR, reverse transcription PCR.
†Assay Ct cutoff value was 40.
‡Sample was subjected to further sequencing analyses.
§Wisconsin Veterinary Diagnostic Laboratory IAV assay, tested in duplicate.
¶National Animal Health Laboratory Network IAV Matrix assay, tested in duplicate.
#Modified National Animal Health Laboratory Network IAV Matrix assay, tested in duplicate.

negative. No detection was reported in any other samples. The IAV RNA detection in bull 1 was confirmed with an additional RNA extraction to rule out laboratory contamination. The IAV strain was further identified as HPAI using the H5N1 2.3.4.4b lineage subtyping RT-PCR.

Targeted IAV sequencing confirmed the presence of H5N1 virus and yielded a partial H5N1 genome (Appendix Table 1), deposited into GISAID (https://www.gisaid.org; accession no. EPI_ISL_20206713). Attempts to assemble the full genome were unsuccessful because of the low viral load in the semen. Phylogenetic analysis of the partial concatenated genome sequences indicated that the viral RNA in bull 1 clustered within predominantly bovine-derived B3.13 genotype sequences and was most closely related to a sample collected from a dairy farm worker in California during the same period (Figure) (*7*).

We processed all samples from bull 1 for virus isolation to attempt recovery of an isolate. Serially

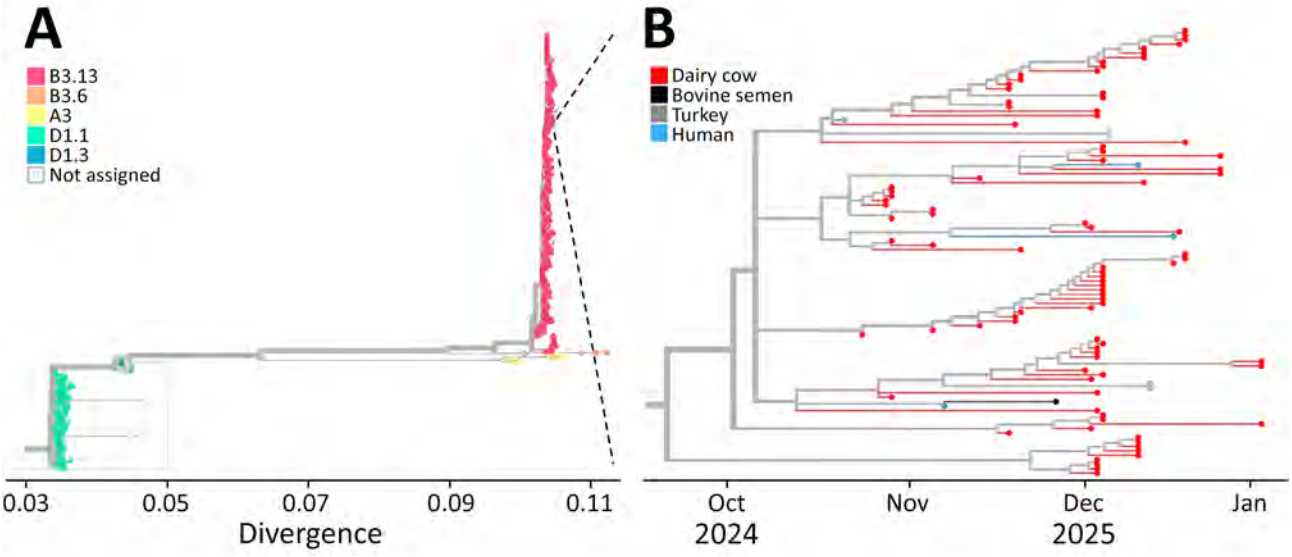

Figure. Phylogenetic analysis of partial concatenated genome sequences confirming detection of highly pathogenic avian influenza A(H5N1) virus genotype B3.13 from bovine semen, California, USA, 2024. A) Tree showing broader phylogeny of H5N1 virus genotypes. B) Timescale tree showing closer examination of the virus from bull 1 semen (bovine semen, black line) and closely related virus sequences.

diluted samples inoculated into 10-day-old specific-pathogen–free embryonated chicken eggs or Madin-Darby canine kidney cells showed no embryo death or cytopathic effect. We confirmed all samples as negative by hemagglutination assay.

The serum samples from all bulls tested negative by antigen-based influenza A ELISA (*8*). However, the sample/positive control ratio for bull 1 was 0.620, close to the validated 0.5 assay cutoff, potentially indicating seroconversion.

Because of the limited semen volume available for analysis, we did not perform further confirmation testing at the national reference laboratory. We requested additional samples several months later for convalescent testing, but bull 1 had been culled from the herd. The significance of identifying HPAI H5N1 in bovine semen remains uncertain. The virus could have been actively shed in semen, or the ejaculate could have been contaminated during collection. Although detecting RNA does not confirm the presence of infectious virus, this finding warrants further investigation into whether HPAI H5N1 can be shed in semen and raises questions about farm biosecurity amid the ongoing outbreak. High viral load in the environment during a herd outbreak was well documented (S. Lakdawala et al., unpub. data, https://www.biorxiv.org/content/10.1101/2025.07.31.666798v3; C. Stenkamp-Strahm et al., unpub. data, https://www.medrxiv.org/content/10.1101/2025.09.03.25335023v1). Good biosecurity measures are essential to prevent infections and, if infection occurs, slow disease spread on the farm.

In conclusion, further research and risk assessments are needed to determine tissue tropism of HPAI H5N1 in reproductive organs and whether naturally infected bulls shed virus in semen, and, if so, evaluate the risk for disease spread on dairy farms and with artificial insemination programs. Repetition and confirmation of these findings would have implications for natural breeding and biosecurity for artificial insemination collection centers, suggesting the need for increased caution in preventing silent intraherd spread.

About the Author

Dr. Lim is a clinical associate professor in the Department of Pathobiological Sciences at the University of Wisconsin–Madison and serves as the Section Head of Virology and Molecular Diagnostics at the Wisconsin Veterinary Diagnostic Laboratory, Madison. She specializes in veterinary diagnostics and infectious disease, with a primary focus on advancing molecular diagnostic assays.

References

1. Burrough ER, Magstadt DR, Petersen B, Timmermans SJ, Gauger PC, Zhang J, et al. Highly pathogenic avian influenza A(H5N1) clade 2.3.4.4b virus infection in domestic dairy cattle and cats, United States, 2024. Emerg Infect Dis. 2024;30:1335–43. https://doi.org/10.3201/eid3007.240508
2. Frye EA, Nooruzzaman M, Cronk B, et al. Isolation of highly pathogenic avian influenza A(H5N1) virus from cat urine after raw milk ingestion, United States. Emerg Infect Dis. 2025;31:1636–9. https://doi.org/10.3201/
3. Givens MD. Review: risks of disease transmission through semen in cattle. Animal. 2018;12(s1):s165–71. https://doi.org/10.1017/S1751731118000708
4. Cardona C, Wileman B, Malladi S, Ceballos R, Culhane M, Munoz-Aguayo J, et al. The risk of highly pathogenic influenza A virus transmission to turkey hen flocks through artificial insemination. Avian Dis. 2021; 65:303–9. https://doi.org/10.1637/aviandiseases-D-20-00132
5. Animal and Plant Health Inspection Service. Real-time RT-PCR detection of influenza A and avian paramyxovirus type-1. Document no. NVSL-SOP-0068, revision 6. Riverdale Park (MD): The Service; 2024.
6. Zimmerman A, Vandenburg-Carroll A, Marthaler DG, Lim A. Optimizing nucleic acid extraction from extended bovine semen for endemic and high-consequence pathogens. Animals (Basel). 2025;15:3411. https://doi.org/10.3390/ani15233411
7. Zhu S, Harriman K, Liu C, Kraushaar V, Hoover C, Shim K, et al.; California Department of Public Health H5 Laboratory Response Team. Human cases of highly pathogenic avian influenza A(H5N1)—California, September–December 2024. MMWR Morb Mortal Wkly Rep. 2025;74:127–33. https://doi.org/10.15585/mmwr.mm7408a1
8. Posey E. Use of IDEXX influenza A ELISA for antibody detection in bovine-origin mik and serum. Document no. NVSL-SOP-1255, revision 3. Riverdale Park (MD): Animal and Plant Health Inspection Service; 2024.

Address for correspondence: Ailam Lim, Wisconsin Veterinary Diagnostic Laboratory, 445 Easterday Ln, Madison, WI 53706, USA; email: allim2@wisc.edu

Human Respiratory Syncytial Virus in Vaccinated and Unvaccinated Adults, Georgia, USA, 2024–2025

Saïd Rachida,[1] Alaa Ahmed,[1] Diana Rojas-Gallardo, Henok Tafesse, Hannah Dakanay, Mackenzie Duford, Collin Tolbert, Ryan S. Springfield, Anne Piantadosi

Author affiliations: Emory University School of Medicine, Atlanta, Georgia, USA (S. Rachida, A. Ahmed, D. Rojas-Gallardo, H. Dakanay, M. Duford, C. Tolbert, R.S. Springfield, A. Piantadosi); Morehouse School of Medicine, Atlanta (H. Tafesse, C. Tolbert); Medical College of Georgia, Athens, Georgia, USA (R.S. Springfield)

DOI: http://doi.org/10.3201/eid3205.251997

We analyzed respiratory syncytial virus genome sequences from adults in Georgia, USA, during 2024–2025. We found multiple co-circulating lineages of both A and B subtypes. We identified few mutations in F protein antigenic sites in this population with low vaccine uptake, highlighting the need for ongoing genomic surveillance.

Respiratory syncytial virus (RSV) is a leading cause of respiratory tract infections in infants, older adults, and immunocompromised persons (*1*). Vaccines are available for adults on the basis of age and underlying conditions (*2*). In the United States during 2024–2025, 47.5% of adults ≥75 years of age and 38.1% of adults 60–74 years of age with high-risk conditions received RSV vaccinations (*3*). RSV vaccines target the fusion (F) protein at conserved epitopes; however, vaccination might create selective pressure for immune escape mutations.

Subtypes RSV-A and RSV-B have been classified into lineages (*4*), enabling surveillance for immune escape variants that might arise across diverse viral genetic backgrounds. US studies during 2022–2024 identified few substitutions in antigenic sites, none of which were clearly associated with vaccination (*5*–*7*). We analyzed RSV sequences during 2024–2025 to assess virus diversity under a changing immune landscape.

Our study included 182 vaccinated and unvaccinated adults within the Emory Healthcare system, in Georgia, USA (Appendix 1, https://wwwnc.cdc.gov/EID/article/32/5/25-1997-App1.pdf); 68.7% were female, 30.7% were male, and the median age was 61 years (Appendix 1 Table 1). Nearly all (98%) persons reported symptoms, including fever (31%), cough (93%), and dyspnea (25%). Hospitalization occurred in 13%, intensive care unit admission in 2%, and death in 3% (Appendix 1 Table 3).

Ninety-six (53%) persons were eligible for RSV vaccination on the basis of age (≥75 years) or age 50–74 years with underlying conditions (*2*); however, only 17 (18% of eligible persons) received vaccinations. We did not perform statistical analyses because of the small sample size, but observed that vaccinated persons were older and had more underlying conditions, which likely contributed to their higher rates of hospitalization and intensive care admission (Appendix 1 Table 1). We detected similar numbers of RSV-A (n = 93) and RSV-B (n = 83) cases. We successfully sequenced 71% of RSV-A samples and 76% of RSV-B samples (Appendix 1 Table 2), generally corresponding to those with quantitative reverse transcription PCR cycle threshold values ≤31 (Appendix 1 Figure 1).

Among RSV-A sequences, lineage A.D.3.1 was predominant (n = 27; 29%), followed by A.D.5.2 (n = 14; 15%) and A.D.1.5 (n = 9; 10%) (Appendix 1 Table 4). Lineage A.D.3.1 was more frequent in our study than previously reported (*8*,*9*). Among RSV-B sequences, most were lineage B.D.E.1 (n = 48; 58%), consistent with other studies (*4*). Among 17 vaccinated persons, 14 had RSV sequences with ≥75% coverage; those sequences represented multiple lineages, with no clear differences in lineage distribution between vaccinated and unvaccinated persons (Appendix 1 Table 4). Phylogenetic analysis showed that sequences from our study were distributed across phylogenetic trees (Figure; Appendix 1 Figure 2), although we observed clusters of Georgia sequences (Appendix 1 Table 4). Sequences from vaccinated persons did not show distinct clustering.

We evaluated mutations in F protein antigenic sites Ø–V for 125 sequences with ≥95% F gene coverage, 13 of which came from vaccinated persons. Across all persons, we identified a total of 25 nonsynonymous substitutions in antigenic sites (Table; Appendix 1 Figures 3, 4). Only 1 substitution was unique to vaccinated persons, K65R in antigenic site Ø in 1 RSV-A sequence. K65R phenotypic effects are unknown, but other substitutions at this site have been associated with nirsevimab resistance (*10*). We found another substitution, S377N, in 43% of vaccinated and 5% of unvaccinated persons, a finding also noted in a report of 2 postvaccine infections during 2023–2024 (*6*), but phenotypic effects of that substitution are unknown. The other substitutions occurred at the same

[1]These authors contributed equally to this article.

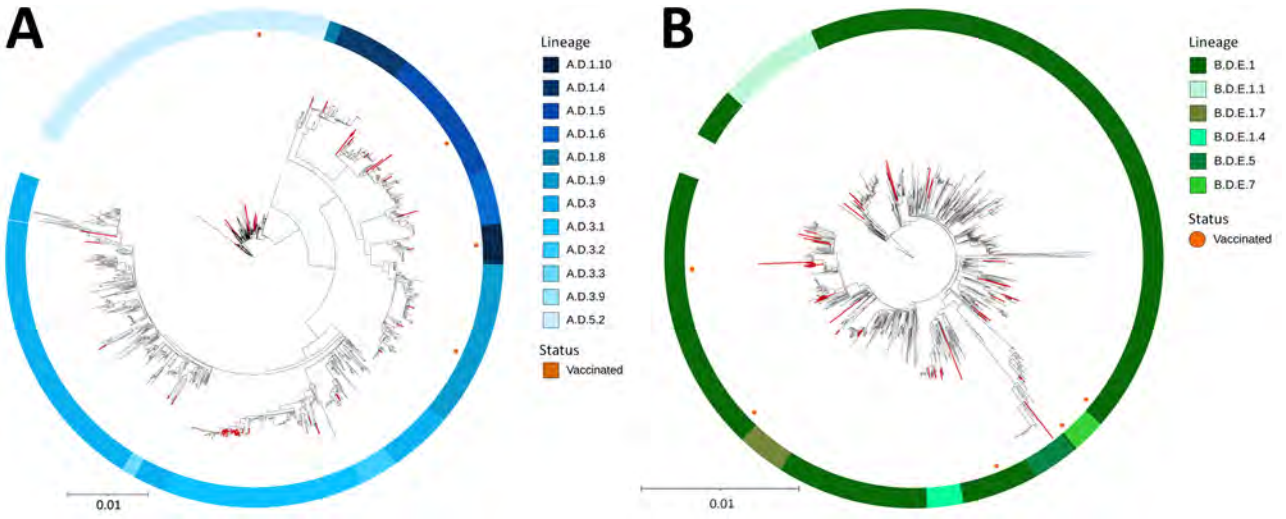

Figure. Maximum-likelihood phylogenetic trees of respiratory syncytial virus (RSV) A and RSV-B sequences from adults with RSV infection in Georgia, USA, 2024–2025. A) RSV-A sequences mainly clustered within lineages A.D.3.1 and A.D.5.2. B) RSV-B sequences mainly clustered within lineage B.D.E.1. There was limited clustering of the Georgia sequences obtained in this study (red branches), and RSV sequences from vaccinated persons (orange dots) were distributed throughout the tree. For ease of visualization, Panel B of this figure omits lineage B.D.4.1.1; that lineage is included in Appendix 1 Figure 2. Reference sequences are listed in Appendix 2 (https://wwwnc.cdc.gov/EID/32/5/25-1997-App2.xlsx). Scale bars indicate nucleotide substitutions per site.

or higher frequency in unvaccinated compared with vaccinated persons.

Among all persons, several substitutions (e.g., I59V and K470R) in RSV-A occurred at higher frequencies than previously reported (*5*). For RSV-B, 9 of the 13 substitutions were characteristic of the B.D.E.1 lineage (*4*). R42K, detected in nearly half of our samples, was also frequently detected in prior reports (*6*); however, F54L, detected in all our sequences, was previously rarely reported. We identified 3 substitutions not reported in prior studies: N63S in site Ø, and K445R and N466S in site IV (*5*–*7*,*9*). Mutations at antigenic sites 384 of RSV-A and 191 of RSV-B, rarely noted in cases of postvaccine infection reported during 2023–2024 (*6*), were widely circulating in our cohort by 2024–2025. Although not likely to be a direct result of immune pressure, these findings highlight ongoing drift in the F protein that might have future consequences for vaccine effectiveness. We also analyzed within-sample minor variants in F and identified only 1 substitution in antigenic site G71E in 37% of reads from an unvaccinated person with RSV-A (Appendix 1 Table 5).

Our analyses demonstrated that RSV strains circulating in Georgia during the 2024–25 season were diverse and resembled strains circulating across the United States and globally. We did not find evidence

Table. Amino acid mutations at antigenic sites in the RSV F protein for a study of human respiratory syncytial virus in vaccinated and unvaccinated adults, Georgia, USA, 2024–2025*

	RSV-A				RSV-B			
	Unvaccinated, n = 58		Vaccinated, n = 7		Unvaccinated, n = 53		Vaccinated, n = 6	
Antigenic site	Sub.	No. (%)	Sub.	No. (%)	Sub.	No. (%)	Sub.	No. (%)
Site ϕ, 62–96, 195–227	T72I	1 (2)	K65R	1 (20)	N63S	1 (2)	I206M	6 (100)
					I206M	53 (100)	Q209R	5 (83)
					Q209R	52 (98)	S211N	6 (100)
					S211N	53 (100)		
Site I, 27–45, 312–318, 378–389	I379V	58 (100)	I379	7 (100)	R42K	25 (47)	R42K	2 (33)
	V384I	58 (100)	V384I	6 (80)	F54L	53 (100)	F54L	6 (100)
					S389P	50 (94)	S389P	4 (67)
Site II, 254–277	N276S	33 (57)	N276S	4 (57)	ND	ND	ND	ND
Site III, 46–54, 301–311, 345–352, 367–378	S377N	3 (5)	S377N	3 (43)	ND	ND	ND	ND
Site IV, 422–471	M447V	58 (100)	M447V	7 (100)	K445R	1 (2)	ND	ND
	K470R	2 (3)			N466S	1 (2)		
Site V, 55–61, 146–194, 287–300	I59V	5 (7)	V152I	7 (100)	L172Q	53 (100)	L172Q	6 (100)
	V152I	58 (100)	L178V	7 (100)	S173L	53 (100)	S173L	6 (100)
	V154I	1 (2)			S190N	52 (98)	S190N	6 (98)
	L178V	58 (100)			K191R	53 (100)	K191R	6 (100)

*Sub., substitution; RSV, respiratory syncytial virus.

of vaccine-driven evolution; however, a primary limitation of this study was the small number of vaccinated persons. Continued large-scale RSV genomic surveillance will be critical for detecting emerging immune-escape variants and understanding viral evolution in the postvaccine era.

All raw sequencing data (cleaned of human reads) are available in the National Center for Biotechnology Information (NCBI) under BioProject no. PRJNA1369004, and assembled virus genome sequences are available in NCBI GenBank (accession nos. listed in Appendix 1 Table 2).

This project has been funded in whole or in part with Federal funds from the Centers for Disease Control and Prevention (CDC) Pathogen Genomics Centers of Excellence under contract no. NU50CK000626 (CDC Pathogens Genomics Centers of Excellence, PGCoE). S.R. was supported by Insight Net cooperative agreement CDC-RFA-FT-23-0069 from the CDC's Center for Forecasting and Outbreak Analytics. This study was supported in part by the Emory Integrated Genomics Core, which is subsidized by the Emory University School of Medicine and is one of the Emory Integrated Core Facilities.

CHATGPT version 5.1 (OpenAI, https://openai.com) was used to review grammar for portions of the text during early drafts. All conceptualization, initial writing, final editing, and generation of figures and tables were done manually.

About the Authors

Dr. Rachida is an associate scientist at Emory University School of Medicine, Atlanta, Georgia, USA. His research focuses on molecular tracking of viruses in wastewater samples. Dr. Ahmed is an associate scientist at Emory University School of Medicine. His work focuses on developing and applying next-generation sequencing methods for viral genomic analysis.

References

1. Tin Tin Htar M, Yerramalla MS, Moïsi JC, Swerdlow DL. The burden of respiratory syncytial virus in adults: a systematic review and meta-analysis. Epidemiol Infect. 2020;148:e48. https://doi.org/10.1017/S0950268820000400
2. Britton A, Roper LE, Kotton CN, Hutton DW, Fleming-Dutra KE, Godfrey M, et al. Use of respiratory syncytial virus vaccines in adults aged ≥60 years: updated recommendations of the Advisory Committee on Immunization Practices—United States, 2024. MMWR Morb Mortal Wkly Rep. 2024;73:696–702. https://doi.org/10.15585/mmwr.mm7332e1
3. US Centers for Disease Control and Prevention. RSVV axView. Weekly RSV vaccination dashboard. [cited 2024 Oct 23]. https://www.cdc.gov/rsvvaxview/dashboard/index.html
4. Goya S, Ruis C, Neher RA, Meijer A, Aziz A, Hinrichs AS, et al. Standardized phylogenetic classification of human respiratory syncytial virus below the subgroup level. Emerg Infect Dis. 2024;30:1631–41. https://doi.org/10.3201/eid3008.240209
5. Holland LA, Holland SC, Smith MF, Leonard VR, Murugan V, Nordstrom L, et al. Genomic sequencing surveillance to identify respiratory syncytial virus mutations, Arizona, USA. Emerg Infect Dis. 2023;29:2380–2. https://doi.org/10.3201/eid2911.230836
6. Lauring AS, Edson C, Surie D, Dawood FS, Self WH, Lucero-Obusan C, et al.; IVY Network. Genomic characterization of RSV in the US by vaccination status. JAMA. 2025;333:1540–3. https://doi.org/10.1001/jama.2025.1225
7. LaVerriere E, Behar S, Sher-Jan C, Liang YM, Sagar M, Connor JH. Genomic epidemiology of respiratory syncytial virus in a New England hospital system, 2024. Open Forum Infect Dis. 2025;12:ofaf334. https://doi.org/10.1093/ofid/ofaf334
8. Evans D, Kunerth H, Mumm E, Namugenyi S, Plumb M, Bistodeau S, et al. Genomic epidemiology of human respiratory syncytial virus, Minnesota, USA, July 2023–February 2024. Emerg Infect Dis. 2024;30:2414–8. https://doi.org/10.3201/eid3011.241000
9. Yunker M, Fall A, Norton JM, Abdullah O, Villafuerte DA, Pekosz A, et al. Genomic evolution and surveillance of respiratory syncytial virus during the 2023–2024 season. Viruses. 2024;16:1122. https://doi.org/10.3390/v16071122
10. Fourati S, Reslan A, Bourret J, Casalegno JS, Rahou Y, Chollet L, et al.; POLYRES investigators. Genotypic and phenotypic characterisation of respiratory syncytial virus after nirsevimab breakthrough infections: a large, multicentre, observational, real-world study. Lancet Infect Dis. 2025;25:301–11. https://doi.org/10.1016/S1473-3099(24)00570-X

Address for correspondence: Anne Piantadosi, Woodruff Memorial Research Building, 101 Woodruff Cir, Atlanta, GA 30322, USA; email: anne.piantadosi@emory.edu

Evidence of Rat Hepatitis E Virus Circulation through Wastewater Surveillance, Central Argentina

Florence Abravanel, Clément Castille, Nicolas Marter, Jean Luc Guerin, Sébastien Lhomme, Jacques Izopet

Author affiliations: CHU Toulouse Purpan, INSERM UMR1291, CNRS UMR5051, Université de Toulouse, Toulouse, France (F. Abravanel, S. Lhomme, J. Izopet); ENVT, Université de Toulouse, INRAE, IHAP, Toulouse (C. Castille, J.L. Guerin); Eau de Toulouse Métropole, Toulouse (N. Marter).

DOI: https://doi.org/10.3201/eid3205.260304

To the Editor: A recently published dispatch about rat hepatitis E virus (rHEV) detected high levels of rHEV in wastewater samples from Argentina (67.7%) (*1*). The study authors claimed their findings supported further investigation of the virus in animal reservoirs and humans, with a focus on hepatitis cases of unknown etiology.

rHEV is genetically distinct from conventional human-infecting hepatitis E virus (HEV; *Paslahepevirus balayani*) and is not detected by the PCRs that detect HEV RNA. A recent study in Spain detected an rHEV frequency of 1.4% among patients with hepatitis of unknown etiology (*2*). The rHEV spillover mechanism to humans is unclear.

We analyzed rHEV in wastewater samples from Toulouse, France, where HEV is endemic (HEV IgG seroprevalence 47.8%) (*3*). We collected 49 wastewater samples weekly during 2025 and detected rHEV in all by using a previously published protocol (*4*). However, we could not sequence the genomes because of low viral concentration. During 2023–2025, we tested 484 immunocompetent patients with a positive HEV IgM result by using Liaison (Diasorin, https://us.diasorin.com), to detect HEV IgM in patients with rHEV infection (*5*), and 578 immunocompromised patients living in the same area. We collected the samples at infection onset when the liver enzymes were elevated and AltoStar HEV PCR Kit (Altona Diagnostics, https://altona-diagnostics.com) results were negative. None of the samples were positive for rHEV RNA.

The high detection rate of rHEV in wastewater reflecting high circulation in urban rodents contrasts with the rarity of human cases. This contrast could be linked to low exposure of humans to contaminated sources, low human infection capability of rHEV, or cross protection because of immunity conferred by HEV in Toulouse, where the seroprevalence is higher than in Spain, where rHEV human cases are more frequent (2). Future studies to evaluate rHEV-specific serologic response could be useful.

References

1. Filoni B, Lucero ME, Di Cola G, Fantilli A, Roccia A, Sicilia P, et al. Evidence of rat hepatitis E virus circulation through wastewater surveillance, central Argentina. Emerg Infect Dis. 2026;32:133–6. https://doi.org/10.3201/eid3201.251218
2. Caballero-Gómez J, Casares-Jiménez M, Gallo-Marín M, Pereira-Pardo S, Beato-Benítez A, Poyato A, et al.; GEHEP-014 Study Group. Rat hepatitis E virus as an aetiological agent of acute hepatitis of unknown origin. J Hepatol. 2025;83:662–9. https://doi.org/10.1016/j.jhep.2025.02.027
3. Dimeglio C, El Rakaawi M, Boineau J, De Smet C, Abravanel F, Lhomme S, et al. Increase in HEV IgG seroprevalence during the past years in southern France. J Med Virol. 2025;97:e70483. https://doi.org/10.1002/jmv.70483
4. Parraud D, Lhomme S, Péron JM, Da Silva I, Tavitian S, Kamar N, et al. Rat hepatitis E virus: presence in humans in south-western France? Front Med (Lausanne). 2021;8:726363. https://doi.org/10.3389/fmed.2021.726363
5. Fourgeaud J, Veyrenche N, Laloum I, Jais J-P, Roger C, Rabant M, et al. Occult rat hepatitis E virus infection as a cause of cirrhosis and posttransplant recurrence: insights into the role of metagenomics. Am J Transplant. 2026; S1600-6135(26):00007-9.

Address for correspondence: Florence Abravanel, CHU Toulouse Purpan, 330 Avenue de Grande Bretagne, 31059 Toulouse CEDEX 9, France; email: abravanel.f@chu-toulouse.fr

Evidence Lacking for Endemic Chagas Disease in the United States

Paul T. Cantey, Marisa Hast, Rebecca J. Chancey, Susan P. Mongomery

Author affiliation: Centers for Disease Control and Prevention, Atlanta, Georgia, USA

DOI: https://doi.org/10.3201/eid3205.251840

To the Editor: The Centers for Disease Control and Prevention Parasitic Diseases Branch (National Center for Emerging and Zoonotic Infectious Diseases, Division of Parasitic Diseases and Malaria)

wishes to comment on the Perspective from Beatty et al. (*1*), published last fall. The authors describe infections in the Americas, the presence of multiple vector triatomine insects and *Trypanosoma cruzi* infection in animals in the United States, and the history of locally acquired human cases. Although this article provides supportive information for classifying this pathogen as endemic to the United States, we would like to highlight that human disease caused locally by the pathogen is sporadic, not endemic.

Fewer than 100 locally acquired, vectorborne human *T. cruzi* infections in the country have been documented (*2*). Other documented routes of infection include vertical, transplant-derived, transfusion-derived (before 2007), and occupational exposure-related transmission (*2*,*3*). This number of infections is small compared with the estimated 288,000 persons currently infected in the country (*4*) who acquired the infection elsewhere.

As indicated by the authors, triatomines were identified in the United States in the 1800s and *T. cruzi* was identified in 1916. Data suggest that triatomine species in the United States are primarily sylvatic but occasionally invade homes (*2*). Although high numbers of infected triatomines and mammalian reservoirs have been found in some focal areas, reported human cases do not demonstrate that Chagas disease is emerging in the United States. A combination of triatomine and human factors likely reduces risk. Declaring human Chagas disease endemic could result in universal patient testing that would lead to overtesting of populations with no major risk and the associated costs of false-positive results (for example, healthcare costs, impacts on organ transplantation processes, and unnecessary anxiety for individual patients).

However, continued effort is needed to identify and treat the 288,000 persons with Chagas disease in the United States, including educating healthcare providers to identify high-risk persons and manage the disease. If state partners wish to make Chagas disease nationally notifiable, the Centers for Disease Control and Prevention welcomes the opportunity to work with them to track cases of Chagas disease in the United States. In the meantime, states could voluntarily report Chagas cases using standardized surveillance definitions (https://ndc.services.cdc.gov/case-definitions/chagas).

References

1. Beatty NL, Hamer GL, Moreno-Peniche B, Mayes B, Hamer SA. Chagas disease, an endemic disease in the United States. Emerg Infect Dis. 2025;31:1691–7. https://doi.org/10.3201/eid3109.241700
2. Bern C, Messenger LA, Whitman JD, Maguire JH. Chagas disease in the United States: a public health approach. Clin Microbiol Rev. 2019;33:e00023–19. https://doi.org/10.1128/CMR.00023-19
3. Herwaldt BL. Protozoa and helminths.. In: Wooley DP, Byers KB, editors. Biological safety: practices and principles, 5th edition. Washington: ASM Press; 2017. p. 105–45.
4. Irish A, Whitman JD, Clark EH, Marcus R, Bern C. Updated estimates and mapping for prevalence of Chagas disease among adults, United States. Emerg Infect Dis. 2022;28:1313–20. https://doi.org/10.3201/eid2807.212221

Address for correspondence: Paul T. Cantey, Centers for Disease Control and Prevention, 1600 Clifton Rd NE, Mailstop H16-4, Atlanta, GA 30329-4018, USA; email: gdn9@cdc.gov

Norman L. Beatty, Gabriel L. Hamer, Bernardo Moreno-Peniche, Bonny Mayes, Sarah A. Hamer[1]

Author affiliations: University of Florida College of Medicine, Gainesville, Florida, USA (N.L. Beatty); Emerging Pathogens Institute, University of Florida, Gainesville (N.L. Beatty); Texas A&M University, College Station, Texas, USA (G.L. Hamer); University of California, Berkeley, California, USA (B. Moreno-Peniche); Texas Department of State Health Services, Austin, Texas, USA (B. Mayes); Texas A&M University College of Veterinary Medicine and Biomedical Sciences, College Station (S.A. Hamer)

DOI: https://doi.org/10.3201/eid3205.260617

In Response: We thank Cantey et al. (*1*) for their work and acknowledge our shared perspective that awareness for Chagas disease in the United States must be raised.

References

1. Cantey PT, Hast M, Chancey RJ, Mongomery SP. Potential endemicity of Chagas disease in the United States. Emerg Infect Dis. 2026;32:829–830.

Address for correspondence: Sarah A. Hamer, Department of Veterinary Integrative Biosciences, 667 Raymond Stotzer Ave, Texas A&M University, College Station, TX 77843, USA; email: shamer@cvm.tamu.edu

The Big One: How We Must Prepare for Future Deadly Pandemics

Michael Osterholm, Mark Olshaker; Little, Brown Spark; New York, New York, USA, 2025; ISBN-13: 978-0316258340; Pages: 384; Price: $30.00 USD (hardcover)

The Big One: How We Must Prepare for Future Deadly Pandemics is the second book by authors Michael Osterholm and Mark Olshaker discussing politics, reviewing previous pandemic responses, and summarizing infectious disease microbiology to guide pandemic preparedness. Osterholm writes with authority from his decades of experience in public health and epidemiology at the Minnesota Department of Health and the University of Minnesota Center for Infectious Disease Research and Policy Research and Innovation. As a bestselling author and award-winning filmmaker, Olshaker displays his talent for engaging storytelling. Combining their skillsets, the authors lead readers through 8 chapters of storytelling and discussion across a myriad of interrelated topics covering the evolution of a viral pathogen of pandemic potential, epidemiology of airborne transmission, mandates, medical interventions, effective communication, policy, and next steps.

Each chapter begins with an excerpt of a fictional yet familiar story that catches the reader's attention by detailing how a novel respiratory pathogen, starting at patient zero, becomes a global pandemic. The story highlights our interconnectedness by describing how a novel pathogen can travel globally before medical or public health communities are aware of its existence. Focusing on the United States, the authors also discuss essential aspects of pandemic response such as vaccine development, air quality and masks, reliable and actionable public health surveillance, effective communication, mandates, and pandemic-related policy.

Each chapter provides a foundational overview of topics such as the epidemiology of airborne transmission, history of public health surveillance, types of vaccinations and their limitations, evolution of viral pathogens, and diagnostic tests for respiratory viruses. Using an evidence-based approach, the authors explain, recommend, and critique previous pandemic responses, particularly COVID-19. Critiques and recommendations are often accompanied by references to scientific literature, subject matter experts, and historical references. The authors are explicitly critical of actions not supported by rigorously evaluated evidence, such as the Emergency Use Approval by the US Food and Drug Administration of the BinaxNOW COVID-19 point-of-use lateral flow diagnostic tests (Abbott, https://www.abbott.com), which were approved on the basis of just 117 positive samples. The authors also praise the rapid and accurate clinical and laboratory surveillance metrics for COVID-19 in countries with centralized healthcare, such as the United Kingdom, Israel, and Canada. The goal of this analysis is to glean lessons from planning failures and mistakes made in previous pandemic responses, as well as to provide a blueprint for mitigating damage from the next pandemic. The authors end each chapter with concise and direct takeaways.

The authors have some self-biases; Osterholm recalls instances where he correctly provided warnings and recommendations that others dismissed. The positive contributions of the Center for Infectious Disease Research and Policy Research and Innovation are also discussed, but little if any criticism is included.

The book is a worthwhile read for professionals in public health, healthcare administration, life sciences, public policy, emergency preparedness, and anyone interested in pandemic preparedness. It provides readers with an opportunity to reflect critically on the interdisciplinary facets of pandemic preparedness and response. The book could serve as a reference guide throughout one's career to reflect on how to incorporate evidence-based strategies to respond to major societal concerns.

Courtney N. Dillingham, Gary A. Brooks, Yolanda M. Brooks

Author affiliations: US Customs and Border Protection, Washington, DC, USA (C.N. Dillingham); Retired, Bradenton, Florida, USA (G.A. Brooks); Pennsylvania Department of Health, Harrisburg, Pennsylvania, USA (Y.M. Brooks)

DOI: https://doi.org/10.3201/eid3205.252036

The views expressed in this article are those of the authors and do not necessarily reflect the position or policy of the US Department of Homeland Security, US Customs and Border Protection, or the US government.

Address for correspondence: Yolanda M. Brooks, Department of Health, Bureau of Epidemiology, Division of Surveillance, 625 Forster St, Harrisburg, PA 17120, USA; email: c-yobrooks@pa.gov

Cassius Marcellus Coolidge, *A Friend in Need*, 1903. Oil on canvas. 129.5 cm × 160.6 cm (51 in × 63.22 in). Smithsonian American Art Museum, Washington, DC, USA.

Gone to the Dogs—The Canon of Kitsch

Lesli Mitchell

This issue's cover art is a work of contradictions. It's immediately recognizable, and yet it's painted by "the most famous American artist you've never heard of." In popular culture, it's known as "Dogs Playing Poker," but its actual title is *A Friend in Need*. Often referenced as a standalone work, in fact, it's the fourth in a series of 16 paintings featuring dogs by artist Cassius Marcellus Coolidge (1844–1944). Although art critics do not consider the paintings fine art, Sotheby's deigned to auction off one of Coolidge's dogs playing poker paintings for an impressive $650,000 in 2015, and *A Friend in Need* currently resides on the wall of the Smithsonian American Art Museum in Washington, DC.

Since the painting's wildly successful introduction in 1903, as an image in an advertising calendar, *A Friend in Need* has continued to be a part of the public imagination. The image is everywhere—in television, movies, music videos, hung as a poster in bars and man caves, even sold, still, as a calendar. The enduring popularity of the image has prompted art critics to explore the source of its lasting appeal. Art critics typically categorize the painting as kitsch, a term introduced in art in 1939 by influential New York art critic Clement Greenberg. In his essay "Avant-Garde and Kitsch," published in *Partisan Review*, Greenberg defined kitsch as commercial art concerned with "magazine covers, illustrations, ads, slick and pulp

Author affiliation: Centers for Disease Control and Prevention, Atlanta, Georgia, USA

DOI: https://doi.org/10.3201/eid3205.AC3205

fiction, comics, Tin Pan alley music, tap dancing, Hollywood movies."

Coolidge's work certainly fits that mold, perhaps even more so since the artist had no formal training. Cassius Marcellus Coolidge was born in New York in 1844 to abolitionist Quaker parents and was named after antislavery crusader Cassius Marcellus Clay. In his youth, he pursued a series of seemingly random jobs—druggist, sign painter, founder of a newspaper, even founder of a bank that still exists today—before settling into a career as an artist. He was hired by the advertising company Brown & Bigelow, which specialized in the production of advertising calendars, and it was there that Coolidge created 16 paintings of dogs known collectively as "Dogs Playing Poker."

The series was an immediate hit: "These calendars proved to be massively successful, and Coolidge's art found its way into millions of homes," according to the blog The Automat. Part of the paintings' success, both then and today, may be that despite Coolidge's lack of professional training, his work ticked the boxes of established principles of composition. The composition is circular, anchored by the table in the center, with the objective of guiding the eye around the circle to each subject. The highly saturated green of the table is value-matched to the complementary strong red above it, in the hanging lamp. The background follows the rule of thirds, dividing the canvas, creating a triangle in the center, and drawing the viewer's eye across the canvas in a diagonal line. In painting the background, Coolidge also makes use of a technique known as scumbling, scrubbing the brush onto the canvas to roughen it. He scumbles as he pairs that texture with the Doberman's coat.

Coolidge's composition also tells a human story, using the dogs as allegory, and upon close inspection the viewer is rewarded with a host of intriguing details. Many people enjoy the image without noticing the circumstances that give the painting its name, *A Friend in Need*. Subtly, in the foreground, we can see that the bulldog is cheating, passing an ace under the table to his companion. Once we see that, we see more: his companion has three aces in hand and needs only a fourth to win. The clock indicates the lateness of the hour, suggesting the game has been going on for a while. The bulldogs are clearly doing very well for themselves, with tall stacks of chips, compared with the pitiful scattering of chips held by the other dogs.

Coolidge also gives the dogs character and complexity. The St. Bernard in the middle eyes the Doberman suspiciously, and the Doberman in turn eyes the bulldog suspiciously. Or perhaps he's looking beyond the bulldog to us, the viewers, asking, "Are you seeing this?" The St. Bernard on the right is lamenting his hand, knowing he's going to lose again. The collie and St. Bernard on the left, who have a few more chips than the others, have half smiles, perhaps hopeful that this will be the hand that changes their fortunes.

For an artist with no formal training, Coolidge nevertheless knows how to engage his viewers and give them a rich and fun experience. In this accomplishment, the painting begins to escape the negative associations in Greenberg's definition of kitsch, which he considers to be about money and ease: "Kitsch pretends to demand nothing of its customers except their money—not even their time." Kitsch at its core is a manipulation, using sentiment to make money. Coolidge's skill in both technique and subject expresses the playfulness of the scene without tipping the scale to sentimentality. The way in which Coolidge anthropomorphizes the dogs feels authentically affectionate. Even art critics respond to that. As Tamar Avishai says in his podcast, *The Lonely Palette*:

> When I look at this painting, of course I think of the Cezanne card player paintings, but then the sort of art critic in me falls away and I just look at the dogs. I love dogs, and I think that everyone probably goes to the breed that appeals to them first or they have some life or childhood connection to.

The work encourages viewers to connect emotionally with the dogs. We are, after all, the only ones who know what the bulldogs are up to. We are invited to enjoy the fun of the scene, and we accept the invitation. In the same podcast, Avishai mentions his friend:

> My buddy Wade has both PhD from MIT and a new Australian shepherd puppy, and he's certainly not above wistfully commenting that if there had been an Aussie at the poker table, you know he would have cleaned up.

The genuine warmth that comes across in this work helps it transcend the derogatory commercial connotations of kitsch. Coolidge's work has a stretchiness to it that accepts the classification as "The Mona Lisa of Kitsch" and at the same time evokes a fondness from those who give it that label. It's a painting that occupies a unique position as an American cultural artifact, and we embrace it whether it hangs on the wall of a museum or a pool hall.

The enduring popularity of *A Friend in Need* also points to the enduring bond that humans have with their canine friends and other domesticated animals. The health of humans is closely connected to the

health of animals and our shared environment. The expansion of the population into new areas, climate changes, and travel and trade have led to the spread of new or emerging zoonotic diseases. Approaches like One Health address such risks by promoting collaboration among experts worldwide in human, animal, and environmental health. The goal is to improve the health of both humans and animals, including livestock, wildlife, and the beloved pets that bring companionship, delight, and enrichment to our lives.

Acknowledgments

Special thanks to T.G. Pelham and artist Susan Pelham for their technical analyses of the painting.

Bibliography

1. Arn J. Why this painting of dogs playing poker has endured for over 100 years. Artsy.net. 2018 Jun 6 [cited 2026 Mar 19]. https://www.artsy.net/article/artsy-editorial-painting-dogs-playing-poker-endured-100-years
2. Avishai T. Episode 26: C.M. Coolidge's Dogs Playing Poker (1903). The Lonely Palette [cited 2026 Feb 18]. https://www.thelonelypalette.com/episode-26-dogs-playing-poker
3. Centers for Disease Control and Prevention. About One Health [cited 2026 Apr 3]. https://www.cdc.gov/one-health/about/index.html
4. Foxpudding. Cassius Marcellus Coolidge. The Automat. 2011 May 19 [cited 2026 Feb 18]. https://foxpudding.wordpress.com/2011/05/19/cassius-marcellus-coolidge
5. Greenberg C. Avant-guard and kitsch. Partisan Review. 1939 [cited 2026 Feb 18]. https://www.nshafer.com/darkvisual-arts/Greenberg.pdf
6. Martinovic J. Beloved by all but the art world—the dogs playing poker painting by Cassius Marcellus Coolidge. 2025 Feb 27 [cited 2026 Mar 19]. https://blog.artsper.com/en/a-closer-look/dogs-playing-poker-painting
7. Moore J. That dogs playing poker painting just sold for over $650,000. GQ. 2015 Nov 20 [cited 2026 Feb 18]. https://www.gq.com/story/dogs-playing-poker-painting-sold-for-650000
8. Scruton R. Kitsch and the modern predicament. City Journal. 1999 [cited 2026 Mar 19]. https://www.city-journal.org/article/kitsch-and-the-modern-predicament

Address for correspondence: Lesli Mitchell, Centers for Disease Control and Prevention, 1600 Clifton Rd NE, Mailstop H16-2, Atlanta, GA 30329-4018, USA; email: aul6@cdc.gov

etymologia revisited

Petri Dish

[pe'tre 'dish]

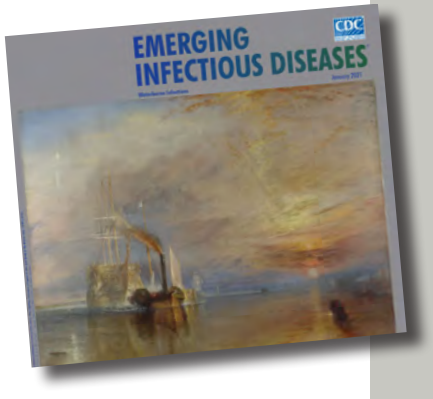

The Petri dish is named after the German inventor and bacteriologist Julius Richard Petri (1852–1921). In 1887, as an assistant to fellow German physician and pioneering microbiologist Robert Koch (1843–1910), Petri published a paper titled "A minor modification of the plating technique of Koch." This seemingly modest improvement (a slightly larger glass lid), Petri explained, reduced contamination from airborne germs in comparison with Koch's bell jar.

References:

1 Central Sheet for Bacteriology and Parasite Science [in German]. Biodiversity Heritage Library. Volume 1, 1887 [cited 2020 Aug 25]. https://www.biodiversitylibrary.org/item/210666#page/313/mode/1up
2. Petri JR. A minor modification of the plating technique of Koch [in German]. Cent für Bacteriol und Parasitenkd. 1887;1:279–80.
3. Shama G. The "Petri" dish: a case of simultaneous invention in bacteriology. Endeavour. 2019;43:11–6. DOIExternal
4. The big story: the Petri dish. The Biomedical Scientist. Institute of Biomedical Science [cited 2020 Aug 25]. https://thebiomedicalscientist.net/science/big-story-petri-dish

Originally published in January 2021

https://wwwnc.cdc.gov/eid/article/27/1/et-2701_article

EMERGING INFECTIOUS DISEASES

Upcoming Issue • June 2026 • Bacterial Infections and Their Treatment

- Cerebrospinal Fluid Findings among Patients with Anaplasmosis and Central Nervous Involvement, Minnesota and Wisconsin, USA
- Public Health Response to Toxigenic Respiratory Diphtheria Outbreaks at Correctional Facility, South Africa, 2023–2025
- Outcomes of Hospitalized and Critically Ill Adults with Murine Typhus, Galveston, Texas, USA, 2019–2023
- Group A *Streptococcus* Outbreak Associated with a Large Congregate Shelter, Chicago, Illinois, USA, October 26, 2023–January 3, 2024
- Emergence of *Klebsiella pneumoniae* Carbapenemase–Producing *K. pneumoniae* with Penicillin-Binding Protein 3 Insertions, Taiwan, 2021
- Association of Frailty and Frailty Trajectory with Risk for Respiratory Infectious Diseases
- Characteristics of Plausible Source Cases Responsible for Recent *Mycobacterium tuberculosis* Transmission, United States, 2018–2022
- Identification of a Novel Recombinant Human Adenovirus Genotype B117 from 2 Pediatric Community-Acquired Pneumonia Cases, China
- Role of Households with Children in the Spread of Multidrug-Resistant Enterobacterales in the Community
- In Vitro Antifungal Susceptibility of 1,178 Clinical Feline *Sporothrix schenckii* Complex Isolates in Thailand, 2023–2025
- Antimicrobial-Resistant Gonorrhea of Public Health Concern, Australia, 2022–2024
- National Surveillance of Enterovirus D68 Upsurge, France, 2024
- Outbreak of *Wickerhamomyces anomalus* (Formerly *Candida pelliculosa*) Bloodstream Infections, Venezuela, 2022–2023
- *Wickerhamomyces anomalus* Fungemia during Healthcare-Associated Outbreak in Pereira, Colombia, 2025
- Yellow Fever Virus Surveillance in *Callithrix* spp. Marmosets during Epizootic Outbreak, Brazil, 2024–2025
- Repeated Extraneous Introduction of Cholera in Thailand, 2007–2025
- Burden of Hospitalization for Disseminated Coccidioidomycosis and Coccidioidal Meningitis, Texas, USA, 2016–2023
- *Caballeronia Bacteremia* in Children with Cancer, United States
- CDC Consultations for Adverse Outcomes of Travel-Related Cosmetic Procedures, January 2014–December 2024
- Suspected Sexual Transmission of Dermatophilosis among Men Who Have Sex with Men, Lyon and Paris, France, 2025–2026
- Suspected Sexual Transmission of Dermatophilosis among Men Who Have Sex with Men, Barcelona, Spain, 2025–2026
- Placental Vascular Pathology Associated with Congenital Lymphocytic Choriomeningitis Virus Infection, Philadelphia, Pennsylvania, USA
- Concurrent Detection of Swine-Origin Influenza A(H1N1) Virus in Pigs and Farmer, Switzerland
- Therapeutic Challenges in Case of *Trichophyton indotineae* Dermatophytosis, Singapore, 2025
- Emergence of Ceftriaxone-Resistant *Neisseria gonorrhoeae penA*-60–Carrying Strains, Thailand, 2025
- Utility of Using Phenotypic and Genomic Analysis to Characterize Antimicrobial-Resistant *Neisseria gonorrhoeae* of Public Health Concern
- *Cutibacterium avidum* Isolation in a Postmastectomy Breast with Prior Silicone Injections
- Outbreak of *Neisseria gonorrhoeae* ST16676 among Disseminated Infections in Minnesota, USA, 2025
- Increase in bla_{NDM} among Carbapenemase-Producing, Carbapenem-Resistant Enterobacterales Collected through Surveillance Initiative, United States, 2016–2023
- Dangerous Miracle: The Astonishing Rise and Looming Disaster of Antibiotics
- Myriad, Microscopic and Marvelous: The World of Antoni van Leeuwenhoek
- Assessing Evidence to Guide Primary Prevention of Pathogen X

Complete list of articles in the June issue at http://www.cdc.gov/eid/#issue-332

Earning CME Credit

To obtain credit, you should first read the journal article. After reading the article, you should be able to answer the following, related, multiple-choice questions. To complete the questions (with a minimum 75% passing score) and earn continuing medical education (CME) credit, please go to http://www.medscape.org/journal/eid. Credit cannot be obtained for tests completed on paper, although you may use the worksheet below to keep a record of your answers.

You must be a registered user on http://www.medscape.org. If you are not registered on http://www.medscape.org, please click on the "Register" link on the right hand side of the website.

Only one answer is correct for each question. Once you successfully answer all post-test questions, you will be able to view and/or print your certificate. For questions regarding this activity, contact the accredited provider, CME@medscape.net. For technical assistance, contact CME@medscape.net. American Medical Association's Physician's Recognition Award (AMA PRA) credits are accepted in the US as evidence of participation in CME activities. For further information on this award, please go to https://www.ama-assn.org. The AMA has determined that physicians not licensed in the US who participate in this CME activity are eligible for AMA PRA Category 1 Credits™. Through agreements that the AMA has made with agencies in some countries, AMA PRA credit may be acceptable as evidence of participation in CME activities. If you are not licensed in the US, please complete the questions online, print the AMA PRA CME credit certificate, and present it to your national medical association for review.

Article Title

Frequency and Duration of Diagnostic Delays Associated with Coccidioidomycosis and Risk Factors for Missed Diagnoses, United States

CME Questions

1. Which of the following statements regarding Coccidioidomycosis is most accurate?

A. *Coccidioides immitis* infection is associated with greater severity and a higher risk for mortality vs *C. posadasii* infection
B. A majority of cases of coccidioidomycosis are asymptomatic
C. The liver is the most common site of extrapulmonary dissemination of coccidioidomycosis
D. Coccidioidomycosis is characterized on chest radiography by mass-like lesions in the upper lobes

2. Missed opportunities to diagnose coccidioidomycosis were most common in which of the clinical settings in the current study?

A. Outpatient
B. Inpatient
C. Emergency department
D. Observational

3. What was the approximate average delay in diagnosis of coccidioidomycosis among patients with at least 1 missed opportunity for diagnosis?

A. 12 days
B. 30 days
C. 75 days
D. 110 days

4. Which of the following variables was most associated with a delay in diagnosis of coccidioidomycosis in the current study?

A. Medicaid health insurance
B. Medicare health insurance
C. Younger age
D. Receipt of antibiotics or inhalers

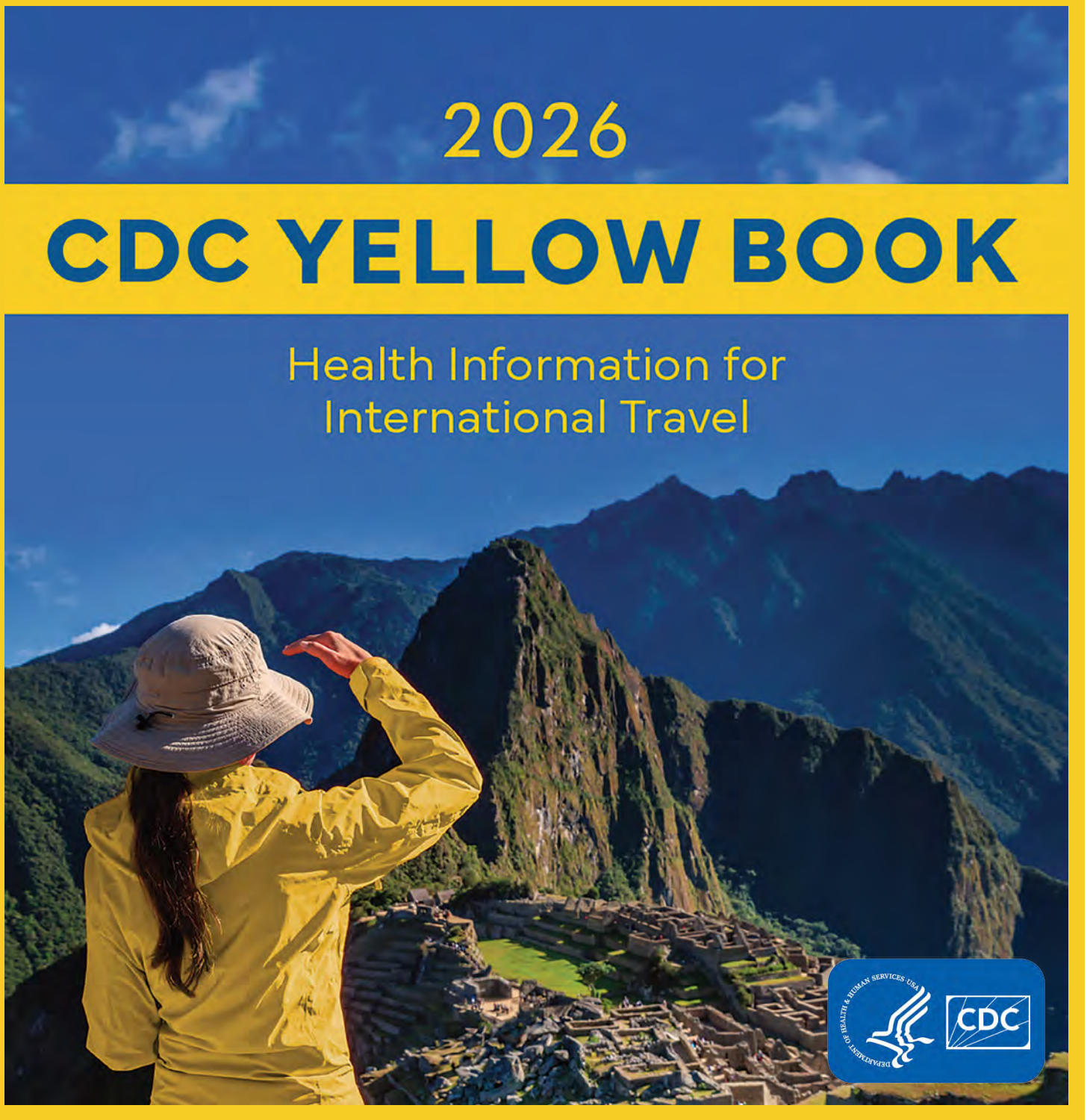

Launch of CDC Yellow Book 2026– A Trusted Travel Medicine Resource

CDC is pleased to announce the launch of the **CDC Yellow Book 2026**. The CDC Yellow Book is a resource containing the U.S. government's travel medicine recommendations and has been trusted by the travel medicine community for over 50 years. Healthcare professionals can use the print and digital versions to find the most up-to-date travel medicine information to better serve their patients' healthcare needs.

The CDC Yellow Book is available online now at www.cdc.gov/yellowbook and in print starting in June 2025 through Oxford University Press and other major online booksellers.